The Dissertation Committee for Rangsan Wongjeeraphat certifies that this is the approved version of the following dissertation:

STABILITY BRACING BEHAVIOR FOR TRUSS SYSTEMS

Committee:

Todd A. Helwig, Supervisor

Karl H. Frank

Michael D. Engelhardt

John L. Tassoulas

Krishnaswamy Ravi-Chandar

STABILITY BRACING BEHAVIOR FOR TRUSS SYSTEMS

by

Rangsan Wongjeeraphat, B.E.; M.E.

Dissertation

Presented to the Faculty of the Graduate School of

The University of Texas at Austin

in Partial Fulfillment

of the Requirements

for the Degree of

Doctor of Philosophy

The University of Texas at Austin

May, 2011

Dedication

To my family for their unlimited love and support.

Acknowledgements

Words are completely inadequate to convey my appreciation for the many people who have helped me throughout the process of this dissertation. First and foremost, I would like to express my deepest gratitude to my advisor, Dr. Todd Helwig. His guidance, advice, and limitless patience over the past five years have been unbelievably helpful and motivational. Without his mentoring and knowledge, I never would have accomplished this major milestone in my life. I would also like to express my sincere gratitude to Dr. Karl Frank, for his advice on the technical details of my work. I am very grateful to the remaining members of my dissertation committee, Dr. Michael Engelhardt, Dr. John Tassoulas and Dr. Krishnaswamy Ravi-Chandar. Their invaluable input and constructive comments to my project are greatly appreciated. I would also like to take this opportunity to express my respect and gratitude to Dr. Joseph Yura for sharing his knowledge with me through numerous discussions and for providing guidance on my experiments, which helped me improve my understanding of truss system buckling behavior.

I would like to thank the Ferguson Structural Engineering Laboratory for providing me the opportunity to work with such a large and fully equipped laboratory. I am indebted to the FSEL staff who have helped me through these years. Thank you to Dennis Fillip, Blake Stasney, Andrew Valentine, Eric Schell and Mike Wason. I am also thankful to Ms. Barbara Howard, Ms. Jessica Harbison and Ms. Cari Billingsley for their administrative help.

Also thanks to my friends at the Ferguson Lab for interesting discussions and for being fun to be with. I would regret it if I did not mention Dr. Craig Quadrato, who was my officemate and has been a great friend to which I can turn to with any engineering or

non-engineering related questions. Special thanks to Dr. Quan Chen who was always willing to help and give his best suggestions regarding analytical techniques. I will also never forget my great times with Dr. Jason Stith and Anthony Battistini. I am grateful to Weihua Wang, Guanyu Hu, Jeremiah Fasl, Dr. Seongyeong Yang, Dr. Gun Up Kwon, Dr. Shiv Shanker Ravichandran and Dr. Seongwoo Jo and the many others for always being such wonderful friends throughout these past five years. Thanks also go to Sean Donahue, Nicholas Olin, Yoav Wolfson, Ryan Hall, and Loren Campos - the undergraduate research assistants who helped me with my research.

I would like to acknowledge the Faculty of Engineering at Kasetsart University and the Royal Thai Government for their financial support. My appreciation also goes to the Minister and staff at the Office of Educational Affairs at Washington D.C., Royal Thai Government, for their coordination and support.

I would also like to recognize my Thai friends in Austin. They made me feel at home and joyful during the time I have been here. I must acknowledge with tremendous and deep thanks Dr. Jaroon Rungamornrat for his mentorship during my early years in graduate school. Thanks to Piyanuch Wonganan for her tremendous help and support in several aspects. I am grateful to Sumalee Thitinan, who is a joy to spend my days with. I also acknowledge the friendship that Kajakorn Chomaitong, Sorawit Watanachet and Punchet Thammarak have given me throughout these years. Thank you to all of you whom I may not have mentioned, but have contributed to my graduate career.

Last but not least, I would like to express my deepest thanks to my family for always encouraging and never doubting any dream I have ever had. They have always supported me and encouraged me with their best wishes.

Rangsan Wongjeeraphat

January, 2011

Stability Bracing Behavior for Truss Systems

Publication No. _____

Rangsan Wongjeeraphat, Ph.D.

The University of Texas at Austin, 2011

Supervisor: Todd A. Helwig

The stability bracing behavior of trusses was investigated using experimental testing and computational modeling. The laboratory experiments were conducted on twin trusses fabricated with W4x13 sections for the chord and web members. Spans of 48 and 72 feet were used in the tests that included both lateral load tests and buckling tests. Most of the tests were done on the regular (Howe) truss, except the lateral stiffness tests which were also done on the inverted (Pratt) truss. Computational models were developed using the three-dimensional finite element program, ANSYS, which were validated using the laboratory test data. A variety of models were used to simulate both as-built and idealized truss models.

The experiments demonstrated that the buckling capacity of the truss with torsional bracing largely depended on the brace stiffness and the number of intermediate braces. Similar behavior was observed in the truss with lateral bracing. The tests results demonstrated that cross sectional distortion dramatically reduces the effectiveness of the torsional braces. The experiments provided valuable data for validating the finite element models that were used to conduct parametric studies on torsional bracing of truss systems. The results from the parametric studies were used to develop stiffness requirements for torsional bracing of trusses.

Table of Contents

List of Tables xv

List of Figures xvii

CHAPTER 1: Introduction 1

1.1 Introduction 1

1.2 Problem Description 4

1.3 Research Purpose 7

1.4 Research Method 7

1.5 Report Organization 8

CHAPTER 2: Background 9

2.1 Introduction 9

2.2 Buckling Behavior of Beams 9

2.2.1 Load Types and Force Distribution 10

2.2.2 Load Locations (Load Height Effect) 12

2.2.3 Total Brace Stiffness 14

2.2.3.1 Brace Stiffness (β_b) 14

2.2.3.2 Cross Section Stiffness and Cross Section Distorsion (β_{sec}) 16

2.2.3.3 Connection Stiffness (β_{con}) 18

2.2.3.4 Girder In-Plane Stiffness (β_g) 19

2.2.4 Brace Locations 21

2.3 Ideal Stiffness Requirements and Initial Imperfections 21

2.4 Stability Bracing Requirements for Columns, Beams and Trusses 23

2.4.1 Column Bracing Requirements 25

2.4.2 Beam Bracing Requirements 30

2.4.3 Truss Bracing Requirements 33

2.4.3.1 Regular Truss 33
2.4.3.2 Half Through Truss (Pony Truss) 37
2.5 Technique to Estimate Buckling Capacity 39
2.6 System Mode Buckling 41
2.7 Summary 42
CHAPTER 3: Experimental Program **44**
3.1 Introduction 44
3.2 General Test Setup 45
3.2.1 Truss Fabrication 45
3.2.2 Gravity Load Simulator 48
3.2.3 Load Beams and Knife Edges 52
3.2.4 Instrumentation 55
3.2.5 Supports and End Conditions 60
3.3 Initial Imperfection Measurement 64
3.4 Lateral Stiffness Test Setup 65
3.5 Effect of Load Position 66
3.6 Test Setup with Lateral Bracing 68
3.7 Test Setup with Torsional Bracing 72
CHAPTER 4: Experimental Test Results **77**
4.1 Introduction 77
4.2 Initial Imperfection 77
4.3 Lateral Stiffness Test 80
4.3.1 Laterally Unrestrained Trusses 81
4.3.2 Laterally Restrained Trusses 85

4.4 Buckling Test of Truss without Intermediate Bracing 88
4.4.1 Lateral Deflection 88
4.4.2 Strain at Midspan 89
4.4.3 Vertical Deflection 92
4.4.4 Cross Section Rotation 94
4.4.5 Estimated Truss Buckling Capacity by Southwell Plot 95
4.5 Buckling Test of Trusses with Lateral Bracing 99
4.5.1 Calibration of Lateral Braces 99
4.5.2 Lateral Deflection 101
4.5.3 Cross Section Rotation 107
4.5.4 Strain in Truss Chord 110
4.5.5 Lateral Brace Forces 112
4.6 Buckling Test of Trusses with Torsional Bracing 113
4.6.1 Lateral Deflection 115
4.6.2 Strain in Truss Chord 117
4.6.3 Torsional Brace Strain 120
4.6.4 Torsional Brace Axial Force 123
4.6.5 Cross Section Distortion and Effect of Connection Stiffeners on Truss Buckling Capacity 123
4.7 Buckling Test of Pony Truss 126
4.7.1 Lateral Deflection 128
4.7.2 Torsional Brace Strain 129
4.7.3 Torsional Brace Axial Force 130
4.8 Buckling Test of Truss with Load Offset 131
4.9 Summary 133
CHAPTER 5: Development of Finite Element Model and Model Verification 136
5.1 Introduction 136
5.2 Developing of the FEA Model 136

5.3 FEA Model Initial Conditions 139

5.4 Model Verification 141

5.4.1 Lateral Stiffness Test 141

5.4.1.1 Lateral Stiffness of Truss without Lateral Stops 142

5.4.1.2 Lateral Stiffness of Truss with Lateral Stop 145

5.4.2 Buckling Test of Truss without Intermediate Bracing (with 48-ft and 72-ft span) 146

5.4.3 Buckling Load Test with Torsional Bracing 151

5.4.4 Brace Force 157

5.5 Summary 160

CHAPTER 6: Parametric Study of Truss Buckling Behavior 162

6.1 Introduction 162

6.2 Criteria of the Analysis and Assumptions 163

6.2.1 Chord and Web Size 163

6.2.2 Torsional Braces 164

6.2.2.1 Beam Elements 164

6.2.2.2 Cross frame 165

6.2.3 Analysis assumptions and scope for parametric study 166

6.2.4 Model verification with structural analysis program of single truss 166

6.3 Calculation of Truss In-Plane Moment of Inertia 170

6.4 Buckling Behavior of Truss with Rigid Web at Brace Point 174

6.5 Trusses with Cross Frame Bracing 176

6.5.1 Comparisons of Bracing Behavior for Cross Frames and Beam Element Torsional Braces 179

6.5.2 Comparison of Buckling Capacity of Trusses with Multiple Intermediate Braces 182

6.5.2.1 Uniform Moment Cases 182

6.5.2.2 Uniform Load Cases 185

6.6 Behavior of Trusses with Simplified Web Connections 189

6.7 Summary 190

CHAPTER 7: Stiffness Requirements for Torsional Bracing of Truss Systems **194**

7.1 Introduction 194

7.2 Buckling Capacity and Ideal Cross Frame Stiffness of Truss with One Cross Frame at Midspan 195

7.2.1 Regular Truss Model 196

7.2.2 Simplified Truss Model 203

7.3 Development of the Stiffness Requirement for the Truss with Single Cross Frame at Midspan 209

7.4 Estimating the Buckling Capacity of Torsionally Braced Truss 211

7.4.1 Truss Subjected to Uniform Load 211

7.4.2 Truss Subjected to Uniform Bending Moment 219

7.5 Summary 223

CHAPTER 8: Conclusion and Recommendation **224**

8.1 Overview 224

8.1.1 Truss Buckling Behavior 225

8.1.2 Recommendation of Stiffness Requirement for Trusses with Midspan Torsional Brace 226

8.1.3 Recommendation for Estimating the Buckling Capacity of Truss with Torsional Brace at Midspan 227

8.2 Recommendation for Future Work 227

APPENDIX A: Test Results and Model Verification **230**

A.1 Lateral Deflection of Lateral Stiffness Test 230

A.2 Lateral Deflection of Buckling Test 233

A.2.1 Truss without Intermediate Bracing 233

A.2.2 Truss with Top Chord Loading and Lateral Bracing 234

A.2.3 Truss with Top Chord Loading and Torsional Bracing 235
A.2.4 Truss with Bottom Chord Torsional Bracing and Loading 236
A.2.5 Pony Truss 239
A.2.6 Comparison of Regular and Pony Truss 242
A.2.7 Truss with Top Chord Torsional Bracing and Loading with Load Offset 243
A.3 Out-of-Plane Cross Section Rotation of Truss without Intermediate Bracing 245
A.4 Vertical Deflection of Truss with Lateral Bracing 247
A.5 Strain in Truss Chord at Midspan 248
A.5.1 Truss without Intermediate Bracing 248
A.5.2 Truss with Lateral Bracing 250
A.5.3 Truss with Torsional Bracing 252
A.6 Torsional Brace Axial Force 253
A.6.1 Regular Truss 253
A.6.2 Pony Truss 254
A.7 Comparison between Brace Strain of Regular and Pony Truss 256
A.8 Initial Imperfection 257
A.8.1 Initial Imperfection Component 257
A.8.2 Comparison of Initial Imperfections of Trusses without Intermediate Bracing 258
A.8.3 Comparison of Initial Imperfections of Trusses with Torsional Bracing 262
A.9 Lateral Stiffness Test Verification 267
A.9.1 48-ft Span Regular Truss without Lateral Restraint 267
A.9.2 48-ft Span Regular Truss with Lateral Restraints 270
A.9.3 72-ft Span Regular Truss without Lateral Restraint 272
A.9.4 72-ft Span Regular Truss with Lateral Restraints 274
A.9.5 72-ft Span Inverted Truss without Lateral Restraint 276
A.9.6 72-ft Span Inverted Truss with Lateral Restraints 278

A.10 Midspan Deflection Verification of Truss without Intermediate Bracing 281

A.11 Midspan Deflection Verification of Truss with Torsional Bracing 282

A.12 Verification of Strain in Torsional Braces 285

A.13 Calibration of Lateral Braces 291

APPENDIX B: Parametric Study Results **294**

B.1 Section Properties 294

B.2 Comparison of Truss with Regular and Rigid Web with Torsional Bracing and Cross Frame Subjected to Uniform Load 296

B.3 Comparison of the Buckling Capacity of Truss with the Same Unbraced Length with Stiffness per Unit Length 298

APPENDIX C: Stiffness Requirements for Torsional Bracing of Truss Systems **299**

C.1 Buckling Capacity (P_{cr}) and Ideal Stiffness (β_i) of Truss with Single Cross Frame at Midspan 299

C.1.1 Truss with Regular Web 299

C.1.2 Truss with Simplified Web 303

C.2 Verification of the Estimation of the Buckling Capacity of Truss with Cross Frame 306

C.2.1 Uniform Load Cases 306

C.2.2 Uniform Moment Cases 311

References **314**

Vita **317**

List of Tables

Table 1.1 Typical ranges of span to depth ratio of truss bridge 4

Table 2.1 Ideal Discrete Stiffness Requirements: N_iP/L 28

Table 3.1 Strain gages offset distances from brace points on the lateral brace 59

Table 3.2 Torsional brace locations 74

Table 4.1 Estimated buckling capacity by Southwell plot 99

Table 4.2 Load height effect ratio 99

Table 4.3 Summary of calibrated lateral brace stiffness 101

Table 6.1 Comparison of buckling capacity from ANSYS and MASTAN2 models 167

Table 6.2 Comparison of P_{cr} from ANSYS and MASTAN2 with gusset plate model 169

Table 6.3 Calculation of in-plane stiffness of 6-ft depth truss 173

Table 6.4 Calculation of equivalent centroidal axis of 96-ft span truss 175

Table 7.1 Eigenvalue and ideal brace stiffness of truss with uniform load 196

Table 7.2 Eigenvalue and ideal brace stiffness of truss with larger web near supports with uniform load 202

Table 7.3 Eigen value and ideal brace stiffness of truss with simplified web 204

Table 7.4 Slope of the straight line between unbraced and fully braced buckling capacity 220

Table B.1 Chord and web elements section properties 294

Table B.2 Torsional brace section properties 295

Table C.1 48-ft span truss with 3-ft depth 299

Table C.2 48-ft span truss with 6-ft depth 300

Table C.3 72-ft span truss with 3-ft depth 300

Table C.4 72-ft span truss with 6-ft depth 301

Table C.5 96-ft span truss with 3-ft depth 301

Table C.6 96-ft span truss with 6-ft depth 302

Table C.7 48-ft span truss with 3-ft depth 303

Table C.8 48-ft span truss with 6-ft depth 303

Table C.9 72-ft span truss with 3-ft depth 304

Table C.10 72-ft span truss with 6-ft depth 304
Table C.11 96-ft span truss with 3-ft depth 305
Table C.12 96-ft span truss with 6-ft depth 305

List of Figures

Figure 1.1 Basic trusses 3
Figure 1.2 Complex trusses 3
Figure 2.1 Load height effect on beam 13
Figure 2.2 Torsional brace stiffness of bending type bracing 15
Figure 2.3 Tension-only cross frame 16
Figure 2.4 Partially stiffened web 18
Figure 2.5 Type of truss connections 20
Figure 2.6 Shear developed at the end of the diaphragm 20
Figure 2.7 Winter's model with no imperfections 22
Figure 2.8 Winter's model with imperfections 22
Figure 2.9 Effect of initial imperfection on the brace force 24
Figure 2.10 Deflection and brace force of Winter column 25
Figure 2.11 Relative bracing system 27
Figure 2.12 Column lateral restraint location 29
Figure 2.13 Equivalent bracing force 36
Figure 2.14 Pony truss bridge 38
Figure 2.15 Southwell plot 40
Figure 2.16 Meck plot 40
Figure 2.17 System mode buckling 42
Figure 2.18 Rigid body rotation of twin girder with stiff cross frame 42
Figure 3.1 General test setup details 46
Figure 3.2 Truss geometry and details 47
Figure 3.3 Bolts connection with marking before fully tightening by turn-of-the-nut method 48
Figure 3.4 Bolt calibration with skidmore 49
Figure 3.5 ½"x13x1½" bolt calibration 49
Figure 3.6 Truss fabrication 50
Figure 3.7 Truss chord splice 50
Figure 3.8 Gravity load simulator geometry 52

Figure 3.9 GLS in the test setup 53
Figure 3.10 Adjustable GLS stop 54
Figure 3.11 Knife edge in the test setup 54
Figure 3.12 Mark of knife edge on steel plate 55
Figure 3.13 Linear potentiometer at support's bottom chord 56
Figure 3.14 Linear potentiometer attached to steel frame and glass plate at the tip 57
Figure 3.15 Tilt sensors across the truss height 57
Figure 3.16 Strain gage on lateral brace 59
Figure 3.17 Zero reference specimen for adjusting steel strain gage on aluminum bar 60
Figure 3.18 Strain gages on torsional brace 60
Figure 3.19 Support for the bottom chord loading case 61
Figure 3.20 Rigid frame attached to the support 62
Figure 3.21 Support frames to prevent the movement of top and bottom chord at support 63
Figure 3.22 Rounded threaded rod at support 63
Figure 3.23 Thrust bearing and steel plate at support 64
Figure 3.24 Initial imperfection measurement by using dial caliper 65
Figure 3.25 Lateral stiffness test of inverted truss 66
Figure 3.26 Test setup for load height effect test of 48-ft span truss 67
Figure 3.27 Bottom chord loading with 10 in. load offset from joint 68
Figure 3.28 Schematic drawing of the lateral brace attached to the truss and details 70
Figure 3.29 Teflon sheet attached to the lateral brace 71
Figure 3.30 Test setup of truss with lateral bracing 71
Figure 3.31 Checking of lateral brace vertical alignment 72
Figure 3.32 Torsional brace with connection plate 73
Figure 3.33 Installation of large torsional braces at bottom chord 73
Figure 3.34 Test setup of truss with 3 small torsional braces at bottom chord 74
Figure 3.35 Adding the stiffener to the torsional brace connection joint 75
Figure 3.36 Top chord support's threaded rod backed up for pony truss test 76

Figure 3.37 Half inch load offset by offsetting the knife edge to the East side 76
Figure 4.1 Initial imperfection of the 48-ft span East truss - Bottom chord loading 78
Figure 4.2 Initial imperfection of the 48-ft span West truss - Bottom chord loading 79
Figure 4.3 Initial imperfection of the 72-ft span East truss - Bottom chord loading 79
Figure 4.4 Initial imperfection of the 72-ft span West truss - Bottom chord loading 80
Figure 4.5 Lateral deflection at midspan of 72-ft regular truss - Top chord loading 83
Figure 4.6 Lateral deflection at midspan of 72-ft regular truss - Bottom chord loading 83
Figure 4.7 Force distribution in unloaded chord 84
Figure 4.8 Lateral deflection at midspan of 72-ft inverted truss - Top chord loading 85
Figure 4.9 Lateral deflection at midspan of 72-ft inverted truss - Bottom chord loading 86
Figure 4.10 Lateral deflection of 72-ft regular truss - Top chord loading and bottom chord restrained 87
Figure 4.11 Lateral deflection of 72-ft regular truss - Bottom chord loading and top chord restrained 87
Figure 4.12 Lateral deflection of 72-ft truss - Top chord loading 89
Figure 4.13 Lateral deflection of 72-ft truss - Bottom chord loading 90
Figure 4.14 Strain at midspan of the 72-ft truss - Top chord loading 91
Figure 4.15 Stress components at midspan of the 72-ft truss - Top chord loading 91
Figure 4.16 Stress from bending component at midspan of the 72-ft truss - Top chord loading 93
Figure 4.17 Comparison of bending stress component at midspan of the 72-ft truss - Top chord loading 93
Figure 4.18 Vertical deflection at bottom chord of the 72-ft truss - Top chord loading 94
Figure 4.19 Effect of string length on the accuracy of string potentiometer 95

Figure 4.20 Cross section rotation at midspan of 72-ft truss - Top chord loading- No intermediate bracing. 96
Figure 4.21 Southwell plot of 72-ft truss - Top chord loading 97
Figure 4.22 Southwell plot of 48-ft truss 98
Figure 4.23 Southwell plot of 72-ft truss 98
Figure 4.24 Calibration of aluminum lateral braces 100
Figure 4.25 Calibration of steel lateral braces 101
Figure 4.26 Lateral deflection of truss with single lateral brace - K = 0.2 kip/in 103
Figure 4.27 Lateral deflection of truss with single lateral brace - K = 0.8 kip/in 103
Figure 4.28 Lateral deflection of truss with 2 lateral braces - K = 0.2 kip/in 104
Figure 4.29 Lateral deflection of truss with 2 lateral braces - K = 0.8 kip/in 104
Figure 4.30 Effect of brace stiffness on buckling capacity of truss with single lateral brace 105
Figure 4.31 Effect of number of lateral brace on buckling capacity of truss 106
Figure 4.32 Relative maximum lateral deflection of truss with and without lateral bracing 106
Figure 4.33 Rotation at 24 feet of truss with single lateral brace - K = 0.8 kip/in 108
Figure 4.34 Rotation at 24 feet of truss with 2 lateral braces - K = 0.8 kip/in 109
Figure 4.35 Rotation at 36 feet of truss with 2 lateral braces - K = 0.8 kip/in 109
Figure 4.36 Truss cross section rotation at 24 feet of truss with 2 lateral braces - K = 0.8 kip/in 110
Figure 4.37 Truss cross section rotation for the cases with the same degree of rotation 110
Figure 4.38 Strain at midspan for truss with single lateral brace and K = 0.2 kip/in 111
Figure 4.39 Strain at midspan of truss with single lateral brace - K = 0.8 kip/in 112
Figure 4.40 Strain in the lateral brace for truss with single lateral brace - K = 0.8 kip/in 113
Figure 4.41 Brace force of truss with single lateral brace at midspan top chord 114
Figure 4.42 Brace force at 24-ft brace of truss with 2 lateral braces 114
Figure 4.43 Lateral deflection of truss with single small torsional brace at bottom chord (without connection stiffener) 116

Figure 4.44 Lateral deflection of truss with 3 large torsional braces at bottom chord (without connection stiffener) 116
Figure 4.45 Lateral deflection of truss with 3 small torsional braces at top chord (with connection stiffener) 117
Figure 4.46 Lateral deflection of truss with 3 large torsional brace at top chord (full sine buckle shape) 118
Figure 4.47 Strain in truss chord at midspan of truss with 3 small torsional braces at bottom chord (without connection stiffener) 119
Figure 4.48 Strain in truss chord at midspan of truss with 3 small torsional braces at top chord (with connection stiffener) 119
Figure 4.49 Strain at 20-ft brace of truss with 3 small torsional braces at top chord 121
Figure 4.50 Strain at midspan brace of truss with 3 small torsional braces at top chord 122
Figure 4.51 Strain at 24-ft brace of truss with 3 large torsional braces at bottom chord 122
Figure 4.52 Axial force in brace of truss with large torsional brace at top chord 124
Figure 4.53 Axial force in brace of truss with large torsional brace at bottom chord 124
Figure 4.54 Effect of stiffener on buckling capacity of truss with 3 large torsional brace at bottom chord 125
Figure 4.55 Cross section rotation of truss with 3 large torsional brace at bottom chord (without connection stiffener) 126
Figure 4.56 Cross section rotation of truss with 3 large torsional brace at bottom chord (with connection stiffener) 127
Figure 4.57 Cross section distortion at brace connection due to stiff torsional brace 127
Figure 4.58 Lateral deflection of pony truss with 3 small torsional braces (without connection stiffener) 128
Figure 4.59 Comparison of midspan lateral deflection of truss with 3 small torsional brace (without connection stiffener) 129
Figure 4.60 Comparison of brace strain at 24-ft brace of truss with 3 small torsional braces 130
Figure 4.61 Comparison of brace force of truss with large torsional brace 131

Figure 4.62 Midspan lateral deflection of 72-ft truss without bracing - Top chord loading 132
Figure 4.63 Midspan lateral deflection of 72-ft truss with 2 large torsional braces at top chord 132
Figure 4.64 Torsional strain at 3S/4 in North brace of truss with 2 large torsional braces at top chord 134
Figure 4.65 Warping strain at 3S/4 in North brace of truss with 2 large torsional braces at top chord 134
Figure 5.1 Dimension of gusset plate and ANSYS connection 138
Figure 5.2 Truss model showing enhanced line element shape 138
Figure 5.3 Comparison of initial imperfection at bottom chord of 72-ft span East truss with 3 small torsional brace at top chord with top chord loading 140
Figure 5.4 Comparison of initial imperfection of 72-ft span East truss with 3 small torsional brace at top chord with top chord loading 141
Figure 5.5 Midspan lateral deflection of 72-ft regular truss with bottom chord loading 143
Figure 5.6 Midspan lateral deflection of 72-ft regular truss with top chord loading 143
Figure 5.7 Midspan lateral deflection of 72-ft inverted truss with bottom chord loading 144
Figure 5.8 Midspan lateral deflection of 72-ft inverted truss with top chord loading 144
Figure 5.9 Midspan lateral deflection of 72-ft regular truss with top chord loading and lateral stop at bottom chord 145
Figure 5.10 Midspan lateral deflection of 72-ft regular truss with bottom chord loading and lateral stop at top chord 146
Figure 5.11 ANSYS model replicate the test setup 147
Figure 5.12 Midspan lateral deflection of 48-ft span truss with top chord loading 148
Figure 5.13 Midspan vertical deflection of 48-ft span truss with top chord loading 148
Figure 5.14 Midspan lateral deflection of 72-ft span truss with top chord loading 149
Figure 5.15 Midspan vertical deflection of 72-ft span truss with top chord loading 150
Figure 5.16 Vertical component of lateral deflection 150

Figure 5.17 Midspan lateral deflection of truss with single small torsional brace at midspan bottom chord without brace connection stiffener 152
Figure 5.18 Midspan vertical deflection of truss with single small torsional brace at midspan bottom chord without brace connection stiffener 153
Figure 5.19 Midspan lateral deflection of truss with 3 large torsional braces at bottom chord with brace connection stiffener 154
Figure 5.20 Midspan lateral deflection of truss with 2 large torsional braces at top chord with brace connection stiffener 154
Figure 5.21 Comparison of idealize and actual connections 155
Figure 5.22 Cross section rotation at 48 feet of truss with 3 large torsional braces at bottom chord 156
Figure 5.23 Cross section rotation at 52 feet of truss with 2 large torsional braces at top chord 156
Figure 5.24 Strain in North brace at quarter point of truss with 3 small torsional braces at top chord 158
Figure 5.25 Strain in midspan brace at quarter point of truss with 3 small torsional braces at top chord 158
Figure 5.26 Strain in North brace at three quarter point of truss with 2 large torsional braces at top chord 159
Figure 5.27 Strain in South brace at quarter point of truss with 3 large torsional braces at bottom chord 159
Figure 6.1 Chord and web sections used in the analysis 164
Figure 6.2 72-ft span truss with 6-ft depth and uniform load at top chord 167
Figure 6.3 Buckling mode shape for Vierendeel truss with stiff chord and stiff web with bottom chord loading 171
Figure 6.4 Large displacement analysis of truss with stiff chord and stiff vertical web with and without very flexible diagonal web with bottom chord loading 171
Figure 6.5 Large displacement analysis of truss with stiff chord and stiff vertical web with and without very flexible diagonal web with top chord loading 172
Figure 6.6 Calculation of truss in-plane moment of inertia 172
Figure 6.7 Buckling capacity of 96-ft moderate chord and flexible web truss with rigid web at midspan 176

Figure 6.8 Buckling capacity of 96-ft stiff chord and flexible web truss with rigid web at midspan 177
Figure 6.9 Truss cross section at midspan with tension only cross frame 178
Figure 6.10 Buckling capacity of 96-ft span with 6-ft depth moderate chord and flexible web truss with cross frame 179
Figure 6.11 Buckling capacity of 96-ft span stiff chord and flexible web truss with one cross frame at midspan (above – uniform load, below – uniform moment) 180
Figure 6.12 Increase in buckling capacity due to the addition of the cross frame of moderate chord and flexible web 96-ft span truss 181
Figure 6.13 Comparison of buckling capacity of 96-ft span moderate chord and very flexible web truss with uniform moment 182
Figure 6.14 Comparison of buckling capacity of 96-ft span stiff chord and web truss with uniform moment 183
Figure 6.15 Buckling capacity of moderate chord and flexible web truss with 24-ft unbraced length with uniform moment 184
Figure 6.16 Buckle between the brace point of truss with three cross frames 185
Figure 6.17 Buckling capacity of flexible chord and flexible web truss with 24-ft unbraced length with uniform moment 186
Figure 6.18 Buckling capacity of moderate chord and flexible web truss with 24-ft unbraced length with brace stiffness per linear length with uniform moment 186
Figure 6.19 Buckling capacity of moderate chord and flexible web truss with 24-ft unbraced length with uniform load 187
Figure 6.20 Buckled mode shape of truss with high stiffness cross frame 188
Figure 6.21 Buckling capacity of 96-ft span 3-ft depth truss with regular and simplified web 191
Figure 6.22 Buckling capacity of 96-ft span 6-ft depth truss with regular and simplified web 191
Figure 6.23 Buckling capacity of 96-ft span 6-ft depth truss with regular and simplified web with top chord loading 192
Figure 6.24 Buckling capacity of 96-ft span 6-ft depth truss with regular and simplified web with bottom chord loading 192
Figure 6.25 Comparison of truss in-plane moment of inertia 193

Figure 7.1 Stiffness requirement by using column formula for truss with regular web and uniform bending moment 198
Figure 7.2 Stiffness requirement by using beam formula for truss with regular web and top chord loading 199
Figure 7.3 Total stiffness requirement by beam equation of 6-ft depth truss with regular web and uniform load at top chord 200
Figure 7.4 Total stiffness requirement by beam equation of 3-ft depth truss with regular web and uniform load at bottom chord 201
Figure 7.5 Total stiffness requirement by beam equation of 3-ft depth truss with regular web and uniform moment 201
Figure 7.6 Comparison of eigenvalue for truss with larger diagonal near support and regular truss 203
Figure 7.7 Stiffness requirement by using beam formula for 6-ft deep truss with pinned web and top chord loading 205
Figure 7.8 Stiffness requirement by using beam formula for 3-ft deep truss with pinned web and top chord loading 205
Figure 7.9 Stiffness requirement by using beam formula for 6-ft deep truss with pinned web and uniform moment 206
Figure 7.10 Stiffness requirement for combine plot of truss subjected to uniform load 207
Figure 7.11 Comparison of stiffness requirement of simplified web and regular web truss subjected to uniform load (exclude outlier) 208
Figure 7.12 Comparison of stiffness requirement of simplified web and regular web truss subjected to uniform moment (exclude outlier) 208
Figure 7.13 Stiffness requirement of proposed equation compared to the analysis – top chord loading 212
Figure 7.14 Stiffness requirement of proposed equation compared to the analysis at low stiffness value – top chord loading 212
Figure 7.15 Stiffness requirement of proposed equation compared to the analysis – bottom chord loading 213
Figure 7.16 Stiffness requirement of proposed equation compared to the analysis at low stiffness value – bottom chord loading 213
Figure 7.17 Stiffness requirement of proposed equation compared to the analysis – uniform moment 214
Figure 7.18 Stiffness requirement of proposed equation compared to the analysis at low stiffness values – uniform moment 214

Figure 7.19 Additional buckling capacity of 96-ft span truss with 72-in depth..... 216
Figure 7.20 Span length adjustment 216
Figure 7.21 Comparison of 72-ft span truss with 6-ft depth – W4x13 chord with bottom chord loading 218
Figure 7.22 Comparison of 72-ft span truss with 6-ft depth – W8x24 chord with bottom chord loading 218
Figure 7.23 Comparison of 72-ft span truss with 6-ft depth – W12x50 chord with bottom chord loading 219
Figure 7.24 Buckling capacity of 48-ft span truss with 6-ft depth with uniform moment. 220
Figure 7.25 Slope plot of truss with uniform moment 221
Figure 7.26 Comparison of buckling capacity of 72-ft span truss with 72-in depth – W4x13 chord 221
Figure 7.27 Comparison of buckling capacity of 72-ft span truss with 72-in depth – W8x24 chord 222
Figure 7.28 Comparison of buckling capacity of 72-ft span truss with 72-in depth – W12x50 chord 222
Figure 8.1 Relative lateral bracing in twin truss system 229
Figure A.1 48-ft regular truss - Top chord loading 230
Figure A.2 48-ft regular truss - Bottom chord loading 231
Figure A.3 48-ft regular truss - Top chord loading and bottom chord restrained 231
Figure A.4 72-ft inverted truss - Bottom chord loading and top chord restrained 232
Figure A.5 72-ft inverted truss - Top chord loading and bottom chord restrained 232
Figure A.6 48-ft span truss - Bottom chord loading 233
Figure A.7 48-ft span truss - Top chord loading 233
Figure A.8 Truss with single lateral brace - K = 0.50 k/in 234
Figure A.9 Truss with 2 lateral braces - K = 0.50 k/in 234
Figure A.10 Truss with 2 small torsional braces (with connection stiffener) 235
Figure A.11 Truss with 2 large torsional braces (with connection stiffener) 235
Figure A.12 Truss with 2 small torsional braces (without connection stiffener) 236
Figure A.13 Truss with 3 small torsional braces (without connection stiffener) 236
Figure A.14 Truss with single large torsional brace (without connection stiffener) 237

Figure A.15 Truss with 2 large torsional braces (with connection stiffener) 237
Figure A.16 Truss with 3 large torsional braces (with connection stiffener) 238
Figure A.17 Truss with single small torsional brace (without connection stiffener) 239
Figure A.18 Truss with 2 small torsional braces (without connection stiffener) 239
Figure A.19 Truss with single large torsional brace (without connection stiffener) 240
Figure A.20 Truss with 2 large torsional braces (with connection stiffener) 240
Figure A.21 Truss with 3 large torsional braces (with connection stiffener) 241
Figure A.22 Midspan lateral deflection of regular and pony truss with 3 large torsional braces at bottom chord (with connection stiffener) 242
Figure A.23 Truss without intermediate bracing with 0.5" load offset (with connection stiffener) 243
Figure A.24 Truss without intermediate bracing with 1.0" load offset (with connection stiffener) 243
Figure A.25 Truss with 2 large torsional braces and 0.5" load offset (with connection stiffener) 244
Figure A.26 Truss with 2 large torsional braces and 1.0" load offset at top chord (with connection stiffener) 244
Figure A.27 Midspan rotation of 48-ft truss - Bottom chord loading 245
Figure A.28 Midspan rotation of 48-ft truss - Top chord loading 245
Figure A.29 Midspan rotation of 72-ft truss - Bottom chord loading 246
Figure A.30 Vertical deflection of 72-ft truss with single lateral brace – K = 0.8 kip/in 247
Figure A.31 Vertical deflection of 72-ft truss with 2 lateral brace – K = 0.8 kip/in 247
Figure A.32 Strain of 48-ft truss - Bottom chord loading 248
Figure A.33 Strain of 48-ft truss - Top chord loading 248
Figure A.34 Strain of 72-ft truss - Bottom chord loading 249
Figure A.35 Strain of 72-ft truss with single lateral brace - K = 0.5 k/in 250
Figure A.36 Strain of 72-ft truss with 2 lateral braces - K = 0.2 k/in 250
Figure A.37 Strain of 72-ft truss with 2 lateral braces - K = 0.5 k/in 251
Figure A.38 Strain of 72-ft truss with 2 lateral braces - K = 0.8 k/in 251
Figure A.39 Strain of 72-ft truss with 3 large torsional braces at bottom chord (with connection stiffener) 252

Figure A.40 Strain of 72-ft truss with 3 large torsional braces at top chord (with connection stiffener) 252
Figure A.41 Truss with small torsional braces at top chord 253
Figure A.42 Truss with small torsional braces at bottom chord 253
Figure A.43 Pony truss with small torsional braces 254
Figure A.44 Pony truss with large torsional braces 254
Figure A.45 Comparison of brace forces of truss with small torsional braces 255
Figure A.46 Strain at 36 feet of truss with 3 small torsional braces 256
Figure A.47 Strain at 48 feet of truss with 3 small torsional braces 256
Figure A.48 Comparison of imperfection at top chord of truss with 3 small torsional braces at top chord - Top chord loading 257
Figure A.49 48-ft truss - Bottom chord loading 258
Figure A.50 48-ft truss - Top chord loading 259
Figure A.51 72-ft truss - Top chord loading 260
Figure A.52 72-ft truss - Bottom chord loading 261
Figure A.53 72-ft truss with single small torsional brace at bottom chord - Bottom chord loading 262
Figure A.54 72-ft truss with 2 large torsional braces at bottom chord - Bottom chord loading (with connection stiffener) 263
Figure A.55 72-ft truss with 3 large torsional braces at bottom chord - Bottom chord loading (with connection stiffener) 264
Figure A.56 72-ft truss with 3 small torsional braces at top chord - Top chord loading (with connection stiffener) 265
Figure A.57 72-ft truss with 2 large torsional braces at top chord - Top chord loading (with connection stiffener) 266
Figure A.58 Lateral deflection at 16 feet - Top chord loading 267
Figure A.59 Lateral deflection at midspan - Top chord loading 267
Figure A.60 Lateral deflection at 32 feet - Top chord loading 268
Figure A.61 Lateral deflection at 16 feet - Bottom chord loading 268
Figure A.62 Lateral deflection at midspan - Bottom chord loading 269
Figure A.63 Lateral deflection at 32 feet - Bottom chord loading 269
Figure A.64 Lateral deflection at 16 feet - Top chord loading and bottom chord restrained 270

Figure A.65 Lateral deflection at midspan - Top chord loading and bottom chord restrained 270
Figure A.66 Lateral deflection at 32 feet - Top chord loading and bottom chord restrained 271
Figure A.67 Lateral deflection at 24 feet - Top chord loading 272
Figure A.68 Lateral deflection at 48 feet - Top chord loading 272
Figure A.69 Lateral deflection at 24 feet - Bottom chord loading 273
Figure A.70 Lateral deflection at 48 feet - Bottom chord loading 273
Figure A.71 Lateral deflection at 24 feet - Top chord loading and bottom chord restrained 274
Figure A.72 Lateral deflection at 48 feet - Top chord loading and bottom chord restrained 274
Figure A.73 Lateral deflection at 24 feet - Bottom chord loading and top chord restrained 275
Figure A.74 Lateral deflection at 48 feet - Bottom chord loading and top chord restrained 275
Figure A.75 Lateral deflection at 24 feet - Top chord loading 276
Figure A.76 Lateral deflection at 48 feet - Top chord loading 276
Figure A.77 Lateral deflection at 24 feet - Bottom chord loading 277
Figure A.78 Lateral deflection at 48 feet - Bottom chord loading 277
Figure A.79 Lateral deflection at 24 feet - Top chord loading and bottom chord restrained 278
Figure A.80 Lateral deflection at midspan - Top chord loading and bottom chord restrained 278
Figure A.81 Lateral deflection at 48 feet - Top chord loading and bottom chord restrained 279
Figure A.82 Lateral deflection at 24 feet - Bottom chord loading and top chord restrained 279
Figure A.83 Lateral deflection at midspan - Bottom chord loading and top chord restrained 280
Figure A.84 Lateral deflection at 48 feet - Bottom chord loading and top chord restrained 280
Figure A.85 Lateral deflection of 48 feet truss - Bottom chord loading 281
Figure A.86 Vertical deflection of 48 feet truss - Bottom chord loading 281

Figure A.87 Lateral deflection of truss with 2 large torsional braces at bottom chord (with connection stiffener) 282
Figure A.88 Vertical deflection of truss with 2 large torsional braces at bottom chord (with connection stiffener) 282
Figure A.89 Lateral deflection of truss with 3 small torsional braces at top chord (with connection stiffener) 283
Figure A.90 Vertical deflection of truss with 3 small torsional braces at top chord (with connection stiffener) 283
Figure A.91 Vertical deflection of truss with 2 large torsional braces at top chord (with connection stiffener) 284
Figure A.92 Vertical deflection of truss with 3 large torsional braces at bottom chord (with connection stiffener) 284
Figure A.93 Strain in South brace at quarter point of truss with 3 small torsional braces at top chord 285
Figure A.94 Strain in North brace at three quarter point of truss with 3 small torsional braces at top chord 285
Figure A.95 Strain in midspan brace at three quarter point of truss with 3 small torsional braces at top chord 286
Figure A.96 Strain in South brace at three quarter point of truss with 3 small torsional braces at top chord 286
Figure A.97 Strain in North brace at quarter point of truss with 3 large torsional braces at bottom chord 287
Figure A.98 Strain in midspan brace at quarter point of truss with 3 large torsional braces at bottom chord 287
Figure A.99 Strain in North brace at three quarter point of truss with 3 large torsional braces at bottom chord 288
Figure A.100 Strain in midspan brace at three quarter point of truss with 3 large torsional braces at bottom chord 288
Figure A.101 Strain in South brace at three quarter point of truss with 3 large torsional braces at bottom chord 289
Figure A.102 Strain in North brace at quarter point of truss with 2 large torsional braces at top chord 289
Figure A.103 Strain in South brace at quarter point of truss with 2 large torsional braces at top chord 290
Figure A.104 Strain in South brace at three quarter point of truss with 2 large torsional braces at top chord 290

Figure A.105 Aluminum brace - K_{design} = 0.2 k/in 291
Figure A.106 Aluminum brace - K_{design} = 0.5 k/in 291
Figure A.107 Aluminum brace - K_{design} = 0.8 k/in 292
Figure A.108 Steel brace - K_{design} =0.2 k/in 292
Figure A.109 Steel brace - K_{design} =0.5 k/in 293
Figure A.110 Steel brace - K_{design} =0.8 k/in 293
Figure B.1 Comparison of buckling capacity of 96-ft span moderate chord and very flexible web truss with uniform load and bottom chord bracing 296
Figure B.2 Comparison of buckling capacity of 96-ft span moderate chord and very flexible web truss with uniform load and top chord bracing 296
Figure B.3 Comparison of buckling capacity of 96-ft span flexible chord and flexible web truss with uniform load and bottom chord bracing 297
Figure B.4 Comparison of buckling capacity of 96-ft span flexible chord and flexible web truss with uniform load and top chord bracing 297
Figure B.5 Comparison of moderate chord and flexible web truss with 24-ft unbraced length 298
Figure C.1 48-ft span truss with 3-ft depth 306
Figure C.2 72-ft span truss with 3-ft depth 307
Figure C.3 48-ft span truss with 6-ft depth 308
Figure C.4 72-ft span truss with 6-ft depth 309
Figure C.5 96-ft span truss with 6-ft depth 310
Figure C.6 48-ft span truss 311
Figure C.7 72-ft span truss 312
Figure C.8 96-ft span truss 313

CHAPTER 1
Introduction

1.1 INTRODUCTION

Trusses are used in a variety of applications in structural engineering and generally consist of a collection of members that are combined to form a structural component to resist loads. Most trusses form a flexural system in which the joints are idealized as pinned. Therefore, if the loads are applied at the joints (nodes), the members of the truss will only be subjected to tension or compression. Trusses are commonly used in long-span applications where efficient systems compared to girder elements can be fabricated to satisfy the structural demand with either constant or variable depth along the length. Trusses have been used in several applications such as bridges, buildings, stadiums, or tower structures. These structural applications may make use of either planar or space trusses. Compared to space trusses, planar trusses are easier to design, fabricate, and erect due to simplicity. However trusses generally require more effort than girders, but are used where the depth or other geometrical demands result in too large of a girder. The design of planar trusses can be done by hand calculations for simple structural systems. For 3-D space trusses, the design can be troublesome and usually necessitates computer analyses to ease the complex equations. This dissertation is primarily focused on 2-D planar trusses.

Trusses began gaining popularity in the nineteenth century where several types of trusses were developed. Figure 1.1 shows some common trusses and the names that are generally attributed to the individual that first developed the system. These commonly used systems include the Howe, Pratt, Warren, and Vierendeel trusses. Most of the truss elements are connected to form an array of triangular shapes with the exception of the Vierendeel truss where the chords are connected together by only one web at each joint with a moment connection, instead of a pin connection. The behavior of Vierendeel

trusses differ significantly from the others due to the moment connections as well as the lack of diagonals. The trusses shown in Figure 1.1 are basic planar trusses that are statically determinate systems. More complex trusses are shown in Figure 1.2. Although these systems have better redundancy compared to those systems in Figure 1.1, the complexity of the analysis and design of the systems are increased since they are statically indeterminate. Examples of 3-D space truss include tower structures or space domes.

Different types of trusses have their own limit and capacity. Typical span lengths for railroad truss bridges are usually longer than 150 feet while the trusses for highway bridges are typically longer than 300 feet, both of which are longer than the capability of rolled beam sections and would require built-up girders (Tall, 1974). Railway trusses have shorter spans due to heavier loads and deflection limits. Typical span to depth (L/d) ratios of truss bridges was summarized by Collings (2005) and is provided in Table 1.1. The angle of the diagonals in the range of 45-65 degrees to the chord is usually considered the most efficient.

A major advantage of trusses compared to other structures is the potential efficiency, especially for the long-span structures where the truss has very high in-plane stiffness values due to the large distance between the chords. Relatively efficient systems are possible for trusses since the verticals and diagonals in the web can be properly sized based upon demand compared to continuous webs in girders that can be inefficient in very deep girder systems. The applied load in trusses is transformed into the axial force in the members. Although some bending is induced in the truss elements, the magnitude is usually negligible compared to the axial force component. For the case of uniform distributed loads, the shear is low and bending moment is high at mid span. Within practical limits, the truss elements can be varied along the span length to match the design forces. Normally, the truss chord is larger near mid span than the chord near supports while the web at mid span is smaller than those near the supports. In contrast, beams have a continuous web that may often lead to inefficient systems for deeper girders that will be necessary for long span applications. Transverse web stiffeners will

often be necessary to improve the web buckling capacity; however even with the stiffening the amount of steel for the web plates is considerable in deep girders. While the bending moment is high at mid span, the size of a girder flange can be adjusted to accommodate the required area similar to varying the chord sizes of the truss.

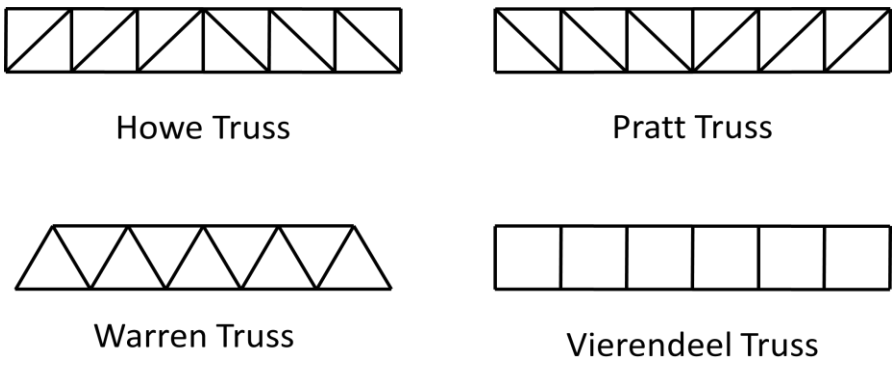

Figure 1.1 Basic trusses

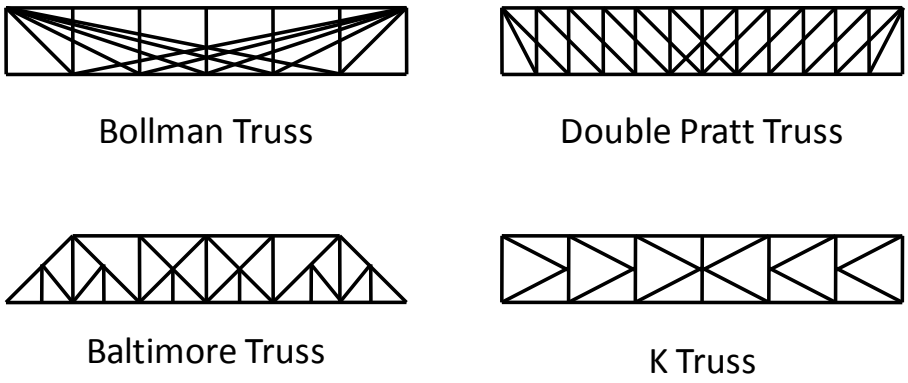

Figure 1.2 Complex trusses

In addition to the efficiency of the member elements, the discrete web elements in trusses also help minimize the self weight, which can be a major load for long-span structures. Combined, the factors outlined above lead to efficiency when using trusses for long-span structures both in terms of load-carrying capacity and minimizing the structures dead load.

Although trusses offer several advantages, they also have some disadvantages. Truss fabrication requires more precision work to prevent problems during erection. The increased number of connections and necessary precision often result in higher fabrication costs compared to girders. With the help of the advancement of high precision fabrication technologies, the cost of fabrication can be less expensive than compared to manually operated machines. In addition, because of the long lengths truss structures will usually require field assembly during erection and often require significant falsework. The painting requirements or other maintenance issues during the service life of the structure can also be significant with the numbers of connections and surface area of the individual members. Another disadvantage of trusses is the relatively low out-of-plane stiffness compared to the in-plane stiffness which can lead to significant stability issues with the truss. From a stability perspective, there are also several different modes that may control the design of the truss including both local and global stability modes.

Table 1.1 Typical ranges of span to depth ratio of truss bridge (Collings, 2005)

Truss form	Typical span to depth ratio
Simply supported highway bridge	10-18
Continuous highway truss bridge	12-20
Simply supported railway truss bridge	7-15
Continuous railway truss bridge	10-18

1.2 PROBLEM DESCRIPTION

Stability bracing is crucial for improving the buckling capacity of structural members and systems. In many instances, stability bracing may only be required at specific times in the life of the structure. For example, in many systems the critical stage for stability occurs during construction. In as such, the bracing may only be necessary during construction stages when not all of the structural elements are active, such as the case of concrete slabs in composite structures. Bracing systems can often be divided into specific types that are a function on how the bracing behaves. The controlling global

mode of stability of beam systems generally includes both lateral and torsional deformation. Effective bracing can therefore be provided by either stopping lateral movement of the compression flange or by preventing twist of the section. Depending on the deformation that is being prevented, bracing systems may often be categorized as either lateral bracing or torsional bracing.

Several systems have structural elements that act as the bracing for the main members. The bracing elements are usually secondary members. The forces induced in these secondary members from bracing are usually additive to the forces induced from the primary loading on the structure. If the stability braces are not considered during design, the member may experience problems that can lead to stability problems in the primary member. Therefore, it is critical to evaluate the global buckling capacity of structural members and systems for ensuring a safe structure. Failure to consider certain stability modes can lead to catastrophic problems during construction or in-service.

In truss design, the joints are often idealized as pins that result in only axial forces in the members. The design of the truss should consider global buckling of the overall truss as well as buckling of an individual member. The limit of the capacity of the individual element can be calculated by using the column formula specified by AISC (2005a) which depends on the effective length of the truss element. The effective length of the truss compression chord may often be taken as is 0.85L for compression chords and $0.7L_d$ for the diagonals where L is the distance between the joints in the chords and L_d is the length of the diagonal (Collings, 2005). These lengths reflect some of the joint restraint that is offered for buckling of the individual element. The member connections in trusses are usually modeled as pinned to simplify the analysis. In reality, the top and bottom chords are usually continuous and the gusset plates often extend a significant distance along the lengths of the verticals and diagonals. Currently, the effects of connection flexibility on the truss stability are not well understood. There is also not much information about the truss buckling behavior and bracing requirements.

Planar trusses are commonly used in bridges, and roofs of buildings or stadiums. The plane truss is normally analyzed and designed in two dimensions (2-D). The use of a

2-D analysis is based on the assumption that the truss has full lateral bracing. The 2-D model is conservative if the truss is fully braced; however the actual truss is a complex structure that involves several internal factors such as out-of-plane stiffness of the web elements, the axial compressive loads in the chords, as well as the alignment of the vertical and diagonal web elements. There are also external factors that affect the buckling behavior of the truss systems such as the local and global initial imperfections, load locations, type of braces, and location of braces on the cross section. These behaviors have not yet been well studied. Some past work has been dedicated towards the behavior of pony trusses and design equations for the buckling capacity of the top chord have been suggested (SSRC, 2010). Pony trusses often consist of deck stiffened trusses where there is no restraint above the bottom chord along the entire truss length. For stability, torsional restraints must be provided usually by the floor beams that connect to the truss at the joint locations along the bottom chord. While there have been several studies on the bracing behavior of pure column systems or pure beam systems, little work has been conducted on the bracing behavior of trusses. The bracing requirements of trusses are generally not well understood due to the complexity of the potential local and global buckling modes of the truss.

The previous studies on column and frame bracing have led to design provisions for these members in the AISC Specification (AISC, 2005a). AISC (2005a) allows the design of bracing systems for trusses when the top chord extends to the supports by using beam provisions. Arguments can be made for the direct application of either the beam bracing provisions or the column bracing provisions. The use of the column bracing provisions is reasonable since the trusses are usually modeled as a collection of axial loaded members, while the use of the beam bracing provisions would be logical since the truss is essentially a collection of members that make up a flexural system. Although engineers often rely on solutions that have been developed for columns and beams, the factors that affect the bracing requirements for trusses can be quite different. Since trusses are generally flexural systems which are composed of a collection of axially loaded members, there are a variety of failure modes that complicate the bracing

requirements. Establishing a clear understanding of the bracing requirements to control the variety of instabilities that can occur in truss systems is vital to a proper design.

1.3 RESEARCH PURPOSE

This research intends to improve the understanding of truss behavior and the stability of truss systems subjected to various bracing and load conditions. The study primarily focuses on the Howe truss. Pony, Vierendeel and Pratt trusses are also addressed. The behaviors of trusses with and without intermediate bracing are considered. Although the behaviors of both lateral and torsional bracing systems were considered, the primary bracing that was studied is torsional braces. Comparisons in the brace stiffness requirements of columns and the beams as applied to trusses were conducted.

1.4 RESEARCH METHOD

The study includes both experimental testing as well as parametrical finite element analyses (FEA). To obtain accurate results from the laboratory buckling tests, gravity load simulators were fabricated and used in the tests to minimize restraint from the load points. The laboratory tests demonstrated the basic truss behavior. The data that was gathered in the experimental tests represents the most detailed tests conducted on lateral and torsional bracing systems for trusses to date. Moreover, the laboratory test results were used to validate three dimensional FEA models which were developed using the finite element program ANSYS Academic Research, Release 11.0 (ANSYS, 2010). Extensive parametric analyses were performed to study the behavior of twin trusses with and without intermediate bracing. In the parametric studies, torsional braces consisting of a beam element at the chord as well as full-depth cross frames were considered. The study led to the development of the stiffness requirement for the truss system with a brace at midspan. Although a comprehensive design methodology was not fully developed, the results of this study provide a valuable experimental and computational basis for the development of design provisions for truss systems.

1.5 REPORT ORGANIZATION

This dissertation has been divided into eight chapters. Background information on beam, column and truss bracing are presented in Chapter 2. An overview of the experimental test setup is outlined in Chapter 3 followed by a presentation of the test results in Chapter 4. Chapter 5 provides a summary of the development of the FEA model along with model verification. Results from the parametric studies are presented in Chapter 6. The development of the stiffness requirement for truss systems with midspan torsional bracing is described in Chapter 7. Finally, a summary of the investigation along with recommendations is provided in the final chapter of the dissertation.

CHAPTER 2
Background

2.1 INTRODUCTION

There have been several studies directed towards the stability bracing requirements of structural elements and systems. Most of the past work has targeted column and beam systems. These studies have demonstrated the impact of a wide variety of factors on the bracing behavior. This chapter provides an overview of some of the past studies on bracing systems and discusses the factors important to effective bracing. Due to limited studies on the buckling and bracing behavior with trusses, factors that affect the buckling capacity of columns and beams will be discussed first. These factors play an important role in understanding the approaches to develop bracing requirements for truss systems later in the dissertation.

2.2 BUCKLING BEHAVIOR OF BEAMS

The shape of beam cross sections can play an important factor in the resulting buckling behavior. Most beams in structural applications have either one or two axes of symmetry. Rolled wide flange beams fit into the classification of doubly-symmetric sections. The expression for evaluating the buckling capacity of doubly-symmetric beams subjected to uniform moment loading was derived by Timoshenko (Timoshenko and Gere, 1961) and is given in the following expression:

$$M_{cr} = \frac{\pi}{L_b}\sqrt{EI_yGJ + \left(\frac{\pi E}{L_b}\right)^2 I_y C_w} \tag{2.1}$$

Where L_b = Unbraced length

E = Young's modulus

I_y = Moment of inertia in the minor axis

J = St. Venant's torsional constant

G = Shear modulus

C_w = Warping constant

In some applications, improved economy is made through using different size flanges to form a beam with a single plane of symmetry about the axis through the web. Such is the case in steel girders designed to act compositely with the concrete slab. The closed-form solution for the buckling capacity of the singly symmetric beam subjected to uniform bending moment was derived by Galambos (1968) as follows:

$$M_{cr} = \frac{\pi^2 E I_y}{L^2}\left\{\frac{\beta_x}{2} + \sqrt{\left(\frac{\beta_x}{2}\right)^2 + \left[\frac{C_w}{I_y} + \frac{GJ}{EI_y}\frac{L^2}{\pi^2}\right]}\right\} \quad (2.2)$$

Where β_x is coefficient of monosymmetry. β_x is equal to zero for doubly symmetric section. The general expression of β_x is shown in Equation (2.3) and has been experimentally verified by Anderson and Trahair (1972).

$$\beta_x = \frac{1}{I_x}\int_A y(x^2 + y^2)dA - 2y_o \quad (2.3)$$

Where I_x = Moment of inertia in the major axis

y_o = Distance from the shear center to the cross section centroid

x = Centroidal x axis coordinate

y = Centroidal y axis coordinate

A = Cross section area

2.2.1 Load Types and Force Distribution

The last section presented the elastic buckling solutions that were derived for beams subjected to uniform moment loading. In most practical situations, beams are not subjected to uniform moment but are instead subjected to moment gradient along the length of the member. The distribution of the moment along the member length can have a significant impact on the buckling strength. Since the maximum moment with moment gradient only occurs over a small region of the beam, the buckling capacity is usually

higher than the uniform moment strength. The benefits of variable moment are usually approximated using a moment gradient factor, C_b, applied to the uniform moment solutions. The AISC Specification (AISC, 2005a) employs the following expression for C_b:

$$C_b = \frac{12.5M_{max}}{2.5M_{max} + 3M_A + 4M_B + 3M_C} \quad (2.4)$$

Where C_b = Lateral torsional buckling modification factor for non-uniform moment diagram

M_{max} = Absolute value of maximum moment in the unbraced segment

M_A = Absolute value of moment at quarter point of the unbraced segment

M_B = Absolute value of moment at center line of the unbraced segment

M_C = Absolute value of moment at three-quarter point of the unbraced segment

The modification of the non-uniform moment in AASHTO (2007) is different from the AISC specification (AISC, 2005a) as shown in Equation (2.5).

$$C_b = 1.75 - 1.05\,\omega + 0.3\omega^2 \leq 2.3 \quad (2.5)$$

Where ω = Stress ratio (more detail can be found in AASHTO (2007))

C_b is permitted to be conservatively used as 1.0 in both the AISC (2005a) and the AASHTO (2007) standards (with exception of some unusual circumstances in AASHTO).

In trusses, the load pattern is similar to beams; however, the truss geometry is different due to the discrete web and joint connections and the introduction of diagonal web elements. In addition, the force distribution in trusses is still similar to beam but is limited by the truss geometry. For loading conditions similar to uniform bending moment in trusses the bending moment is transformed into axial force on the top and bottom chords and the force is constant throughout the span length of the truss where the web has theoretically zero force. This makes the individual chord of the truss behave

similar to columns subjected to axial force. For the point loads applied at the joints, the shear is transformed into axial force in the web where the axial force is generally the maximum in the diagonal web elements next to the support and minimum at midspan. The bending moment, which causes axial force in the chords on the other hand, is generally maximum at midspan and minimum near the supports. In contrast to beams, the web and the chord of the truss can be specified to the required size to maximize the efficiency of the cross section. This therefore leads to the non-uniform cross section throughout the span length where larger chords and smaller web members can be expected near midspan while the opposite might be used near support locations. Even with the ability to vary the chord and web members along the length, practicality often limits excessive variability in these members along the length. For example, the chord is usually continuous over several panels to minimize splice points. In addition, the web member sizes are usually controlled by geometry and therefore the same size is often used for several panels of verticals and diagonals along the length. Unfortunately, there has been little work focused on the impact of the variation of the chord and web elements on the buckling capacity of the truss. This dissertation will discuss mostly on the case of members with uniform cross section throughout the span length.

2.2.2 Load Locations (Load Height Effect)

The C_b factors discussed in the last section generally apply to beams with concentrated or distributed loads applied at midheight of the section. In reality, loads applied to beam systems can be applied at several different locations on the cross section. The self-weight of the beam would generally be idealized to act at the geometric centroid while externally applied loads may be applied either at the top or bottom flange depending on the structural application. The point of load application on the cross section can have a substantial impact on the buckling behavior. In general, loads applied at the bottom flange result in increases in the buckling capacity relative to midheight loading because the load results in a restoring force as the section twists during buckling as depicted in Figure 2.1. In a similar fashion, loads applied at the top flange result in a

reduction in the buckling capacity compared to midheight loading because the load causes an overturning force as the section twists during buckling.

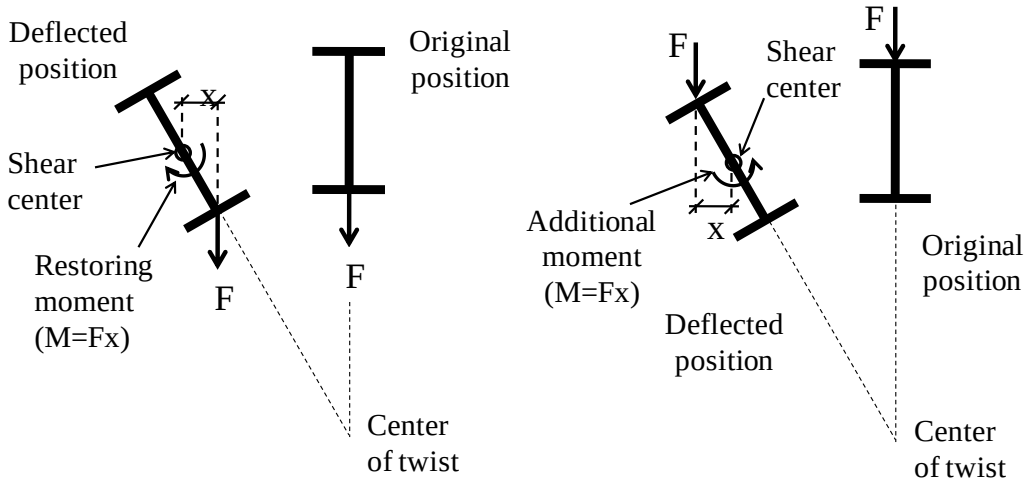

Figure 2.1 Load height effect on beam

To account for the effect of the load height on the buckling capacity of beam, the load height effect factor, Equation (2.6), is imposed into the calculation of beam buckling capacity, Equation (2.1) (Helwig et.al., 1997).

$$C_b^* = \left(1.4^{2y/h_o}\right)C_b \tag{2.6}$$

Where C_b^* = Modified moment gradient factor accounting for load position

y = Location of the applied load relative to the midheight
Positive for loading below midheight
Negative for loading above midheight

h_o = Beam depth

C_b = Moment gradient factor from appropriate equations such as Equations (2.4) and (2.5)

The bracing behavior of beams is affected by the position of the loading on the cross section. Dux and Kittipornchai (1986) found that beams with top flange loading experienced a larger relative increase in the buckling load when intermediate bracing was

introduced compared to beam with loading at the shear center or at the bottom flange when intermediate bracing was introduced.

2.2.3 Total Brace Stiffness

Lateral braces for beams or columns are primarily subjected to only the axial force in the brace. Provided a good connection is used between the brace and the beam or column, the stiffness of the brace is primarily only a function of the lateral brace itself. In contrast, for torsional braces, several factors can affect the performance of the bracing system. The total stiffness (β_T) of the bracing system comes from the combination of several factors and can be calculated by using the expression for springs in series (Yura, 2001) as follows:

$$\frac{1}{\beta_T} = \frac{1}{\beta_b} + \frac{1}{\beta_{sec}} + \frac{1}{\beta_g} \tag{2.7}$$

Where β_b = Stiffness of the attached brace

β_{sec} = Cross section stiffness

β_g = Girder in-plane stiffness

The following subsections focus on each of the individual components in the expression shown in Equation (2.7).

2.2.3.1 Brace Stiffness (β_b)

Torsional braces that are used in beam systems primarily consist of either plate diaphragms or cross frames systems. Plate diaphragms can either be rolled sections or built up members. Cross frames consist of a combination of axial loaded members to form a truss system that resists twist of the beam by linking the section to an adjacent beam. Diaphragm systems may frame into the middle of the web of the beam or near the top or bottom of the web depending on the structural requirements. In through girder systems, the floor beams may consist of the diaphragm that frame into the girders near the bottom flange. Depending on the length to depth ratio of the brace, the stiffness of many "diaphragm" systems may be dominated by the flexural stiffness of the bracing

member. The location of the diaphragm brace on the cross section can have a significant impact on the stiffness of the brace itself. For example, diaphragm braces that frames into the beams near the top flanges of two adjacent beams will often bend the brace in reverse curvature as shown in Figure 2.2A, which will have a 6EI/S stiffness, where E is the modulus of elasticity, I is the moment of inertia of the brace about the bending axis, and S is the length of the brace. On the contrary, diaphragm braces that frame into the beams lower on the cross section will often bend in single curvature and have a 2EI/S stiffness.

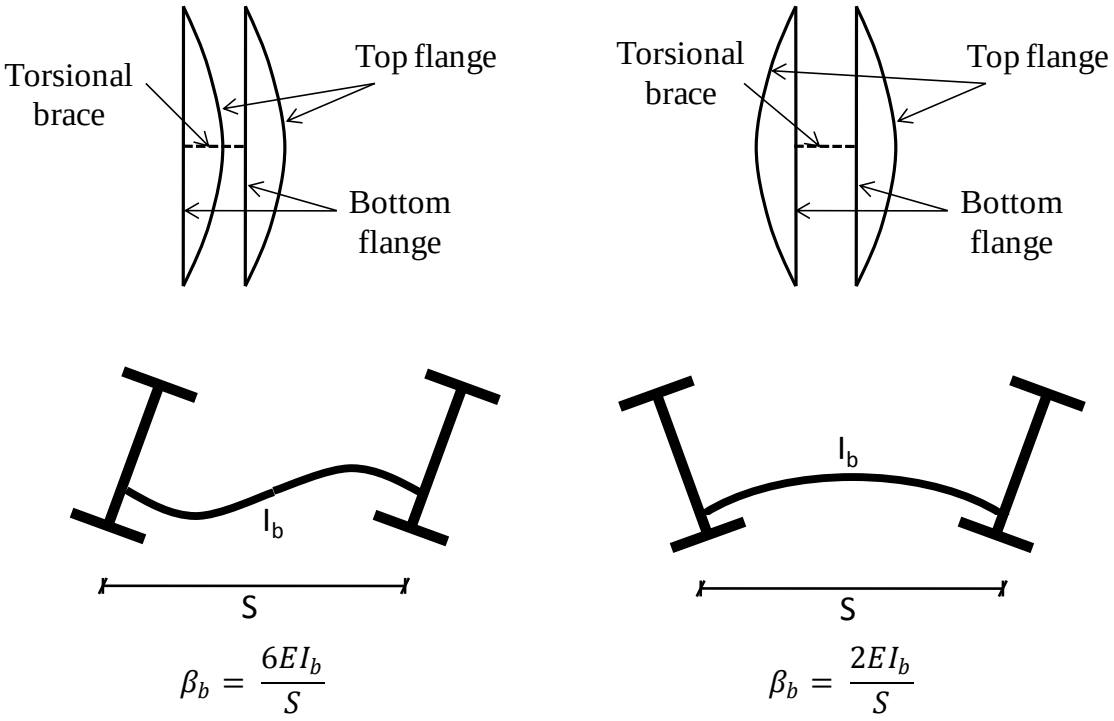

Figure 2.2 Torsional brace stiffness of bending type bracing

For the cross frame, the stiffness comes from the elongation and shortening of the axial loaded elements. Cross frames can be tension-only systems, compression systems, K-brace system or other types. The stiffness values of the various types of cross frame

are summarized and can be found in Yura (2001). For example, the stiffness of the tension-only cross frame, Figure 2.3, is shown in Equation (2.8).

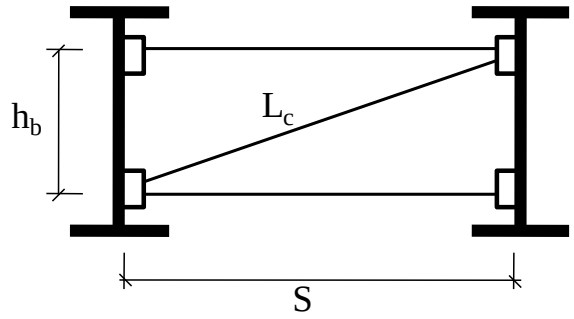

Figure 2.3 Tension-only cross frame

$$\beta_b = \frac{ES^2 h_b^2}{\frac{2L_c^3}{A_c} + \frac{S^3}{A_h}} \tag{2.8}$$

Where E = Young's modulus

S = Girder spacing

h_b = Cross frame depth

L_c = Length of diagonal member

A_c = Area of diagonal members

A_h = Area of horizontal member

2.2.3.2 Cross Section Stiffness and Cross Section Distorsion (β_{sec})

The stiffness behavior of torsional bracing systems can be substantially affected by cross sectional distortion. Phillips (1991) found that the use of beams with slender webs can cause a substantial decrease in the bucking strength. Most torsional bracing systems for beams require web stiffeners at the brace locations to provide a suitable connection between the brace and the beam as well as controlling the web distortion. The SSRC (2010) recommends extending the diaphragm to at least three-quarters of the beam depth. Similarly, to minimize the cross section distorsion of beams with cross frames,

Yura (2001) suggested that the cross frame depth should be at least three-quarters of the beam depth.

In order to calculate the cross section stiffness (β_{sec}) in Equation (2.7), Yura (2001) provided the following equation to calculate the stiffness at each part throughout the depth of the beam:

$$\beta_i = \frac{3.3\,E}{h_i}\left(\frac{h}{h_i}\right)^2 \left(\frac{(N + 1.5\,h_i)t_w^3}{12} + \frac{t_s\,b_s^3}{12}\right) \tag{2.9}$$

Where h = Beam web depth

h_i = Depth of considered portion

N = Width of brace connection

t_w = Thickness of web

t_s = Thickness of stiffener

b_s = Width of stiffener

If partially stiffened webs are used, Figure 2.4, the stiffness of the cross-section (β_{sec}) is obtained by combining the stiffness values of the individual parts. The stiffness values in each part are combined by using the equation:

$$\frac{1}{\beta_{sec}} = \frac{1}{\beta_1} + \frac{1}{\beta_2} + \frac{1}{\beta_3} + \frac{1}{\beta_4} \tag{2.10}$$

Where each individual portion of the web (β_i) is obtained using Equation (2.9). The SSRC Guide (2010) provides Equation (2.9), without the variable N.

The effects of cross-sectional distortion in beams can be controlled by using a web stiffener to control the web flexibility. Cross-sectional distortion primarily occurs in portions of the web above and below the cross frame or diaphragm. Generally the portion of the web within the depth of the brace is very stiff and does not distort. Distortion can also occur in columns if lateral braces frame into the web, or if torsional braces are used to improve the torsional buckling capacity. Web stiffeners also are effective at controlling the cross sectional flexibility for the column systems (Helwig and Yura, 1999).

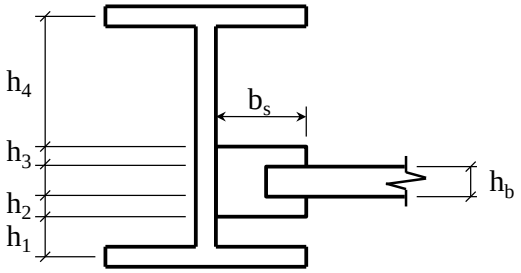

$$h = h_1 + h_2 + h_3 + h_4 + h_b$$

Figure 2.4 Partially stiffened web

The cross section of trusses can also have different stiffness values depending on type of the web of the truss. The cross section stiffness varies along the length of the truss since the diagonals and verticals frame into the chords at discrete locations along the length. Using wide flange sections for the web members of the truss provides stiffer webs than smaller members such as angles; however good connections are still necessary between the web-to-chord members. Zhi-Gang (2008) found that, in steel pipe trusses, the buckling capacity decreases with increases in the web slenderness ratio. It was also found that the influence of the slenderness ratio can affect the truss buckling capacity in the range of 5 to 25 percent. With wide flange sections for the web, the truss benefits from stiffer connections with the chord that tends to result in smaller cross-section distortion. However, even if the web has high stiffness value; flexibility in the gusset plate connections can lead to distortion that affects the bracing behavior for the truss. Web stiffeners may often be necessary to control flexibility in the webs of the chords. This is particularly true in pony truss systems where the floor beams provide torsional restraint to the truss at the lower chord, or cases where a flexural member is provided as a torsional restraint at the top chord. The use of full depth cross frames eliminate the cross-section distortion of the truss.

2.2.3.3 Connection Stiffness (β_{con})

Besides the web distortion, the connection flexibility also affects the buckling capacity of the truss. Even though this stiffness component was not included into

Equation (2.7); previous studies have shown connection flexibility can have significant effects on the bracing behavior (Quadrato, 2010).

In trusses with hot rolled sections, four details are commonly used in medium to long span trusses (DeBlauw, 2007). As depicted in Figure 2.5, these details consist of (1) wide flange to wide flange section with gusset plate on both sides of the chord commonly used in long span systems; (2) angle to tee section chords which are usually used in lightweight roofing systems; (3) double angle web members to wide flange chords with a single connection plate; and (4) structural tubes for both the web and chord members which are often used for aesthetic reasons. The types of connections that are used between the web members and the chords can have a significant effect on the buckling mode and resulting capacity of the truss systems. The single thin-web connection in truss type (3) can lead to very low connection stiffness while the double gusset plate in (1) generally provides the highest stiffness compared to the other three cases. In (4), the connection stiffness seems to be high due to the large cross section of the elements; however, the local buckling might occur due to the thin walls of the tubes and can affect the buckling behavior.

2.2.3.4 Girder In-Plane Stiffness (β_g)

The in-plane stiffness of beams has been shown to affect the bracing and buckling behavior in beam systems. Shears are developed at the ends of cross frames or diaphragms that result in in-plane deformations of the girders that in turn impact the effectiveness of the brace, Figure 2.6. Helwig et al. (1993) showed that the in-plane stiffness of the girder can become significant for the twin girder systems braced by either cross frames or diaphragms. The girder in plane stiffness can be calculated by (Helwig et al., 1993, Yura, 2001):

$$\beta_g = \frac{12S^2EI_x}{L^3} \tag{2.11}$$

Where S = Girder spacing

I_x = Major axis moment of inertia of single girder

L = Girder length

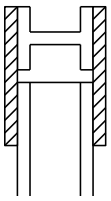

1) Wide flange to wide flange connection

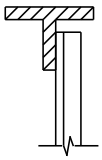

2) Angle to tee connection

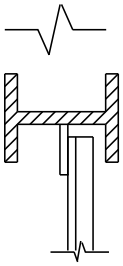

3) Double angles to wide flange connection

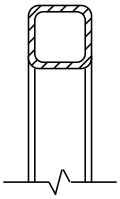

4) Structural tubes connection

Figure 2.5 Type of truss connections

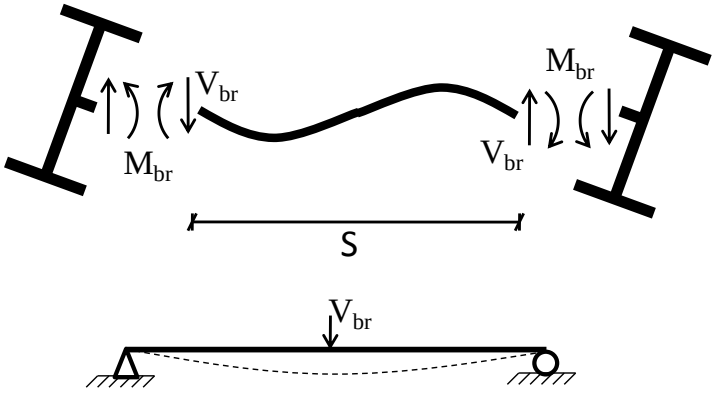

$$V_{br} = 2M_{br} / S$$

Figure 2.6 Shear developed at the end of the diaphragm

2.2.4 Brace Locations

The location of the lateral braces on the cross section and along the length can have significant effects on the bracing behavior for both columns and beams. Columns with the same unbraced length for torsion and about the minimum principal axis will always be controlled by weak-axis buckling. However, if bracing details are used that do not restrain twist, torsional buckling may control. In some instances, lateral braces are offset from the shear center/centroid of the section which can cause a lower torsional mode of buckling with the brace point acting as the center of twist. For lateral bracing of trusses, Masoumy (1980) found that attaching the lateral bracing to the tension chord of the truss has negligible influence on the buckling capacity of the truss. Similarly, Hribar (1965) found that removing the lateral brace at the bottom chord (tension chord) of trusses with lateral braces on both top and bottom chord reduces the buckling capacity by less than 10 percent.

The location of torsional braces on the cross sections of columns and beams does not significantly affect the buckling capacity provided that cross section distortion is controlled (Yura et.al., 1992; Yura, 2001; Helwig and Yura 1999). However, due to the potential lower stiffness, the connection of the intermittent web members of truss systems, the location of the brace might affect the performance of the brace and the buckling capacity of the truss. In these cases, connection flexibility might have significant effects on the bracing performance.

2.3 IDEAL STIFFNESS REQUIREMENTS AND INITIAL IMPERFECTIONS

Many bracing requirements are expressed as a function of the ideal stiffness requirements, which is the bracing required so that a perfectly straight member will buckle between the braces. Winter (1960) developed a simple model for determining the stiffness and strength requirements for lateral bracing systems. The model consisted of rigid links with pinned connections and the location of the lateral braces as depicted in Figure 2.7. By taking equilibrium on the displaced structure, the required brace stiffness to stabilize the column can be determined. The ideal stiffness for the system in Figure

2.7 is $\beta_i = 2P/L$. Although Winter's model allows the evaluation of the ideal stiffness requirements, imperfect systems can also be considered with his model. The magnitude and shape of the initial imperfection has a significant impact on the magnitude of the brace forces. Large initial imperfections result in secondary effects that amplify the forces in the bracing system. The initial imperfection can be included in Winter's model so that brace strength requirements can be evaluated as shown in Figure 2.8 and Equation (2.12).

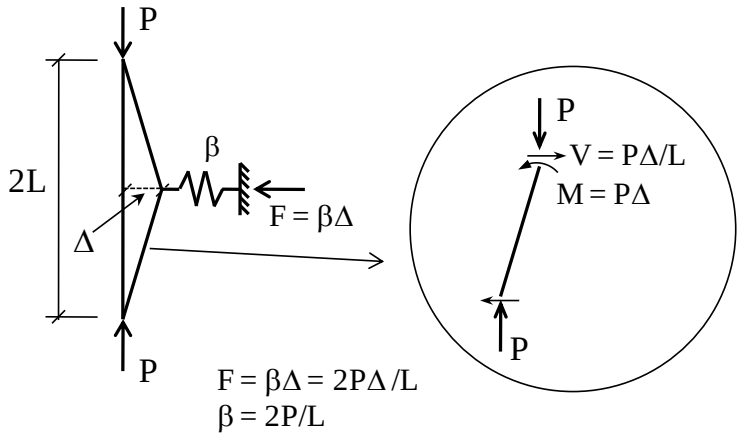

Figure 2.7 Winter's model with no imperfections

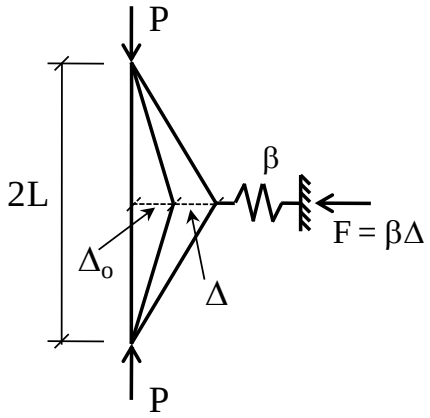

Figure 2.8 Winter's model with imperfections

$$F = \frac{2P}{L}(\Delta_o + \Delta) \tag{2.12}$$

It can be seen from Equation (2.12) that the brace force depends directly on the initial imperfection value. In addition, the expression in the fraction is simply the ideal stiffness that was derived from Winter's model of a perfectly straight system. Results will be presented later in this chapter that demonstrate that providing the ideal stiffness results in large deformations and brace forces. However, providing a larger stiffness than the ideal value can limit deformations and brace forces. The stiffness requirements are often determined so that amount of lateral deformation, Δ, is equal to the initial imperfection, Δ_o. Practically, the column can have any shape of initial imperfection such as the half sine shape as shown in Figure 2.9A where the brace force would be slightly different from the Equation (2.12). Wang and Helwig (2005) found that the critical imperfection in columns is the zigzag shape with one wave less than the number of the braces.

Similar to column systems, the magnitude and shape of the initial imperfection also affects the brace forces and deflections in beams. Figure 2.9B shows the typical imperfection that might exist in a beam. The offset of the applied load from the brace point caused by initial twist creates the additional moment in the brace and results in larger brace forces and rotations. Phillips (1991) and Wang and Helwig (2005) found that the initial imperfection significantly affects the bracing behavior for beam. Wang and Helwig (2005) found the critical shape imperfection for beams has a lateral deformation of the compression flange while the tension flange remains straight. The AISC Code of Standard Practice (AISC, 2005b) limits the values of the initial imperfection for the beam to L/1000 which equal to $L_b/500$ for the case of beam with single brace at midspan. Applying the critical shape imperfection with one of the flanges has an initial out-of-straightness equal to $L_b/500$ while the other flange is straight results in a twist of $L_b/500d$ where d is the beam depth.

2.4 STABILITY BRACING REQUIREMENTS FOR COLUMNS, BEAMS AND TRUSSES

The bracing elements must have adequate strength and stiffness to effectively brace the main members against buckling. Historically, many designers have used rules

of thumb such as sizing the brace for 2% of the compression force in the member being braced. While this may provide sufficient strength, such an approach neglects the stiffness requirements and therefore may result in inadequate bracing.

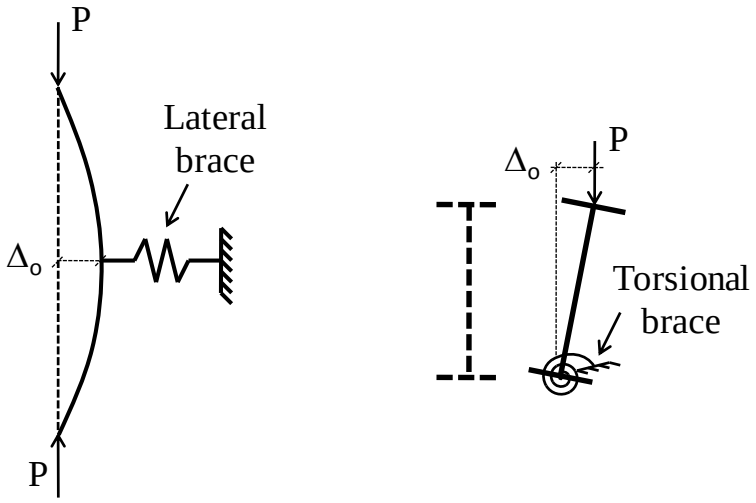

Figure 2.9 Effect of initial imperfection on the brace force

There are generally two types of bracing that are commonly used to improve the buckling capacity of beams and columns: lateral and torsional bracing systems. As noted in the last section, the stiffness requirements for most braces are usually expressed as a function of the "ideal stiffness", β_i, which is the stiffness required so that a perfectly straight member buckles between the brace points. While it is desirable for structural members to be as straight as possible, limitations in production and fabrication lead to initial imperfections in the members in practice. The effects of these imperfections need to be taken into consideration in the design of the braces. Using the ideal stiffness (β_i) for column and beam with an initial imperfection will result in very large brace forces as well as significant deformations. Most bracing provisions recommend providing at least twice the ideal stiffness to control brace forces and deformations.

Previous investigations on the bracing requirements of column and beam systems have shown that the connections between the braces and the main members must be detailed to avoid excessive distortion that may otherwise render the brace ineffective (Yura, 2001; Deaver, 2003). The AISC Specification (AISC, 2005a) provides requirements for the bracing of beam and column systems. The bracing requirements for each type of element are outlined in the following two sections.

2.4.1 Column Bracing Requirements

The critical load for a perfectly straight prismatic column is given by the Euler buckling load which can be calculated from the following expression:

$$P_{cr} = \frac{\pi^2 EI}{L_b^2} \tag{2.13}$$

To reach the Euler load requires sufficient lateral restraint which is usually provided by braces at the ends or at intermediate locations along the length of the member. Effective bracing must have both adequate stiffness and strength. Most bracing systems fit into one of four categories: relative, discrete (nodal), continuous and lean-on bracing.

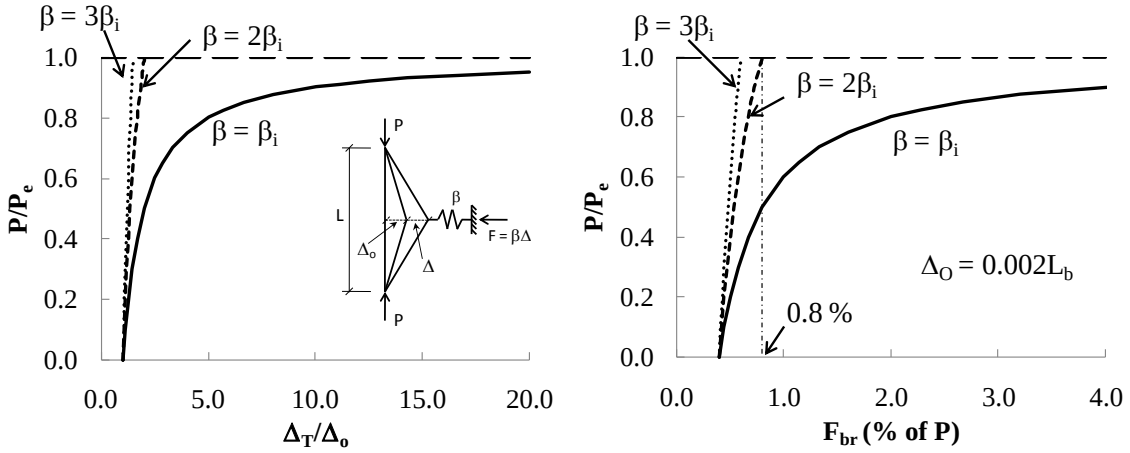

A) Lateral deflection B) Brace force

Figure 2.10 Deflection and brace force of Winter column

Engineers should be aware of the potential controlling torsional buckling modes that might control depending on the lateral bracing details that are used. For lateral bracing, Figure 2.10A shows the lateral deflection of the Winter column with an initial imperfection. Using the ideal stiffness results in very large lateral deflections as the load approaches $P/P_e = 1.0$. Providing a brace stiffness equal to twice the ideal brace stiffness provides much better control of the column deformation and the amount of deformation equal to the initial imperfection occurs at $P/P_e = 1.0$. Larger values of the brace stiffness above twice the ideal stiffness provide further control of the deformations; however the difference is not as significant as the improvement in comparing curves for β_i and $2\beta_i$. The brace stiffness that is provided also affects the brace forces as demonstrated in Figure 2.10B. Providing the ideal stiffness results in very large braces forces and the load level $P/P_e = 1.0$ is never reached. However, with an imperfection of $L_b/500$, Winter's model with twice the ideal stiffness results in a brace force of 0.8%P, where P is the axial force in the column. Winter's rigid link model is actually slightly unconservative compared to continuous columns. An FEA analysis on a column with a single brace at midheight and an imperfection of $L_b/500$ results in a brace force of 1.05%P. For larger number of intermediate braces, the force does tend towards the 0.8%P predicted by Winter's model; however the provisions in the AISC Specification (AISC, 2005a) use a value of 1%P to match the case of a single intermediate brace. Brace forces are generally a linear function of the magnitude of the initial imperfection. Therefore brace forces for columns with larger imperfections than the design value can simply be scaled accordingly.

Winter's model was for predicting the behavior of columns with discrete brace located along the column length. In many applications, braces are provided such as that shown in Figure 2.11 that controls the relative movement of two adjacent points. The ideal stiffness requirements for the relative bracing system is $\beta_i = \Sigma P/L$, where ΣP is the sum of the load that is stabilized by a single brace. Similar to the discrete bracing systems, the ideal stiffness should be doubled, which produces a required stiffness of $\beta_{req'd} = 2\beta_i = 2\Sigma P/L$. The resulting strength requirements are 0.4%P. For design in the

Load and Resistance Factor Design formulation, a resistance factor, ϕ, of 0.75 is recommended along with the use of factored design loads. Therefore, the requirements for relative and discrete (nodal) bracing systems are as follows:

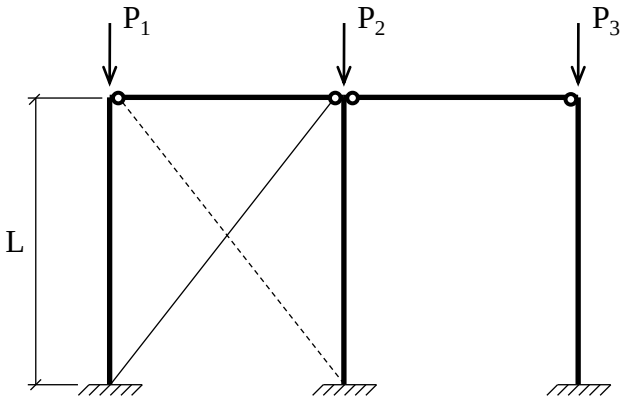

Figure 2.11 Relative bracing system

Relative Bracing

Stiffness requirement

$$\beta_{req} = \frac{2\sum P}{\Phi L} \tag{2.14}$$

Strength requirement

$$F_{br} = 0.004 \sum P \tag{2.15}$$

Where P = Column load

L = Column length

ϕ = 0.75

Discrete (Nodal) Bracing

Stiffness requirement

$$\beta_{req} = N_i \frac{2P}{\Phi L} \tag{2.16}$$

Strength requirement

$$F_{br} = 0.01P \tag{2.17}$$

Where N_i = (4-2/n)

n = Number of brace

The N_i expression shown above accounts for the difference in the stiffness requirements as a function of the number of intermediate discrete braces. The previous derivation was for the case of a single intermediate brace. As braces are added, the stiffness required for full bracing increases based upon the following table:

Table 2.1 Ideal Discrete Stiffness Requirements: N_iP/L

Number of Intermediate Braces, n	Exact Solution, N_i	Approximate Solution, N_i=4-2/n
1	2.00	2.00
2	3.00	3.00
3	3.41	3.33
4	3.62	3.50
Several braces	Approaching 4.00	Approaching 4.00

As mentioned earlier, torsional buckling may control the capacity of columns when the bracing prevents lateral movement but not twist. Columns in which the lateral bracing frames into the flange are particularly susceptible to torsional buckling about a restrained axis, such as cases where shear diaphragms, in form of siding, restrain the columns at the locations of the girts. The girts frame into the columns on the outer flange and provide a stiff lateral bracing system; however the girts usually have relatively simple connections that do not restrain twist. Torsional buckling capacity of column with lateral restraint offset to the X and Y axes from the centroid, Figure 2.12A and B, can be calculated by Equations (2.18) and (2.19) (Timoshenko and Gere, 1961), respectively. For the case with centroid bracing, the variable “a” and “b” drop to zero.

$$P_T = \frac{P_{ey}[(d^2/4) + a^2] + GJ}{a^2 + r_x^2 + r_y^2} \tag{2.18}$$

$$P_T = \frac{P_{ey}\left[(d^2/4) + (I_x/I_y)b^2\right] + GJ}{b^2 + r_x^2 + r_y^2} \tag{2.19}$$

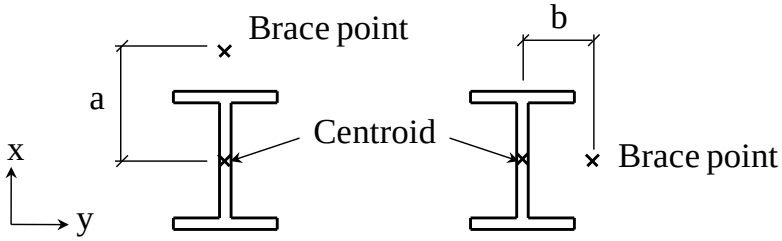

A) X axis offset B) Y axis offset

Figure 2.12 Column lateral restraint location

The girts can be designed to act as a torsional brace, provided a suitable detail is provided to restrain column twist. The torsional bracing requirements for columns with lateral bracing offset along either the X or Y axes are provided by Helwig and Yura (1999). The stiffness requirement for the case where the brace is offset along the X axis (i.e. the girt/shear diaphragm is fastened on the outer flange of a W-shape) is provided in Equation (2.20). The requirements for the case where the brace aligns in the Y axis is similar to the case in the X axis with the changing of "A" to 4 and "a^2" to $(I_x/I_y)b^2$ where b is the offset distance from centroid along the minor axis.

$$\beta_T = A\,\frac{\left\{Pr_s^2 - P_o\left[\frac{d^2}{4} + a^2\right]\right\}^2}{\frac{n_b 4EI_y}{L}\left[\frac{d^2}{4} + a^2\right]} \tag{2.20}$$

where

$$A = 4 - \frac{2a}{d} \geq 2.0 \tag{2.21}$$

Where P = Applied axial load

P_o = Weak axis flexural buckling load with full column length

r_s^2 = $r_x^2 + r_y^2 + a^2$

r_x = Radius of gyration about x axis

r_y = Radius of gyration about y axis

a = Offset of lateral support from centroid

d = Column depth

n_b = Number of intermediate torsional brace

The stiffness provided in Equations (2.20) and (2.21) were developed so that the amount of twist that the member will experience at the design axial load P is equal to the initial imperfection $\theta_o = L_b/500d$. Therefore the brace strength of the torsional brace is given as $M_{br} = \beta_T\theta_o$

The most efficient way for column bracing is the combination of the lateral and torsional bracing where not only the column is forced to buckle between the brace points but also the torsional mode is prevented. Roof trusses are also highly susceptible of the torsional buckling about a restrained axis since the top chord is often restrained by profiled sheeting and joists along the length. The torsional bracing requirements given above are applicable to these truss systems.

2.4.2 Beam Bracing Requirements

Similar to column systems, bracing systems for beams are also usually divided into either lateral or torsional bracing. Lateral bracing can be divided into the same categories (relative, discrete (nodal), continuous, or lean-on) similar to column bracing whereas torsional bracing is typically divided into the categories of either discrete (nodal) or continuous bracing.

The buckling capacity of a doubly-symmetric unbraced beam given in Equation (2.1) is for uniform moment loading. The beneficial effects of variable moment are usually accounted for by a moment gradient factor, C_b that is applied to the uniform moment solution (Equation (2.4) or (2.5)). The moment gradient factor is applicable when transverse loads are applied at midheight. When the loads are applied away from

midheight, load position relative to midheight can have a significant impact on the buckling capacity and can be modified by Equation (2.6).

The important parameter in Equation (2.1) for improving the buckling capacity is the unbraced length, L_b. Reducing the unbraced length requires effective bracing which is a function of the factors discussed previously. Extensive studies have been conducted in the past on beam bracing systems and expressions were developed to account for these many factors (Yura, 2001).

For discrete lateral beam bracing the following expressions were developed by Yura (2001):

For stiffness requirement:

$$\beta_L = \frac{2N_i M_f C_l C_d}{L_b h} \tag{2.22}$$

For strength requirement:

$$F_{br} = \frac{0.01 C_l C_d M_f}{h} \tag{2.23}$$

Where N_i = 4-(2/n)

M_f = Maximum beam moment

h = Beam depth

L_b = Unbraced length

C_l = 1+(1.2/n) for top flange loading

= 1.0 for other loading

C_d = 1.0 for single curvature

= $1+(M_s/M_L)^2$ for double curvature

n = Number of braces.

The solution for the buckling capacity of doubly symmetric beams with continuous torsional bracing on the compression flange subjected to uniform moment is given by Yura (2001) and is based on the Taylor and Ojalvo (1966) torsional bracing solution:

$$M_{cr} = \sqrt{M_o^2 + \overline{\beta_T} E I_y} \tag{2.24}$$

Where $\overline{\beta_T}$ = Equivalent continuous torsional brace (in-k/rad)/in

Yura (2001) modified this equation to account for the loading condition and yield stress limit and suggested the general formula of beam with torsional bracing as

$$M_{cr} = \sqrt{C_{bu}^2 M_o^2 + \frac{C_{bb}^2 \bar{\beta}_T E I_{eff}}{C_T}} \quad \leq \quad M_y \ \ or \ \ M_{bp} \tag{2.25}$$

Where M_o = Buckling capacity of unbraced beam with uniform moment loading

C_{bu} = Moment gradient factor for beam with no intermediate bracing

C_{bb} = Moment gradient factor for beam with full bracing

$\bar{\beta}_T$ = Continuous torsional bracing system stiffness

I_{eff} = Effective moment of inertia of weak axis ($I_{eff} = I_y$ for doubly symmetric cross section

C_T = 1.2 for top flange loading and 1.0 for centroid loading

M_y = Beam yield moment

M_{bp} = Moment corresponding to buckling between brace points

This equation can be used for beams with discrete torsional brace by summing the stiffness of the individual braces along the length of the beam and dividing by the length ($\overline{\beta}_T = n\beta_T / L$).

The stiffness requirements in the AISC Specification (AISC, 2005a) are based upon Equation (2.25); however the first term under the radical was conservatively neglected and M_{cr} was replaced with the design moment, M_f. Assuming top flange loading and doubly the stiffness to account for imperfections results in the following stiffness expression:

For stiffness requirements

$$\bar{\beta}_T^* = \frac{2.4M_f^2}{nC_{bb}^2 EI_{eff}} \tag{2.26}$$

Since this stiffness requirement is essentially twice the ideal value, the magnitude of the twist when the design moment is reached is assumed to be equal to the initial imperfection, $\theta_o = L_b/500d$. Therefore the resulting brace moment is $\beta_T\theta_o$, which results in the following brace strength requirement:

$$M_{br} = 0.005\left(\frac{L_b}{h}\right)\frac{LM_f^2}{nEI_{eff}C_{bb}^2} \tag{2.27}$$

Where M_f = Maximum beam moment

n = Number of intermediate braces along the span.

2.4.3 Truss Bracing Requirements

2.4.3.1 Regular Truss

The difficulty in establishing clear bracing formulations for truss systems is inherent in the complexity added by the variety of possible failure modes. The buckling of trusses can occur by either local or global modes. The low out-of-plane stiffness of the truss is an important factor in the global buckling capacity of the truss. The web elements connecting the top and bottom chords provide some out-of-plane stiffness to restrain the compression chord, similar to the web of beams that restrain the compression flange. The flexibility of the web to chord connections also introduces uncertainty into the general behavior of the system. The ability of the truss web members to help restrain the compression chord depends on the stiffness of both the web elements and the connections.

The buckling behavior can be further complicated by the lateral bracing details that are used. Secondary members attached to the truss may act as lateral braces, torsional braces, or a combination. In roof trusses, metal cladding and joists often provides lateral restraint at the top of the truss; however the lateral restraints are often

offset from the centroid of the top chord. The eccentricity can result in the torsional modes of buckling about a restrained axis that were discussed earlier. Therefore, truss systems may be susceptible to a variety of buckling modes including flexural or torsional modes of individual members and the overall truss system.

Because the truss is a collection of members that comprise a flexural system, a logical choice for establishing the stability of the overall system is to employ the beam bracing requirements. However, because the truss also consists of a collection of axial loaded members, the applicability of the column bracing provisions may also be viable solutions to ensure a stable system.

Effective bracing must have sufficient stiffness and strength. Full bracing is often defined as bracing the member to reach a load corresponding to an unbraced length equal to the spacing between braces. This does not necessarily mean that the member does not displace at the braced point. Iwicki (2007) conducted elastic analyses with non-linear geometry on trusses with lateral braces with a variety of different brace angles. He found that the buckling length of the compressed truss chord is usually greater than the brace spacing.

Masoumy (1980) found that the buckling capacity of the truss top chord alone was about 11 percent less than the buckling capacity of the truss system analyzed as a frame. This indicates that the web member and bottom chord of the truss have a relatively small effect on the lateral buckling capacity of the truss with lateral bracing.

Leigh (1972) found that the lateral buckling of the top chords of trusses can be related to an Euler column with appropriate boundary condition. By using the Euler column equation (Equation (2.13)) to estimate the buckling capacity of the truss, Masoumy (1980) found that the effective length of the truss with third-point loading is less than 1.0. It was also found that, for trusses with discrete lateral bracing, the end condition of the lateral brace does not generally affect the buckling capacity of the truss.

Historically, many designers have used the 2% rule for sizing braces, where the brace is sized for 2% of the compression force in the member being braced. For bracing systems with insufficient stiffness, the brace forces can get significantly larger than the

forces predicted by the 2% rule. AISC (2005a) does not specify bracing requirements for trusses; however, in the commentary, AISC states that parallel chord trusses with both chords extended to the end of the span and attached to the supports can be treated like beams. The American Institute of Timber Construction (AITC, 2005) specifies that:

> *"To provide lateral support for truss members subject to compression, the bracing system should be designed to withstand a horizontal force equal to at least 2% of the compressive force in the truss chord if the members are in perfect alignment. If the members are not aligned calculation of the force should be based on the eccentricity of the members due to the misalignment"*

The guidance in the provisions is somewhat unclear since all members have initial imperfections and the engineer is left to select the appropriate magnitude.

Iwicki (2007) found that the brace forces have a non-linear relationship with the compression force in the chord and can be greater than 3% of the chord compression force. However, this does not affect the 2% rule in the development of the bracing requirements of the lateral bracing by AISC (2005a) due to the fact that the author did not limit the lateral deflection at $2\Delta_o$ where Δ_o is taken as $L_b/500$ and some braces were not perpendicular to the truss. The truss was also not the parallel chord truss with the both chord extended to the end of the span as specified by AISC (2005a).

In Europe, the bracing requirements for trusses can be found in the Polish steel design code (PN-90, in Iwicki, 2007) with a strength requirement for the lateral braces given as:

$$F = 0.01N \quad \text{and} \quad F \geq 0.005A_c f_y \tag{2.28}$$

Where N = Axial force in the compression chord

A_c = Cross sectional area of the compression chord

f_y = Yield stress of steel

The Polish code also limits the maximum displacement of the brace to $L_b/200$.

Additional lateral bracing requirement for trusses are given in Eurocode 3 (CEN, 2005) where the bracing requirements are issued for beams and compression members. The code specifies that the brace must be able to carry at least the equivalent uniform load due to the initial imperfection, Figure 2.13 , of:

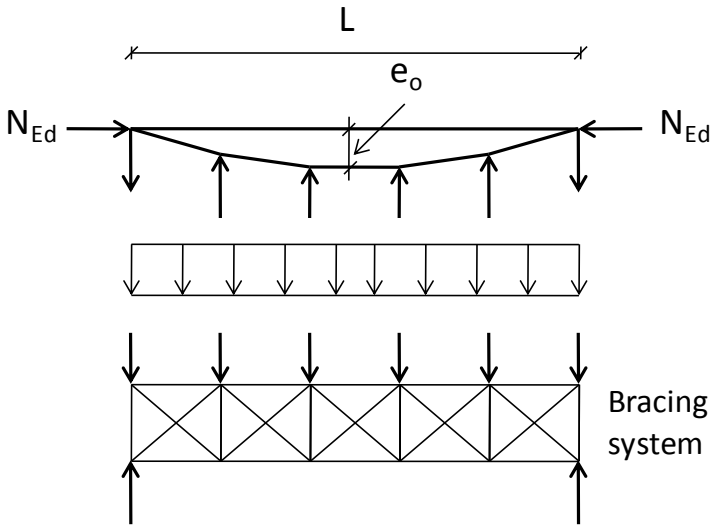

Figure 2.13 Equivalent bracing force

$$e_o = \frac{\alpha_m L}{500} \tag{2.29}$$

Where

$$\alpha_m = \sqrt{0.5\left(1 + \frac{1}{m}\right)} \tag{2.30}$$

Where e_o = Initial imperfection

m = Number of members to be restrained

The equivalent uniform load can be calculated from

$$q_d = \sum N_{Ed}\ 8\ \frac{e_o + \delta_q}{L^2} \tag{2.31}$$

Where q_d = Equivalent force per unit length

δ_q = In plane deflection of the bracing system due to q plus any external loads calculated from first order analysis

For the case of a compression flange of a beam with constant height, the force N_{Ed} can be calculated by:

$$N_{Ed} = M_{Ed}/h \tag{2.32}$$

Where M_{Ed} = Maximum moment in beam

h = Beam depth

In a recent study of trusses, Iwicki (2007) found that the buckling capacity increases for larger values of the stiffness of the brace and decreases with increase in the angle of the brace. When the angle of the brace reaches 30 and 45 degrees, the horizontal displacement was greater than the limit set by the Polish code (PN-90), which is $L_b/200$. Also, the brace force ranged from -0.25% to 3.0% of the compression force in the top chord.

2.4.3.2 Half Through Truss (Pony Truss)

The bracing requirements can be further complicated by the basic geometry that depends on the types of trusses. For example, pony trusses such as the one shown in Figure 2.14, are often used in half through truss systems where bracing of the top chord is not possible. As a result, the stability of the top chord must be provided by a combination of the deck members as well as the web members of the trusses. This bracing behavior is therefore sensitive to the flexibility of the web members and the associated connections. While there have been past studies on the stability of pony trusses that have resulted in design expressions for the buckling capacity of top chords, these expressions do not consider connection flexibilities, which can have dramatic effects on the behavior. Within the limited studies of bracing requirements for trusses, the most developed bracing design recommendations in the literature are perhaps for the half through truss (pony truss).

Figure 2.14 Pony truss bridge

Engessor (1885, 1893) and Holts (1952, 1956) focused on the bracing behavior in pony trusses and suggested equations for the required out-of-plane stiffness of the truss vertical members. Holts (1952) also considered some secondary factors such as the torsional stiffness of the chord and web members, effect of diagonal web members, and the effect of restraint provided by the chord with axial stresses. It was found that these secondary effects are small and can be neglected. Schibler (1946) also found that the effect of torsional stiffness from the web diagonal members is small. In their bridge design specifications, AASHTO (2007) treats the compression chord as a column with elastic lateral supports at the panel points. The vertical truss members and floor beams must be designed to be able to resist the lateral force of not less than 0.30 kips per linear foot applied to the top chord at the truss panel points. A summary of the design recommendations for half-through trusses is provided in the SSRC Guide (2010).

2.5 TECHNIQUE TO ESTIMATE BUCKLING CAPACITY

In many buckling tests, the determination of the critical buckling load is often complicated by imperfections in the structural members. As a result, the determination of the critical buckling capacity is difficult since the member tends to exhibit deformations immediately when the load is applied. These deformations increase as the structure approaches the buckling load; however there is usually a desire to limit the amount of total deformation to keep the specimen elastic so that multiple tests can be conducted on the same specimen. Methods are available to estimate the buckling capacity based upon basic measurements of the applied load and resulting displacement. These methods are usually referred to as Southwell plots (Southwell, 1932) or Meck plots (Meck, 1977). The Southwell plot technique can be used to estimate the buckling capacity and initial imperfection of a column subjected to axial force using some of the basic measurements of the applied load and the resulting deformation. This plot was developed from the assumption of the rectangular hyperbola load-deflection relationship. A typical Southwell plot is depicted in Figure 2.15, and consists of a graph of the lateral deflection (Δ) on the X-axis and the ratio of lateral deflection to the applied load (Δ/P) on the Y-axis. The relationship of the graph is generally linear. The X-intercept provides an estimate of the effective initial imperfection. The inverse of the slope of the graph is the estimated buckling capacity.

The Southwell technique is intended for application in columns with force distributions that are uniform throughout the member length. Meck plots were specifically developed for the lateral buckling of beams and can include systems with non-uniform loading. The Meck plot contains two plots of the lateral deflection and twist, Figure 2.16. For beams subjected to uniform bending moment, the first plot is the plot between the ratio of angle of twist over applied moment (ϕ/M) and the lateral deflection (Δ). The second plot is the plot between the ratio of lateral deflection over the applied moment (Δ/M) and the angle of twist (ϕ). The X-intercept of the first plot represents the initial lateral deformation imperfection while the second plot indicates the

initial twist imperfection. The inverse of the slope of the first and second plots represent the term α and β where the buckling moment is the square root of $\alpha\beta$. The plot can be applied to the case with point load at the centroid by substituting the bending moment (M) by the point load (P). The plot can also be modified to use with the case where the point load is above the centroidal axis of the beam.

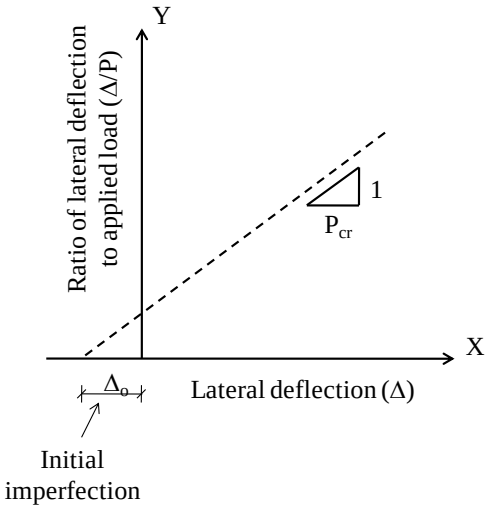

Figure 2.15 Southwell plot

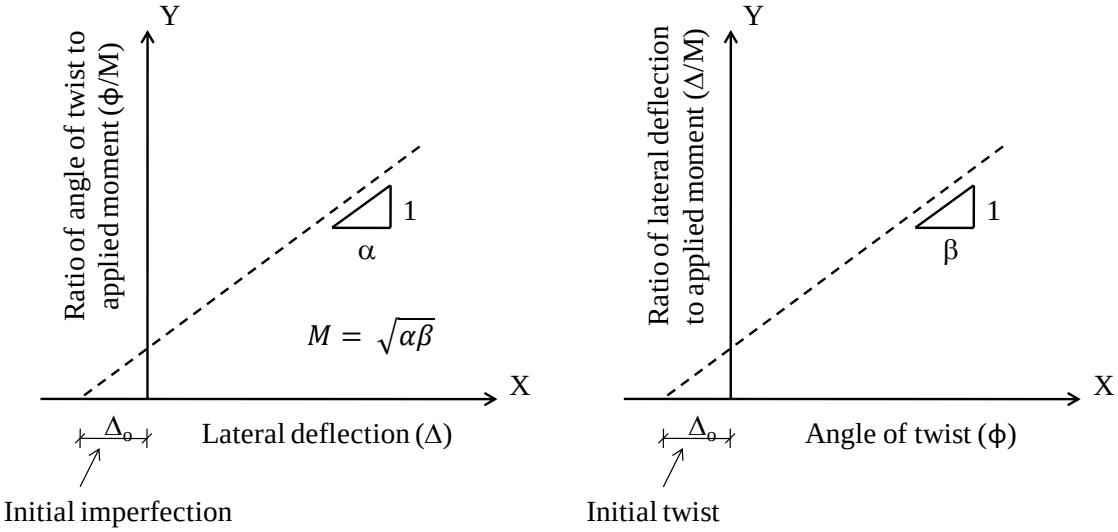

Figure 2.16 Meck plot

2.6 SYSTEM MODE BUCKLING

The system mode of buckling has recently been discussed by Yura et.al. (2008). The system mode of buckling can occur in girder systems with relatively large length-to-width ratios. Twin girder systems are particularly susceptible to the system mode of buckling which has recently been the cause of both failures and problems that have happened during construction. The system mode of buckling generally involves a global instability of the members of the system, in which the primary members buckle as a unit. The mode is relatively insensitive to the spacing between the braces. For example, considering the twin girder system shown in Figure 2.17 the system mode buckling involves both girders buckling as a half sine curve instead of buckling between the brace points. The two beams act as a unit such as the system shown in Figure 2.18.

The system mode of buckling results in a capacity that may be significantly less than the buckling capacity calculated by conventional methods, such as those given in Equation (2.24). Yura et al. (2008) used the combined warping rigidity of the system to derive an expression to account for the global buckling capacity for both singly and doubly symmetric twin girder systems as:

$$M_{gl} = 2C_b \frac{\pi E}{L_g} \sqrt{\frac{I_{yc}J}{1.3} + \frac{\pi^2 I_{yc}^2 h_o^2}{L_g^2} + \frac{\pi^2 I_{eff} I_x S^2}{4L_g^2}} \quad (2.33)$$

Where M_{gl} = System mode buckling capacity of twin girder

L_g = Girder length

I_{yc} = Moment of inertia of compression flange in y axis

I_{yt} = Moment of inertia of tension flange in y axis

I_{eff} = $(I_{yc} + (b/c)I_{yt}$

b = Distance from centroidal axis to tension flange

c = Distance from centroidal axis to compression flange

J = Torsional constant

h_o = Girder depth

S = Girder spacing

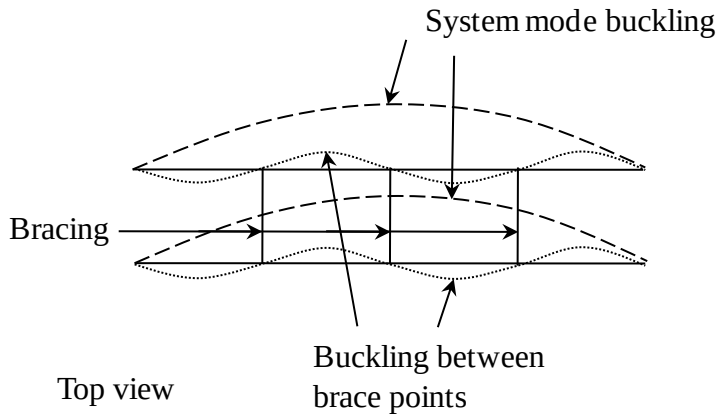

Figure 2.17 System mode buckling

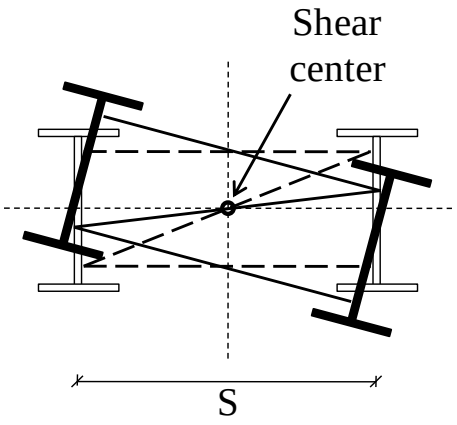

Figure 2.18 Rigid body rotation of twin girder with stiff cross frame

The system mode buckling capacity can be improved by controlling the out of plane effective length of the top chord of the beam by adding diagonal bracing at the top chord to increase the warping end restraint (Yura et.al., 2008). Increasing the girder spacing or the in-plane moment of inertia of the individual girders can also help in preventing the system mode buckling.

2.7 SUMMARY

The buckling behavior of columns and beams has been well-studied resulting in solutions for the bracing requirements that include both stiffness and strength criteria. There are several factors that must be considered when evaluating the bracing behavior.

Although many past studies have focused on column and beam systems, relatively little work has been conducted on the bracing behavior for truss systems. The most knowledge of the buckling behavior of trusses belongs to the half-through-truss (pony truss) for which buckling solutions have been developed. However, there are still many questions about the bracing requirements for pony trusses. Although the truss bracing requirements have not been developed, AISC (2005a) allows the truss with some conditions to be treated as the beam for determining the bracing requirements; however this recommendation is not based upon previous research. Questions still exist about whether trusses should be treated more like beams or columns with regards to developing bracing provisions. The remainder of the chapters in this dissertation focuses towards improving the fundamental understanding of the bracing behavior for trusses. The studies in this dissertation were restricted to the elastic buckling analysis of the trusses only. Many of the solutions that are developed later in the dissertation were developed based upon some of the past studies highlighted in this chapter.

CHAPTER 3
Experimental Program

3.1 INTRODUCTION

The purpose of the experimental test program was to improve the understanding of the numerous factors that affect the buckling behavior of truss systems, while also providing data for validating the accuracy of the finite element models. The trusses were designed to buckle elastically so that several tests could be carried out on the same specimens. The trusses maximum span was 72 feet; however the trusses were also supported with a span of 48 feet to provide additional data. The same trusses were used for both tests; however the truss was allowed to overhang the supports by approximately 12 feet on each end for the cases with the 48-ft spans. The loading was applied using gravity load simulators that were specifically fabricated for the tests. Tests were conducted with top chord and bottom chord loading. The initial series of tests were conducted on the trusses with no intermediate bracing. Several tests were also conducted on the trusses with a variety of bracing layouts, including torsional braces and lateral braces. Lateral braces were positioned at either one or two locations along the length of the truss and three different brace stiffness values were considered. For the cases with lateral bracing, the loads were applied at the top chord. Torsional braces were also used in the tests. The torsional braces consisted of flexural members that were connected to the truss chords so that the flexural stiffness of the brace resisted twist of the trusses. Two different braces sizes were used to vary the brace stiffness. The torsional braces were attached to either the top or bottom chord with the applied loads at the same braced chord. The trusses with torsional bracing were also tested using support conditions similar to that of a pony truss.

To ensure the proper validation of the FEA model with good laboratory data, the experiments were carefully designed, fabricated, tested and monitored to ensure that the

best results were obtained. Key elements of the test setup are discussed in this chapter. The results of the laboratory tests are explained in Chapter 4 and the model verification is presented in Chapter 5.

3.2 GENERAL TEST SETUP

3.2.1 Truss Fabrication

The trusses were designed to buckle elastically, thereby permitting several different tests to be conducted with the same specimen. To prevent inelasticity in the trusses, a large enough span was necessary so that the buckling stress was relatively low compared to the material yield strength. The maximum span for the truss was 72 feet and the truss depth was 4 feet. The details of the general test setup are shown in Figure 3.1 and the truss geometry and details are shown in Figure 3.2. To avoid complexity and minimize the number of variables in the setup, the truss was designed to have a symmetric section. The twin trusses were fabricated with W4x13 sections for the chord and web members with 3/8" gusset plates. The truss fabrication began by cutting 40-ft long W4x13 sections into the required lengths for the chord, vertical and diagonal web elements. The connection layouts on the members were marked using a center punch along with a hole template that was fabricated in the computer numerically controlled (CNC) mill for accuracy. The 9/16 in. diameter holes were then punched or drilled in the truss members. The gusset plates were also prepared by cutting the 3/8" plate to the specified shape and marked by center punch and template. The 9/16 in. diameter holes were then punched.

Bolted connections were used for all the gusset plate connections. Two lines of bolts with two bolts per line were used in the connections as shown in Figure 3.3. The bolts were structural bolts ASTM grade A325. To prevent slip of the bolts that would affect the buckling behavior of the truss, the connections were designed with fully-tightened bolts to prevent slip. The proper bolt tension was obtained using the turn-of-the-nut method with an impact wrench. The numbers of turns required for the pretension

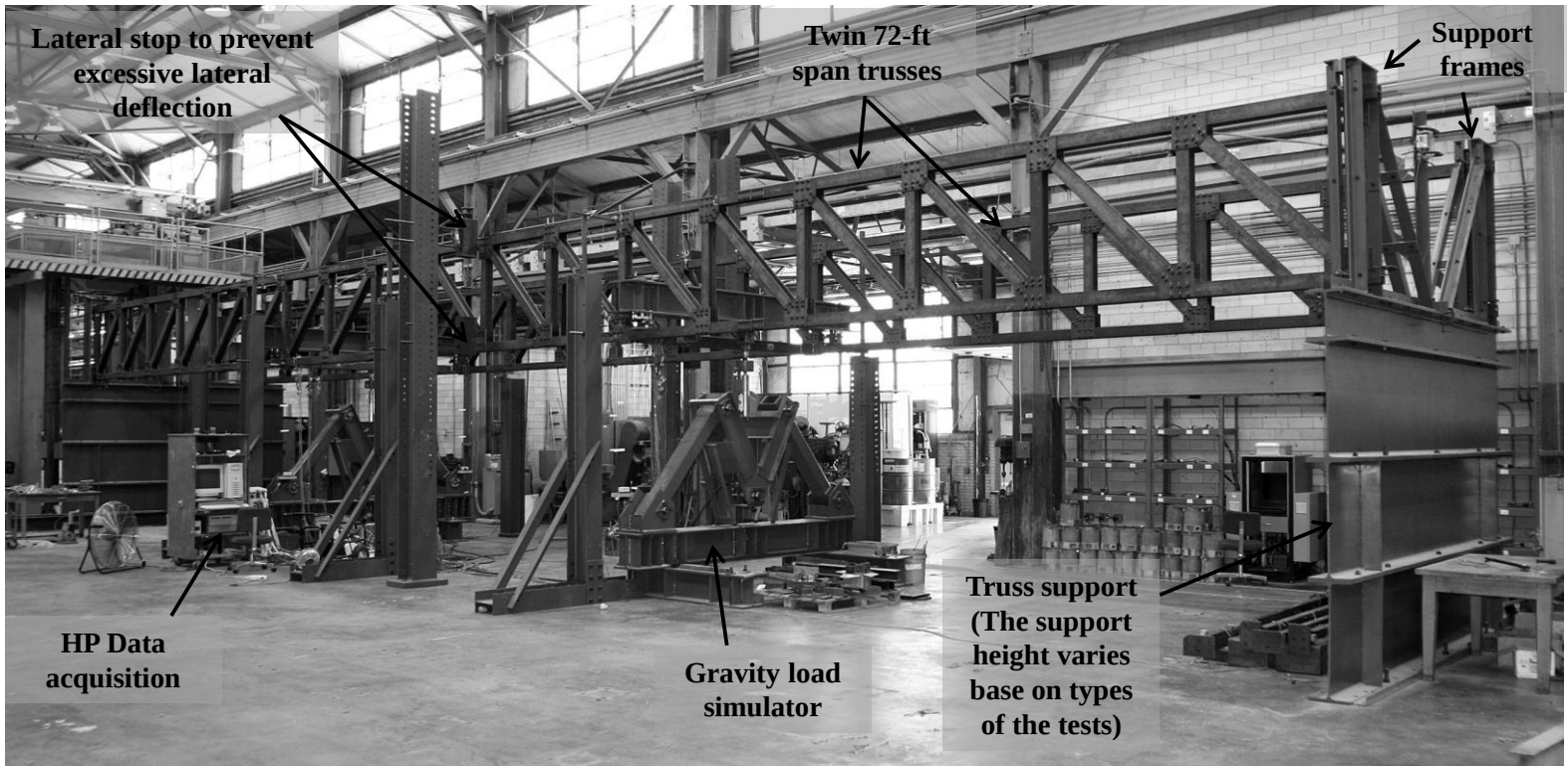

Figure 3.1 General test setup details

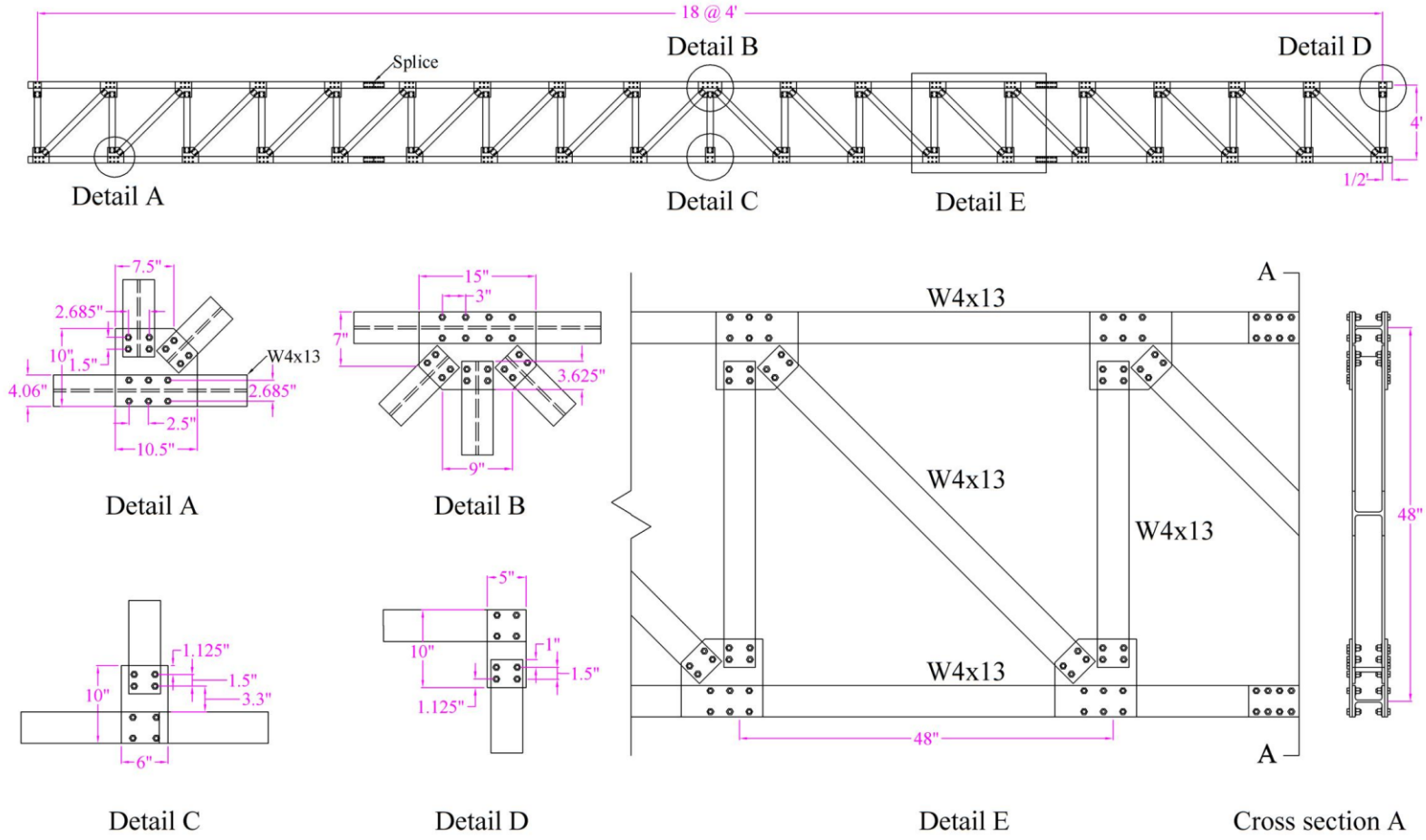

Figure 3.2 Truss geometry and details

value specified by ASTM were calibrated by using a Skidmore. Figure 3.4 show the bolt setup with the Skidmore for the calibration of the ½"x13x1½" bolts. Figure 3.5 shows the results of the bolt calibration. A minimum of ½ turn from snug-tight conditions was used for the ½"x13x1½" bolt. More than 2,300 bolts were used in the fabrication of the twin trusses. Figure 3.6 shows the truss during fabrication. The trusses could not be fabricated as single 72-ft span pieces due to the limits of the wide flange section length. The chords of the trusses were spliced at 18 and 54 ft. These splice locations created symmetrical connections about midspan. The chord splices were made using gusset plates with fully-tightened bolts. The detail of the splice is shown in Figure 3.7. The spacing between the erected trusses was 10 ft.

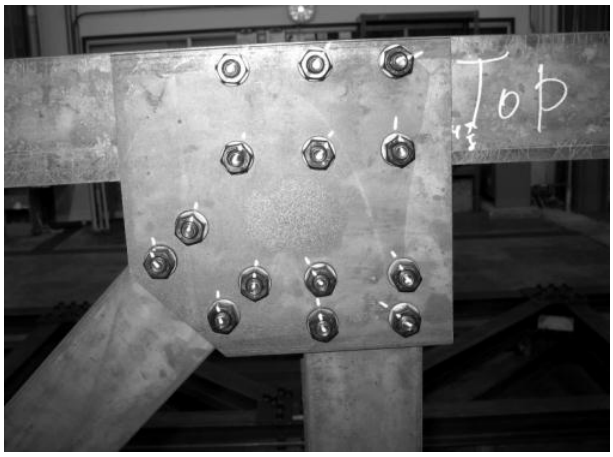

Figure 3.3 Bolts connection with marking before fully tightening by turn-of-the-nut method

3.2.2 Gravity Load Simulator

One of the most difficult aspects of conducting laboratory buckling tests is the ability to apply loads in a fashion that does not restrain member deformation. To serve this purpose, Yarimci et al. (1966) proposed the use of Gravity Load Simulators (GLS). Gravity Load Simulators consist of a mechanism that minimizes lateral restraint at the

load point while ensuring that the applied load remains vertical as the test specimens displaces laterally and twists.

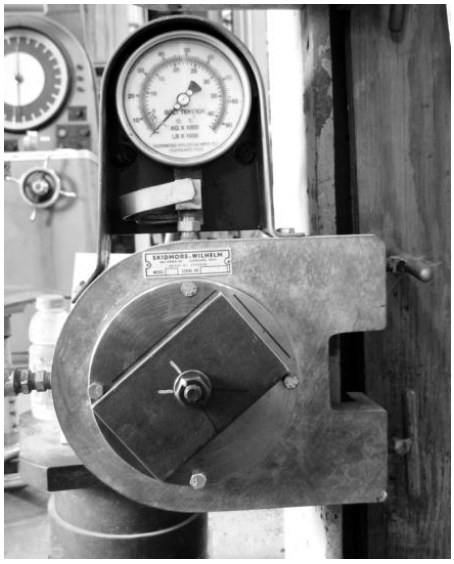

Figure 3.4 Bolt calibration with skidmore

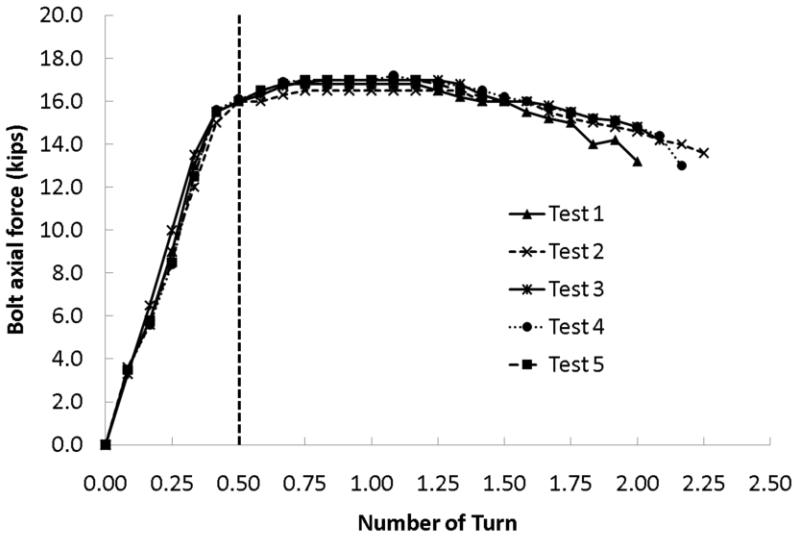

Figure 3.5 ½"x13x1½" bolt calibration

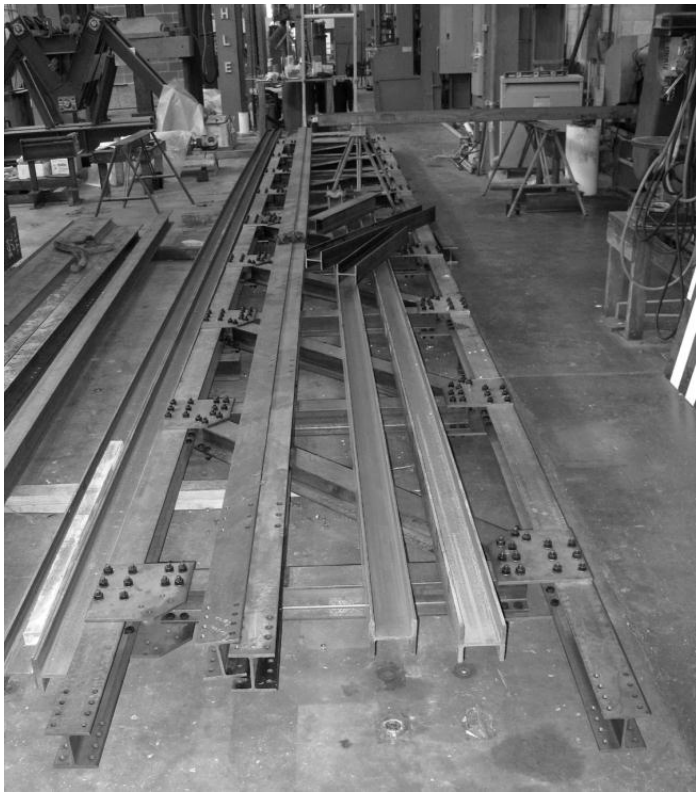

Figure 3.6 Truss fabrication

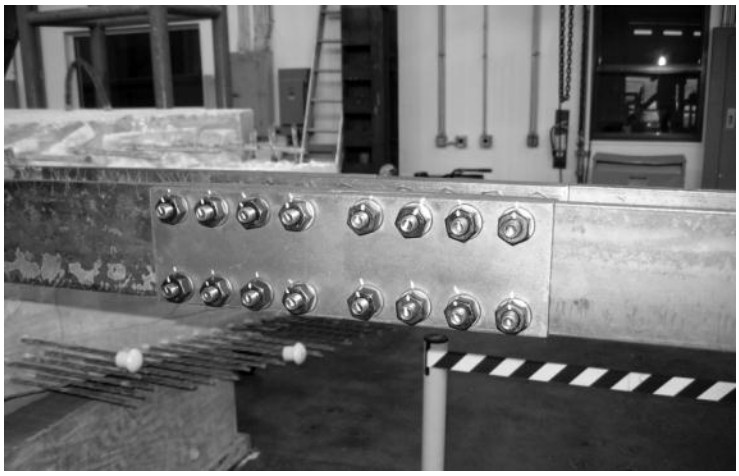

Figure 3.7 Truss chord splice

The GLSs that were fabricated and used in this experiment were slightly modified from the designs developed by Deaver (2003) to accommodate the slight difference of the

actuator geometry. The dimensions of the GLSs used in this experiment are shown in Figure 3.8. With the provided dimension, the load will be vertical at the 0 and 6 inches lateral movement and slightly offset from vertical at the lateral movement between 0 and 6 inches. Figure 3.9 shows one of the two gravity load simulators fabricated for this study. The rigid triangular frame in the middle of the GLS is connected to a hydraulic actuator at the bottom node of the triangle. Two struts that are free to rotate about the base provide the anchor point for the rigid triangular frame. The struts are anchored to a reaction beam that is tied down to the reaction floor. In some cases, the reaction beam could be directly anchored to the floor, while in the case shown in Figure 3.9 the GLS needed to be positioned between floor anchors which required two transfer floor beams. All parts were precisely machined to ensure the accurate assembly geometry and to minimize friction in the system. Timken Torrington heavy duty needle roller bearings were used to minimize friction between the members of the GLS. Bearing housings that could be bolted into place were fabricated to precisely hold the needle bearings. Holes larger in diameter than the housing were cut into the members of the GLS and the gaps were packed with steel-filled epoxy to create bearing connections between the housing and the structural members. To minimize friction in the system, the GLSs were preassembled and the housings were leveled with shim stock until the pin could be removed while the elements of the GLS were fully tightened. This process minimized additional friction due to unaligned component connections.

Bosch Rexroth hydraulics actuators with an 8 in. bore and an 18 in. stroke were attached to the GLSs. An Interface load cell with a 100 kip capacity was mounted on the actuator to monitor the force applied to the trusses. The design capacity of the GLS was approximately 160 kips based upon the rating of the needle bearings. Vibco SCR-100 vibrators were attached to the frame of the GLS to help minimize the system friction. The vibrators contained a rheostat so that the vibration frequency could be adjusted so as to minimize friction, while also not causing any resonance in the setup. Gravity load simulators are inherently unstable until some amount of load is applied to the system. To create a stable system in the unloaded condition, two adjustable struts were used on either

side of the rigid triangular frame. The struts can be rotated and adjusted so that when extended they are in contact with angle stops welded to the struts of the GLS. Figure 3.10 shows a threaded rod that has been adjusted to allow movement in the GLS once a minimum load level of approximately 500 lbs was applied.

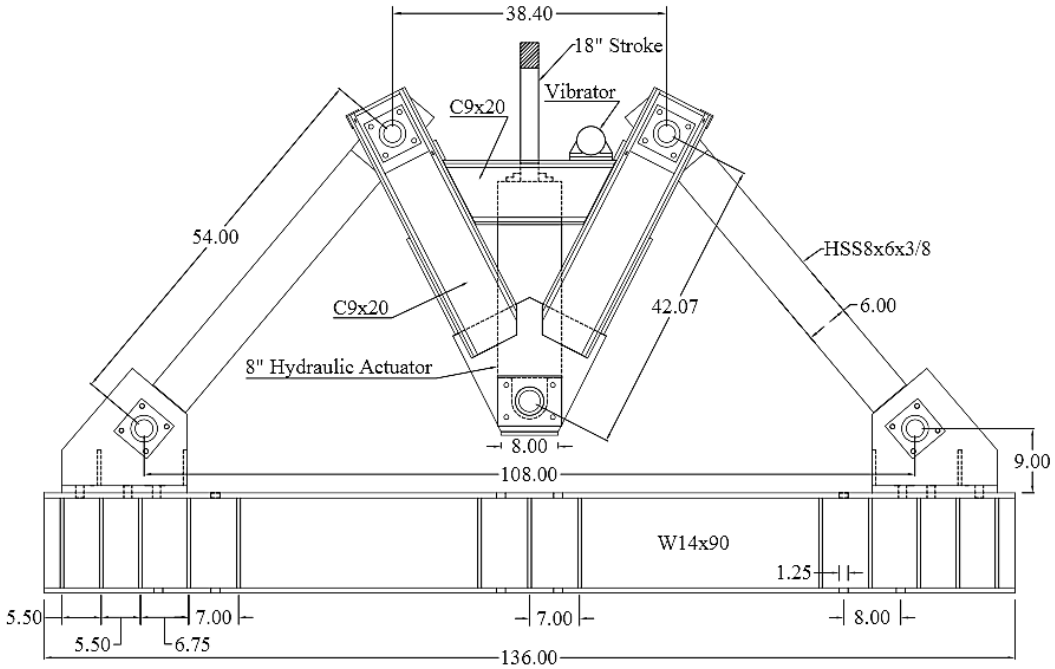

Figure 3.8 Gravity load simulator geometry

3.2.3 Load Beams and Knife Edges

The GLS in the previous subsection connects to a loading beam that transfers the applied force to the test specimen as shown in Figure 3.9. The loading beam used in the truss tests was a W12x87. Transverse bearing stiffeners were provided at the connection point to the actuator and also at the load point on the specimens to prevent local distortions in the load beam. To minimize tipping restraint between the load beam and the trusses, the load was applied through knife edges that were heat treated to increase the hardness and prevent dulling of the sharp edge. To facilitate the heat treating, the steel grade for the knife edges was AISI 4130 annealed steel. The steels were precisely

machined to the proper dimensions and knife-edge shapes followed by heat treatment to increase the hardness to approximately 45-50 Rockwell hardness C. Although the knife edges allow the trusses to twist without restraint, there were concerns that the 5 inch long fixtures could result in some warping restraint if the buckled shape of the loaded truss chord was to experience a twist about the vertical axis of the truss. To minimize a potential warping restraint, thrust bearings were utilized between the knife edge and the load beam. As shown in Figure 3.11, four bolts were used to connect the knife edge assembly to the load beams; however the bolts were loose to allow the knife edge to twist and allow warping deformation in the truss chord. The loads were applied to the truss chords through 6 in. x 6 in. by 1 in. plates that were tac welded to the loaded truss chord. As a result of the hardened knife edges, the sharp edges of the fixture marked onto the steel plate and had no slip, as can be seen in Figure 3.12.

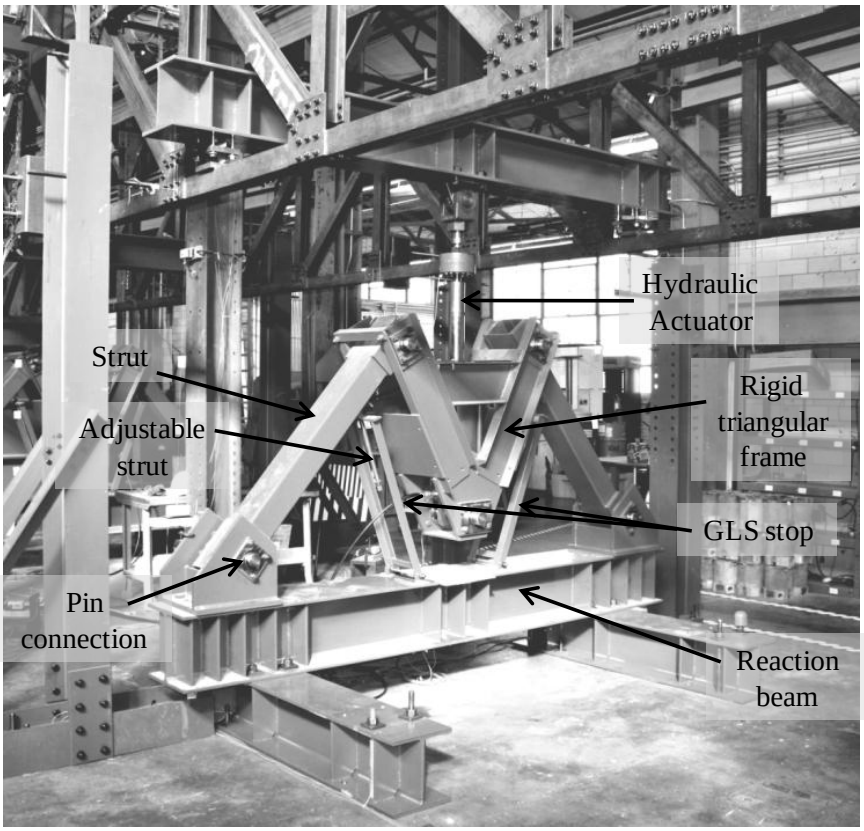

Figure 3.9 GLS in the test setup

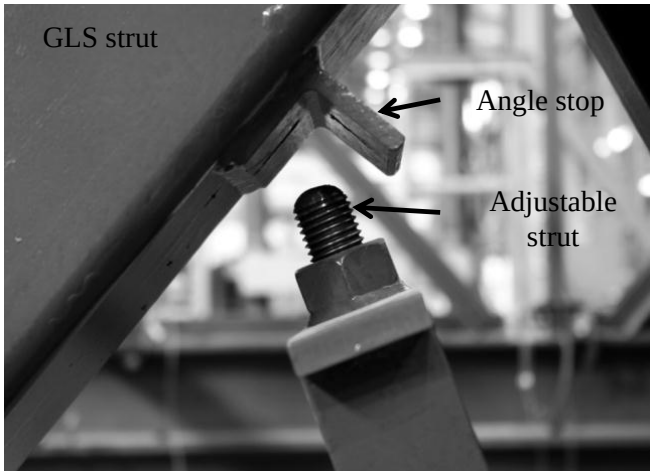

Figure 3.10 Adjustable GLS stop

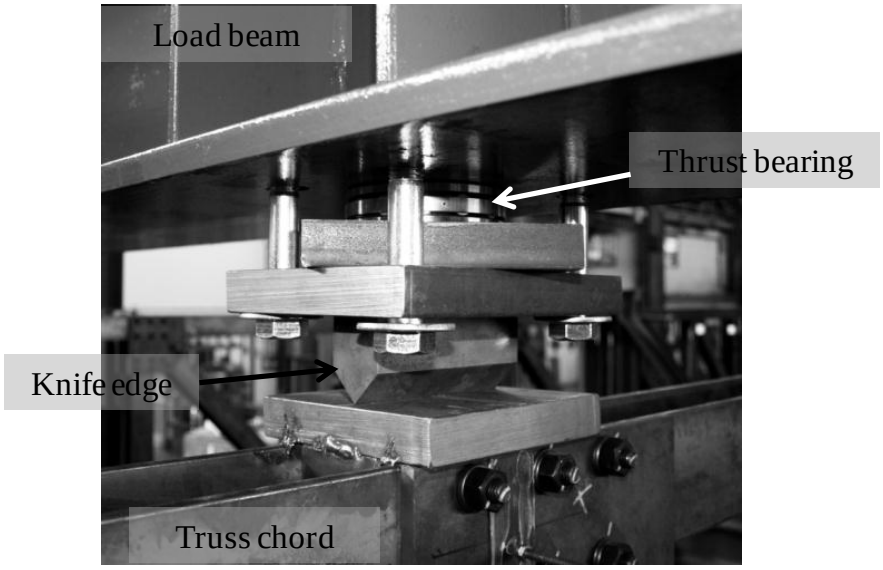

Figure 3.11 Knife edge in the test setup

Since the buckling test is sensitive to the load position and initial imperfection, the position and the alignment of the knife edges and the alignment of the loose connection bolts were checked before every test to ensure that the load were applied at the center line of the truss chords and the knife edges could rotate freely. The weight of

the load beam with 2 knife edges was 1,256 lbs, which was used in the model verification that will be discussed later.

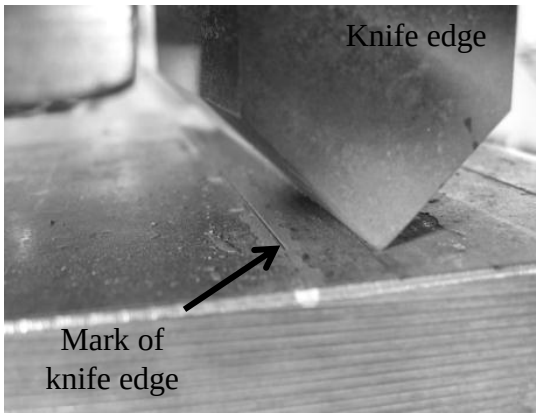

Figure 3.12 Mark of knife edge on steel plate

3.2.4 Instrumentation

Several sensors were used to monitor the truss behavior during the tests. The sensors were calibrated prior to use to ensure that the sensors functioned properly and that accurate readings were obtained. The cable to connect the sensor to the data acquisition was shielded to prevent interference from the environment. To avoid the possibility for electromagnetic interference, the instrumentation cables were arranged so as to avoid high current electric lines. The data acquisition system that was used in the tests was an HP 3852A scanner. The data was captured by the National Instruments LabVIEW program. The sensors were placed in the various locations to monitor the desired truss behavior.

Lateral movement was prevented at the top and bottom chord at the support locations. Linear potentiometers were attached to the bottom chord of the truss at the support location to ensure no lateral movement of the chord. The linear potentiometer at the support bottom chord is shown in Figure 3.13. String potentiometers were used to measure deformations at the top chord at the supports. The string potentiometers were

isolated from the test setup to provide a measurement of the absolute movement of the top chord.

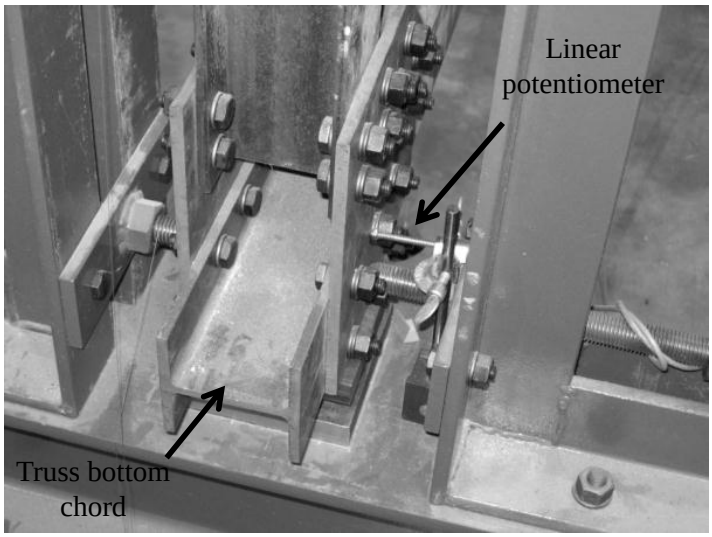

Figure 3.13 Linear potentiometer at support's bottom chord

The major instrumentation consisted of lateral and vertical deflections at various locations. A combination of linear and string potentiometers were used to capture these deflections on both top and bottom chords at both third points and midspan of the two trusses. At the location where the linear potentiometers were installed, 2"x8" glass plates were glued to the trusses to minimize friction between the linear potentiometer tip and specimen. The potentiometers were connected to a rigid frame to prevent the movement and to obtain accurate measurements. Figure 3.14 shows the linear potentiometer with the glass plate in the test setup.

Tilt sensors were used to measure the rotation of the West truss at the same locations as the lateral deflections were measured (both third points and midspan of the truss). The tilt sensors were used to measure the rotation along the depth of the truss. The sensors were attached to small pieces of wood that were clamped or glued to the truss elements. The tilt sensors were mainly located on the web of bottom chord (BC), the top chord (TC), as well as three locations along the web elements labeled bottom (BW), mid height (MW) and top (TW). Tilt sensors were also attached to other locations

to capture the rotation behavior of the truss, including the rotations of the torsional braces. Figure 3.15 shows the tilt sensor along the height of the truss cross section.

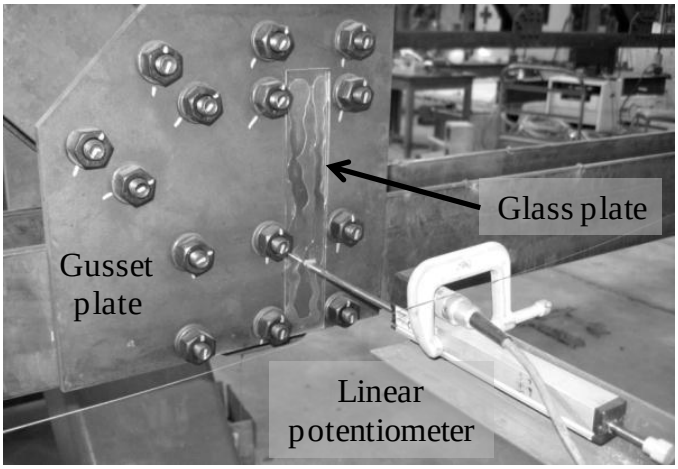

Figure 3.14 Linear potentiometer attached to steel frame and glass plate at the tip

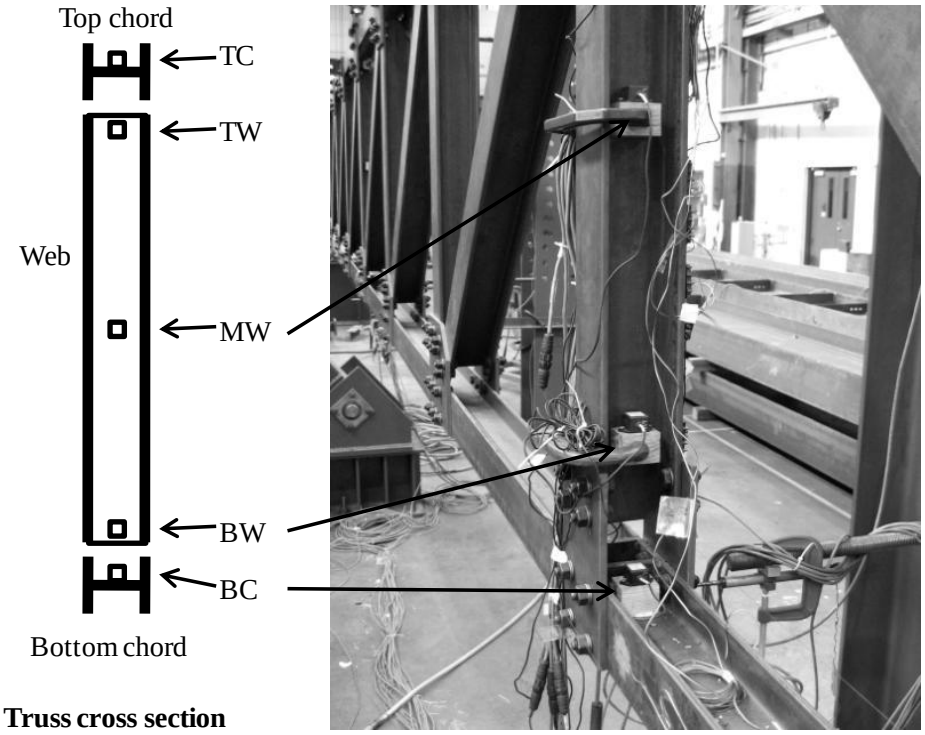

Figure 3.15 Tilt sensors across the truss height

Strain gages were used to measure the stress in the top and bottom chord of the truss during the test to provide an indicator of the point to stop the test to avoid exceeding the elastic limit of the material. The strain gages used in the tests were general purpose strain gages CEA-06-250UN-350/P2 from Vishay micro-measurements. These strain gages were temperature compensated for structural steel.

The strain gages were placed at the top and bottom chord at midspan of the West truss on both East and West sides of the chords. The strain gages were located at the center of the flanges of the W4x13 chords on the exterior surface. The strain gages were offset 5 and 10 inches from the midspan of top and bottom chords respectively to avoid the gusset plate and stress concentrations from the bolts. The strain gages were also placed on the lateral and torsional braces to provide a measure of the brace forces. For the lateral brace, two strain gages were placed on the top and bottom side in the direction of bending and between 20 and 30 inches away from the braced points to avoid the stress concentration so as to obtain a uniform stress distribution. The offset distances between the brace points and the strain gages are shown in the Table 3.1. Figure 3.16 shows the strain gages on the lateral braces. For the case of a single brace at midspan, an aluminum bar was used, while steel bars that were used for the other cases. Although aluminum was used, a strain gage compensated for steel was still used to monitor the brace force. To account for the temperature compensation, another strain gage was installed on a separate (unstressed) aluminum bar as shown in Figure 3.17 to provide a measure of the temperature effects on the gage reading. This gage provided data that could therefore be used to correct the primary gages on the brace in the event the temperature changed during the test. In general, the temperature in the laboratory was relatively constant and temperature effects were minimal.

For the torsional braces, the strain gages were placed at quarter points along the length of the braces on all 4 sides to capture the brace force. The braces were HSS tubular sections with a length of 114.5 inches. Therefore, the locations of the strain gages were 28 5/8" and 85 7/8" from the West end. The strain gages were placed on all center sides on the HSS tubes. Figure 3.18 shows the strain gages on the torsional braces.

Table 3.1 Strain gages offset distances from brace points on the lateral brace

Braces types and locations	Offset distance from the brace points (in)
Aluminum brace - major axis (K = 0.80 k/in)	30
Aluminum brace - minor axis (K = 0.20 and 0.50 k/in)	20
Steel brace HSS 2x2x1/4 (K = 0.20 and 0.50 k/in)	25
Steel brace HSS 2 1/2x2 1/2x1/4 (K = 0.80 k/in)	25

To measure the load applied by the hydraulic actuator, the 100 kip capacity load cell was placed between the actuator and the clevis before attaching to the loading beam. The raw output while there were nothing attached to the load cell were recorded and used as the reference zero value.

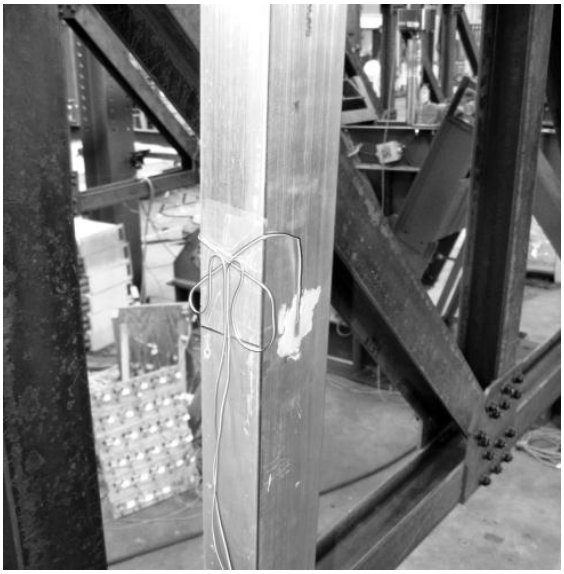

Figure 3.16 Strain gage on lateral brace

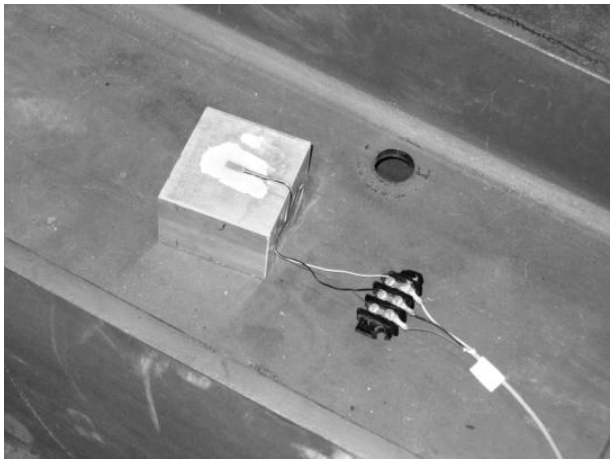

Figure 3.17 Zero reference specimen for adjusting steel strain gage on aluminum bar

Figure 3.18 Strain gages on torsional brace

3.2.5 Supports and End Conditions

The support for the twin truss needed to be high enough to accommodate the GLS and still provide enough space for the truss to be able to deflect laterally without interference in the loading system. The required heights for the respective cases with top chord loading and bottom chord loading were approximately 45 inches and 100 inches. The supports consisted of wide flange sections that were stacked upon each other. The supports were designed to minimize the number of wide flange sections to be used. The spacing of the trusses was 10 feet. The required support length was 14 feet to

accommodate the lateral braces at the supports. One W30x99 and one W12x48 were used for the support for top chord loading cases. Three W30x99 were used for the support for bottom chord loading cases. The wide flange sections were stacked on top of each other to create three layers of wide flanges for the support for the bottom chord loading cases. Stiffeners were welded to the wide flange sections at the truss support locations to reduce the web slenderness of the supporting wide flange sections. The buckling capacity of the webs of the supporting W-shapes was checked for the most severe cases to ensure that the support had adequate strength. The supports were tied to the strong floor using six 1" diameter threaded rods to ensure rigid connections at the bottom of the support. The support for the case with the bottom chord loading tests is shown in Figure 3.19. For cases with higher loads, the frame shown in Figure 3.20 was attached to one of the supports to prevent the lateral movement of the supports. The support on the other end was allowed to move freely to replicate a roller support. The movement of the support on the free end was checked by the use of spirit level to prevent excessive movement.

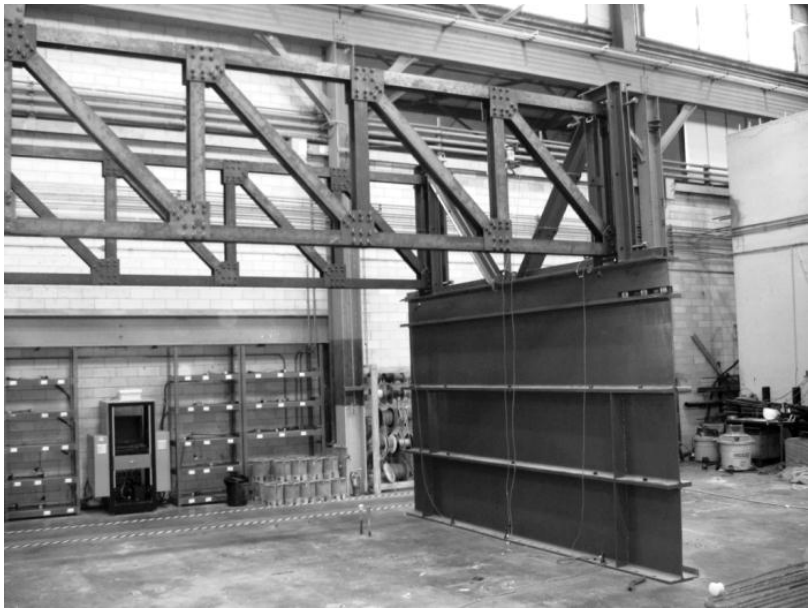

Figure 3.19 Support for the bottom chord loading case

Figure 3.20 Rigid frame attached to the support

The support details were designed to restrain lateral movement and twist of the trusses, but to allow warping deformations. The trusses were restrained at the top and bottom chords at the support using lateral restraints fabricated from L 3x3x1/2 angles and threaded rods. The frames were installed on both sides of the truss at each end. The support frames are shown in Figure 3.21. Twist was restrained at the ends by threaded rods that reacted on the top and bottom chords. The threaded rods were connected to support frames using a nut welded to the frames. The ends of the threaded rods were rounded to permit warping deformations in the top and bottom chords. One of the rounded threaded rods is shown in Figure 3.22. The threaded rods allowed adjustments to be made at the supports to plumb the trusses. The vertical alignments of the top and bottom chords were checked at locations near all supports using a plumb line to ensure the trusses were vertically aligned at the supports.

Figure 3.21 Support frames to prevent the movement of top and bottom chord at support

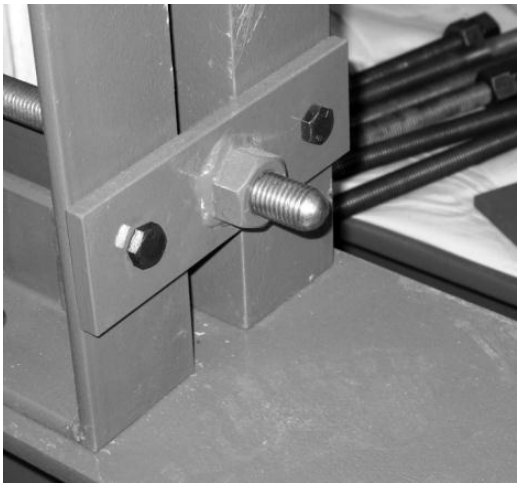

Figure 3.22 Rounded threaded rod at support

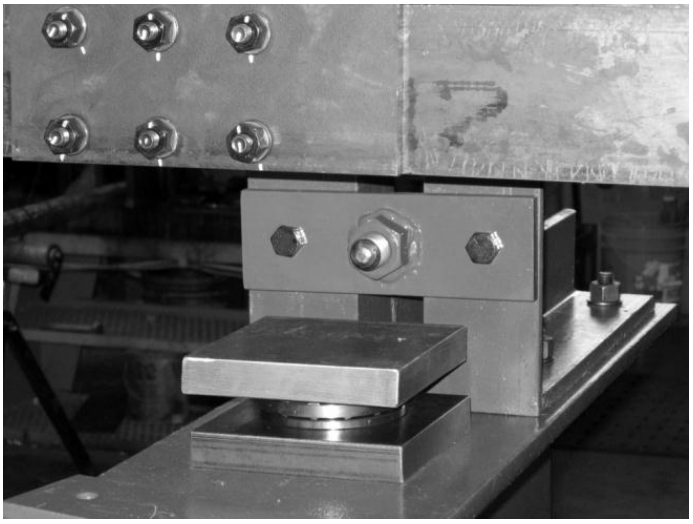

Figure 3.23 Thrust bearing and steel plate at support

Thrust bearings, as shown in Figure 3.23, were used between the bottom chords of the truss and the supports to minimize warping restraint. Pins with the diameter equal to the internal diameter of the thrust bearing were inserted into the bearing and bolted to a 1" steel plate to prevent the slip of the thrust bearing and the ring.

3.3 INITIAL IMPERFECTION MEASUREMENT

Accurate measurement of the initial imperfections was a key factor in verification of finite element analytical (FEA) models of the test setup. The initial imperfections were included into the developed FEA model to analyze the buckling behavior. The initial imperfections were measured in every test setup. The initial imperfections in the top and bottom chords along the length of the trusses on the East and West truss were measured using a taut wire and a dial caliper. The wires were run straight between the two ends of the truss. The wires were placed at the midheight position the chord. One end of the wire was tied to the support frame and the other passed over a threaded rod that served as a "pulley". A 30 lb. weight hung freely from the wire to create the tension and prevent the wires from sagging due to self weight. The wires were then checked to make sure there was no interference along the length so that the wire represented a straight line. The distance between the wire and the gusset plates was then measured at

every 8 feet at the center of the joint by using a dial caliper. The imperfections were measured on both sides of the truss and the average values were used. At each gusset plate, the imperfection reading on each side was measured 3 times and averaged. Figure 3.24 shows the taut wire on the truss for initial imperfection measurement.

Figure 3.24 Initial imperfection measurement by using dial caliper

3.4 LATERAL STIFFNESS TEST SETUP

An important aspect of the experimental tests was to obtain a measure of the effects of connection flexibility. The experimental setup for the lateral stiffness test made use of a turnbuckle to pull the trusses laterally. The turnbuckle and threaded rod passed through a hole in the web of a wide flange column and reacted on a load cell as shown in Figure 3.25. The load cells in the tests ranged in size from 1, 5 and 25 kips capacities. The turnbuckles were attached at the top or/and bottom chord at the third points of the truss. The lateral loads were applied by adjusting the turnbuckle and measuring the rod force with a load cell. The maximum lateral chord displacement was limited to 2.5 inches to ensure that the trusses remained elastic. Although most of the tests were conducted on a Howe truss, tests were also done with the truss inverted (Pratt Truss) to investigate the impact of the diagonal orientation relative to the compression chord. The

inverted truss configuration is shown in Figure 3.25. The lateral stiffness tests were done at 48 and 72-ft span in the regular (Howe truss) truss. Two cases, top chord loading with and without the lateral stop, were tested on 72-ft inverted truss.

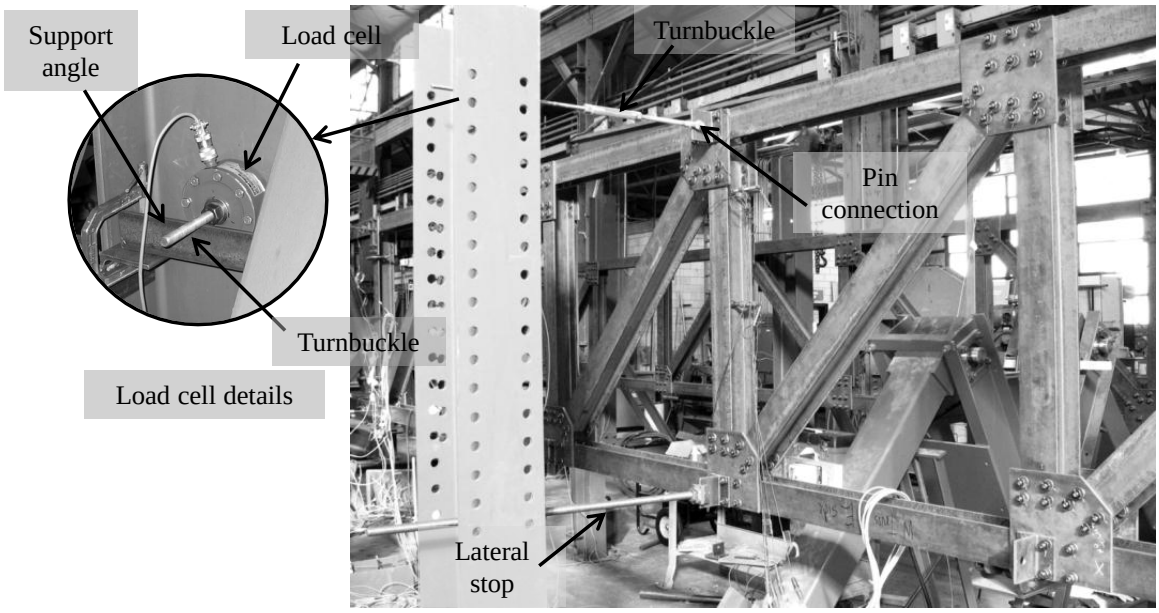

Figure 3.25 Lateral stiffness test of inverted truss

3.5 EFFECT OF LOAD POSITION

The first buckling test was conducted on the truss without intermediate bracing. Tests were conducted to investigate the impact of load position on the buckling behavior of the truss. These tests were conducted on trusses with both 48 and 72-ft spans. Figure 3.26 shows the test setup to measure the load height effect with a 48-ft span and top chord loading.

The loads were applied at 16 and 32 feet from the North support for the 48-ft span and 24 and 48 feet from North support for the 72-ft span on either top or bottom chords. For the top chord loading, the loads were applied directly at the joints through the knife edges from the loading beam. For the bottom chord loading cases, the loads were not able to be placed directly at the joint due to the obstruction of the web elements.

Therefore, the loads were applied 10" offset from the joints to the outside direction on the chord. Figure 3.27 shows the load offset for the bottom chord loading case.

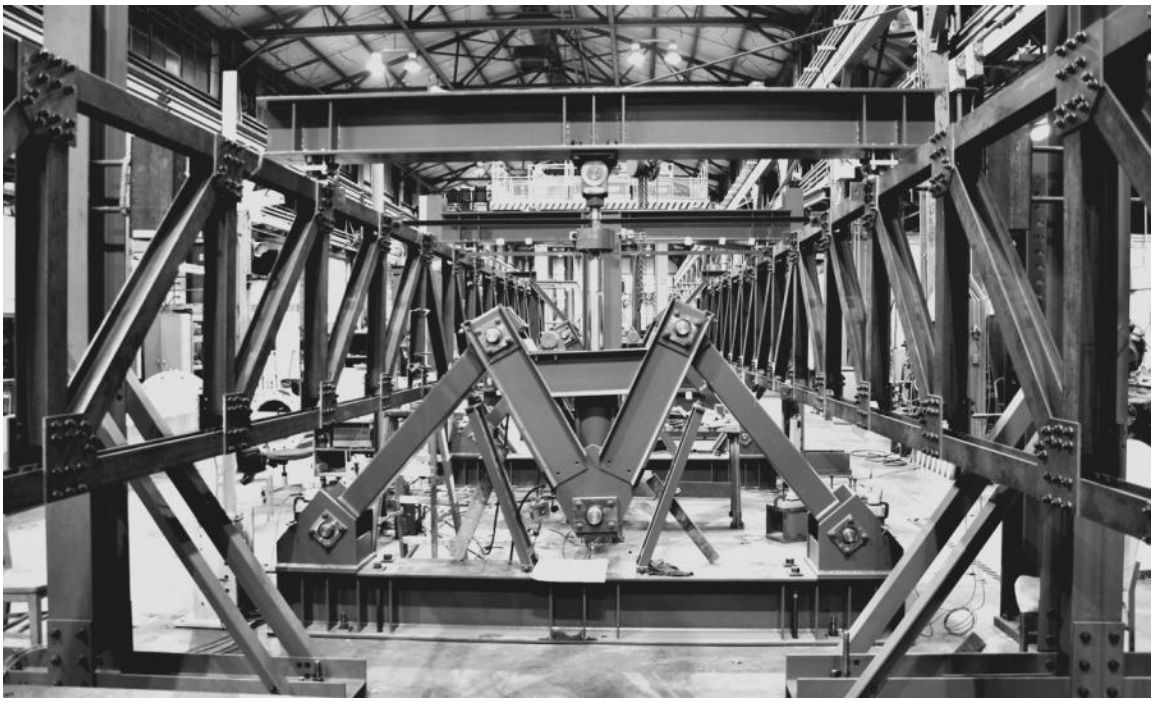

Figure 3.26 Test setup for load height effect test of 48-ft span truss

Before starting the tests, the trusses were shaken and the system stop was allowed to stop by themselves to ensure a lack of restraint. The loads were gradually applied from zero to approximately 0.5 to 1.0 kips while keeping the lateral struts engaged in the GLSs. The vibrator was then switched on. The lateral stops used to stabilize the GLSs were then released when there was some amount of load applied to the loading apparatus. After the GLS lateral stops were released, the loads were then gradually applied to the desired increment level. The vibrator was then turned off and vibrations in the system were allowed to settle for approximately 1-2 minutes before taking the measurements. Ten readings were obtained at each point and the average values were used for the data.

Figure 3.27 Bottom chord loading with 10 in. load offset from joint

3.6 TEST SETUP WITH LATERAL BRACING

The lateral brace tests were only conducted on the trusses with the 72-ft span. Configurations with either one or two braces were tested. For the case with one brace, the brace was located at midspan and attached to the truss at top chord. The truss with the lateral bracing was allowed to deflect approximately 3 inches laterally at midspan. Due to the requirements in both strength and stiffness of the brace, aluminum was used instead of the steel section for the case with a single brace at midspan. The brace was fabricated from 2"x3" ASTM B 221 grade 6160 aluminum bar. For the tests with two lateral braced points, HSS 2"x2"x1/4" were selected for the low and medium stiffness braces and HSS 2½"x2½"x1/4" for the high stiffness braces. The lateral brace geometry is depicted in Figure 3.28. The brace was connected to a rigid frame with a hinge at the bottom and by an adjustable lateral stop at a specified height. The lateral stop connected to the brace by a collar with bolts on 3 sides. The height of the lateral stop was adjustable to change the stiffness of the brace. A 2"x6"x1/4" Teflon sheet was placed at the top of the brace where the link from the truss came in as shown in Figure 3.29. One side of the

Teflon sheet was chemically etched so that the Teflon could be glued to the brace. To ensure a flat Teflon surface was achieved, the flat and stiff steel plate was placed on the expected contact surface and then C-clamps were installed every 2 inches along the length of the Teflon sheet and left in place until the glue dried. A threaded strut was used to allow the truss chord to engage the lateral brace. The threaded strut had a diameter of 1". A nut was welded to the gusset plate on the top chord to provide a connection for the threaded strut. A second nut was used with the threaded strut to provide a tight connection with the welded nut (ie. double nut connection to facilitate tightening). Two nuts were also used at the other end of the threaded strut to provide a connection to a 2"x2"x1/2" plate with bonded Teflon that would react on the 2"x6"x1/4" Teflon sheet bonded to the brace. The threaded strut was then adjusted and aligned so that the Teflon sheets from the link and from the brace were aligned in contact without bending the brace. Figure 3.30 shows the actual test setup with lateral bracing at midspan. As shown in Figure 3.31, the vertical alignment of the brace was also checked using a spirit level before starting the tests. The twin trusses were loaded at the third points on the top chord with variations of stiffness of lateral bracing. Since the lateral brace was only on one side of the twin trusses, the trusses were linked together at the brace location so that both trusses were in contact with the lateral brace. For the case with one lateral brace at midspan, double angles of 1½"x1½"x1/8" with a back–to-back connection were used to link the twin truss together at the brace point. For the truss system with two braces, the braces were located at the load points; therefore, the angle links could not be attached at the brace locations. The links were offset to the midspan side by one truss joint, which were 28 and 44-ft locations from the North support. The links were single angles.

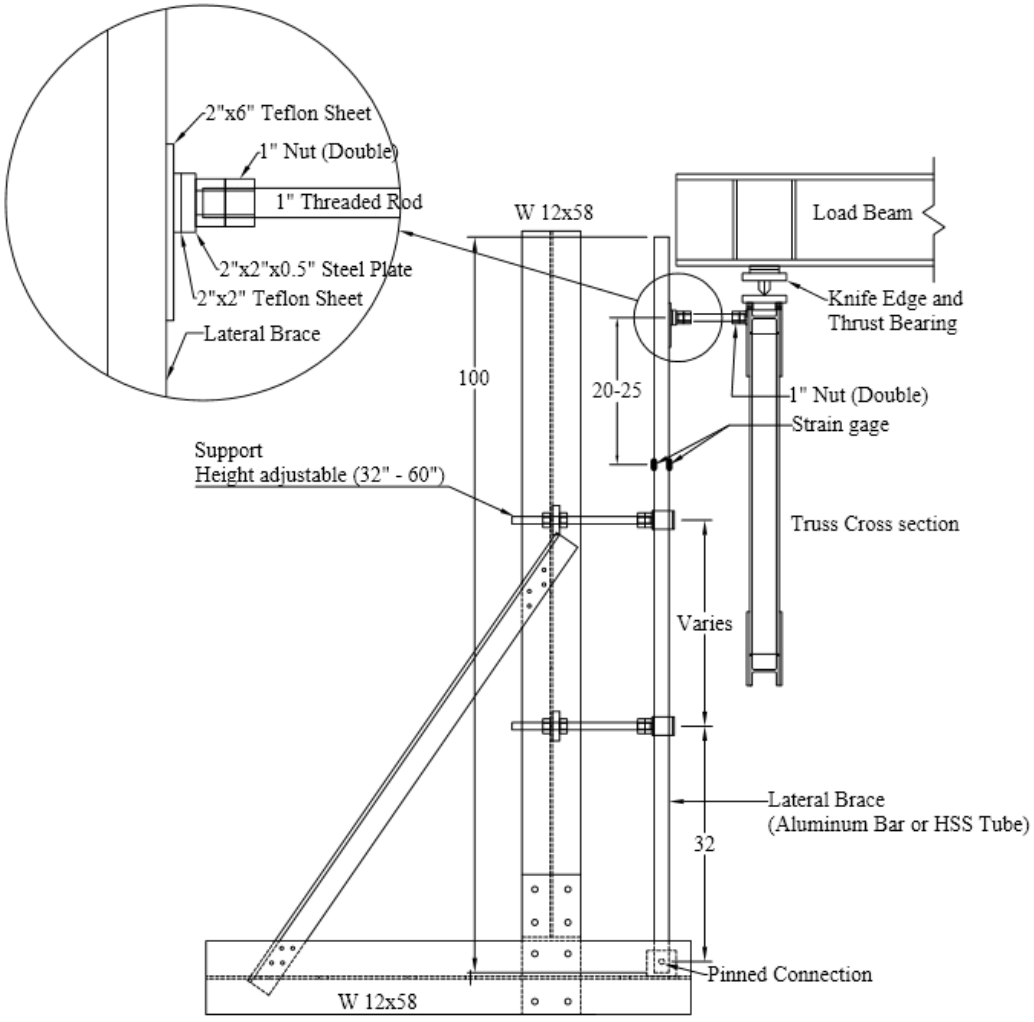

Figure 3.28 Schematic drawing of the lateral brace attached to the truss and details

Figure 3.29 Teflon sheet attached to the lateral brace

Figure 3.30 Test setup of truss with lateral bracing

3.7 TEST SETUP WITH TORSIONAL BRACING

For the tests with torsional bracing, two torsional stiffness values were used. Only the 72-ft span was used for trusses with torsional bracing. Bolted connections were used between the trusses and the braces to facilitate multiple brace configurations and positioning. The brace connections were designed to be bolted at the gusset plate locations in the truss chords. The selection of the torsional braces was limited by the bolt distances and the bolt tightening accommodation. HSS 3"x2½"x1/4" was selected for the low stiffness braces and HSS 5"x2½"x1/4" for the high stiffness braces. The braces were attached to the trusses by fully-tightened bolted connections. Efforts were made to create a relatively rigid connection between the trusses and the braces. The connection plates are shown in Figure 3.32 in which ½" side plates were welded to a ¾" thick end plate that was then bolted to the gusset plate connection. The end plates on both sides were installed during the welding process so that they were parallel. This type of connection was relatively rigid and provided both torsional and warping restraints to the truss chords. Figure 3.33 shows the brace installation to the truss. The setup for the test with torsional braces connected to the bottom chord is shown in Figure 3.34. The torsional braces were attached to the trusses at various locations as noted in Table 3.2.

Figure 3.31 Checking of lateral brace vertical alignment

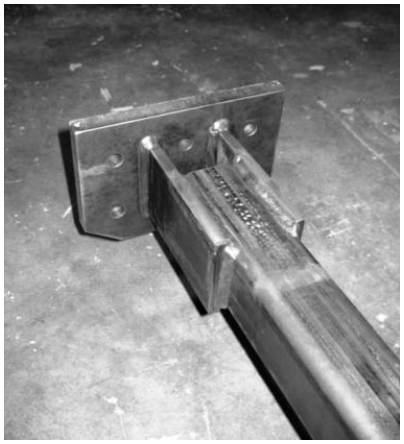

Figure 3.32 Torsional brace with connection plate

Figure 3.33 Installation of large torsional braces at bottom chord

Table 3.2 Torsional brace locations

Number of braces	Brace locations (ft from North support)	
	Pony and Bottom chord cases	Top chord cases
1	36	-
2	24, 48	20, 52
3	24, 36, 48	20, 36, 52

During the initial tests, significant cross section distortion occurred in the wide flange chord in the joints where the torsional braces were connected. The distortions were small and not discernable by eye; however, the effect on the buckling capacity was significant. To prevent the cross section distorsion at the brace points, stiffeners were added to the torsional brace joints between the bolts as shown in Figure 3.35. Two 3¼"x½" stiffeners for each side which resulted in a total of four stiffeners per joint. The stiffeners were welded to the flange and web of the wide flange chord sections.

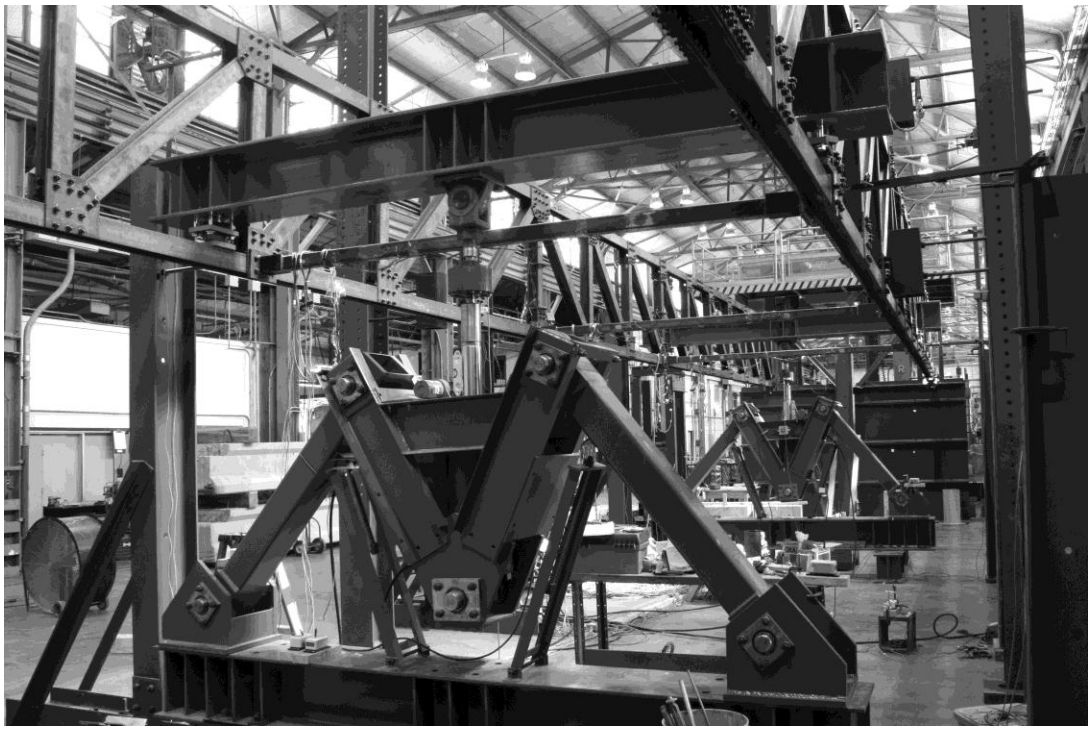

Figure 3.34 Test setup of truss with 3 small torsional braces at bottom chord

In addition to tests with lateral restraints at the supports on both top and bottom chords, torsional bracing tests were also conducted using boundary conditions similar to a pony truss in which the top chord was free to displace laterally. The test setup of the pony truss was very similar to that of the regular truss. However, the rounded threaded rods at the top chord at the supports were removed from contacting the trusses. This allowed the top chord of the truss to move laterally with the only restraint coming from the truss vertical. Figure 3.36 shows the support frame with the threaded rod not in contact for the pony truss setup.

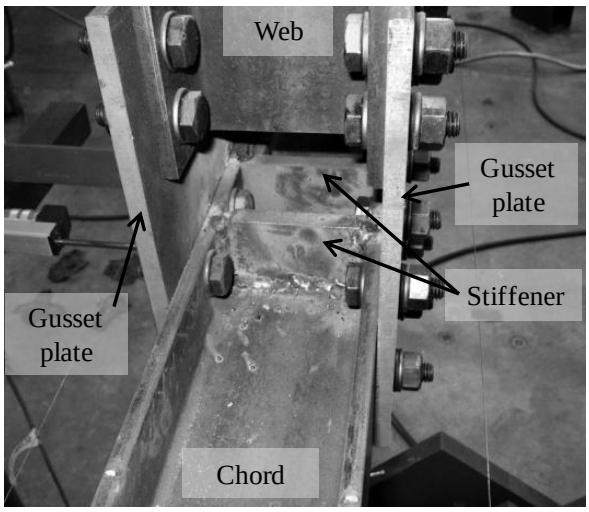

Figure 3.35 Adding the stiffener to the torsional brace connection joint

Trusses with torsional bracing were also tested with 0.5 and 1 inch load offsets to replicate the same truss with different initial imperfections. The test setup was the same as the truss outlined previously in the chapter except that the knife edges were offset to the East side for 0.5 and 1 inch. Figure 3.37 shows the load offset for the truss with torsional bracing test.

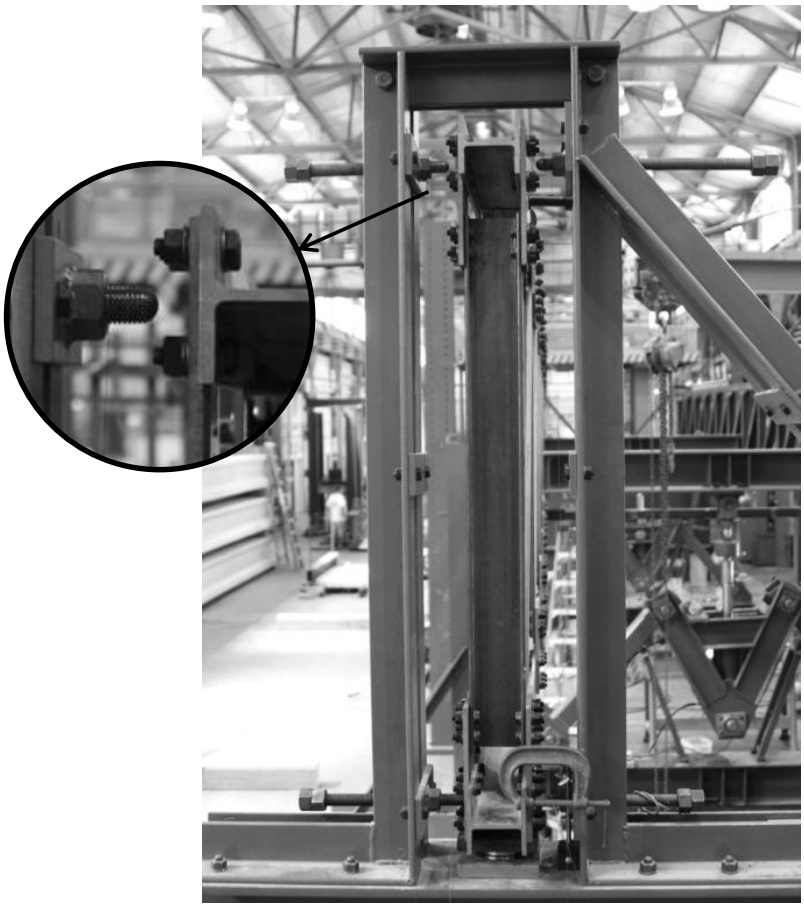

Figure 3.36 Top chord support's threaded rod backed up for pony truss test

Figure 3.37 Half inch load offset by offsetting the knife edge to the East side

CHAPTER 4
Experimental Test Results

4.1 INTRODUCTION

An overview of the experimental test setup was provided in Chapter 3. The data that were gathered on each setup consisted of the measurements of the initial imperfections in the specimen, lateral stiffness tests, and several buckling tests with a variety of bracing scenarios. This chapter provides an overview of each of the different measurements that were taken. The data recorded from the initial imperfection measurements are presented first followed by the results from the lateral stiffness tests. Finally, results from the buckling tests are presented including cases with and without bracing.

4.2 INITIAL IMPERFECTION

Obtaining accurate measurements of the initial imperfections is an important step in achieving accurate geometry for the finite element modeling. Since the test results provide validation data for the FEA model, care was taken in measuring the magnitude and distribution of the imperfections. The trusses used in the test had relatively low out-of-plane stiffness and therefore the buckling and bracing behavior is very sensitive to the magnitude and shape of the initial imperfection. Obtaining accurate and repeatable measurements of the initial imperfection was therefore a crucial step in the testing process.

The initial imperfections were measured in every test setup. For the 48-ft support span, the initial imperfections were only measured for the portions of the 72-ft long trusses that were between the supports. The 12-ft overhang parts on each side were neglected. The initial imperfections were measured every 8 feet along the truss length to coincide with the panel points of the truss. The imperfections at the brace locations and

at midspan were also measured. The imperfections were measured on the East and West sides of each truss chord and an average value was used for the chord. Using the average of the two readings eliminated local inconsistencies in the chord geometry or plate thicknesses. Figure 4.1 and Figure 4.2 show the respective initial imperfections that were measured for the East and West trusses with the 48-ft span for the bottom chord loading case. Initial imperfections for the same bottom load case with 72-ft span truss are shown in Figure 4.3 and Figure 4.4. Generally, the strength requirement for the brace was developed based on the assumed $L_b/500$ initial imperfection which corresponds to 1.15 in. and 1.73 in. for the respective cases of the 48 and 72-ft span trusses. The measured initial imperfections were generally significantly less than the limit. There was generally variability between both the magnitude and shape of the imperfections from test to test. These initial imperfections were important in the analysis to verify the FEA model. The initial imperfections were input into the FEA model so that the computational results could be compared to the experimental test results. The results shown below are representative of the typical measurements that were taken of the test specimen. Additional initial imperfection measurements used for the FEA model verification are provided in Chapter 5 and Appendix A.

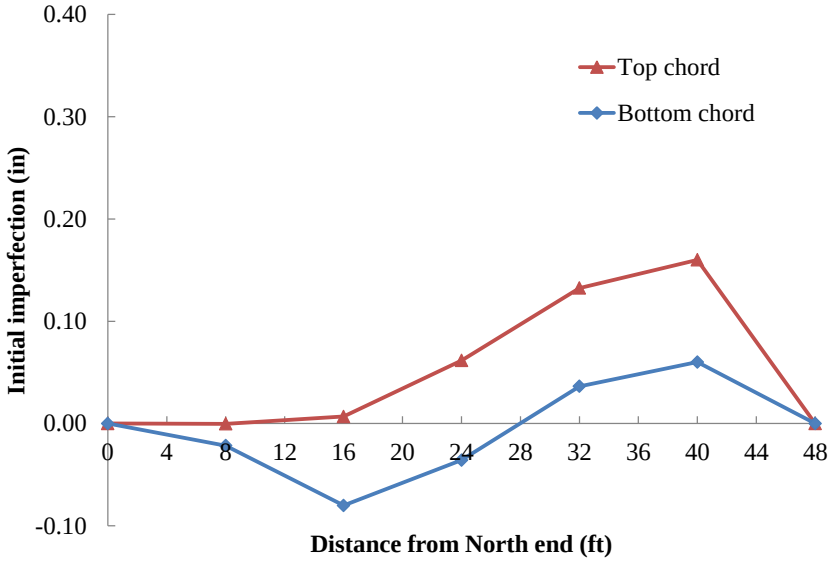

Figure 4.1 Initial imperfection of the 48-ft span East truss - Bottom chord loading

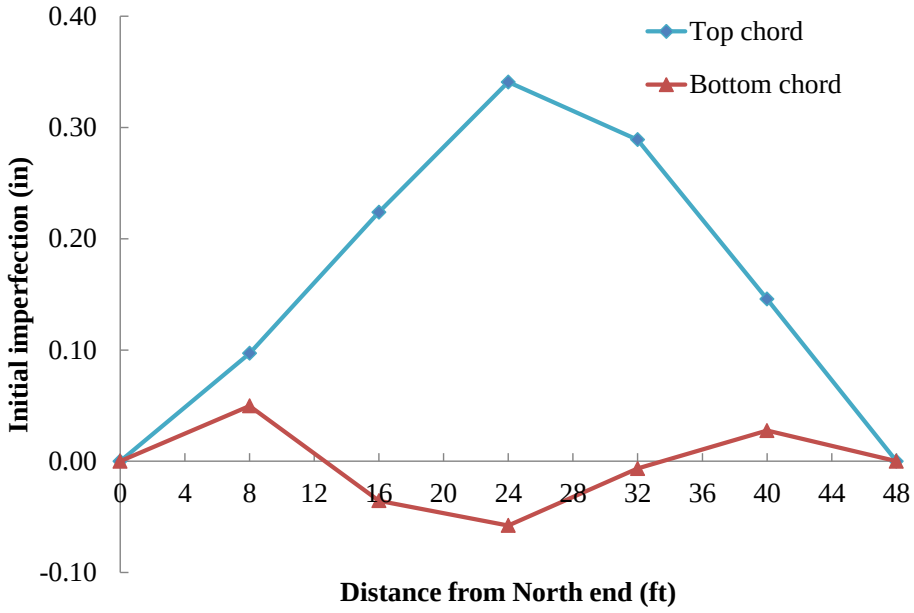

Figure 4.2 Initial imperfection of the 48-ft span West truss - Bottom chord loading

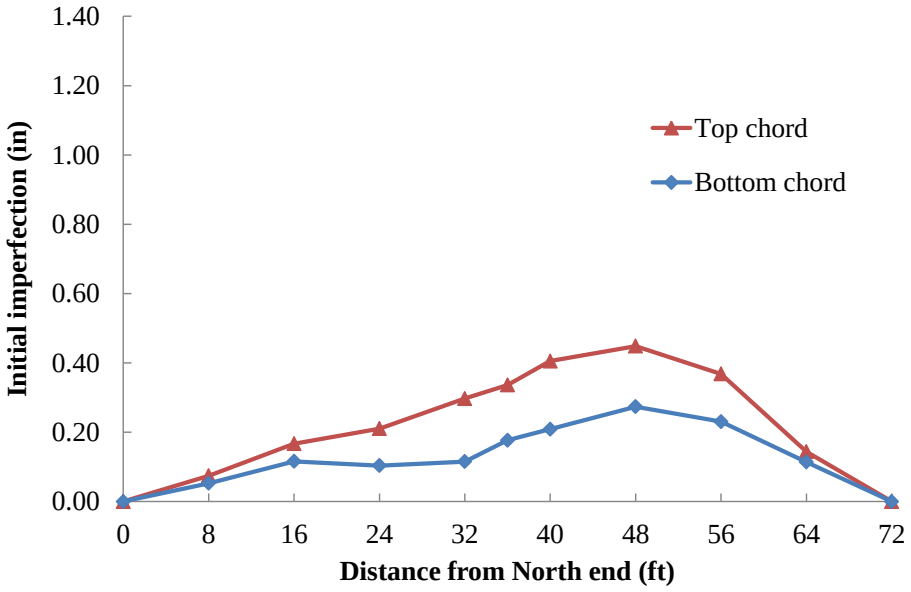

Figure 4.3 Initial imperfection of the 72-ft span East truss - Bottom chord loading

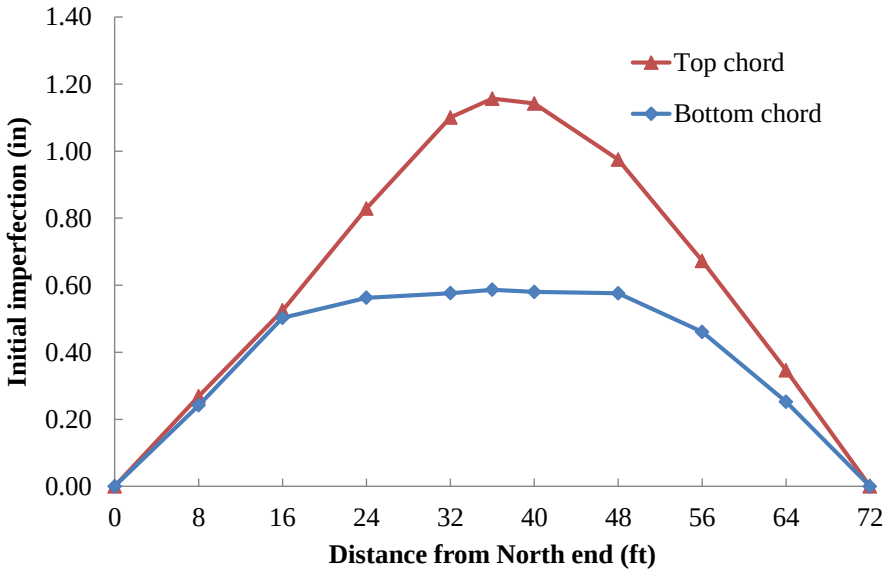

Figure 4.4 Initial imperfection of the 72-ft span West truss - Bottom chord loading

4.3 LATERAL STIFFNESS TEST

The lateral stiffness tests were done on both the 48-ft and 72-ft span trusses with a variety of loading conditions. The tests were done to ensure that accurate models of both the members and joints were used in the finite element analyses. Measurements of both the lateral and torsional stiffness of the trusses were therefore desired. To accomplish these tests the loads were applied at the top and/or bottom chord of the West truss. Tests that were conducted with no lateral restraints between the supports are referred to as Lateral Unrestrained Trusses. To increase the torsional deformation in the truss, cases were considered in which a lateral stop was placed on the chord without the lateral load as shown previously in Figure 3.22. Tests in which the un-loaded truss chord was restrained from movement are referred to as the Lateral Restrained Trusses. For the 72-ft span, tests were conducted with the Howe truss configuration and also by inverting the truss to form a Pratt truss. The two different orientations of the same truss provide measurements to help improve the understanding on the impact of the orientation of the

diagonal and nature of the state of stress (compression or tension) in the truss members on the lateral stiffness behavior.

4.3.1 Laterally Unrestrained Trusses

Figure 4.5 and Figure 4.6 show the relationship of the lateral load and lateral deflection of the unrestrained 72-ft trusses with the load positioned at the top chord and bottom chord, respectively. The lateral loads were applied at the third points (24 feet from the two supports). The midspan lateral deflection of the loaded chord is graphed on the X-axis, while the applied load is graphed on the Y-axis. Although the applied third point loads were nearly identical, there was a small variation in the load magnitude and therefore the average load is graphed. The lateral deflection behavior of the top and bottom chord loading was generally the same in the 48-ft span truss, and the results are provided in Appendix A. For the case of top chord lateral loading, the top chord deflected more than the bottom chord, which is expected. With the load applied at the top chord, some of the load is transferred to the bottom chord through the web elements. Therefore, the bottom chord helps transfer some of the force to the supports.

In contrast to the top chord lateral loading, for the bottom chord loading case, the top chord still deflected more than the bottom chord. There are primarily two factors that might contribute to the difference in behavior for the top and bottom chord loading cases: 1) Orientation of the web diagonals, and 2) The stiffness of the respective truss chords.

For the Howe truss, with the lateral load applied at Point B at the top chord of the truss, Figure 4.7, the diagonals point outward toward the supports. When the load was applied at Point B at the bottom chord, the diagonals point inward toward midspan.

The other factor affecting the truss behavior is the chord stiffness. Since the chord sizes were the same, the primary difference in stiffness is the effects of compressive stress in the top chord due to self weight of the truss. As the compressive stress approaches the buckling capacity of a member, the stiffness in that member reduces. Tensile stresses on the other hand tend to increase the stiffness of the member. Therefore, the self-weight of the trusses results in a decrease in the stiffness of the top

chord and an increase in the stiffness of the bottom chord due to the compression and tension in these respective chords.

The chord stiffness may also be affected by the diagonal alignment. The effect of the diagonal alignment can be explained by considering the distribution of the applied load to the chords, Figure 4.7. Although the load was applied either at the top or bottom chord, because the web members have some connection restraint they provide some load transfer to the opposing chord. The load that is transferred through the opposite chord through the vertical web from the applied load F is labeled as F_1. The load, F_2, is the load that gets transferred through the diagonal to the opposing chord. Because of the flexibility in the members and joints, in general, $F_2<F_1$. For the bottom chord loading case, the diagonal distributes some of the load, F_2, towards the middle of the truss since the diagonal at the loaded joint is oriented towards midspan. For top chord loading, the diagonal transmits some of the load, F_2, to the joint closer to the support since the diagonal slants in that direction. In general, transmitting the load towards the midspan will result in a lower lateral stiffness of the truss due to the increased flexibility of the truss system at nodes further from the supports. Therefore, the diagonal orientation, combined with the lower stiffness of the top chord due to the compression is likely responsible for the larger deformation of the top chord when the load is applied at the bottom chord. However, to confirm this behavior, tests were conducted on the inverted (Pratt) truss so that the diagonal orientation was reversed.

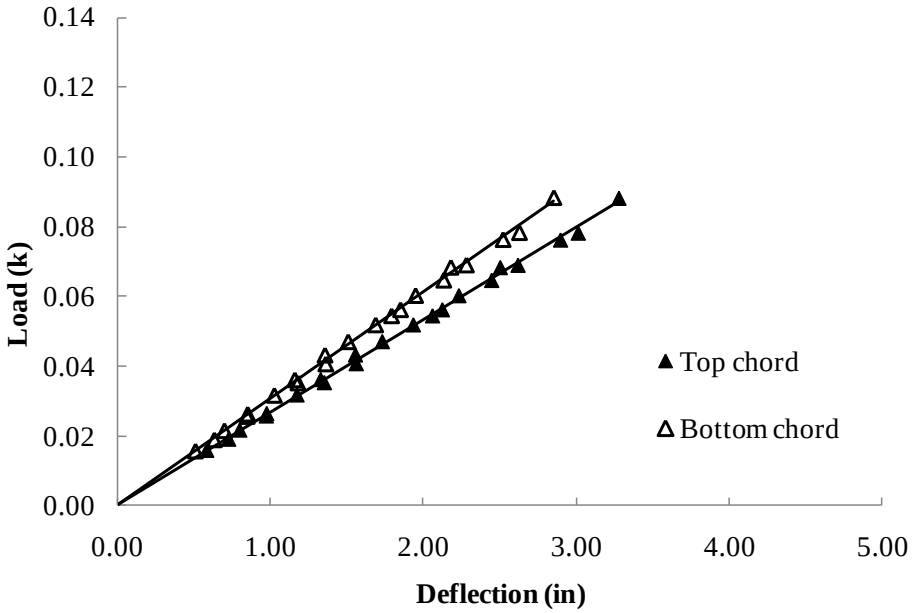

Figure 4.5 Lateral deflection at midspan of 72-ft regular truss - Top chord loading

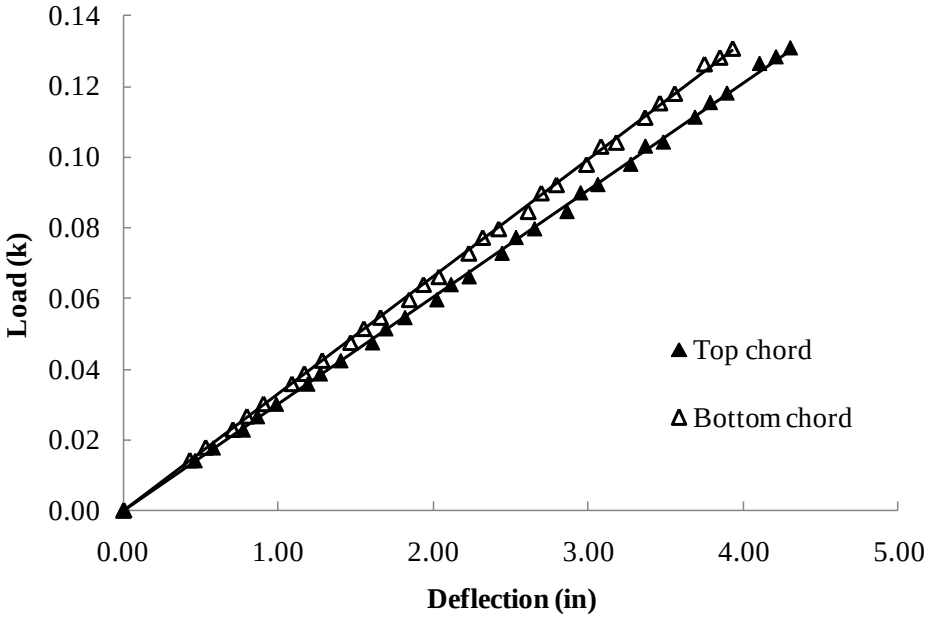

Figure 4.6 Lateral deflection at midspan of 72-ft regular truss - Bottom chord loading

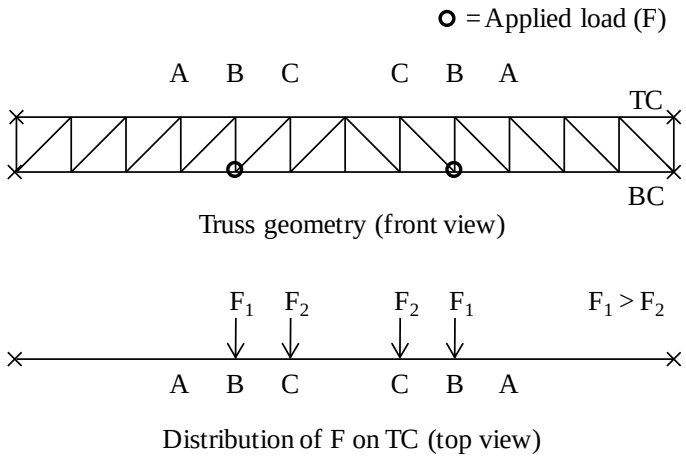

A) Bottom chord lateral loading

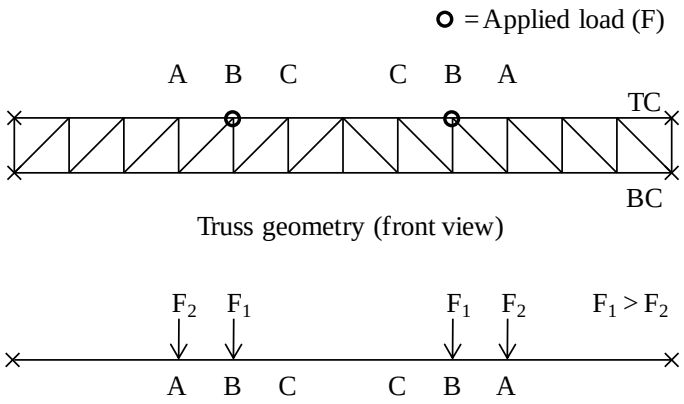

B) Top chord lateral loading

Figure 4.7 Force distribution in unloaded chord

The lateral deflections at midspan of the inverted truss (Pratt Truss) with top chord and bottom chord loading at the third points compared to the regular truss at the same load locations are shown in Figure 4.8 and Figure 4.9. The inverted truss was stiffer than the regular truss in both load cases. For the top chord loading case, the lateral deflections at midspan of the top and bottom chords were similar while the lateral deflections on top chord were slightly higher than the bottom chord at the third point locations. The results of the bottom chord loading cases show that the bottom chord

deflected slightly higher than top chord at midspan while the top and bottom chords deflected the same amount at the third points. Based upon the comparisons between the two truss orientations, the diagonal orientation has a significant effect on the stiffness of the trusses. The Pratt trusses (diagonals slant towards the support) tend to be stiffer with than the Howe truss since the diagonals direct the load towards the support.

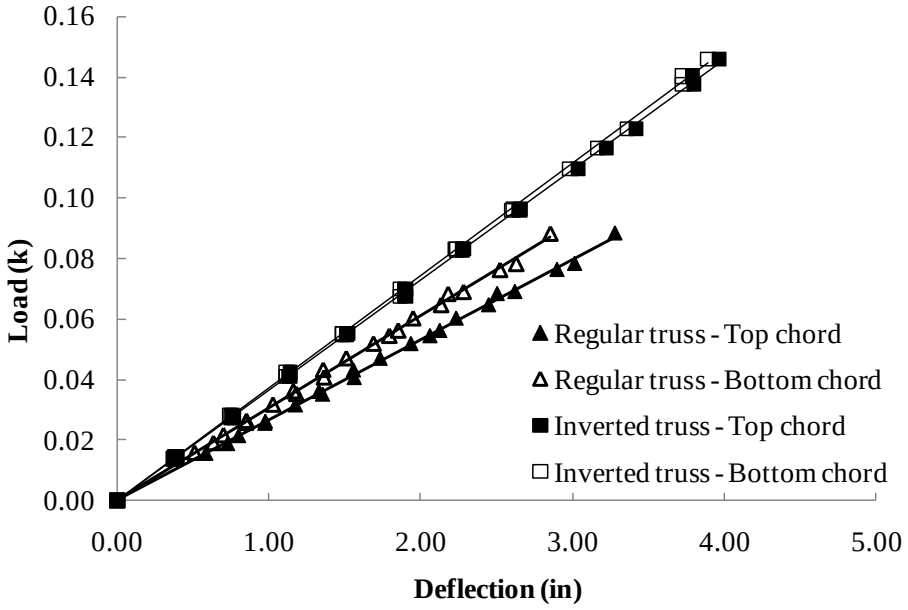

Figure 4.8 Lateral deflection at midspan of 72-ft inverted truss - Top chord loading

4.3.2 Laterally Restrained Trusses

To obtain a different condition for measuring the torsional stiffness of the trusses, lateral stops were added to the unloaded chord at the turnbuckle locations. Graphs of the applied load versus the lateral deformation for the cases of the 72-ft span truss with top chord loading and bottom chord restrained and with bottom chord loading and top chord restrained are shown in Figure 4.10 and Figure 4.11, respectively. Additional results for the inverted truss and the 48-ft span truss are provided in Appendix A. Comparing the behavior with the cases of no lateral restraint shows that the required load to achieve the same lateral deformation was more than 10 times higher with the lateral restraints, which

is expected since the torsional stiffness of the truss increases significantly with the inclusion of the lateral stops.

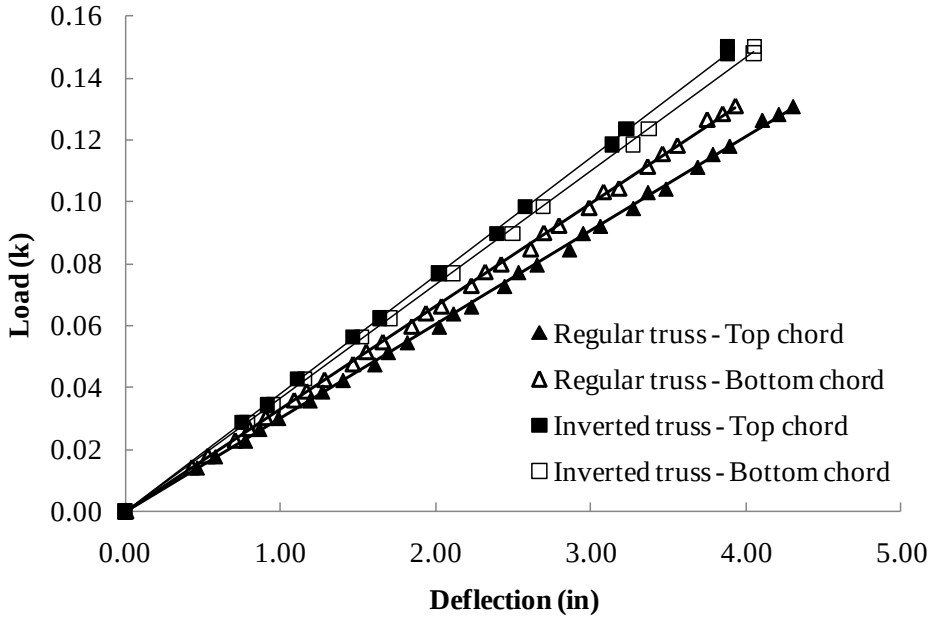

Figure 4.9 Lateral deflection at midspan of 72-ft inverted truss - Bottom chord loading

The top chord lateral deflection (loaded chord) at 24, 36 and 48 feet along the truss length were almost the same and the bottom chord (restrained chord) midspan deflected in the opposite direction in top chord loading case. In contrast, for the bottom chord loading case, the midspan of the top chord (restrained chord) deflected in the same direction of the applied load and the midspan of the bottom chord (loaded chord) deflected more than the third point. The results of the cases with the inverted (Pratt) truss exhibited similar behavior except that the bottom chord of the regular (Howe) truss behaved similar to top chord of the inverted (Pratt) truss and vice versa, which is consistent to the geometry of the truss. The results for the inverted (Pratt) truss are provided in Appendix A.

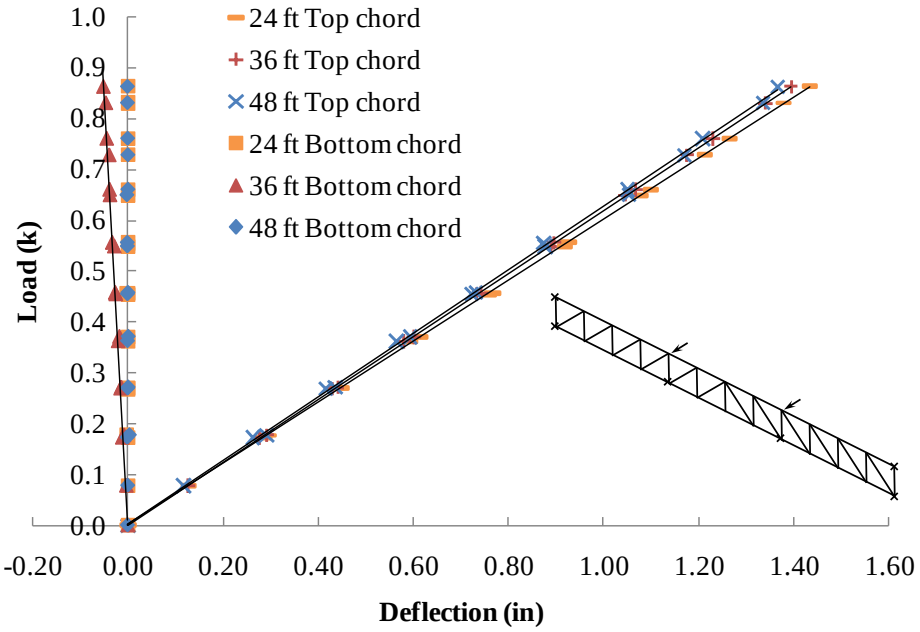

Figure 4.10 Lateral deflection of 72-ft regular truss - Top chord loading and bottom chord restrained

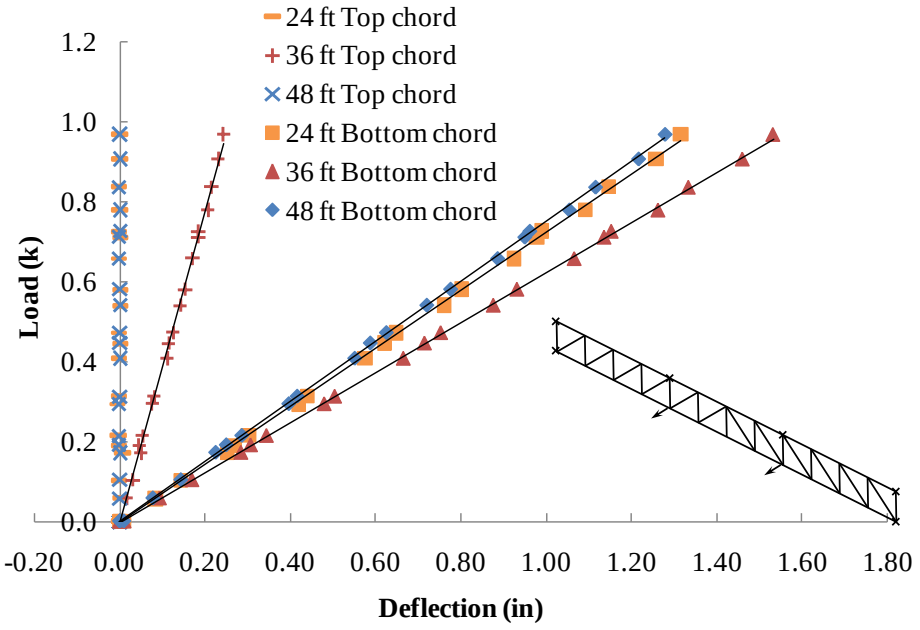

Figure 4.11 Lateral deflection of 72-ft regular truss - Bottom chord loading and top chord restrained

4.4 BUCKLING TEST OF TRUSS WITHOUT INTERMEDIATE BRACING

Several series of buckling tests were done on the trusses without intermediate bracing. These tests were conducted on trusses with 48 and 72-ft spans. The loads positions that were considered on the cross section consisted of top chord and bottom chord loading. The total amount of lateral deformation and maximum chord stress were limited so that the trusses remained elastic during tests. Southwell plots were used to estimate the buckling capacity and initial imperfection of the truss. The imperfections from the Southwell plots provided supplementary imperfection information to the magnitudes and distributions that were measured prior to the tests.

4.4.1 Lateral Deflection

The lateral deflection from the buckling tests of the 72-ft span truss with the respective cases of top chord loading and bottom chord loading are shown in Figure 4.12 and Figure 4.13. Data for the displacements at the third points and midspan are provided. The buckling capacities from the eigenvalue buckling analyses of the trusses are also shown in the graphs by the straight dashed lines to indicate the capacities of the trusses. The results for the 48-ft span were also similar and are provided in Appendix A. The lateral deflection which was limited to maximum values of approximately 3.0 inches is graphed on the X-axis. The summation of load applied to the single truss at the third points is graphed on the Y-axis. The lateral displacement data that is graphed provides an indication of both the lateral translation and cross section twist. The measure of the twist is provided since the top chord deflected more than the bottom chord. Since the gravity load simulators (GLS) are not stable for low magnitudes of the load imposed through the mechanism, the lateral stops of the GLS were left in place until sufficient load levels were reached. Since the lateral stops prevented lateral deformation of the load points, the graphs are not smooth for the first few data points. The lateral deflections of the 72-ft. span trusses were more sensitive to support conditions and load application than the 48-ft. span trusses since the longer trusses were much more flexible. The slope of the load

versus deformation curves decrease substantially with increasing load level, as is expected in buckling problems.

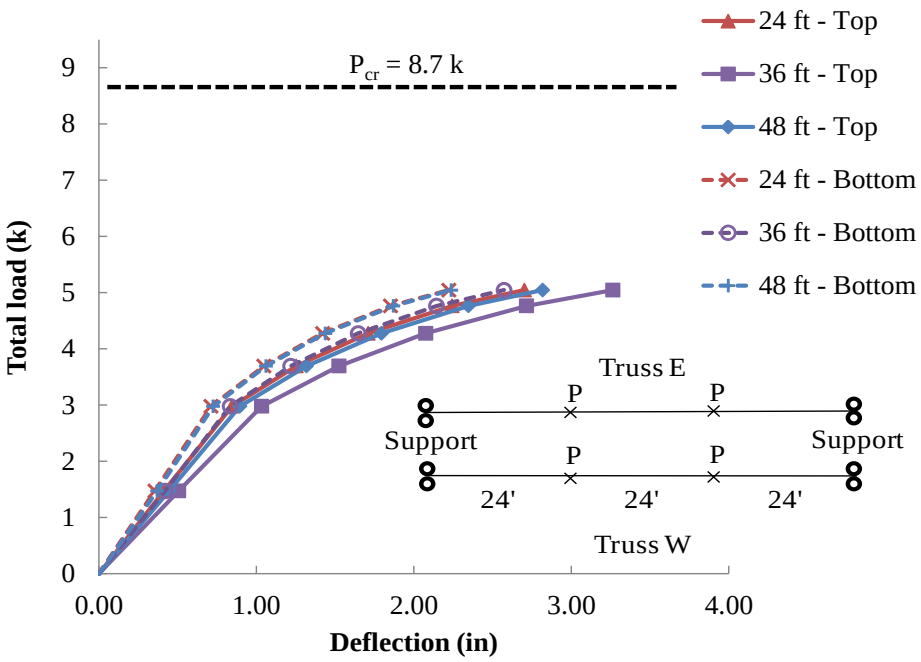

Figure 4.12 Lateral deflection of 72-ft truss - Top chord loading

4.4.2 Strain at Midspan

Top (TC) and bottom (BC) chord strains near midspan of the West truss are plotted in Figure 4.14. Strains were measured on both the East (E) and West (W) side of the chords so that lateral bending stresses could be accounted for in addition to axial strains. The strains were positive on the bottom chord due to the tension force on the chord. The top chord was under compression which is indicted by negative values of the strain. The strains from first two readings up to 3 kips were almost linear due to the low chord axial force and lateral displacement. The strains then diverted from each other at the same chord. The strain at the top chord on the East side was almost back to zero at the end of the test. As the total load increased and approached the buckling capacity, the strains changed rapidly for small increases in the applied load due to the larger lateral deflections.

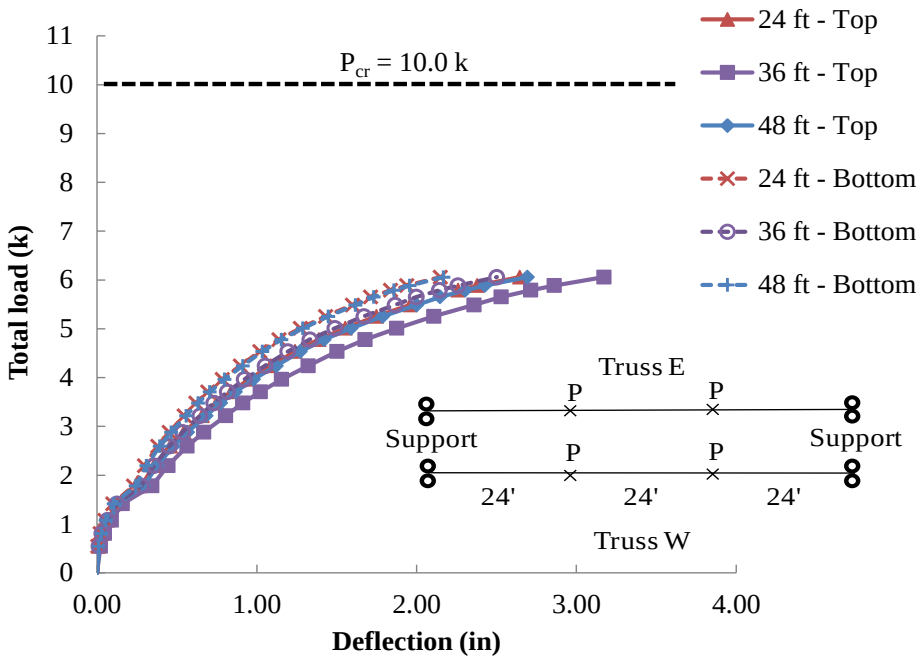

Figure 4.13 Lateral deflection of 72-ft truss - Bottom chord loading

Theoretically, the strain on the same chord in the East and West sides are the same for the in-plane bending. Secondary effects due to lateral deflection of the truss chords contributed some strains in the chord. In general for columns, the contribution of the axial force and secondary effect to the stress can be calculated using the following expression:

$$\sigma = \pm\frac{P}{A} \pm \frac{MC}{I} = \pm\frac{P}{A} \pm \frac{Pey}{I} \qquad (4\text{-}1)$$

Equation (4-1) is intended to be used for the case of constant axial force acting throughout the column length. Since the trusses were not subjected to uniform bending, the axial force in the simply-supported trusses varied along length from the smallest at the panels next to the supports to the maximum at the panels near midspan.

According to the Equation (4-1), the stresses in the chord were broken down into 2 parts, axial and bending stress components. The absolute values of stress components for each part are shown in Figure 4.15. The axial forces in the top and bottom chords

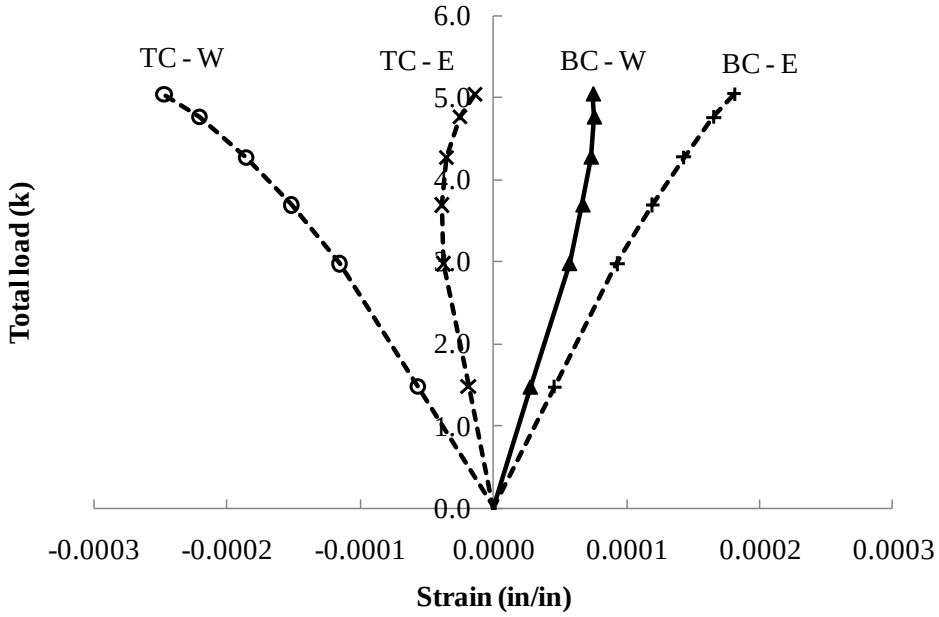

Figure 4.14 Strain at midspan of the 72-ft truss - Top chord loading

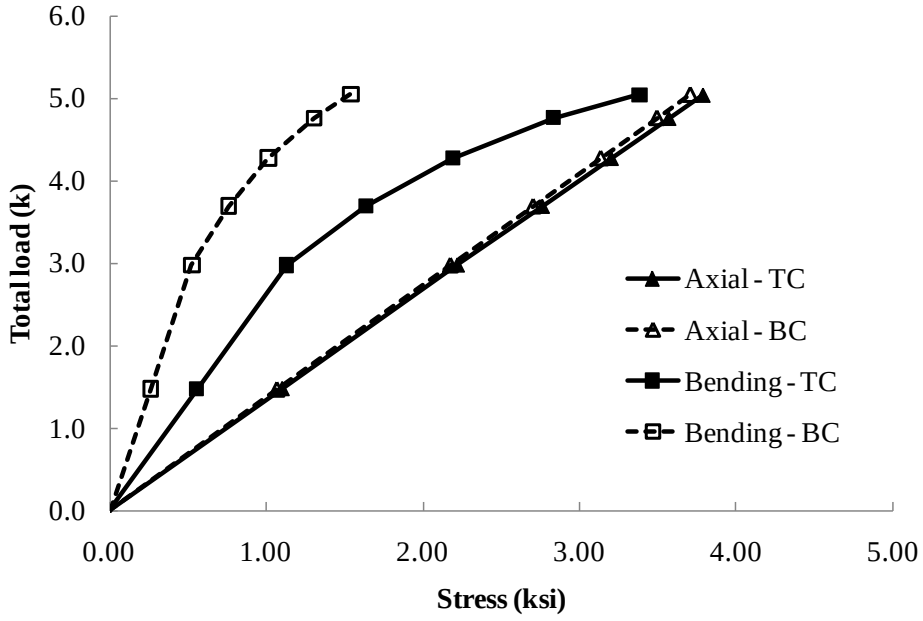

Figure 4.15 Stress components at midspan of the 72-ft truss - Top chord loading

were similar in magnitude except that top chord was subjected to axial compression and bottom chord was subjected to axial tension. Within a given panel, the difference in the magnitude of the axial force component between top and bottom chord was carried by the diagonal web element, which was minimal at midspan panel for this load pattern. The stress from the bending component was almost linear for low load levels and tended to increase at a faster rate as the load approached the buckling capacity. The magnitudes of the stresses from the bending component are graphed with the lateral deflection in Figure 4.16. The stresses measured in the top and bottom chords are graphed versus the lateral deflection of the respective chord. The relationship of the stress from the bending component with the lateral deflection is linear.

Chord stresses from the bending component were plotted with the expected stress from the bending component from the column formula given by Eq. (4-1) in Figure 4.17. It can be seen that the stress from test results were less than the calculation. This was due to the non-uniform axial force in the chord and also the restraint that might come from the vertical and diagonal. It can be concluded that stress in the truss chord cannot be calculated by using equation for column; however, the stress from bending component is directly relate to the lateral deflection of the truss.

4.4.3 Vertical Deflection

The measured results of the vertical deflection at 24 and 36 feet of the 72-ft span truss with top chord loading are shown in Figure 4.18. The vertical deflection at midspan (36 feet) was measured by using a string potentiometer while the deflection at 24 feet was measured by using a spring potentiometer. The vertical deflections were linear. Besides deflecting down, the trusses also deflected laterally, which has an additional effect on the deformation measured by the string potentiometer. Although this additional lateral deformation can affect the accuracy of the measurement (particularly at loads near the bucking capacity), the string potentiometer is easier to mount to the support especially for the bottom chord loading where the trusses were elevated more than 100 inches above the ground. Using longer string lengths reduces the impact of the lateral deformation on

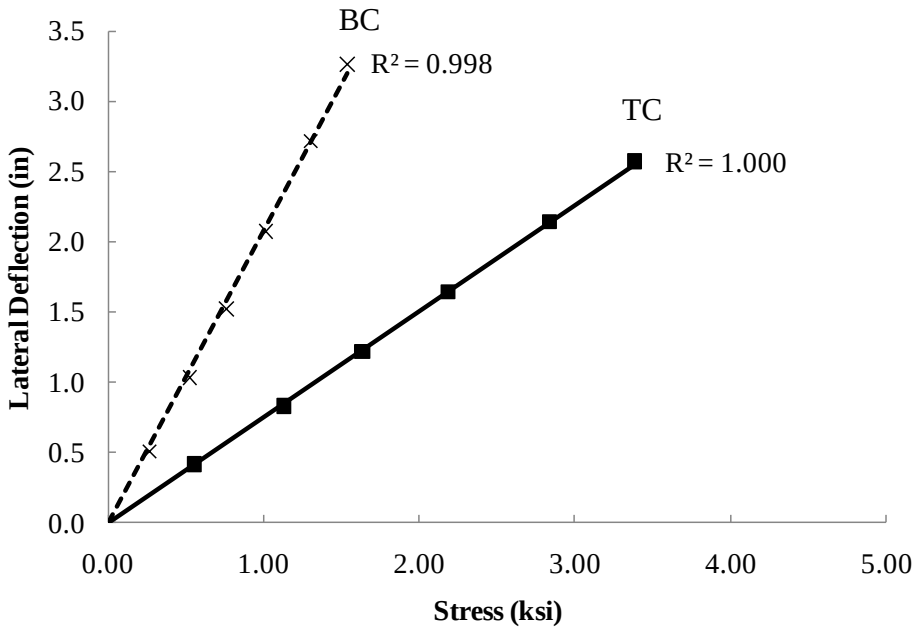

Figure 4.16 Stress from bending component at midspan of the 72-ft truss - Top chord loading

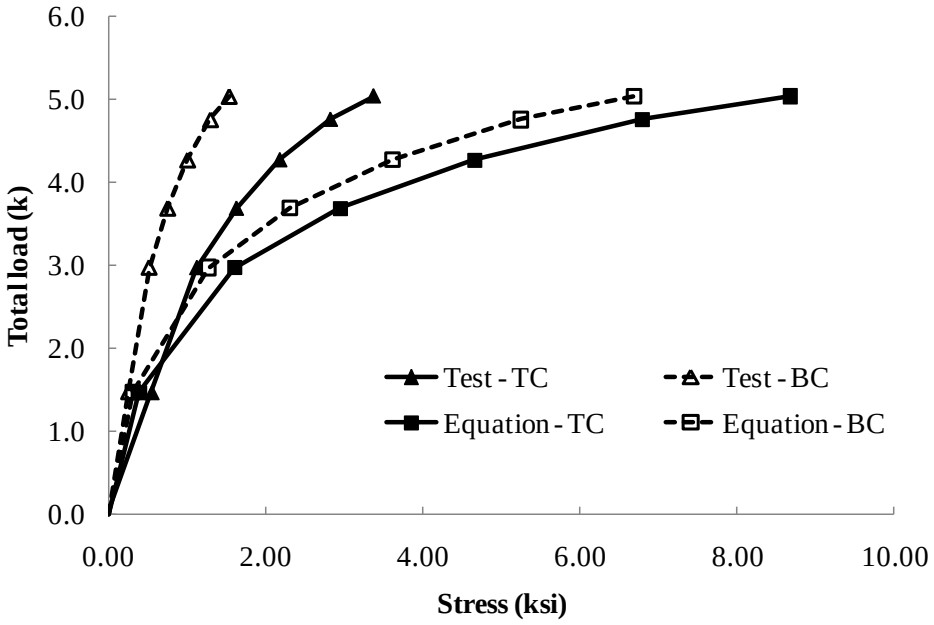

Figure 4.17 Comparison of bending stress component at midspan of the 72-ft truss - Top chord loading

string potentiometer reading since the angle, θ, is reduced, Figure 4.19. In contrast to the string potentiometer, the linear potentiometer was less affected by the lateral movement of the truss; however, it required more fixtures to mount to the support. String potentiometers were therefore used for most of the vertical deflection measurements. From Figure 4.18, it can be seen that the measured vertical deflection at 24 ft. and at midspan (36 ft.) were both reasonably linear. Additional results of the selected vertical deflections are provided in Chapter 5 and Appendix A.

In design, the vertical deflections of the trusses are usually calculated based upon the axial deformations of the truss elements. However, the gusset plate connections and continuous chords do provide some additional restraints that provide some slight changes in the truss stiffness. The truss vertical stiffness is discussed in Chapter 5.

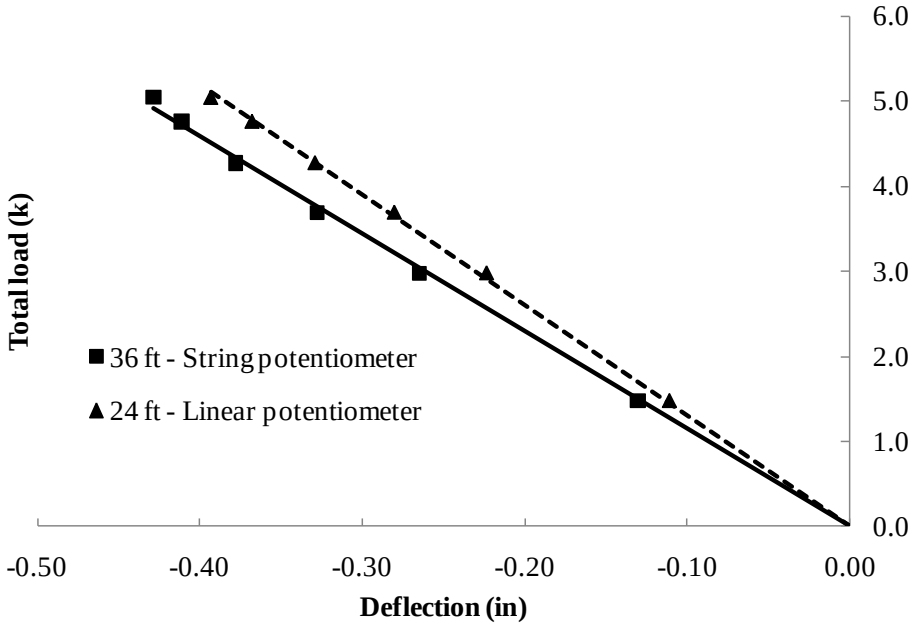

Figure 4.18 Vertical deflection at bottom chord of the 72-ft truss - Top chord loading

4.4.4 Cross Section Rotation

The cross section rotation was measured by using tilt sensors and inclinometers. The sensors were located at 16 and 24 feet for the 48-ft span truss and at 24 and 36 feet

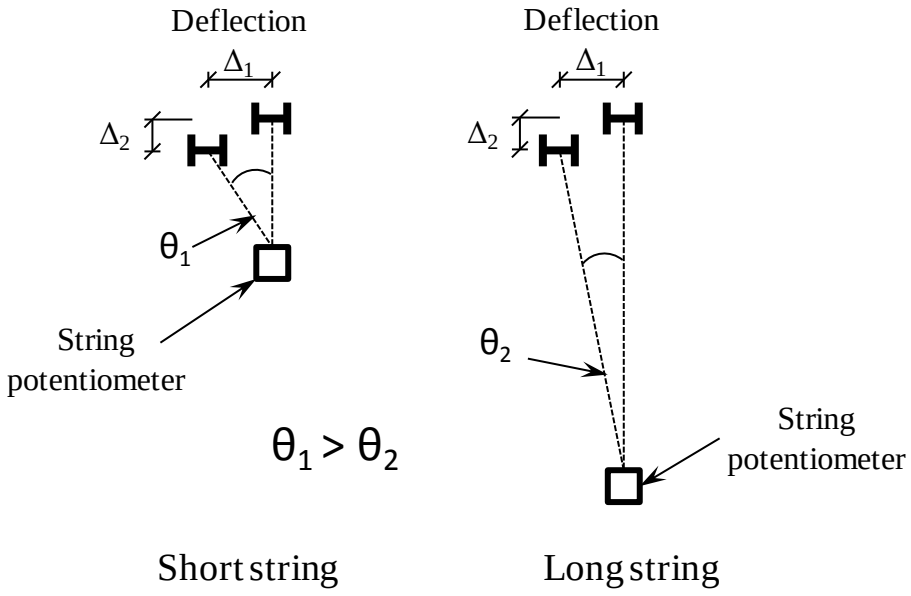

Figure 4.19 Effect of string length on the accuracy of string potentiometer

for the 72-ft span truss on the West truss. The rotation of the truss through the depth of the section was recorded by positioning 5 sensors through the depth of the truss as follows: top chord (TC), top of web vertical (TW), mid height of web vertical (MW), bottom of web vertical (BW) and bottom chord (BC). The readings for the 72-ft span truss with top chord loading are shown in Figure 4.20. Addition results can be found in Appendix A. The curves for the rotations from the 4 sensors are essentially coincident throughout the load range in every location along the cross section, which indicates that the cross section of the truss experienced a uniform rotation with no measurable distortion. The same sensors were also used to measure distortion in the trusses with braces, which is discussed later in the chapter.

4.4.5 Estimated Truss Buckling Capacity by Southwell Plot

As mentioned earlier, the magnitude of the maximum lateral deformation in the trusses was limited to ensure that the truss remained elastic during the tests. Although these tests did provide a measure of the buckling capacity since the load versus deformation curves were beginning to flatten out, Southwell Plots were used to determine

the critical buckling capacity and a measure of the effective imperfection in the trusses. The Southwell Technique (Southwell, 1932) is primarily intended for use in column experiments; and the method was found to work very well with the truss systems. The load-deflection curve was expected to be the rectangular hyperbola shape which is a general requirement of the method. Therefore, the Southwell plot was able to be used. Figure 4.21 shows the Southwell plot of the 72-ft span truss of the East and West trusses. The relationship of the plots were essentially linear, with the square of the correlation coefficient (r^2) very close to 1, indicating the parabolic shape function mentioned by Southwell. The East and West truss behaved almost the same, leading to approximately the same critical load from both trusses.

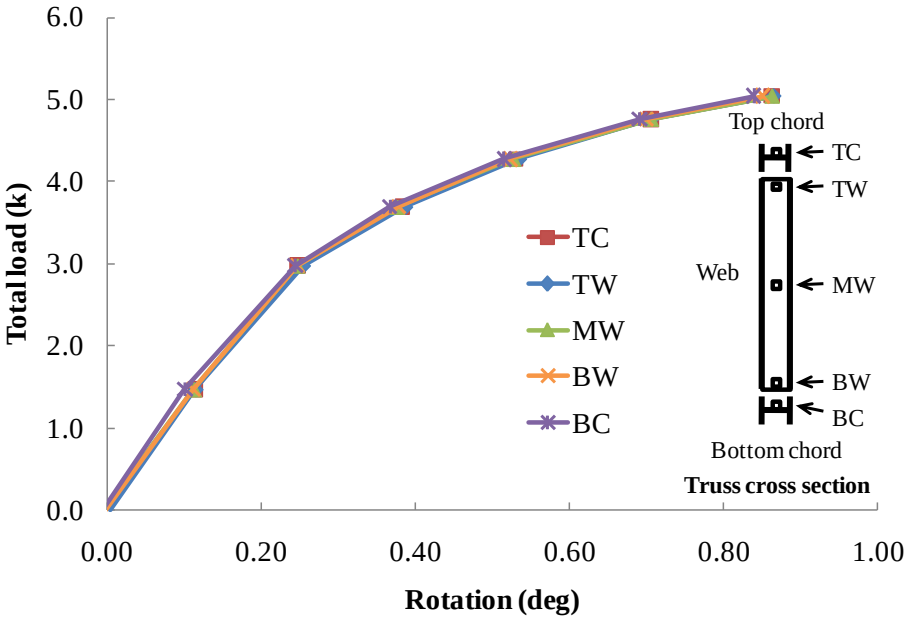

Figure 4.20 Cross section rotation at midspan of 72-ft truss - Top chord loading- No intermediate bracing.

The results of the Southwell plot of the 48-ft and 72-ft span West truss are shown in Figure 4.22 and Figure 4.23, respectively. Because the behavior at the beginning of the test is more likely to be affected by other factors such as friction from the system and have a slightly different slope (Southwell, 1932), the data from zero to 50 percent of

maximum applied load was not included in the plot. According to the graph, the Southwell plot seemed to work very well regarding to linearity of the plot with the R-square value of almost 1 for all plots of the buckling test without bracing. The estimated buckling capacity and initial imperfection were calculated and are summarized in Table 4.1. Table 4.1 includes the results of both the East and West trusses. To determine the estimated buckling capacity of the twin truss system, the individual values for the two trusses were averaged. The estimated buckling capacities represent the total load applied to a single truss at the third points.

The estimated buckling capacity of the truss between the top chord loading and bottom chord loading were compared to obtain a measure of the effects of load position, as indicated in Table 4.2. The estimated ratio of buckling capacity of bottom chord to top chord ratio was about 1.16 for both spans, indicating the potential effect of the load position that has been previously found for beam buckling problems.

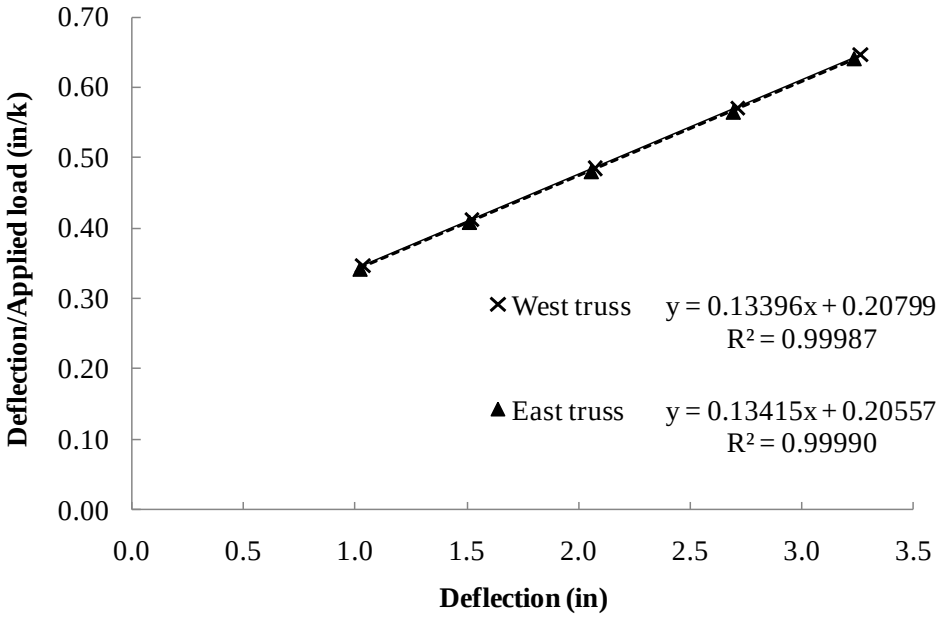

Figure 4.21 Southwell plot of 72-ft truss - Top chord loading

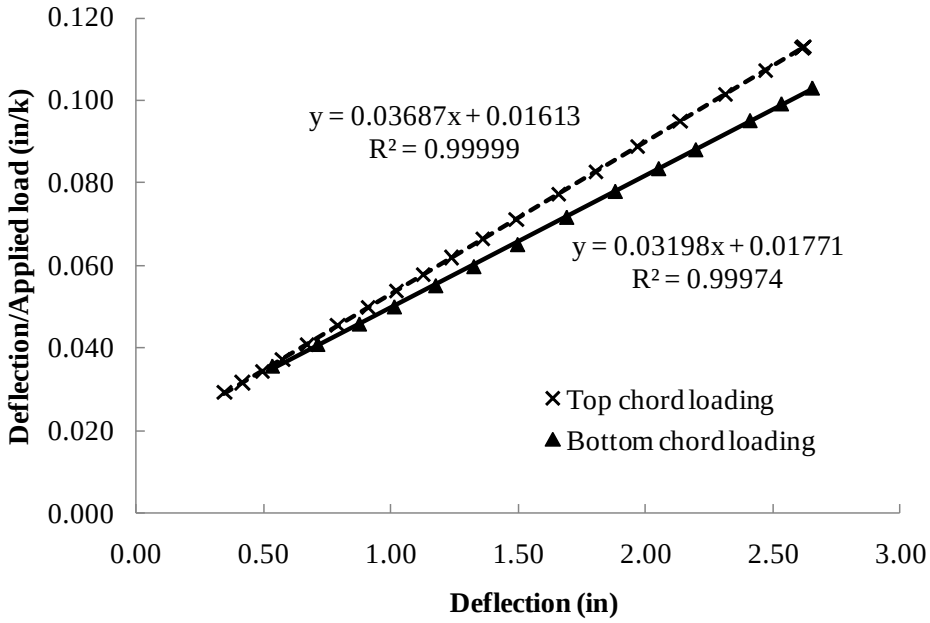

Figure 4.22 Southwell plot of 48-ft truss

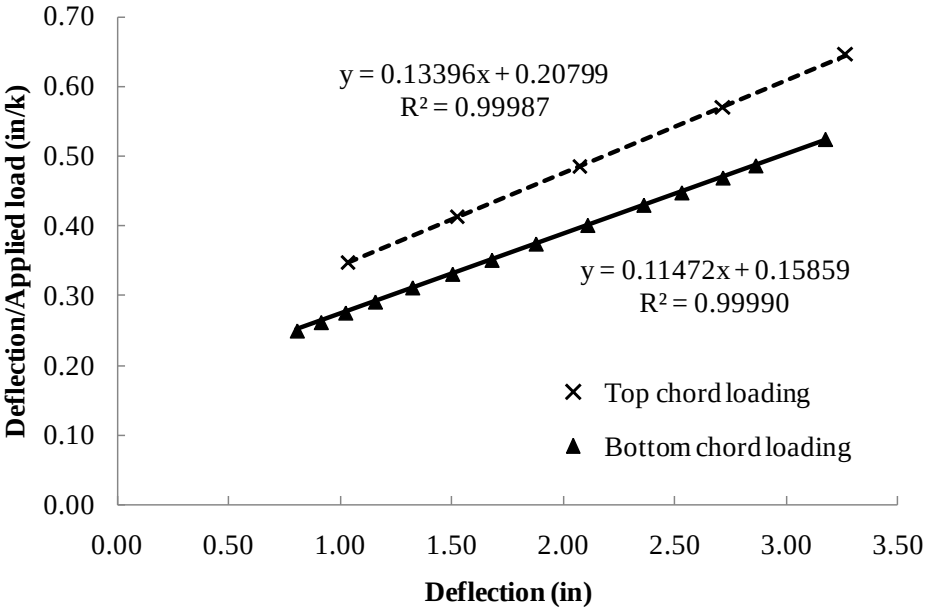

Figure 4.23 Southwell plot of 72-ft truss

Table 4.1 Estimated buckling capacity by Southwell plot

Span	48-ft span				72-ft span			
Load	Bottom chord		Top chord		Bottom chord		Top chord	
Truss	P_{cr} (kip)	Int Imp (in)	P_{cr} (kip)	Int Imp (in)	P_{cr} (kip)	Int Imp (in)	P_{cr} (kip)	Int Imp (in)
West	31.27	0.554	27.12	0.437	8.72	1.382	7.46	1.553
East	31.45	0.563	27.02	0.429	8.58	1.274	7.45	1.532
Average	31.36	0.558	27.07	0.433	8.65	1.328	7.46	1.543

Table 4.2 Load height effect ratio

Case	48-ft span truss	72-ft span truss
Bottom chord loading	31.36	8.65
Top chord loading	27.07	7.46
Bottom to top chord ratio	1.158	1.160

4.5 BUCKLING TEST OF TRUSSES WITH LATERAL BRACING

Several tests were done on the truss systems with lateral braces. The braces consisted of an aluminum bar for the brace for the case with single brace at midspan and HSS (Hollow Structural Section) steel tubes for the brace for case with braces at the third points. The braces were positioned at the top chord. The design brace stiffness values were 0.2, 0.5 and 0.8 kip/in. However, in the actual test setup, the brace stiffness values were not the same because the top truss chord deflected vertically, which resulted in a relatively small change in the brace stiffness. The calibration of the lateral brace stiffness is discussed in the following section.

4.5.1 Calibration of Lateral Braces

Braces were calibrated to obtain the actual stiffness values. The values of the design lateral stiffness were 0.2, 0.5, and 0.8 kips/in based upon the elastic deflection equations for an overhanging beam. However, due to the friction of the system and the test configuration, the actual brace stiffness varied slightly from the design value. During

the test, the truss moved vertically and laterally. The vertical movement changed the contact point, resulting in changes in the brace stiffness values. The calibration tests were performed at the contact points and at 3 inches below the contact points to cover the range of the vertical truss deflection that occurred during the tests. Figure 4.24 and Figure 4.25 show the results of the calibration of the aluminum bar and HSS steel braces, respectively. The dashed lines represent the calibrated values and the solid lines represent the calculated values. The two graphs show that three of the brace sizes had very good agreement between the measured and calculated stiffness. The other three braces had a larger stiffness than the calculated values with a maximum difference of approximately 20%. For all the braces, the relationship between the brace length and stiffness behavior were nearly linear. Therefore, it is reasonable to assume that the variation of the brace stiffness has linear relationship with the overall length of the brace. The calibrated brace stiffness values are summarized in Table 4.3. Although there was some variation in the actual stiffness, the design stiffness is referenced in the remainder of this dissertation in discussions of the behavior.

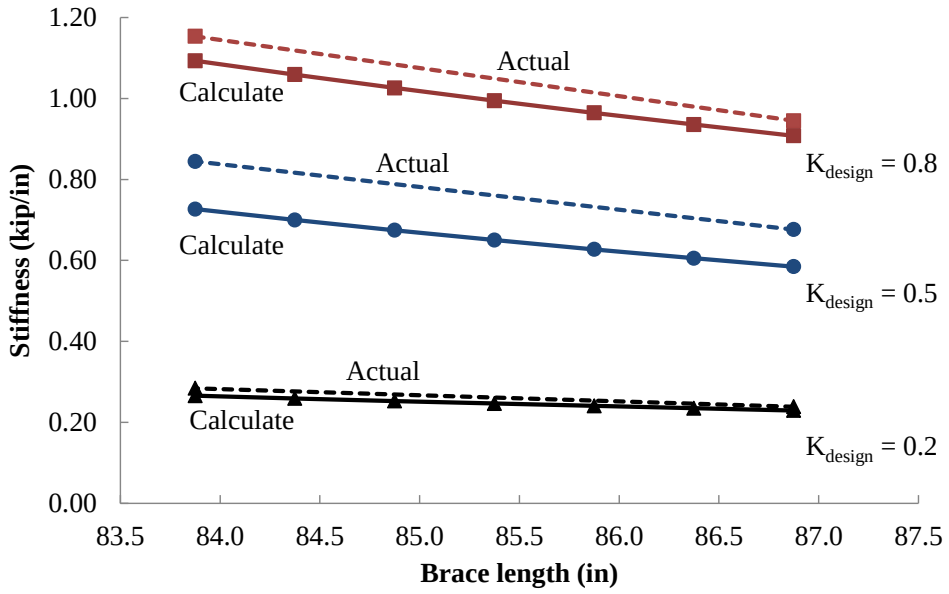

Figure 4.24 Calibration of aluminum lateral braces

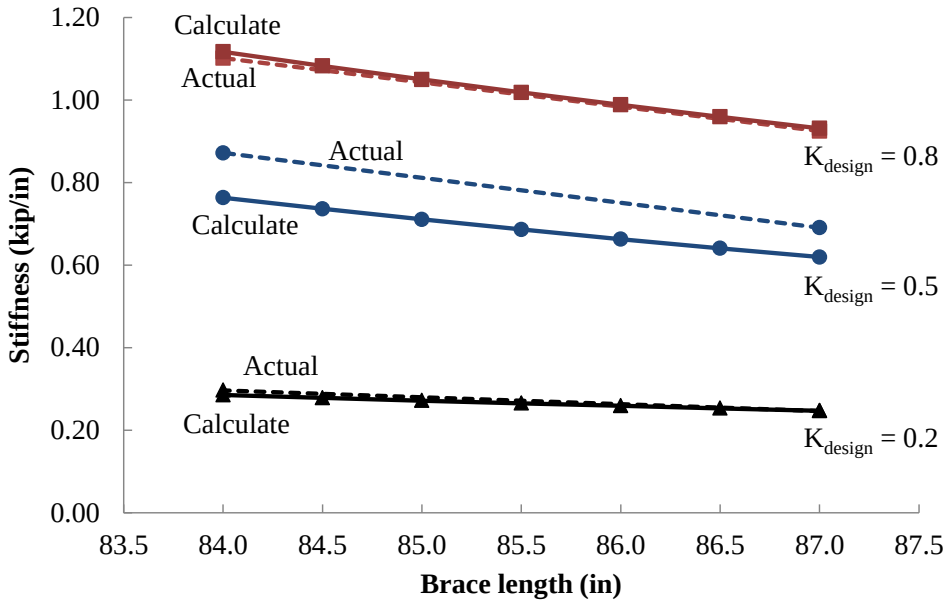

Figure 4.25 Calibration of steel lateral braces

Table 4.3 Summary of calibrated lateral brace stiffness

Material	Design stiffness (kip/in)	Brace stiffness (kip/in)	
		Undeflected	3" Vertical deflection
Aluminum	0.2	0.239	0.284
Aluminum	0.5	0.676	0.845
Aluminum	0.8	0.945	1.153
Steel	0.2	0.247	0.297
Steel	0.5	0.691	0.872
Steel	0.8	0.925	1.102

4.5.2 Lateral Deflection

Results for the case with single lateral brace at midspan with brace stiffness of 0.2 and 0.8 kip/in are shown in Figure 4.26 and Figure 4.27, respectively. Figure 4.28 and Figure 4.29 show results for the case with 2 lateral braces at third points with brace stiffness of 0.2 and 0.8 kip/in, respectively. The lateral deflections at the 24 and 48-ft

locations were similar for the case with 1 and 2 low stiffness braces. For the high brace stiffness, the lateral deflection at 48 feet for the case with single brace increased at a faster rate and was larger than the lateral deflection at midspan for larger load levels. One concern in this case is that the truss might be susceptible to a snap-through buckling mode where the truss flips from a half-sine curve to a full-sine curve. To avoid the truss to snap through from half sine to full sine mode, the tests were stopped at the point where the lateral deflection at the third points was equal to the lateral deflection at the midspan top chord. For the case of 2 braces with high stiffness, the lateral deflection at 48 feet also deviated from the 24 feet location. However, the value was still far less than the midspan deflection at the end of the test which was limited by the stress in the truss chord. For the case of the truss with the low brace stiffness value, the bottom chord experienced large deflection relative to the top chord. On the other hand, top chord bracing with high brace stiffness values were efficient in controlling the bottom chord deflection as can be seen in Figure 4.27 and Figure 4.29 where the bottom chord deflections were less than half of the top chord deflections. The midspan top chord deflection of truss with 2 braces at the third points was almost twice that of the braced points while the unbraced lengths were the same. The midspan top chord was the weakest point due to the high compression and lateral deflection.

Figure 4.30 demonstrates the effect of brace stiffness on the buckling capacity of the truss at the midspan top chord. It can be seen that the buckling capacity of the truss without bracing was very low. Adding only one low stiffness lateral brace to the truss system dramatically improved the behavior of the truss by increasing the capacity from approximately 5 kips to 15 kips. For the cases with the 0.5 k/in and 0.8 kip/in braces, the capacity increased to more than 30 kips. As expected, the 0.8 kip/in brace provided much better control over the magnitude of the maximum lateral deformations.

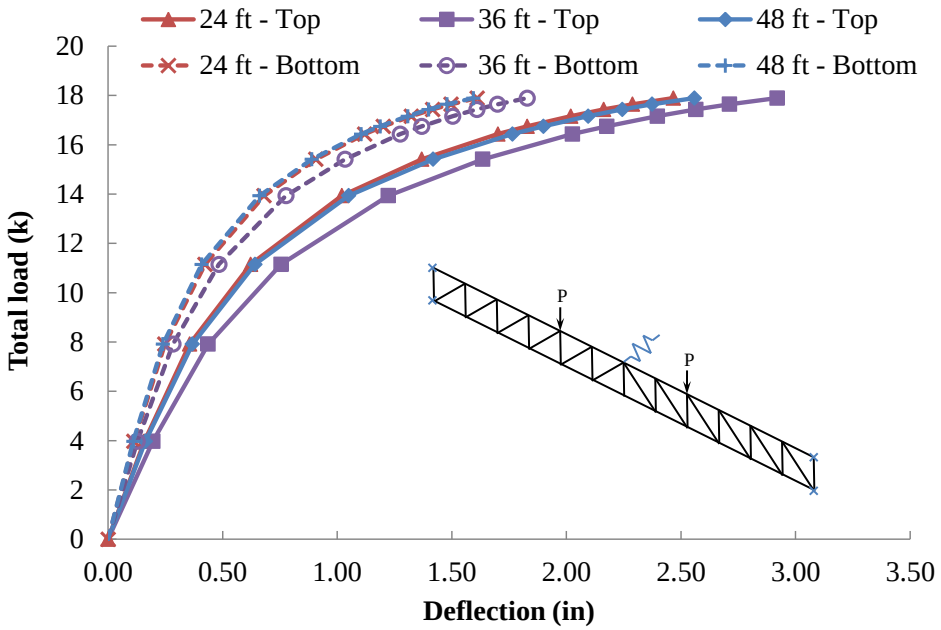

Figure 4.26 Lateral deflection of truss with single lateral brace - K = 0.2 kip/in

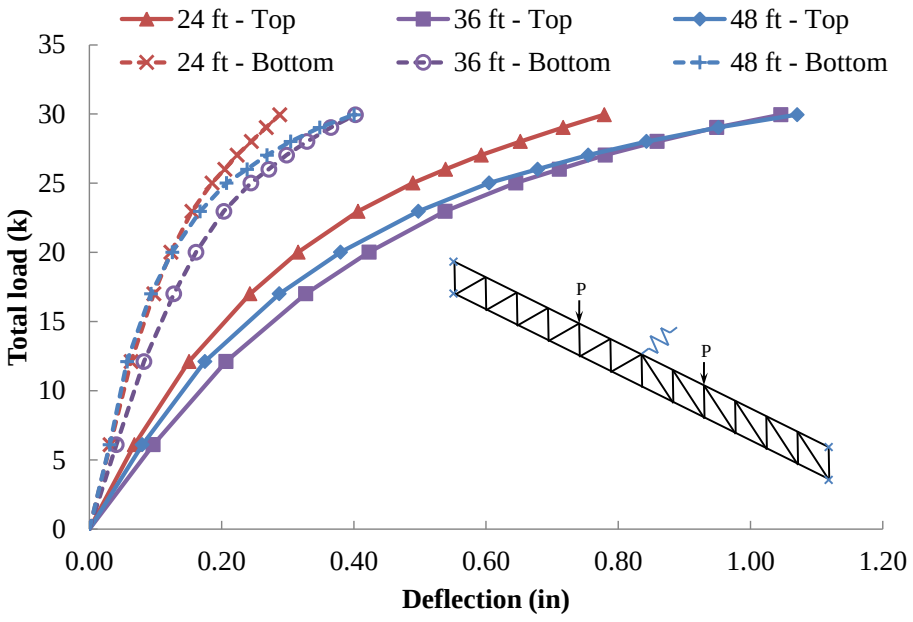

Figure 4.27 Lateral deflection of truss with single lateral brace - K = 0.8 kip/in

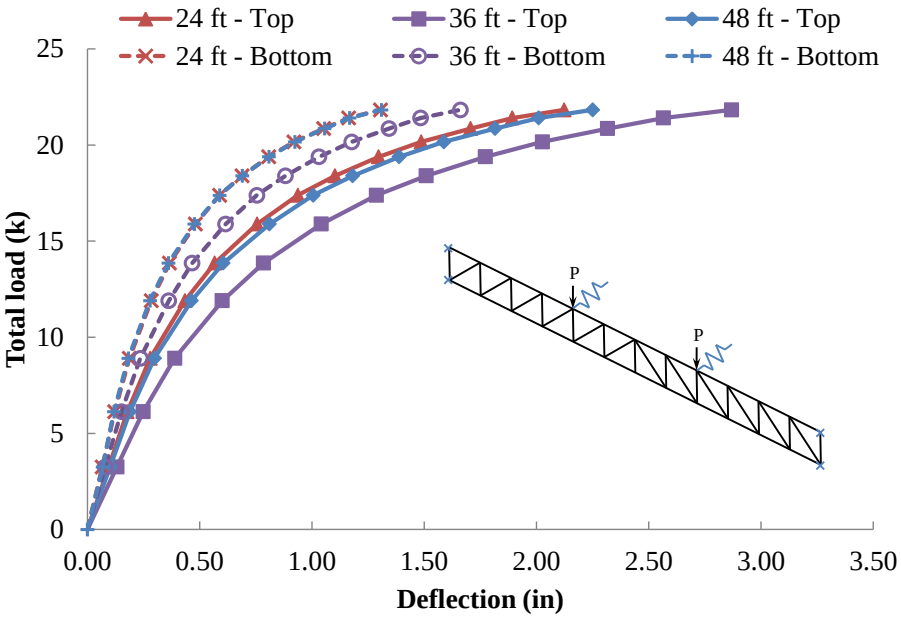

Figure 4.28 Lateral deflection of truss with 2 lateral braces - K = 0.2 kip/in

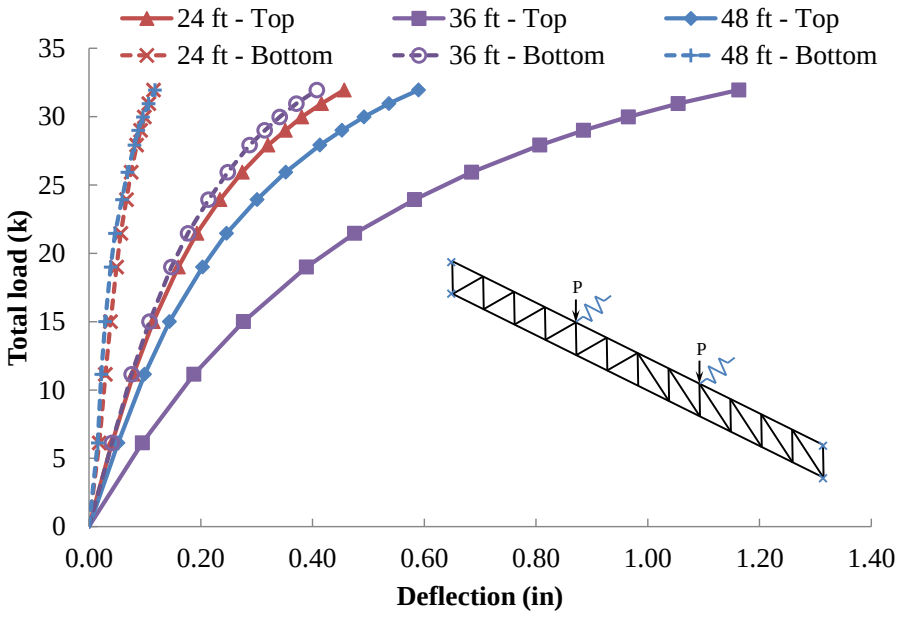

Figure 4.29 Lateral deflection of truss with 2 lateral braces - K = 0.8 kip/in

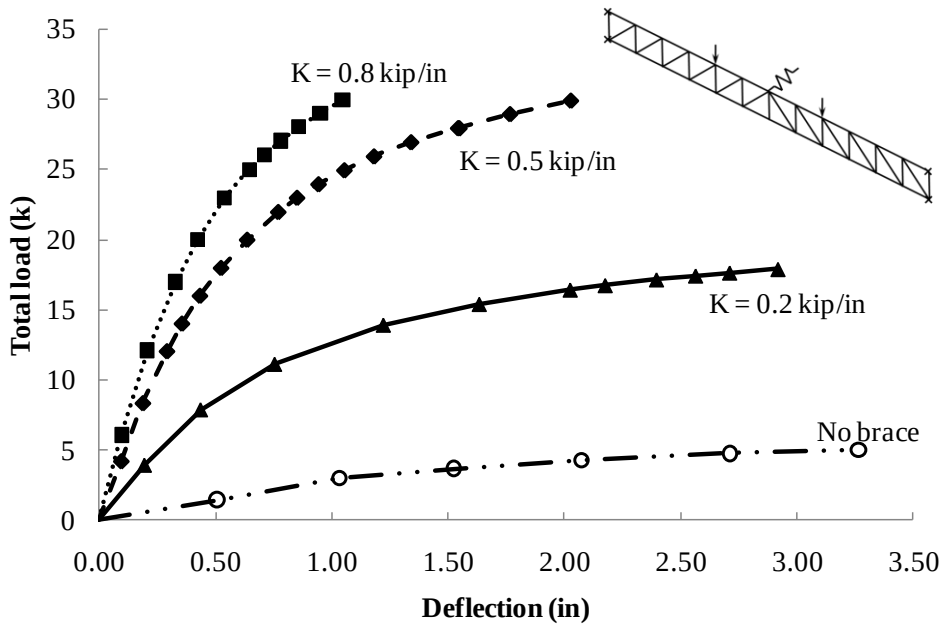

Figure 4.30 Effect of brace stiffness on buckling capacity of truss with single lateral brace

The effect of number of braces on the buckling capacity of the truss is shown in Figure 4.31. From the graph, increasing number of braces from 1 to 2 enhanced buckling capacity; however, with less effectiveness. Theoretically, changing the brace from 1 to 2 decreases the unbraced length and doubled the brace stiffness, resulting in increase in buckling capacity of truss. However, due to high axial force at midspan and lack of lateral brace at midspan, changing the number of the brace from 1 to 2 was much less dramatic than the difference observed between the cases with no intermediate brace and a single brace.

Figure 4.32 shows the relationship of the applied load and relative deflections at the locations limited by the braces. For the case without bracing and cases with single brace at midspan, the relative lateral deflections were the deflection at midspan relative to the support. For the cases with 2 braces, the relative deformation consisted of the maximum deflections resulting from the following three cases:

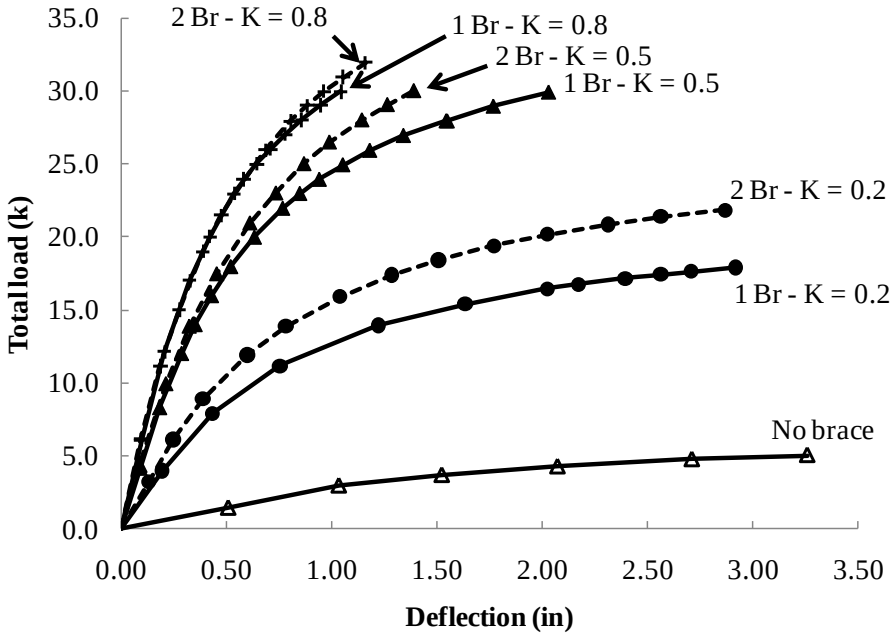

Figure 4.31 Effect of number of lateral brace on buckling capacity of truss

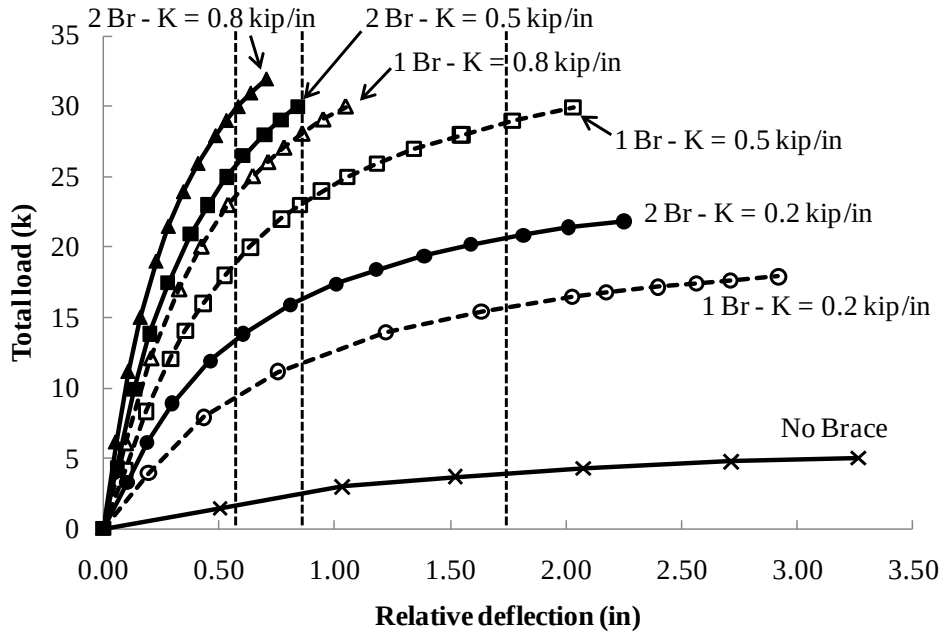

Figure 4.32 Relative maximum lateral deflection of truss with and without lateral bracing

1) The deflection at 24 feet relative to the support at 0 foot,

2) The lower of the deflections at 24 or 48 feet relative to deflection at 36 feet

3) The deflection at 48 feet relative to the support at 72 feet.

For the case with stiffness values (K) of 0.2 and 0.5 kip/in, the maximum relative deflections were controlled by the case 3) above between 48 and 72 feet. The second case relative deflections between 24 and 36 feet was controlled for the case with K = 0.8 kip/in. The first case was never control because the deflections at 48 feet were all larger than at 24 feet. If the maximum lateral deflection of the trusses was limited by the initial imperfection of $L_b/500$, where L_b is unbraced length, the maximum deflections are 1.73, 0.86 and 0.58 inch for trusses without bracing, with single brace at midspan and with 2 braces at third points, respectively. The maximum load at the limit of deflection for truss without bracing was about 4 kips. The maximum loads for the cases with single brace at midspan were 11, 22.5 and 27.5 kips for the brace stiffness values of 0.2, 0.5 and 0.8 kip/in, respectively. The maximum loads for the cases with 2 braces were 13, 25 and 30 kips for the brace stiffness values of 0.2, 0.5 and 0.8 kip/in, respectively. By limiting the lateral deflection to the $L_b/500$, the test showed that changing the brace from single brace to 2 braces improve the load carrying capacity, even though the load-deflection at midspan was the same for the case with brace stiffness of 0.8 kip/in, Figure 4.31. When the stiffness values were varied from 0.2 to 0.8 kip/in, the improvement in the buckling capacity seemed to be the same, about 5 kips, for every stiffness increment.

4.5.3 Cross Section Rotation

The applied load versus the rotations of the truss cross sections at 24 feet for the case with a single midspan brace are graphed in Figure 4.33. The truss cross section appeared to rotate at the same degree throughout the cross section and the behavior was also the same at midspan. This indicated that the truss with wide flange web section had a high web stiffness and that the gusset plates for the connection was sufficient in controlling the distortion of the cross section.

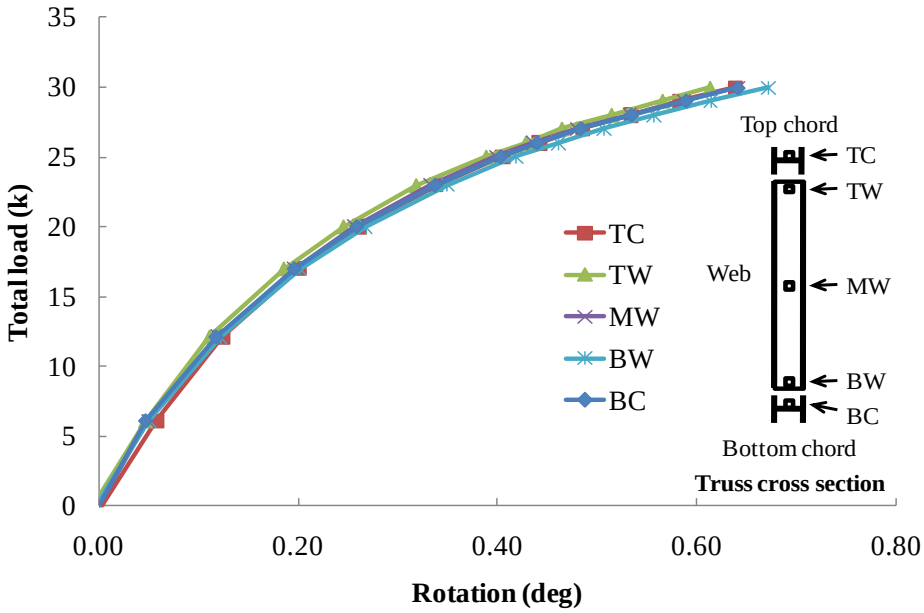

Figure 4.33 Rotation at 24 feet of truss with single lateral brace - K = 0.8 kip/in

For the case with two intermediate braces, graphs of the applied load versus rotations on the cross section at 24 and 36 feet are shown in Figure 4.34 and Figure 4.35, respectively. The rotation at 24-ft location indicates some distortion of the cross section since there was variability in the twist on the cross section. The measured rotations near the top of the truss were smaller than those at the bottom of the truss. A schematic depicting the variation in the rotation is shown in Figure 4.36. The rotations at midspan were the same throughout the cross section. The schematic drawing of the rotation with the same degree of rotation throughout the cross section is shown in Figure 4.37.

According to the cross section rotation, the cross section distortion only affected the case with the load and the brace at the same location which was the third points with the high brace stiffness. This may be an important consideration for trusses with low web stiffness such as when the chord is a tee section and the web is angle which is directly attached to the web of the tee section.

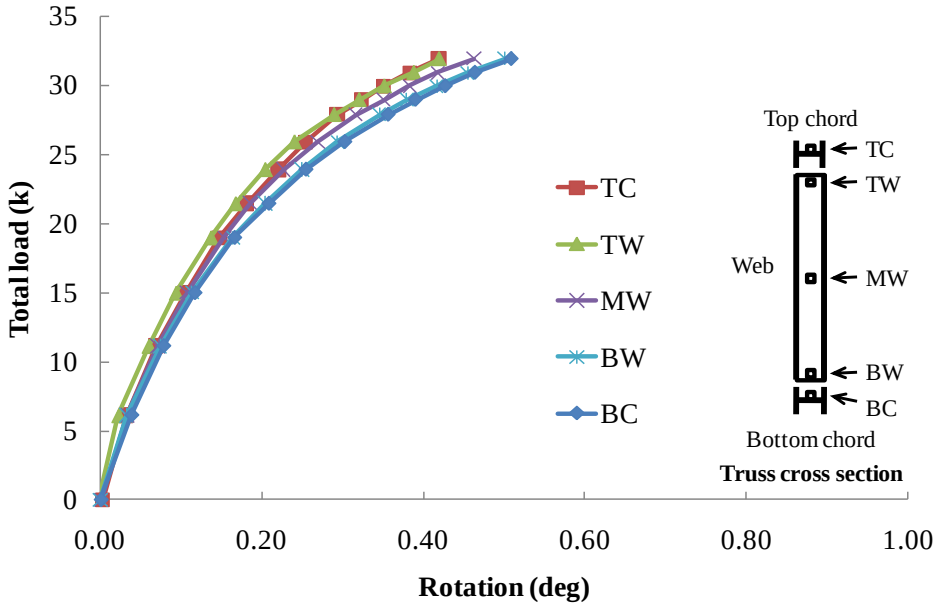

Figure 4.34 Rotation at 24 feet of truss with 2 lateral braces - K = 0.8 kip/in

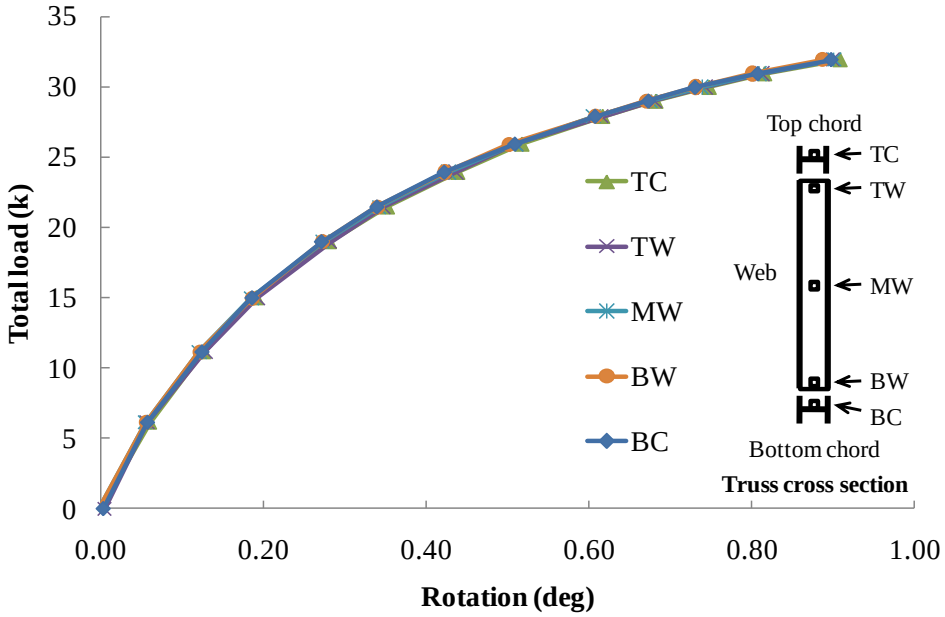

Figure 4.35 Rotation at 36 feet of truss with 2 lateral braces - K = 0.8 kip/in

Figure 4.36 Truss cross section rotation at 24 feet of truss with 2 lateral braces - K = 0.8 kip/in

Figure 4.37 Truss cross section rotation for the cases with the same degree of rotation

4.5.4 Strain in Truss Chord

Figure 4.38 shows the strain on the East and West sides of the truss top and bottom chords at midspan of the West truss for the case of truss with single brace at midspan with K = 0.2 kip/in. The top chord was in compression and the bottom chord

was in tension. According to the test results, the truss chords primarily experienced axial force as can be seen that the graph for each chord were not far apart from each other. The behavior was similar for all cases with 2 lateral braces.

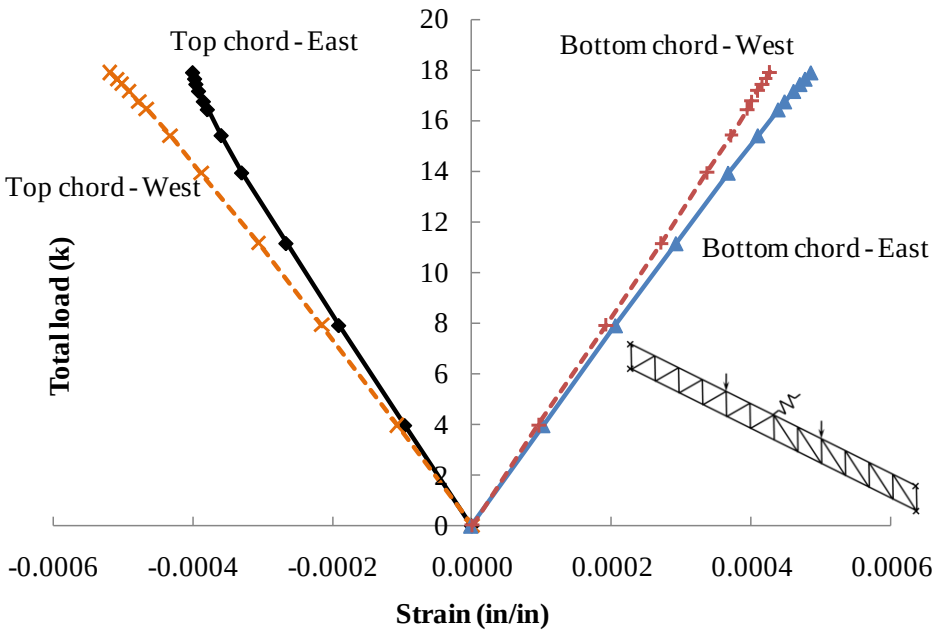

Figure 4.38 Strain at midspan for truss with single lateral brace and K = 0.2 kip/in

Figure 4.39 shows the results of strain at the midspan truss chords for the case with one lateral brace at midspan with K = 0.8 kip/in. The results of strain on the East and West sides on the truss at the same chord were very close to each other, suggesting that there was little lateral bending component. This could be explained by considering the lateral deflection along the length of the truss shown previously in Figure 4.27. The lateral deflection at midspan was close to, about quarter inch, the lateral deflection at 24 feet, and it was similar to that at 48 feet. Thus, the truss profile from 24 to 48 feet was almost straight line and the secondary effect was minimal. The behavior also occurred in the case with K = 0.5 kip/in. Most of the cases with 2 lateral brace strain, shown in Appendix A, were similar to the case of 0.2 kip/in of truss with one lateral brace.

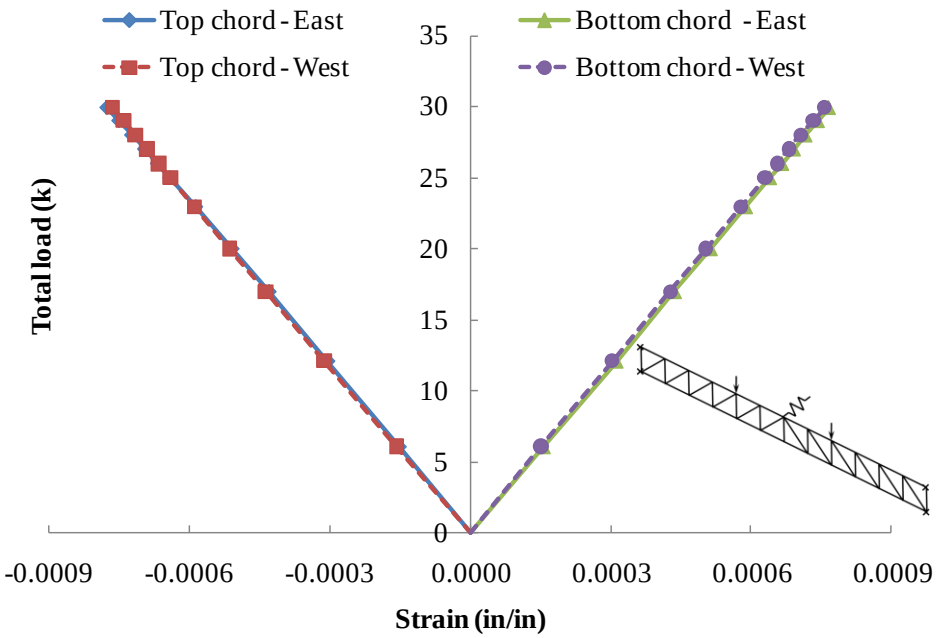

Figure 4.39 Strain at midspan of truss with single lateral brace - K = 0.8 kip/in

4.5.5 Lateral Brace Forces

Brace forces were captured by measuring the strain in the braces approximately 20-30 inches from the contact points of the truss. Stresses in the brace were determined using Hooke's Law. Based upon the stress, the moment in the brace could be determined and then the lateral force between the brace and the truss chord was determined. A graph of the applied load versus the strain in the lateral brace of the case with a single lateral brace at midspan with K = 0.8 kip/in is shown in Figure 4.40. The strain gages that were used were temperature compensated for steel. Therefore, temperature changes during the tests were not a concern with the steel HSS sections for the braces. For the aluminum bar, on the other hand, the temperature compensation was not applicable. However, since the tests were short and were conducted inside the laboratory building, the temperature was relatively constant and did not have a significant effect. The brace strains were almost the same for both sides of the brace which indicates that the strain gages were placed in the proper locations.

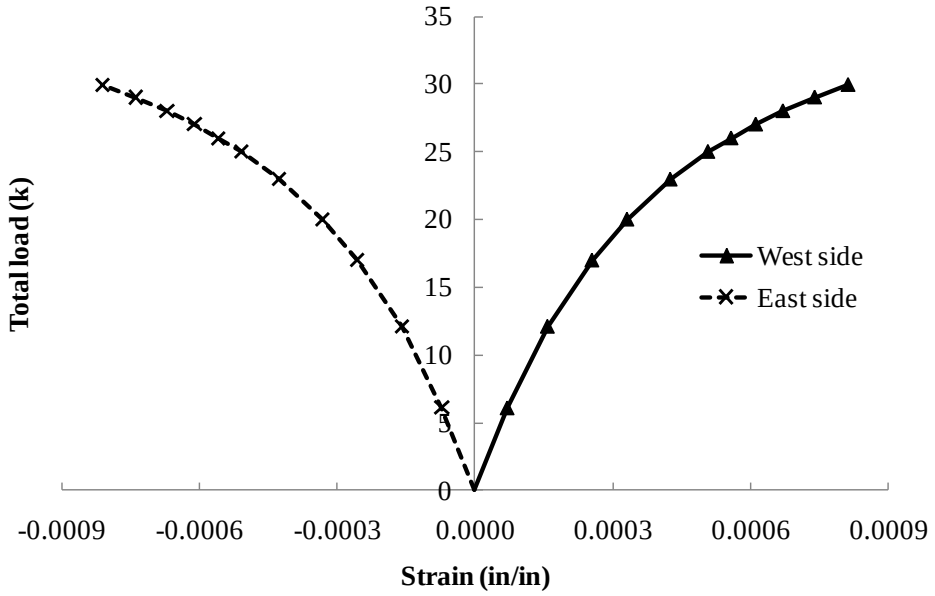

Figure 4.40 Strain in the lateral brace for truss with single lateral brace - K = 0.8 kip/in

Figure 4.41 and Figure 4.42 show graphs of the applied load versus the brace force for the respective cases of a truss with a single lateral brace at midspan and with lateral braces at the third points. The brace force is directly related to the lateral deflection and brace stiffness. At the beginning of the test where the load and lateral deflection was a relatively linear relationship, the brace forces from all tests were also linear. For larger loads, the nonlinearity in the load versus lateral deformation occurred and the brace force had a similar relationship. In these cases, the brace force was sensitive to the brace stiffness. For a given load level, stiffer braces resulted in smaller brace forces.

4.6 BUCKLING TEST OF TRUSSES WITH TORSIONAL BRACING

Similar to the tests with the lateral braces, the tests that were conducted with torsional braces utilized different brace stiffness values. For the torsional braces, the brace position was varied between the top and bottom chord. The brace was always positioned on the loaded chord. The number of intermediate braces ranged from one to

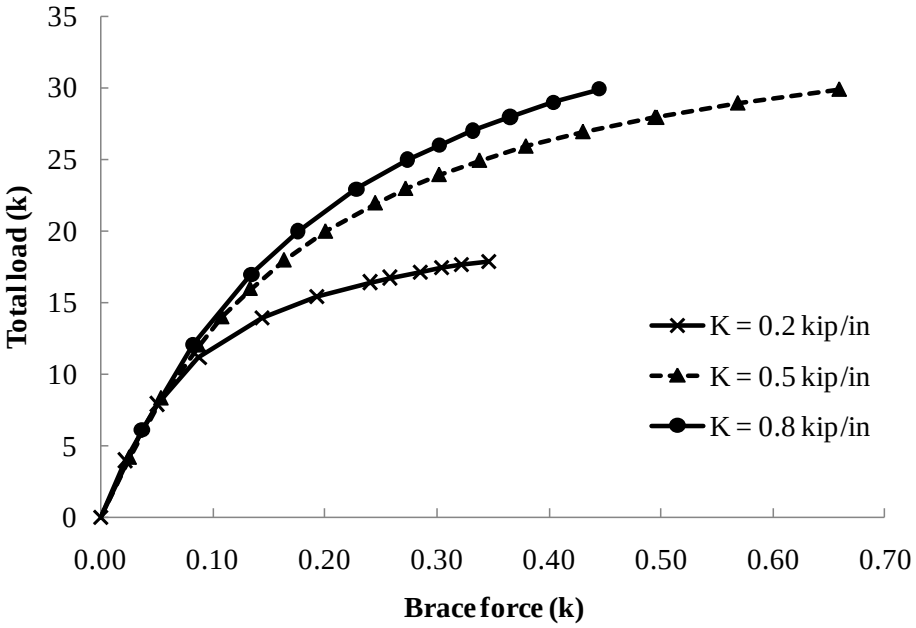

Figure 4.41 Brace force of truss with single lateral brace at midspan top chord

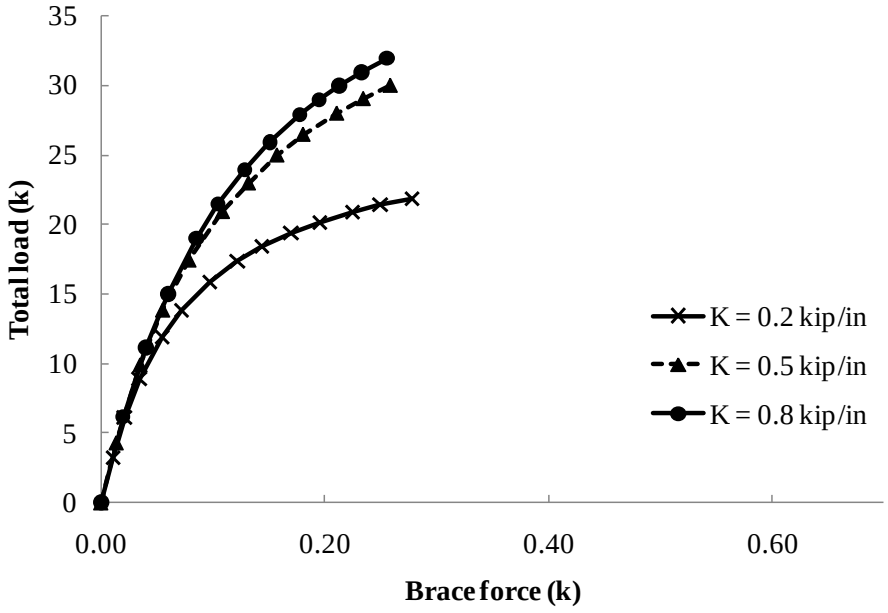

Figure 4.42 Brace force at 24-ft brace of truss with 2 lateral braces

three. For the tests with three large torsional braces at the bottom chord, the results demonstrated that significant distortion occurred in the connection between the brace and the bottom chord. Stiffeners were added to the braced joints for the remaining tests. All buckling tests of the trusses with torsional bracing at the top chord included stiffened brace connections.

4.6.1 Lateral Deflection

The applied load versus the lateral deflection of the trusses with a single small torsional brace on the bottom chord at midspan is presented in Figure 4.43. Additional results are provided in Appendix A. The lateral deflections of the trusses with torsional bracing were similar to the cases without bracing and with lateral bracing where the midspan top chord deflected the most in all cases. For the test with three large torsional braces attached at the bottom chord, distortion of the cross section occurred at the braced connections. The applied load versus the lateral deflection is graphed in Figure 4.44. Although the shape of the load versus deformation behavior is the same with and without the connection stiffener, the load level that was reached is significantly different. A similar graph for the case of three small torsional braces on the top chord with connection stiffener is shown in Figure 4.45. When the stiffeners were added to the braced connection, the behavior of the truss was still the same, but buckling capacity was higher. With one low stiffness torsional brace, the truss had low buckling capacity and uniformly deflected as the deflections at 24 and 48 feet were approximately the same, Figure 4.43. Using more than one high stiffness brace, the truss started to deflect unequally. It can be seen that the lateral deflection at 48-ft in Figure 4.44 and Figure 4.45 was very close to the deflection at midspan and the lateral deflections at top and bottom chord at 24-ft were also close to each other, suggesting that the truss will buckle in the sine mode, instead of half sine mode.

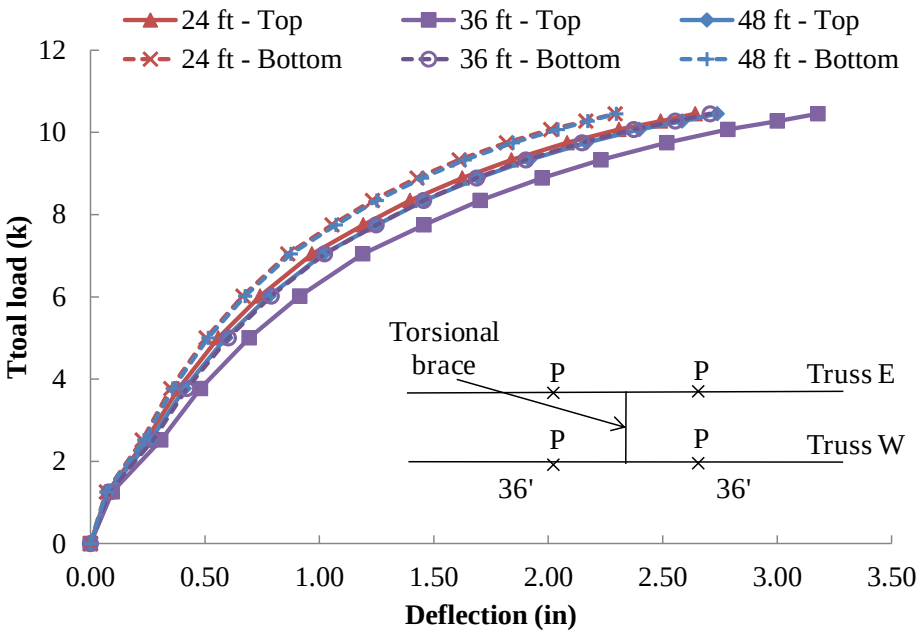

Figure 4.43 Lateral deflection of truss with single small torsional brace at bottom chord (without connection stiffener)

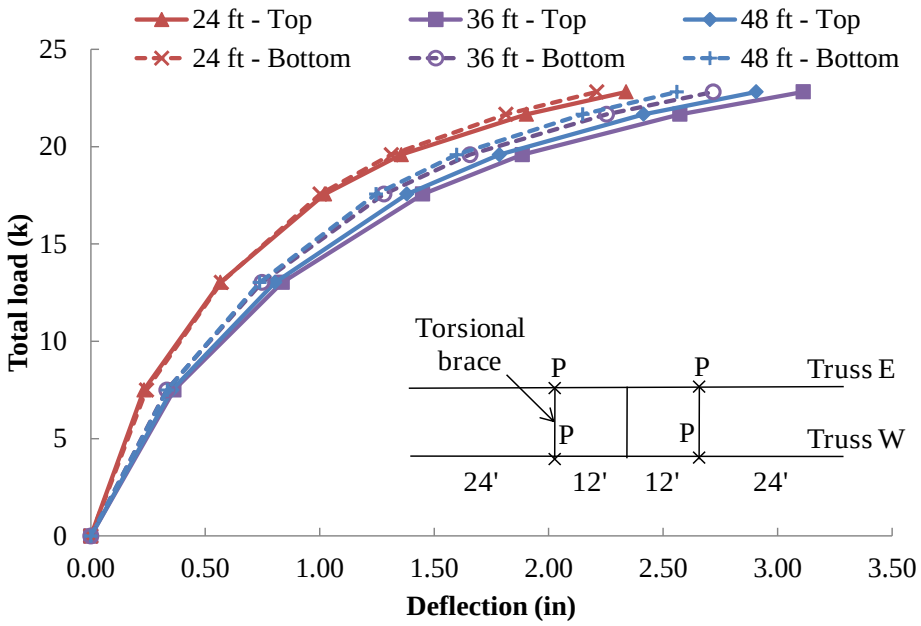

Figure 4.44 Lateral deflection of truss with 3 large torsional braces at bottom chord (without connection stiffener)

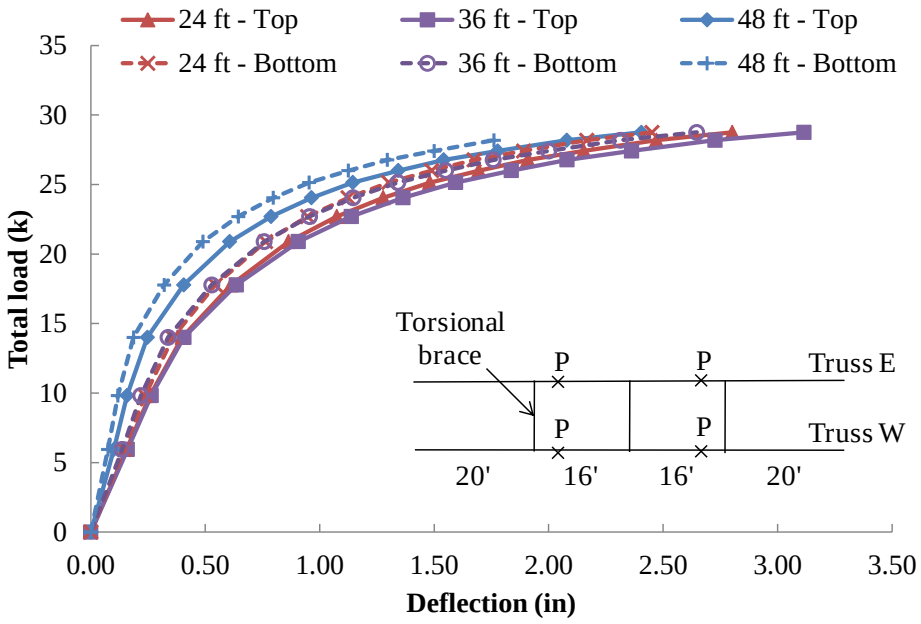

Figure 4.45 Lateral deflection of truss with 3 small torsional braces at top chord (with connection stiffener)

The distribution of the lateral deflection was unsymmetrical in several cases, particularly with the stiffer braces when multiple braces were used. The unsymmetrical buckled shape of the truss, makes the system more likely to experience a snap-through buckling mode had the trusses continued to be loaded. The tests were stopped for safety precautions. The exception case was the case with 3 large torsional braces at the top chord. The truss was originally deflected in the half sine shape. However, during the trial test, the truss snapped from the half-sine shape to the sine shape at a relatively high load level. Subsequent tests with the same test set up had a mode consisting of the full sine shape on top and bottom chord throughout the tests as can be seen in Figure 4.46. The lateral deflections were small, less than 0.5 inch, compared to other tests.

4.6.2 Strain in Truss Chord

Figure 4.47 shows the strains in the chords at midspan of truss with three small torsional braces. The results that are shown are representative of the test results and

additional results are provided in Appendix A. The strain for the cases with small braces was impacted by secondary effects more than the case with large brace as the line tend to be less linearity at the buckling load.

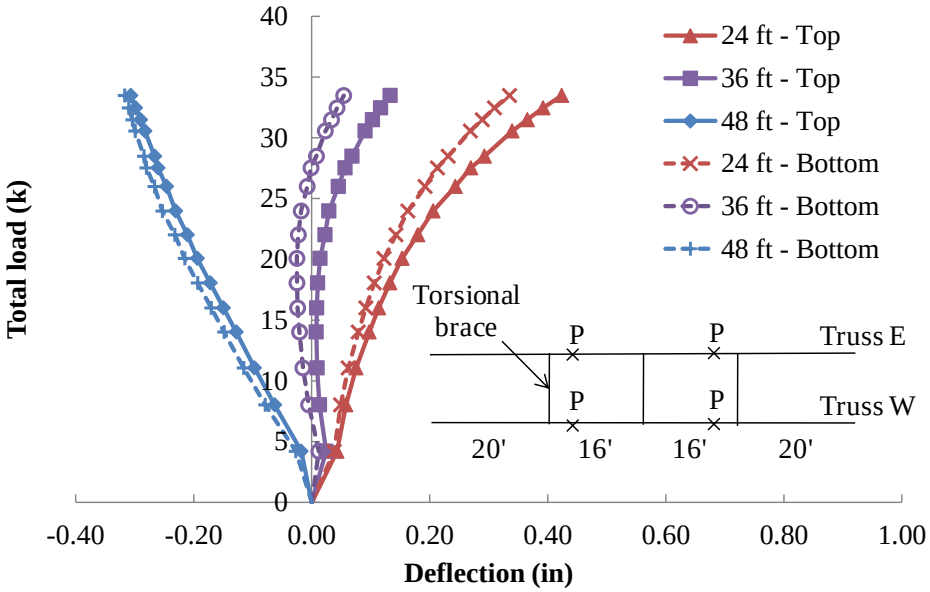

Figure 4.46 Lateral deflection of truss with 3 large torsional brace at top chord (full sine buckle shape)

The strains at midspan on the truss with three small torsional braces at the top chord are shown in Figure 4.48. The behavior was similar to the bottom chord with the same braces, except the buckling capacity was higher due to the added stiffeners. The differences of the strain on the East and West sides were smaller in the case with top chord bracing throughout the test until the load was close to the buckling capacity. Increasing the brace stiffness was also decrease the difference between the East and West side strain due to the high axial force and smaller lateral deflection.

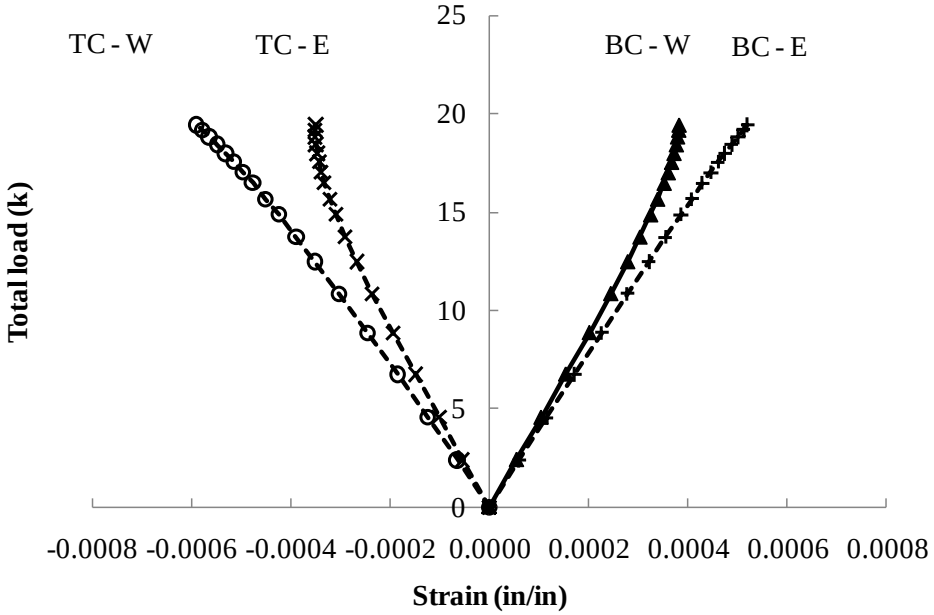

Figure 4.47 Strain in truss chord at midspan of truss with 3 small torsional braces at bottom chord (without connection stiffener)

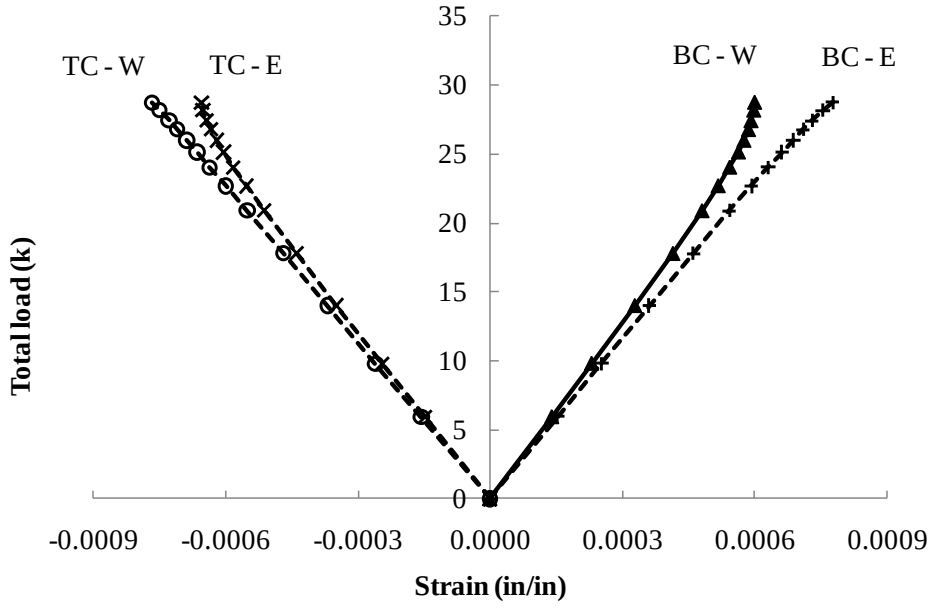

Figure 4.48 Strain in truss chord at midspan of truss with 3 small torsional braces at top chord (with connection stiffener)

4.6.3 Torsional Brace Strain

Strain gages were placed at the quarter points of the torsional braces so that the brace forces could be measured. Gages were placed on all four sides of the braces. The gages on the top and bottom of the brace were used to measure the torsional brace moments. The gages on the sides provided an indication of the amount of warping restraint that the brace provided. Figure 4.49 and Figure 4.50 show the strain on the respective braces at 20-ft and at midspan for the case with three small torsional braces at the top chord. Additional results are provided in Chapter 5 and Appendix A. The strains at the three quarter points of the braces showed similar trends where the strain increased with the increase of the applied load, however the values were not equal due to a slightly difference in lateral deflection and rotation of the trusses. Because the deformations were slightly different, the braces also experienced some axial strains that caused the strains at the quarter points to be slightly different. The strains on top and bottom sides were in the opposite direction on the same side at the three quarter points, indicating that the brace bent into reverse curvature bending.

Theoretically, at midspan, the warping direction should be zero for the case of the symmetrical half-sine buckle shape; however, in most of the cases the truss did not deflect symmetrically in the half-sine shape. In some cases, the lateral deflection at 48 feet was almost the same as at midspan. This caused the brace at midspan to bend into sine shape in the warping direction; however, at the lesser degree than at 24 and 48-ft locations. The warping strains in the braces at midspan essentially maintained the same rate of change even at the higher load levels near the buckling load, as can be seen as almost straight lines in Figure 4.50.

For the torsional direction, top and bottom sides, the brace behave in the same manner as the warping direction where the brace bent into the sine shape, but into the same direction on all 3 braces which was consistent to the half sine buckling mode shape of the truss. For the case of the strain at 24-ft location of truss with 3 large torsional braces at bottom chord with connection stiffeners, Figure 4.51, the first few strain reading

on the top side on both S/4 and 3S/4 were positive which indicated that the top chord of the truss was initially deflected apart from each other and created upward half sine shape on the brace. The deflection shape of the truss was then changed to the half sine with the same side deflection and the brace deflected shape changed to the full sine shape. According to the lateral deflection test result, the trusses deflected into the same direction as almost in the rigid body translation with the East truss top chord slightly deflected more than the West truss. This was possibly due to the results of the truss initial imperfection combined with the high stiffness brace. The graph was not symmetrical along the Y-axis between the top and bottom side which was because of the lean-on-effect axial force in the brace which was directly related to the initial imperfection.

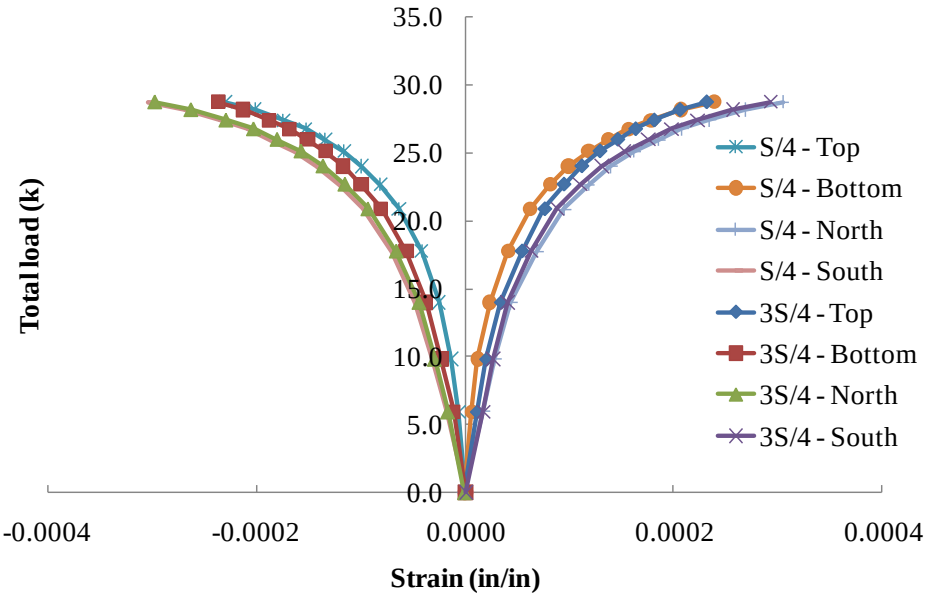

Figure 4.49 Strain at 20-ft brace of truss with 3 small torsional braces at top chord

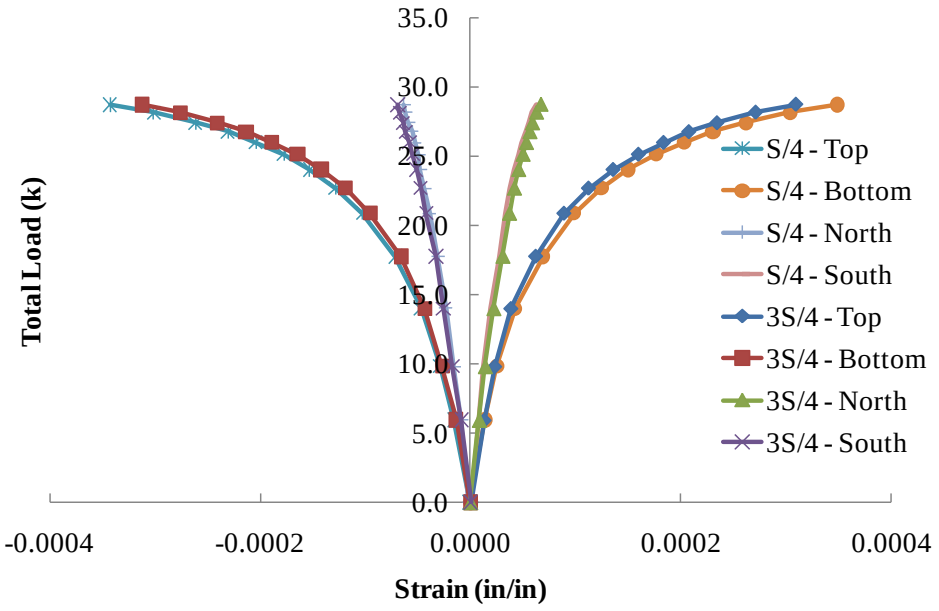

Figure 4.50 Strain at midspan brace of truss with 3 small torsional braces at top chord

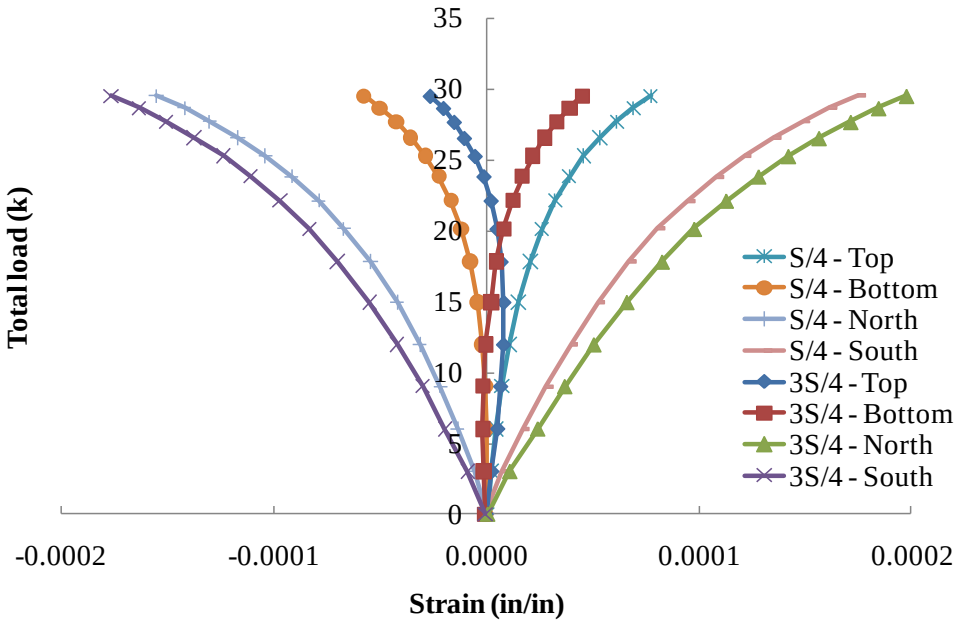

Figure 4.51 Strain at 24-ft brace of truss with 3 large torsional braces at bottom chord

4.6.4 Torsional Brace Axial Force

The strain gages that were mounted on the torsional braces were used to determine the brace forces from the buckling tests. The brace forces were divided into two components: axial and bending. The axial components of the brace forces were determined by averaging the reading from the braces so that the bending components were eliminated. The axial components are shown in Figure 4.52 and Figure 4.53 for large braces at top chord and bottom chord, respectively. The positive values indicate tension force and negative values indicate compression force. The results shown were representative of the wide range of tests that were conducted and additional results are provided in Appendix A. The applied load is graphed on the vertical axis versus the percentage of the brace axial force to the total load applied to one truss on the horizontal axis. The forces ranged from -1 to 4 percent. The axial force came from the unsymmetrical initial imperfection between the two trusses that created a lean-on effect between the trusses. Since the axial force was related to the initial imperfection, the axial force can be either tension or compression. Theoretically, in trusses with a symmetric imperfection, there should be relatively small axial force in the torsional brace since the trusses will deflect and rotate in the same direction. Small differences would be likely since the moments and shears that develop in the brace will affect the buckling behavior slightly; however this effect would be relatively small. For some problems the axial force component may be large enough that it might become important to consider when designing the torsional brace.

4.6.5 Cross Section Distortion and Effect of Connection Stiffeners on Truss Buckling Capacity

It was mentioned previously that adding the stiffeners to the braced joints improved the buckling capacity of the trusses as can be seen in Figure 4.54 for the lateral deflection at midspan of the trusses with three large torsional braces at the bottom chord. At the last load step, with similar magnitudes of the lateral deflection, incorporating the

stiffeners increased load carrying capacity from 23 kips to 30 kips, which was about a 25 percent increase.

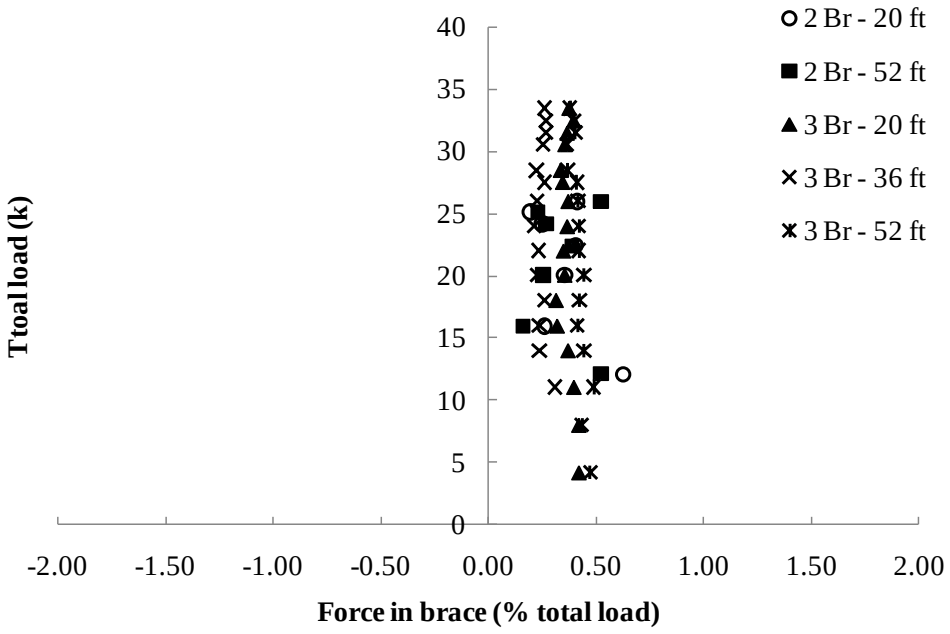

Figure 4.52 Axial force in brace of truss with large torsional brace at top chord

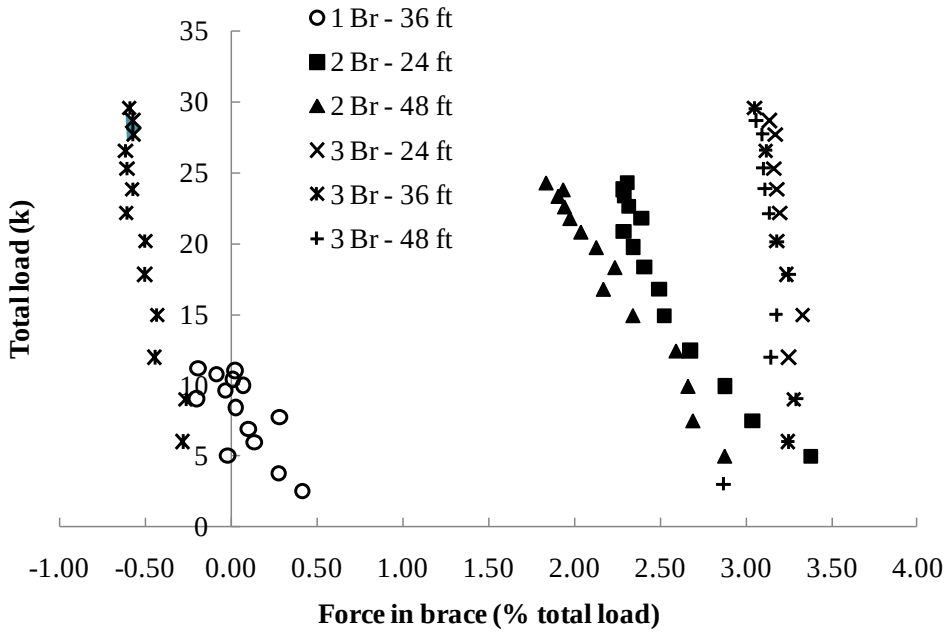

Figure 4.53 Axial force in brace of truss with large torsional brace at bottom chord

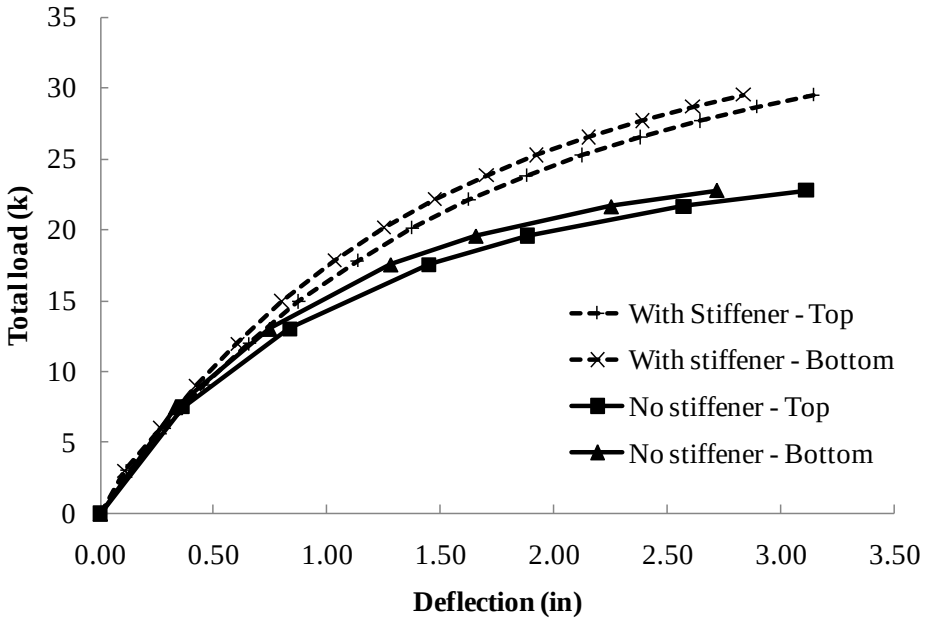

Figure 4.54 Effect of stiffener on buckling capacity of truss with 3 large torsional brace at bottom chord

The results of the adding the connection stiffeners can also be seen in the cross section rotation. Figure 4.55 and Figure 4.56 show the results of the rotation of the cross section at midspan of truss with three large torsional braces at the bottom chord for the respective cases of unstiffened and stiffened connections. Without the stiffeners, rotation at the bottom chord (BC) was larger than other locations in the cross section. The rotation of the brace was expected to be comparable to that of the cross section because it was attached directly to the braced joints; however there was a substantial difference in the rotation of the brace and the rotation of the cross section of the truss due to the connection distortions. By using the rotation of the cross section at bottom chord, the schematic deflection of the connection was drawn and shown in Figure 4.57. According to the cross section rotation data, it can be said that the cross section distortion primarily resulted from the distortion of the web of the wide flange bottom chord and the gusset plate attached to the truss on the braced side. Unfortunately, the web of the chord and the

gusset plate were thin and flexible, resulting in the distortion of the chord web and gusset plate that attached on the brace side.

Adding the stiffeners to the braced connections, Figure 4.56, provided better control of the cross section rotation by reducing the distortion. The effectiveness of bracing system improved since the distortion was reduced. The stiffeners reduced the difference of the rotation between the brace and the joint. The rotation of the torsional brace was increased closer, but not the same, to the rotation of the cross section. According to the test results, it can be concluded that preventing cross section distortion is important in order to acquire higher buckling capacity.

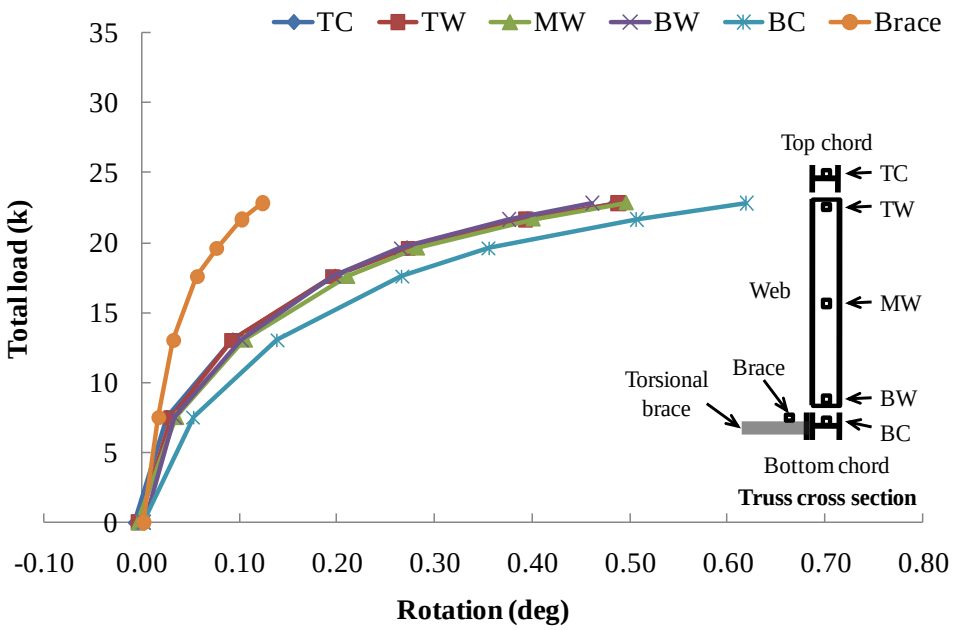

Figure 4.55 Cross section rotation of truss with 3 large torsional brace at bottom chord (without connection stiffener)

4.7 BUCKLING TEST OF PONY TRUSS

The twin truss system was modified to simulate a pony truss by backing off the rounded threaded rods at the top chord at supports to allow the top chord of the truss to move freely. Most of the pony truss tests were done before the connection stiffeners were added. The pony truss test with connection stiffeners were done on the some cases

of truss with large torsional braces. These tests still provided valuable data on the behavior of pony truss systems.

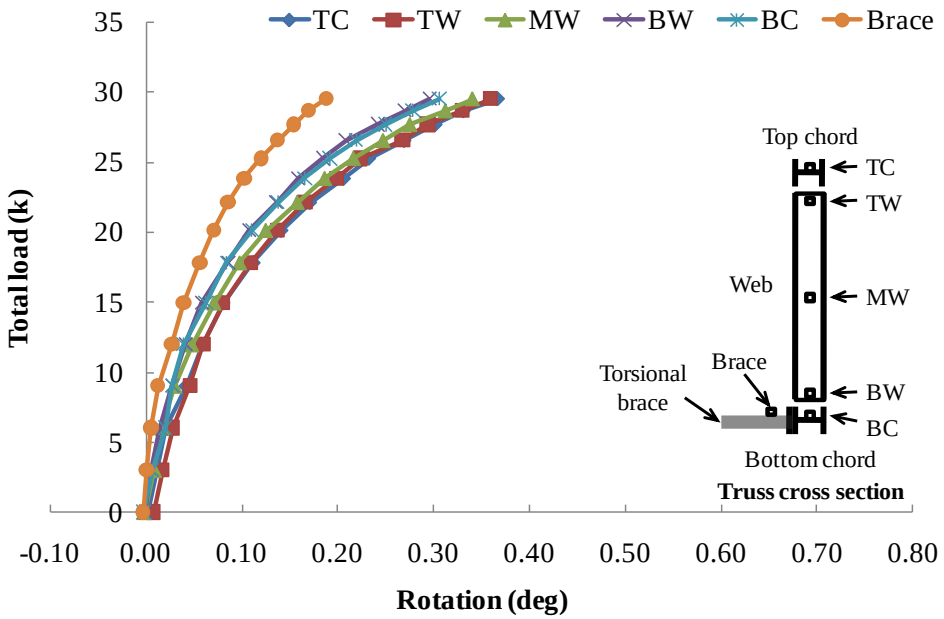

Figure 4.56 Cross section rotation of truss with 3 large torsional brace at bottom chord (with connection stiffener)

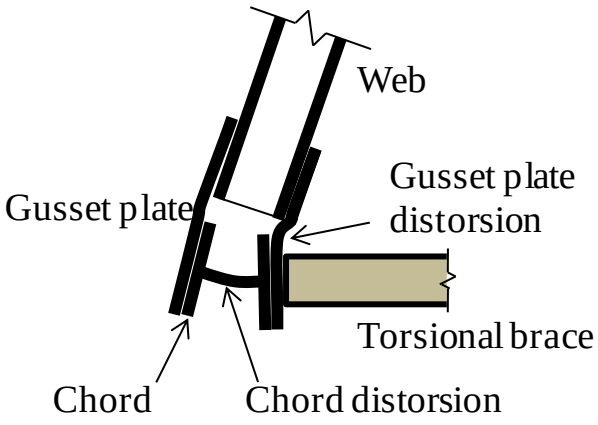

Figure 4.57 Cross section distortion at brace connection due to stiff torsional brace

4.7.1 Lateral Deflection

The pony truss exhibited similar behavior as the regular truss with torsional bracing where the top chord deflected more than the bottom chord along the length of the truss as shown in Figure 4.58 that show the applied load versus the lateral deflection of the truss chords. The top chord lateral deflections at the supports was small compared to the rest and had a relatively linear relationship to the applied load, which differed from the deflections at third points and at midspan, which were nonlinear. Since there was not significant torsional restraint provided at the supports, it was anticipated that there might be significant torsional rotations. The small torsional support rotations are likely caused by a combination of factors including the low axial force at the support top chord, and also the tipping restraint at the support footprints.

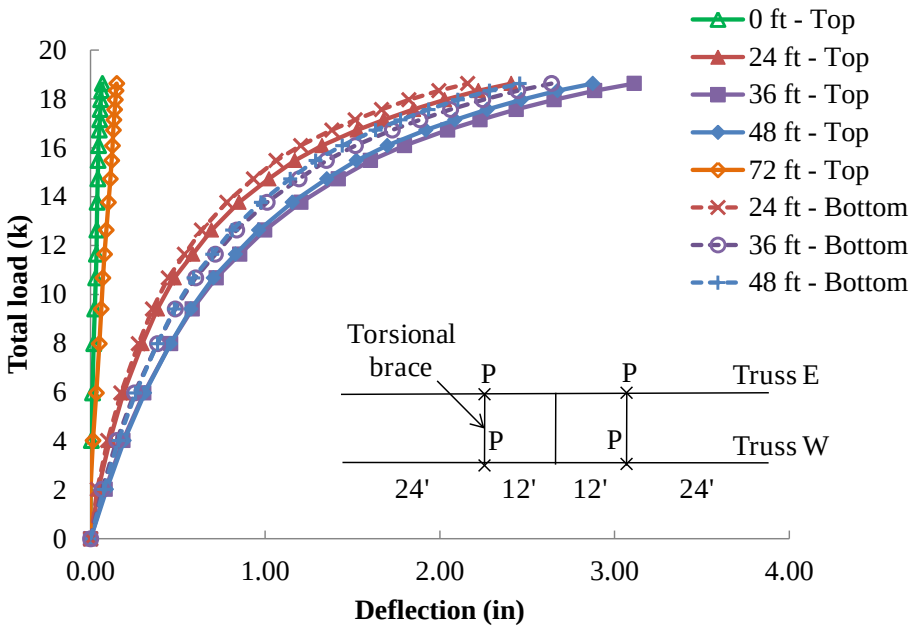

Figure 4.58 Lateral deflection of pony truss with 3 small torsional braces (without connection stiffener)

Figure 4.59 shows the comparison of the buckling capacity of the regular truss and the pony truss with a similar torsional bracing configuration. It can be seen that

regular truss and pony truss had similar behavior. The buckling capacity of the pony truss was less than 10 percent different from the regular truss. This behavior agreed with the small lateral deflection at the top chord at support where only small force was transferred through the top chord at support. The lateral deflection of the cases with connection stiffeners were similar to the case without the stiffeners, shown in Appendix A.

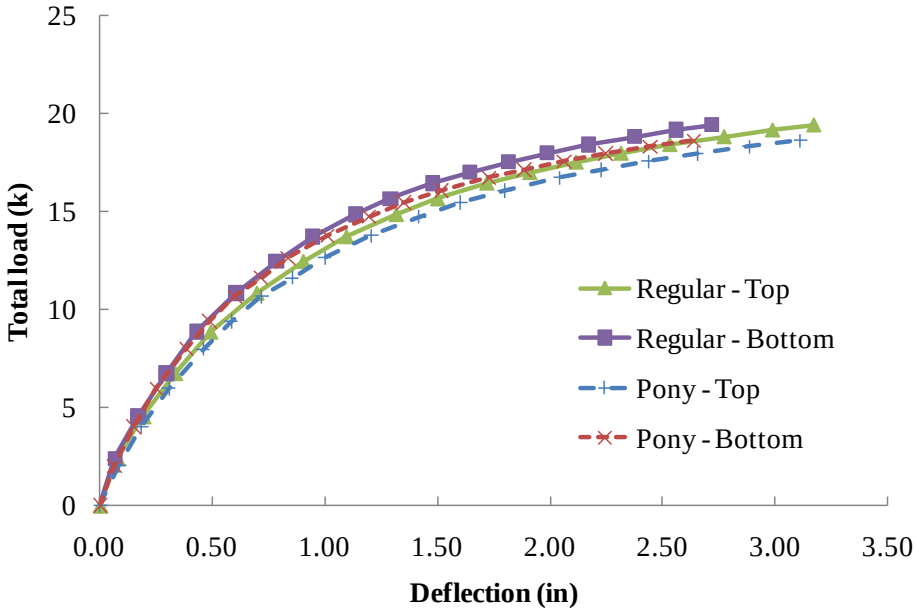

Figure 4.59 Comparison of midspan lateral deflection of truss with 3 small torsional brace (without connection stiffener)

4.7.2 Torsional Brace Strain

The comparison of the brace strain for the cases of truss with three small torsional braces without connection stiffeners are shown in Figure 4.60 for brace at 24 feet. The strains were from the sets of the gages at three quarter point on the brace. As mentioned previously that the buckling capacity of the pony trusses without connection stiffeners was within 10% of the capacity of the regular trusses. Similar behavior was observed in the torsional brace strains. The difference might come from the differences in initial

imperfection, especially for the pony truss where the top chord moved after releasing the threaded rod at the support top chord before the test. The behavior was also similar for the pony truss with connection stiffeners, shown in Appendix A.

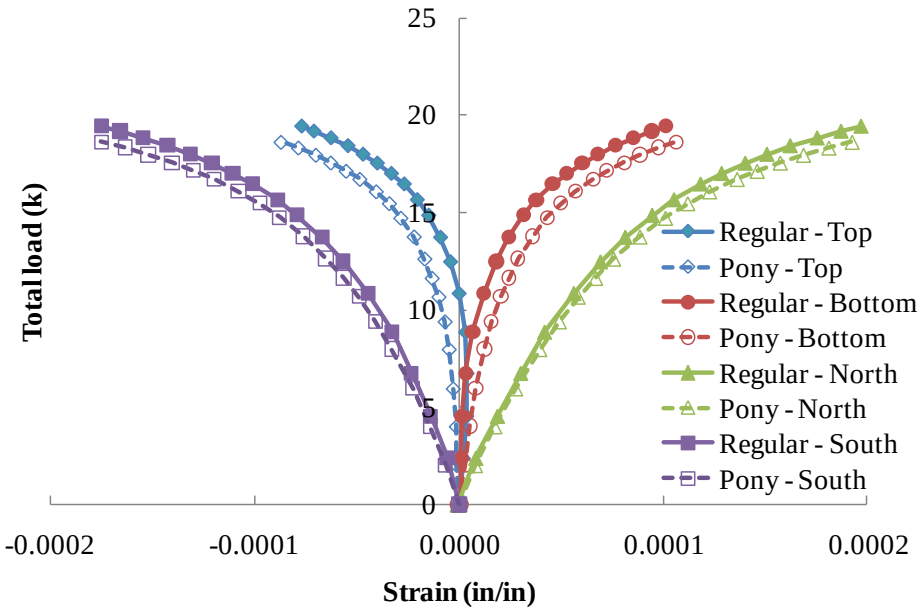

Figure 4.60 Comparison of brace strain at 24-ft brace of truss with 3 small torsional braces

4.7.3 Torsional Brace Axial Force

The axial force of pony truss ranged from -2.0 to 4.0 percent of the total applied load. Comparing the brace forces of the pony truss to the regular truss as shown in Figure 4.61 shows a comparison of the brace forces in the pony trusses and regular trusses. While there were some small differences in the axial brace forces of the regular and pony trusses, a trend in the behavior was not clear from the test data. In many cases the data was similar between the pony trusses and the regular trusses. .

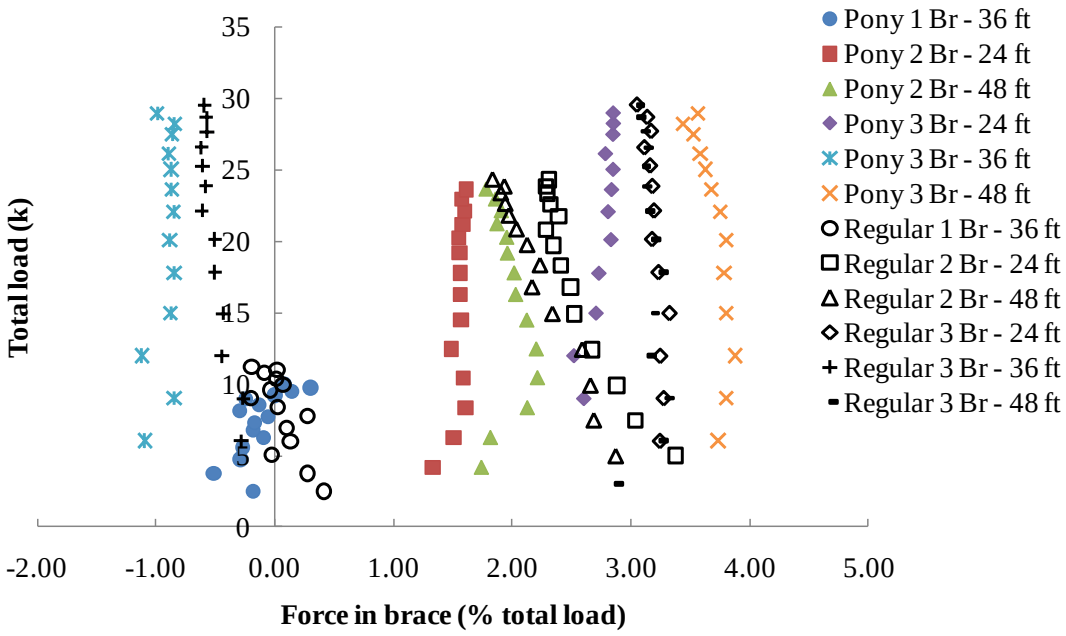

Figure 4.61 Comparison of brace force of truss with large torsional brace

4.8 BUCKLING TEST OF TRUSS WITH LOAD OFFSET

The knife edges were offset 0.5 and 1.0 inch to replicate the initial imperfection at other levels besides the original initial imperfection. The tests were done on the 72-ft truss with and without two large torsional braces with top chord loading. Figure 4.62 shows the results of the comparison of the lateral deflection of the trusses with 0.5 and 1.0 inch load offset to the no-offset case. It can be seen that the truss deflected laterally at the faster rate when load offset distance was higher, resulting in a lower buckling capacity of the truss. The lateral deflection of truss without bracing was not as consistent as the case of the truss with two large torsional braces, as shown in Figure 4.63; however the offset was still within reasonable range.

During the tests of the trusses without bracing, the hydraulics rams tilted approximately 0.5 degree for the case with 0.5" load offset and tilted about 1.0 degree at the beginning and continuously reduced to 0.5 degree at the end of the tests of the case with 1.0" offset. At load below 1.5 kips of 1.0" offset case, the applied load was higher than the other cases due to the use of the GLS strut to stabilize the test setup. The

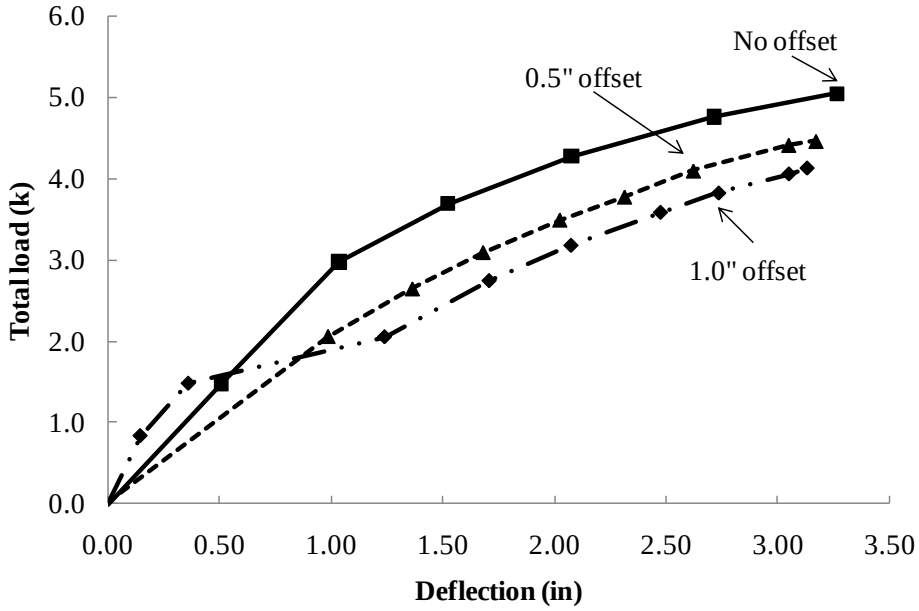

Figure 4.62 Midspan lateral deflection of 72-ft truss without bracing - Top chord loading

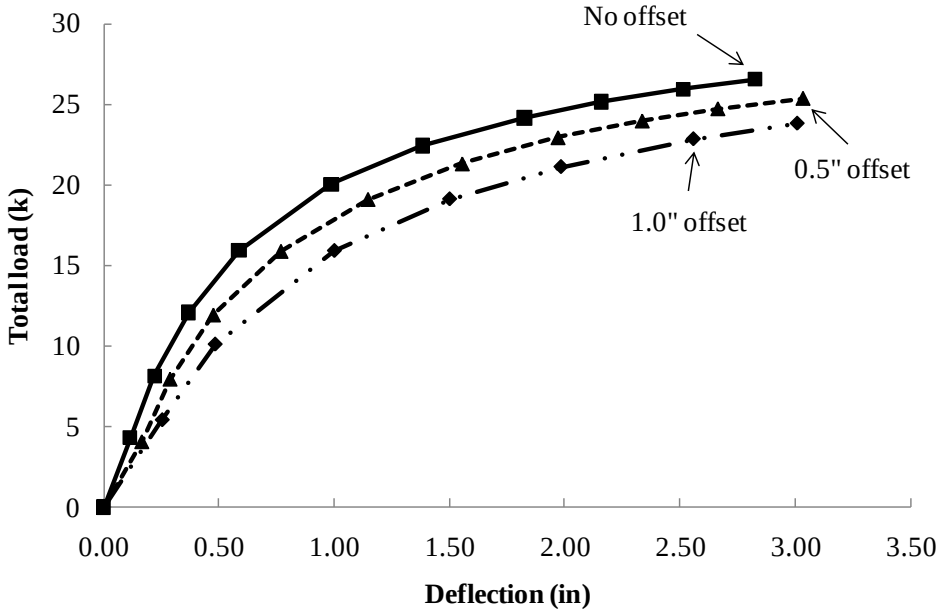

Figure 4.63 Midspan lateral deflection of 72-ft truss with 2 large torsional braces at top chord

deflection shifted to below the 0.5" offset case after the release of the struts. The applied load for the case with 1.0 inch offset without bracing was the lowest applied load in this experiment. The small tilt angle may be due to the low load level and the weight of the GLS's and some internal friction. This tilt angle created the restraint force to pull the system back and might cause the higher buckling capacity than normal. However, with the combination of small angle and low load level, at about 0.5 degree, the system should not be affected much while the load was still far from the buckling capacity, but still can be noticeable from the shift of the load and lateral deflection curves. There was no sign of tilt of the truss with two large torsional braces with load offset cases where the applied load was a lot higher. Thus, this might explain the difference of the non-uniform shifting of the load-lateral deflection curve of the truss with and without torsional braces in the load offset cases.

In the truss with two large torsional braces with load offset, the torsional moment and warping moment in the brace was also uniformly shifted, as can be seen in Figure 4.64 and Figure 4.65 for the torsional moment and warping moment in the North brace, respectively.

4.9 SUMMARY

This chapter provided sample results from the various tests that were conducted on the twin truss systems. The data that was gathered included the initial imperfections of the trusses, the lateral stiffness test, and the buckling tests of trusses with and without lateral bracing and torsional bracing system. The lateral stiffness of truss was shown to be dependent on the truss direction due to the reduction in stiffness from secondary effect and the alignment of the diagonal element. The Southwell plot was used for predicting the buckling capacity of truss without bracing. By using the Southwell technique, the load height factor can be estimated from the laboratory test results. As expected, the buckling capacity of trusses increased with the presence of the bracing system and the increase in the brace stiffness of both lateral and torsional braces. The efficiency of the bracing decreased with the increasing number of the braces due to less deflection and

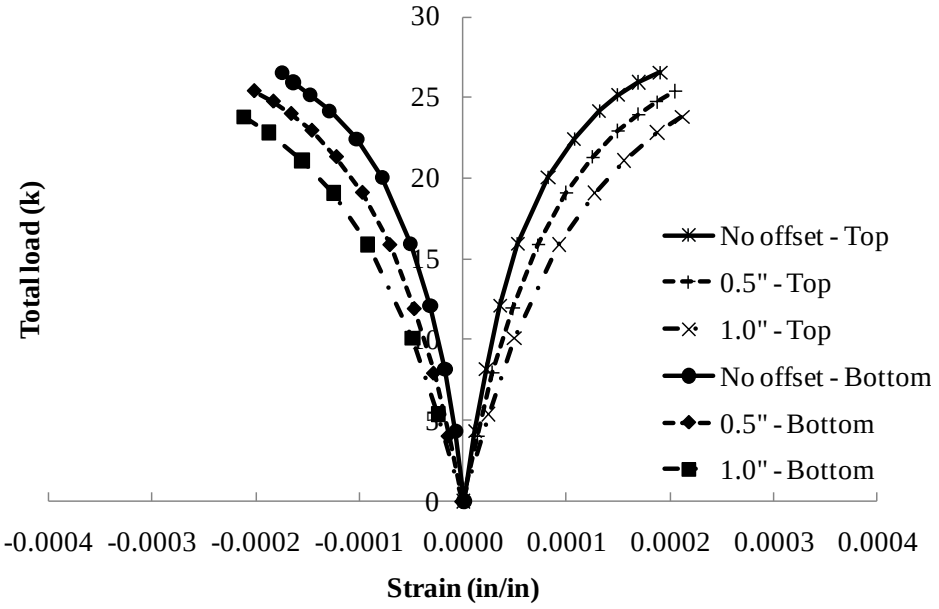

Figure 4.64 Torsional strain at 3S/4 in North brace of truss with 2 large torsional braces at top chord

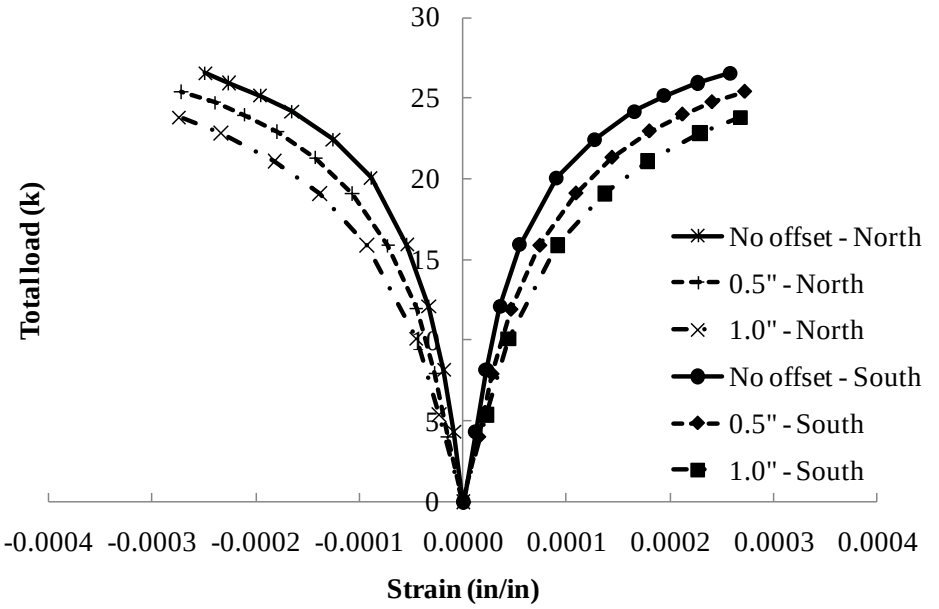

Figure 4.65 Warping strain at 3S/4 in North brace of truss with 2 large torsional braces at top chord

rotation at the location further away from the midspan. Pony trusses were tested and exhibited similar behavior to regular truss with torsional bracing although the pony truss buckling capacity was slightly lower. For torsional bracing systems, providing connection stiffeners at the braced joint is important in terms of improving the buckling capacity by controlling distortion of the connection region. Offsetting the load provides another way to simulate the initial imperfection of the truss. The effect of the load offset tended to reduce the buckling capacity of the truss.

CHAPTER 5
Development of Finite Element Model and Model Verification

5.1 INTRODUCTION

Verification of the modeling techniques in finite element studies is an important step before the model can be used to conduct a parametric investigation. In this study, the ANSYS Academic Research, Release 11.0 program (ANSYS, 2010) was used to develop the finite element model of the truss systems. The verification focuses on behavior of the individual trusses as well as the behavior of the trusses with torsional bracing. To accurately compare the model to the test results, the initial condition of the truss model must be carefully compared to the test setup which includes the support and boundary conditions, self weight and initial imperfection. The verification included the lateral stiffness test, lateral and vertical deflections of buckling test of truss with and without torsional bracing.

5.2 DEVELOPING OF THE FEA MODEL

The finite element model was developed using line elements for the major truss elements. The element type was BEAM44 was employed for the different elements of the truss and bracing system. BEAM44 element is a two node elastic line element with six degrees of freedom at each node with the tension, compression, torsion and bending capabilities (ANSYS, 2010). The shear deformation and the warping degree of freedom were not included in this element; however the shear deformation is available as an option. Although both the BEAM44 and BEAM4 elements were considered, a drawback of the BEAM4 element is that all of the cross section properties need to be input into the BEAM4 element. The advantage of the BEAM44 element is that the user can input the

actual cross-section into the BEAM44 element using the predefined ANSYS cross-section with the input of the geometric properties of the cross section.

The model consisted of the line element model with W4x13 cross-section at the chords and web with the length equal to the actual length of the tested trusses. The connection elements were also modeled using BEAM44 elements and were used to connect the line elements together at the connections. This connection replicated the gusset plate. However, it was difficult to determine the stiffness contribution of the gusset plate to the chord, vertical and diagonal web that intersected at the gusset plate. Thus, several trials were conducted for fitting the results to the model. Several variables were studied in comparing the models with the laboratory results on the lateral stiffness of the truss. These variables included variations in the size and lengths of the vertical and diagonal connection elements, different cross sectional shapes, flange and web thickness of the chord/web members. Although a wide range of the parameters were considered, the accuracy of the model still differed substantially from the test results. The aspect of the model that proved critical for achieving good comparisons with the test results was the length of the connection element. The lengths of the connection elements were adjusted by changing the distance from the virtual node (point of intersection of the center lines from each element) to the center of the group of bolts at the chord or web to the distance from the virtual node to the edge of the gusset plate, which were 5.25, 8.0, 8.8 inches for the connection elements of chord, vertical and diagonal web, respectively, Figure 5.1. The thickness of the gusset plate plus the thickness of the element section were used with proper width for connection elements model. The width of the connection elements was 6.0 inches and was verified by the test results. Figure 5.2 shows the final truss model with the line element shape enhanced.

The load beams from the test setup were modeled with a MASS21 element. A MASS21 element is a point element with six degree of freedom including mass components and rotational inertias and can be defined by a single node (ANSYS, 2010). The MASS 21 elements were attached to the nodes where the actual loading points were at 24 and 48 feet for the top chord loading tests and at 10 inches offset to the support side

from 24 and 48 feet locations for the bottom chord loading tests. The load of the load beam was the actual weight of the beams including the two knife edges, which was 1,260 lbs. For the cases without bracing, the nodes for the load beam on both trusses were coupled together in the out-of-plane degree of freedom to simulate the effect of the load beam for linking the trusses together.

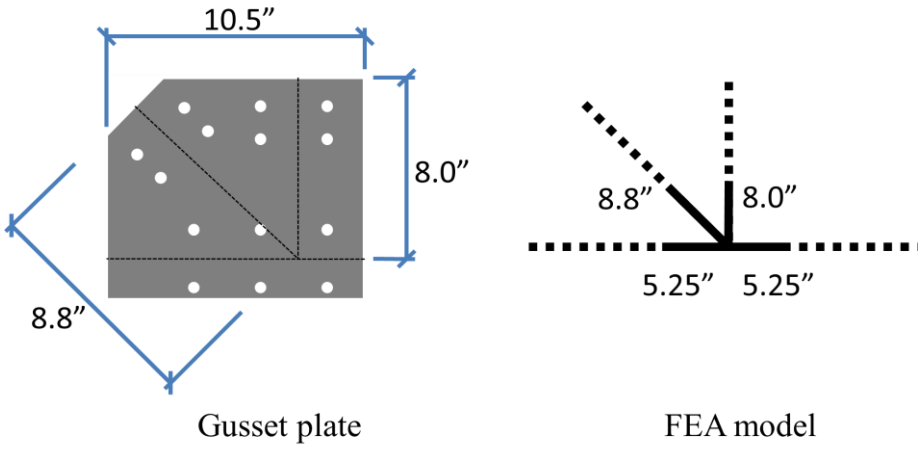

Figure 5.1 Dimension of gusset plate and ANSYS connection

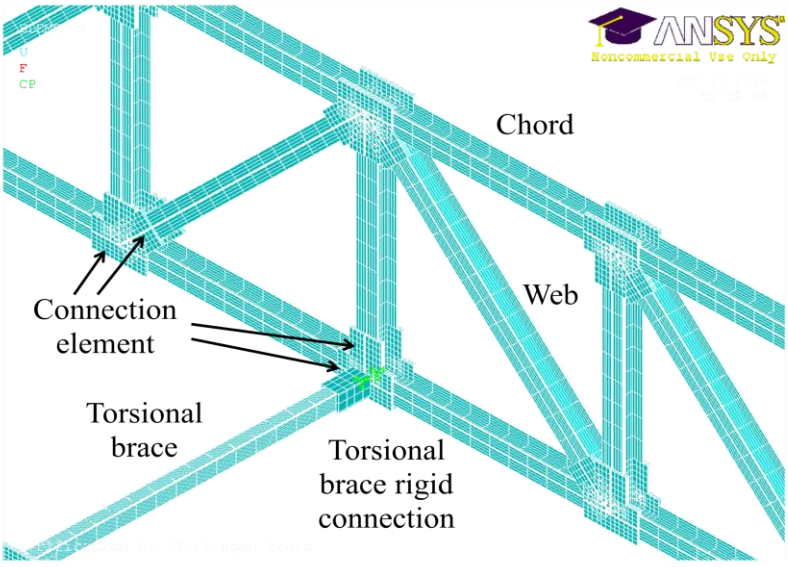

Figure 5.2 Truss model showing enhanced line element shape

The BEAM44 elements were also used to model the torsional braces. Since the predefined model did not include the bend radius at the corner of the HSS section, the section properties were slightly different from the values specified in the steel manual (AISC, 2005a).

5.3 FEA MODEL INITIAL CONDITIONS

The results from the lab tests were used to verify the modeling techniques in the ANSYS model. An important step in this process was ensuring that the FEA model accurately captured the boundary conditions, load conditions and locations, and initial imperfection. The boundary conditions from the test setup were designed to achieve the commonly idealized support conditions for buckling by using simple supports with thrust bearing and rounded threaded rod so that warping restraint was minimized. As mentioned in Chapter 3, thrust bearings were also used at the knife edges. In the FEA model, these boundary conditions limited the translational degrees of freedom in the model but the nodal rotational degrees of freedom were unrestrained in the support boundary conditions.

Another important factor for the verification of the FEA model to the lab test results was modeling of the initial imperfections. The measured initial imperfection was input into the model to replicate the actual initial imperfection before the tests. The process to obtain the initial input imperfection was done with several iterations per each setup condition until the imperfection in the model had good correlation with the actual measured imperfection. The iteration processes were started by inputting the measured initial imperfection into the model. It should be noted that if the model had the torsional braces attached to the truss system, these elements were deactivated. A static analysis was then done with the actual self weight of the truss and loading apparatus to obtain the deflection. This deflection was subtracted from the input initial imperfection. The difference was used as the adjustment factor. The modeled initial imperfection was then reduced by the multiplication of the adjustment factor, which was less than one. The process was repeated until the final modeled imperfection had good correlation with the

measured imperfections. Figure 5.3 to Figure 5.4 show examples of the measured initial imperfection, the input initial imperfection and the lateral deflection due to the self weight. Figure 5.3 shows the results at the bottom chord of the 72-ft East truss with 3 small torsional braces attached at the top chord where the load was applied. Several iterations were conducted until the final imperfection (input + self weight deflection) was close to the measured imperfection. Figure 5.4 shows the final imperfection used in the large displacement analyses along with the measured imperfection. The agreement was not perfect; however the modeled imperfection provided reasonable agreement with the laboratory measurements. Additional imperfection comparisons are provided in the Appendix A. These graphs suggested that this technique works very well in matching the measured versus modeled initial imperfections.

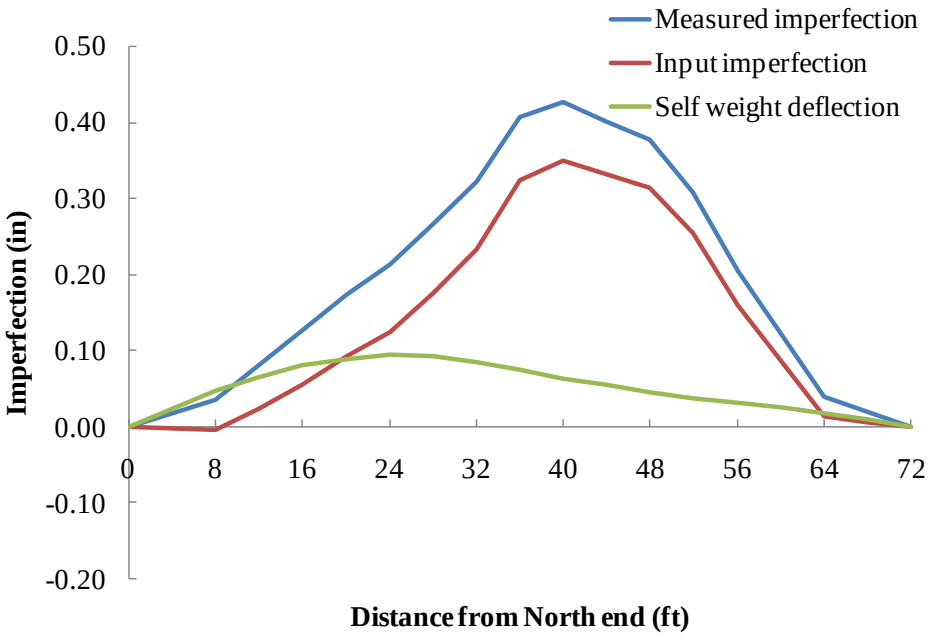

Figure 5.3 Comparison of initial imperfection at bottom chord of 72-ft span East truss with 3 small torsional brace at top chord with top chord loading

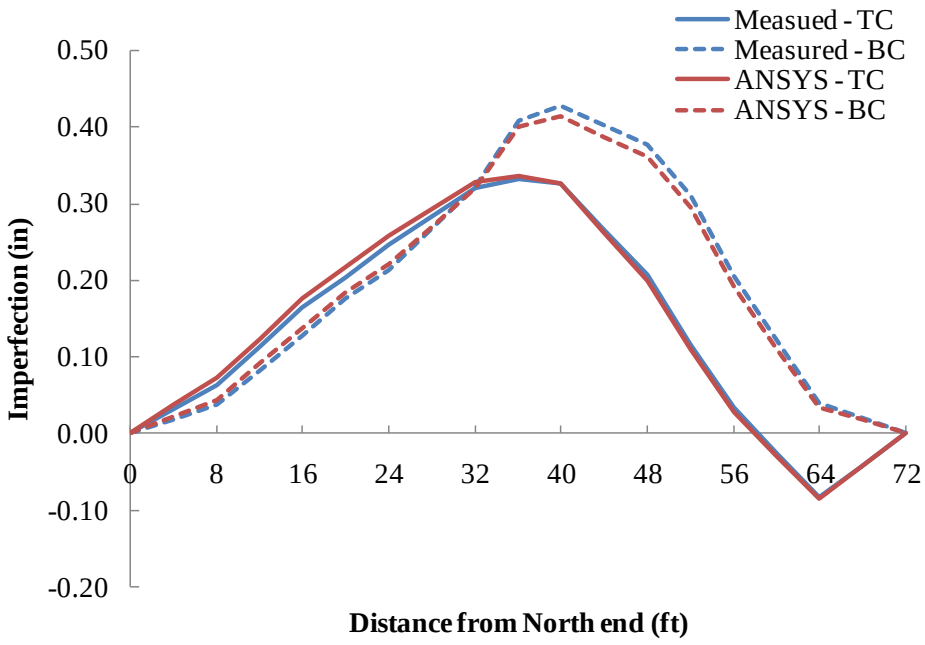

Figure 5.4 Comparison of initial imperfection of 72-ft span East truss with 3 small torsional brace at top chord with top chord loading

5.4 MODEL VERIFICATION

Comparisons between the laboratory test results and the FEA models were made for all of the different types of tests to ensure that the modeling assumptions were correct. The verification was done on the lateral stiffness, the vertical stiffness, and the buckling performance of the regular trusses. Selected results of the 72-ft span verification are shown in this chapter. The results that are shown are representative of the trends that were observed in the comparisons. Additional results from the 72-ft span trusses as well as the 48-ft span trusses are provided in Appendix A.

5.4.1 Lateral Stiffness Test

The results from the lateral stiffness tests were used to verify the lateral stiffness of the FEA model by comparing the lateral displacements at 16, 24 and 32 feet of the 48-ft span trusses and at 24, 36 and 48 feet of the 72-ft span trusses. Depending on which test was under consideration, the lateral loads were applied at the top or bottom chord at

the third points. The verification was conducted with and without lateral stops on the unloaded truss chord. The different boundary conditions with and without the lateral stops provided variations in the lateral and torsional stiffness of the trusses to improve the confidence in the modeling of the trusses and the connections. The lateral stops increased the stiffness of the trusses and also provide more information on the contribution of vertical and diagonal web elements and the gusset plate to the truss out-of-plane stiffness. Since the self weight and the alignment of the diagonal members might affect the model, the model was verified in both regular (Howe) and inverted (Pratt) trusses.

5.4.1.1 Lateral Stiffness of Truss without Lateral Stops

The verifications were done at 24, 36 and 48 feet on top and bottom chords of the 72-ft span truss. However, only the results at the midspan location are shown here. Figure 5.5 and Figure 5.6 show the results of the lateral deflection of the respective cases for top and bottom chord loading with the 72-ft span regular truss. Figure 5.7 and Figure 5.8 show the results of the same load cases for the inverted truss. The graphs show that good agreement between the FEA and measured results was achieved in the lateral stiffness of the trusses for all the load cases and truss orientations. The FEA results confirmed the behavior found in the laboratory test results that the top chord deflected more than bottom chord in both top and bottom chord loading cases of the regular truss. The results also agreed with the inverted truss cases where the bottom chord deflected almost the same as the top chord for top chord loading case and it deflected more than top chord for bottom chord loading cases.

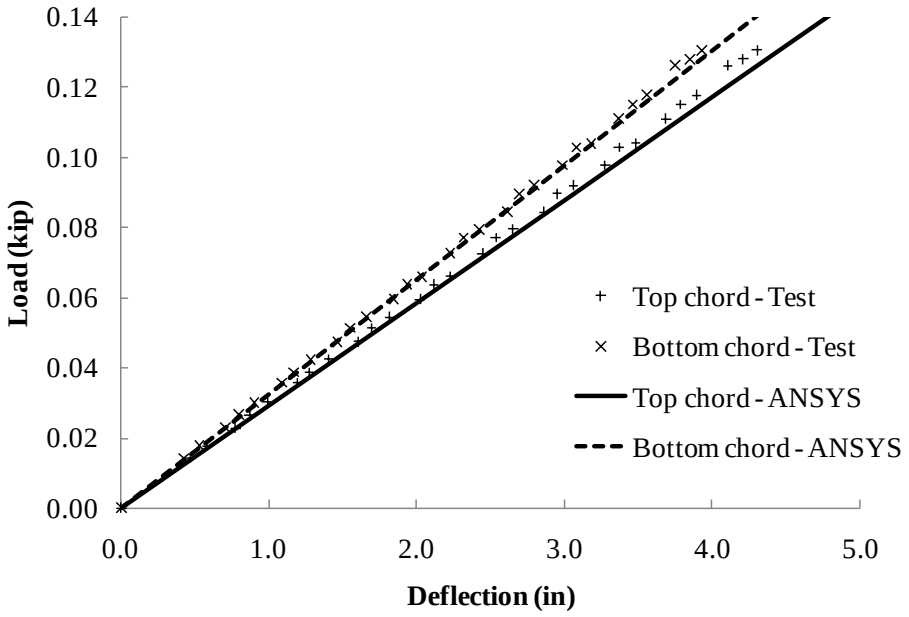

Figure 5.5 Midspan lateral deflection of 72-ft regular truss with bottom chord loading

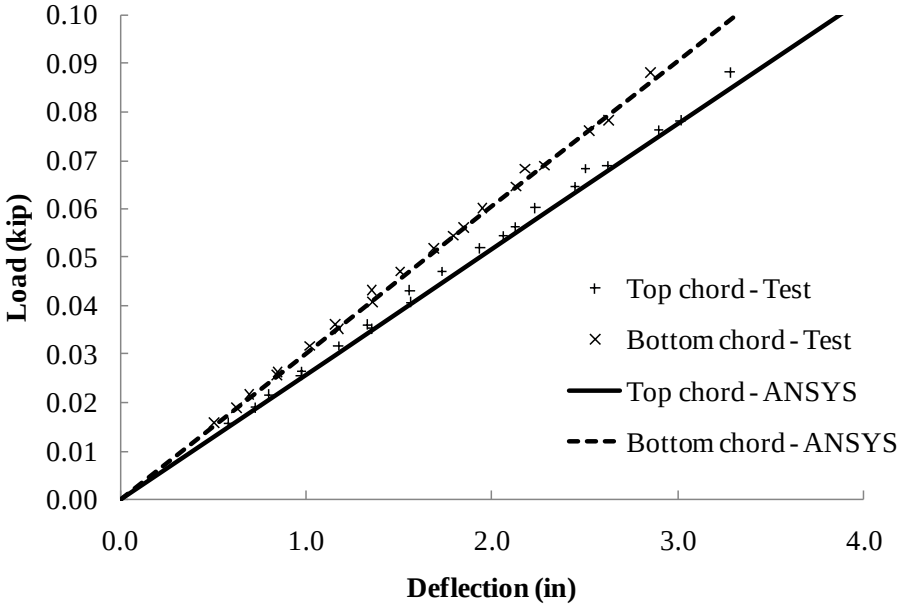

Figure 5.6 Midspan lateral deflection of 72-ft regular truss with top chord loading

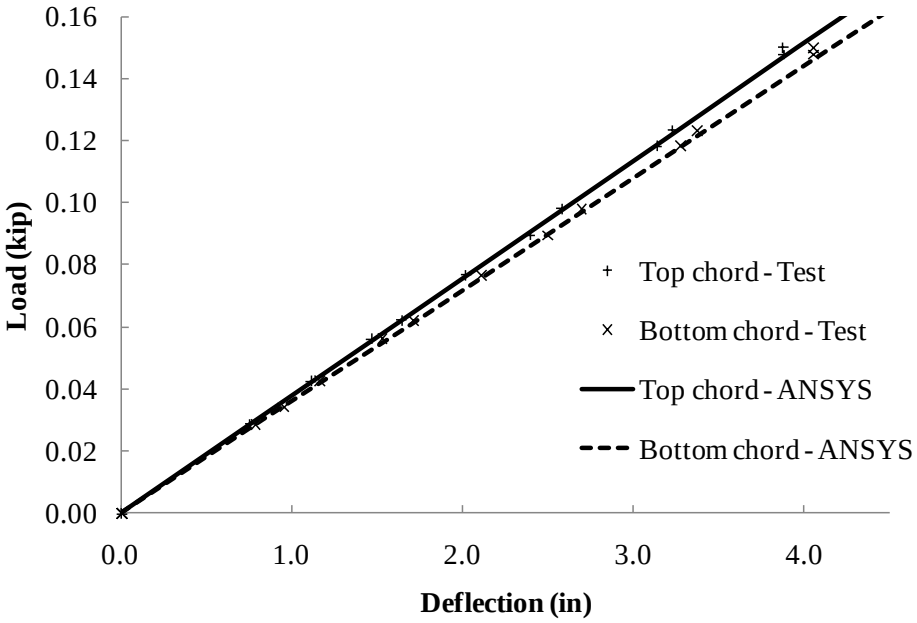

Figure 5.7 Midspan lateral deflection of 72-ft inverted truss with bottom chord loading

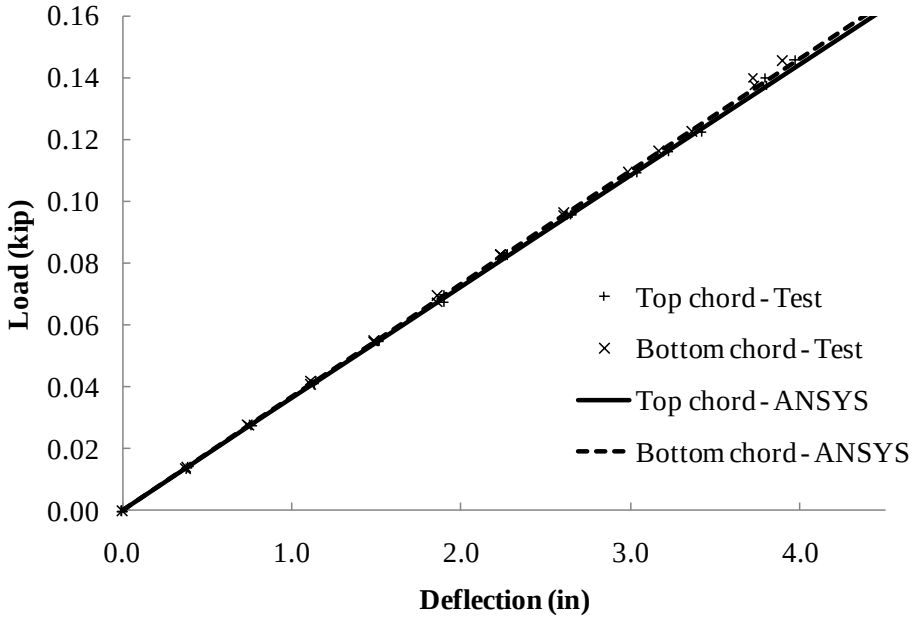

Figure 5.8 Midspan lateral deflection of 72-ft inverted truss with top chord loading

5.4.1.2 Lateral Stiffness of Truss with Lateral Stop

Results of the trusses with the lateral restraints are presented in this subsection. The results of the verification of lateral stiffness of the restrained regular trusses are shown in Figure 5.9 and Figure 5.10 for the respective cases of top chord loading with restraint at bottom chord and bottom chord loading with restraint at top chord. Additional results of regular and inverted trusses are provided in Appendix A. Most of the analysis results matched extremely well to the test results except one case where the analysis result of the top chord was about 10 percent different from the test result which was the case of regular truss with top chord loading and lateral stop at bottom chord shown in Figure 5.9.

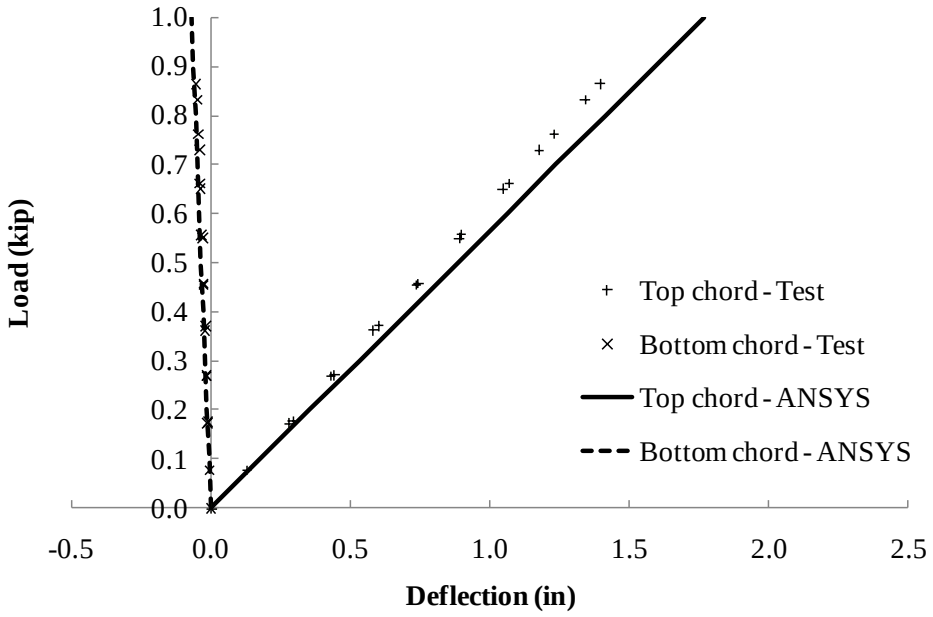

Figure 5.9 Midspan lateral deflection of 72-ft regular truss with top chord loading and lateral stop at bottom chord

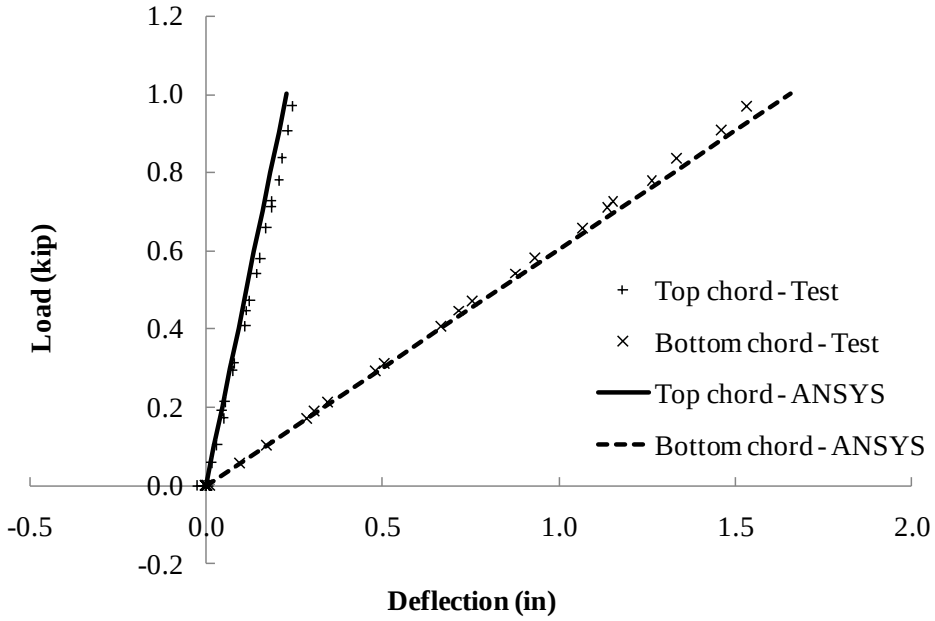

Figure 5.10 Midspan lateral deflection of 72-ft regular truss with bottom chord loading and lateral stop at top chord

5.4.2 Buckling Test of Truss without Intermediate Bracing (with 48-ft and 72-ft span)

The accuracy of the FEA model was also verified with the laboratory test data for the vertical stiffness and bucking behavior. The model was verified first with the trusses without the brace. Since most of the lab tests were done on the 72-ft span truss, the majority of the verification results were done on the 72-ft span. However, to ensure that the model works correctly with other span lengths, the buckling capacity with the 48-ft span was also verified. Figure 5.11 shows that the FEA model replicated the actual test setup for 48-ft span truss. The trusses were modeled as they were tested, which consisted of the 72-ft span trusses supported at 12 and 60 feet to create the 48-ft span. The support points are indicated in Figure 5.11. The model subjected to the bottom chord loading at 16 and 48 feet from the support with 10" offset from the load joints to the support sides and three inches vertical offset to the actual knife edge position. Simple support conditions were modeled and the trusses were restrained from lateral translation at the top

and bottom to prevent twist of the cross section. The large displacement analysis was performed with top chord loading and the deformation results at midspan are shown in Figure 5.12 and Figure 5.13 for the lateral deflection and the vertical deflection. The applied load of the FEA truss model was approximately 10% larger than the measured results. The angles of twist, the difference between the top and bottom chords, between the test and the model were very similar. Several factors could affect the test results such as the friction of the test setup at the supports and at the GLSs and also the sensitivity of the buckling test. These could lead to the difference in the lateral deflection as shown in this test. Reasonable agreement was achieved between the FEA and experimental results in the vertical stiffness of the truss, however the computational model was slightly stiffer in the vertical direction than the test results indicated. Similar correlation was achieved between the FEA model and the test results for the bottom chord loading that are shown in Appendix A. The FEA model was a slightly stiffer than the test results in both the lateral and vertical deflections with the differences within 10 percent.

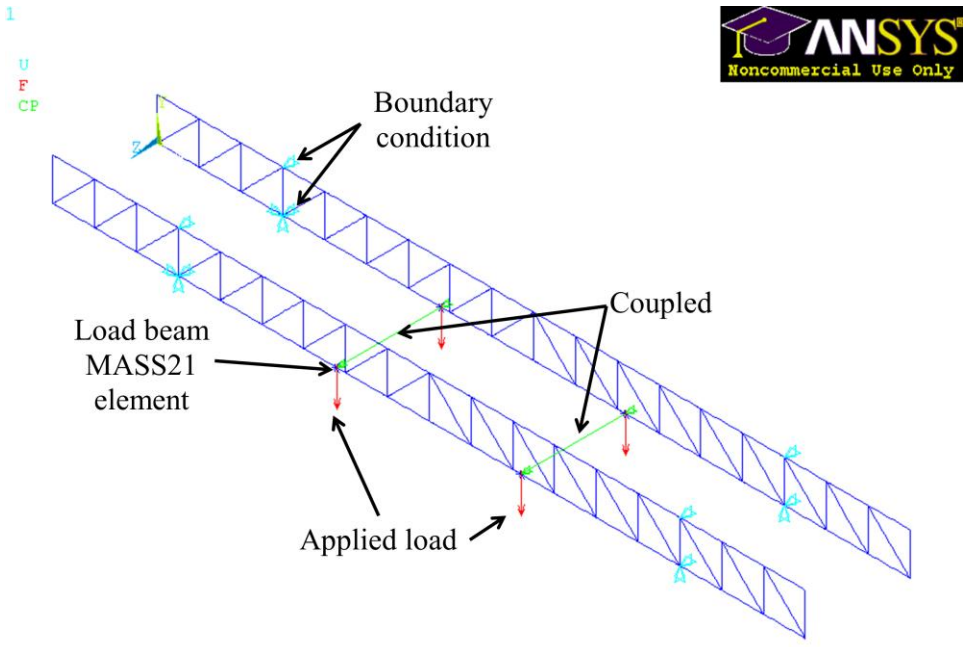

Figure 5.11 ANSYS model replicate the test setup

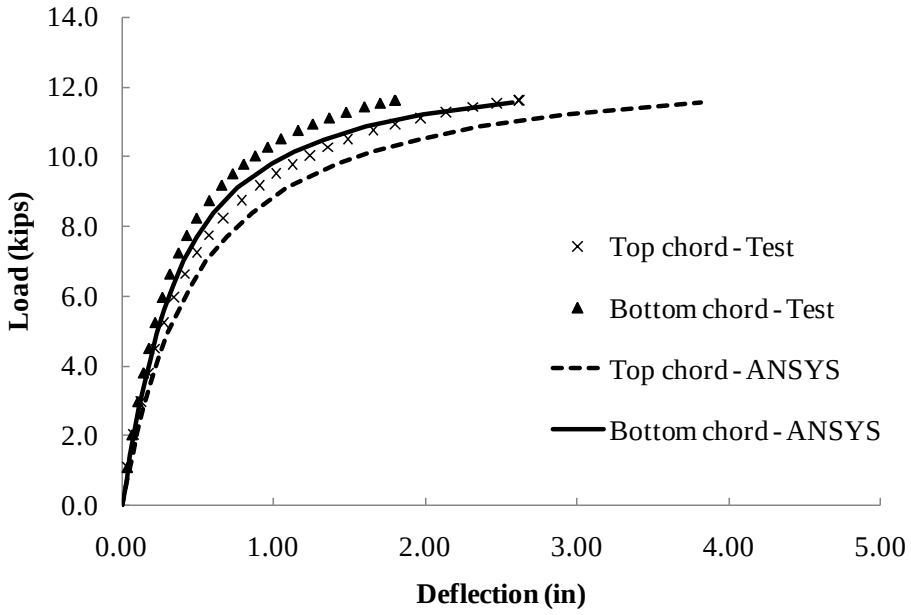

Figure 5.12 Midspan lateral deflection of 48-ft span truss with top chord loading

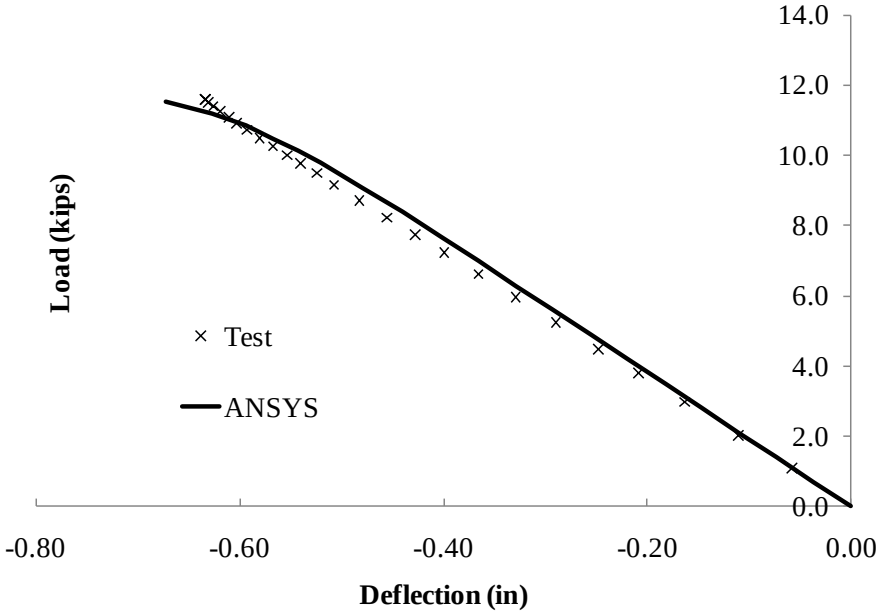

Figure 5.13 Midspan vertical deflection of 48-ft span truss with top chord loading

As mentioned earlier, several factors can affect the buckling test results that can lead to difference in the buckling capacity between the FEA model and the test measurements. Most of these factors generally have a more significant effect on the 72-ft span trusses due to the relatively low out-of-plane stiffness. Figure 5.14 shows the verification of the truss with the 72-ft span truss with top chord loading. The difference between the load of the truss and the model was within 20 percent and the model was stiffer than the test results. The accuracy between the FEA model and the measured results for the vertical stiffness was about the same between the 72-ft and 48-ft span trusses. As shown in Figure 5.15, the vertical deflection of the 72-ft span truss model showed a very good agreement with the test result. As the load approached the buckling capacity, the truss tended to deflect laterally a significant amount and resulted in the larger measured vertical deflection, as can see that the straight line at the beginning started to bend down in Figure 5.15. The vertical deflection did not only come from the in-plane vertical deflection, but also from the vertical component of the lateral deflection due to the twist of the truss, Figure 5.16. This led to higher FEA vertical deflection and

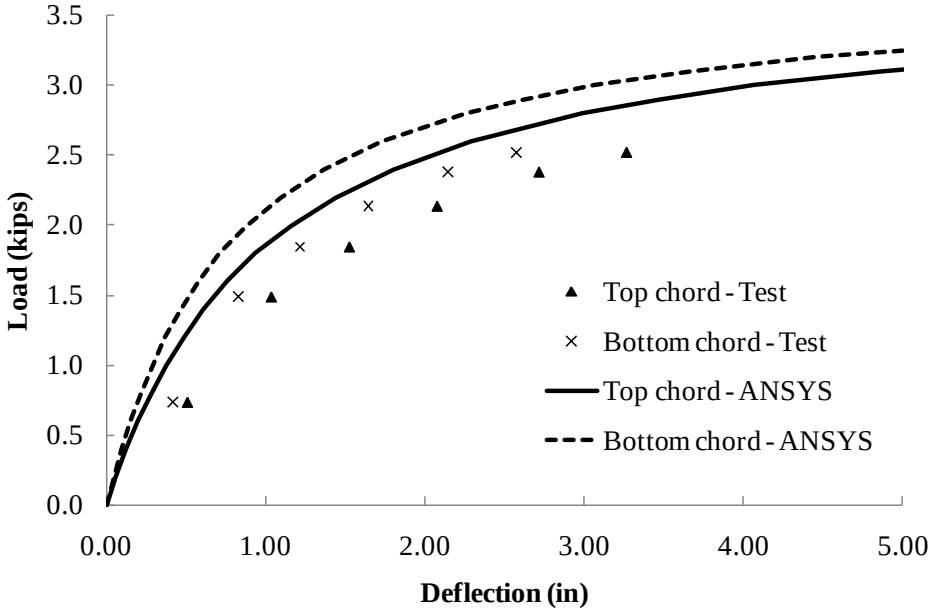

Figure 5.14 Midspan lateral deflection of 72-ft span truss with top chord loading

the graph tended to bend down when the load approached the buckling capacity where the lateral deflection increased rapidly.

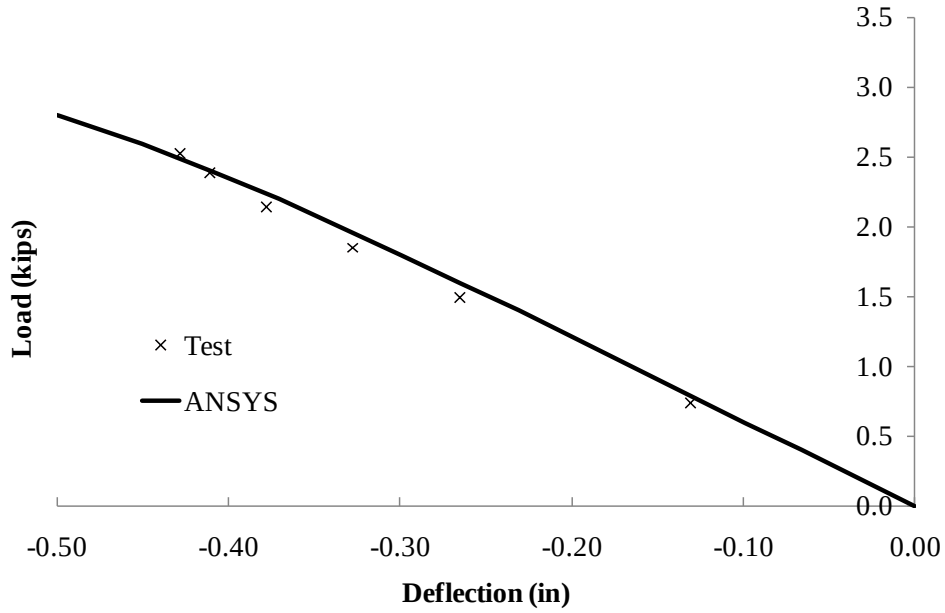

Figure 5.15 Midspan vertical deflection of 72-ft span truss with top chord loading

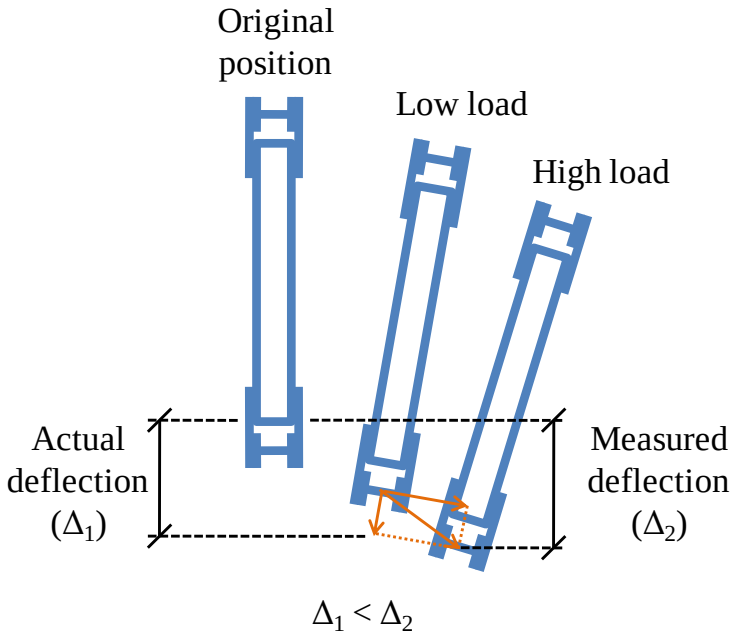

Figure 5.16 Vertical component of lateral deflection

5.4.3 Buckling Load Test with Torsional Bracing

With the low out-of-plane stiffness of the truss without bracing, the friction can play an important role in the difference between the test results and the FEA model. On the other hand, the truss with torsional bracing increases the out-of-plane stiffness of the truss. Thus, the frictions contribute less to the difference in this model. However, it is worth to mention that there are several other factors that can affect the models which are mainly the geometry and the modeling techniques of the bracing. Figure 5.17 shows the verification of the midspan lateral deflection of the truss with a single small torsional brace on the bottom chord at midspan. The results shown in Figure 5.17 are for the case with no connection stiffener. As mentioned in Chapter 4, the cross section distortion occurred at the brace connections of the truss with torsional bracing. The results from the FEA model and test results explicitly show that the buckling capacity of the model was significantly higher than the test result. Even though the cross section distortion was very small and cannot be noticeable in this case, the distortions largely affected the performance of the truss by reducing the buckling capacity by approximately 30%. Therefore, larger difference would be expected for the truss with larger torsional brace. Although the distortion is a local deformation, the impact affects the global lateral stiffness. The factor that clearly was less affected by the local distortion was the twist of the truss. From the graph, the twist of the truss was not noticeably different between the measured and FEA solution as evidenced by approximately the same difference between the top and bottom chord deformations in the FEA model and the measured deformation.

According to the geometry of the Howe truss configuration, there is only a single web vertical element attached to bottom chord at midspan, while the other bottom chord joints have both a vertical and a diagonal web member that frame into the joint. In addition, the gusset plate used for the midspan bottom chord connection was also smaller than the other joints where two members framed into the joint. Taken together, this led to lower connection stiffness at the midspan bottom chord joint. For the case with torsional brace attached to the bottom chord of the regular (Howe) truss, the torsional brace was a

significantly stiffer than the connection plate, which amplified the cross section distortion and resulted in the larger difference in the buckling capacity of the truss model. This was a limitation of the line elements used in the FEA model since the line element does not include the connection cross section distortion into the calculation. A shell element model could be used which would capture the localized cross sectional distortion; however, such a model dramatically increases the size and complexity of the model.

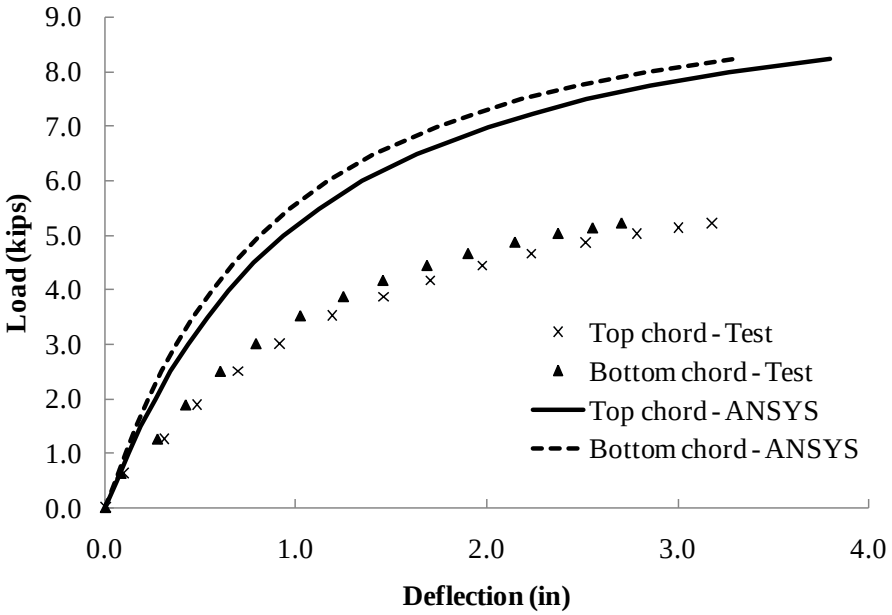

Figure 5.17 Midspan lateral deflection of truss with single small torsional brace at midspan bottom chord without brace connection stiffener

The torsional brace primarily improved the lateral stiffness of the truss. Therefore, the vertical deflection of the model was still in a good agreement with the test results in all verified cases as shown in the last section without intermediate braces. Figure 5.18 show the example of the vertical deflection verification of the truss with one small torsional brace at bottom chord. Additional results are provided in Appendix A.

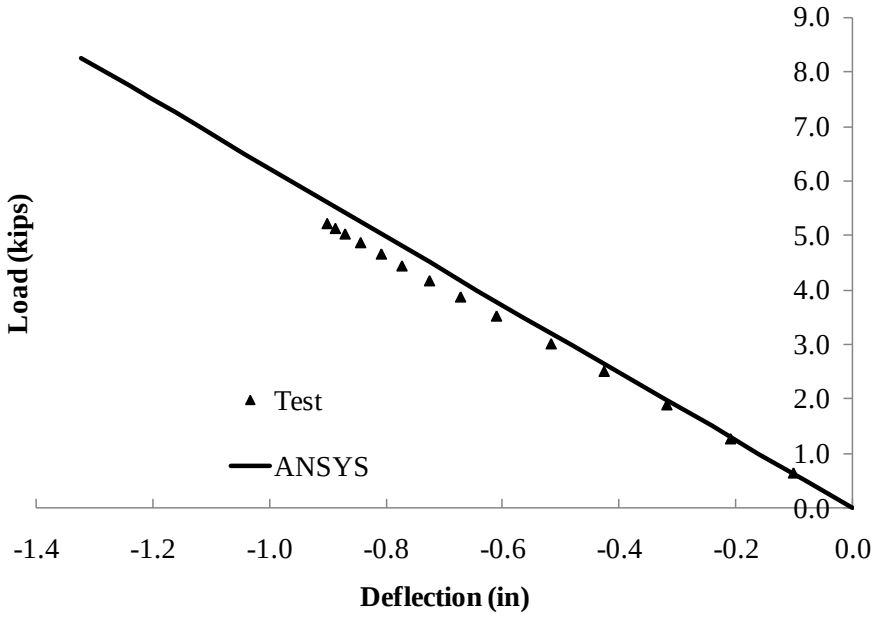

Figure 5.18 Midspan vertical deflection of truss with single small torsional brace at midspan bottom chord without brace connection stiffener

Once the stiffeners were added to the braced connection joints, the chord cross section distortion would expect to be greatly reduced and the results from the FEA model should match the test results better. Figure 5.19 and Figure 5.20 show the verification of the lateral deflection of the truss with three large torsional braces at the bottom chord and the truss with two large torsional braces at the top chord, respectively. The model was in a good agreement with the top chord bracing, but not with the bottom chord bracing. The model still had a higher buckling capacity than the test results. This could be explained by the difference of the gusset plate in the model and actual test setup. The gusset plates for the web, both vertical and diagonal, were modeled in the form of wide flange section which was ideal to prevent connection distortion, Figure 5.21. This was different from the actual model where only the gusset plate was used to connect the chords to the web members. The wide flange model was stiffer than the actual gusset plate. For the truss with small torsional brace, the applied load was low and the brace was flexible. The connection should have not contributed much to the system compared to stiffer braces.

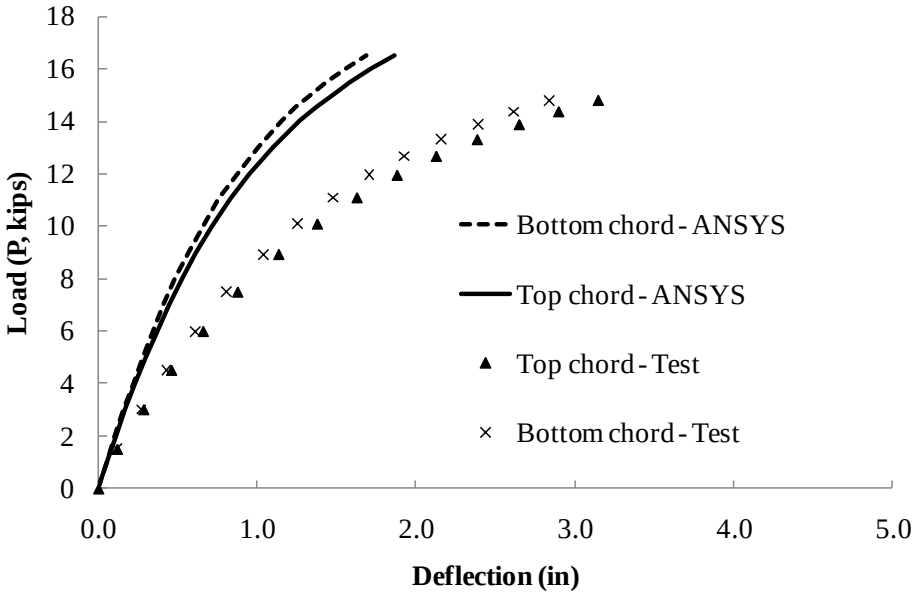

Figure 5.19 Midspan lateral deflection of truss with 3 large torsional braces at bottom chord with brace connection stiffener

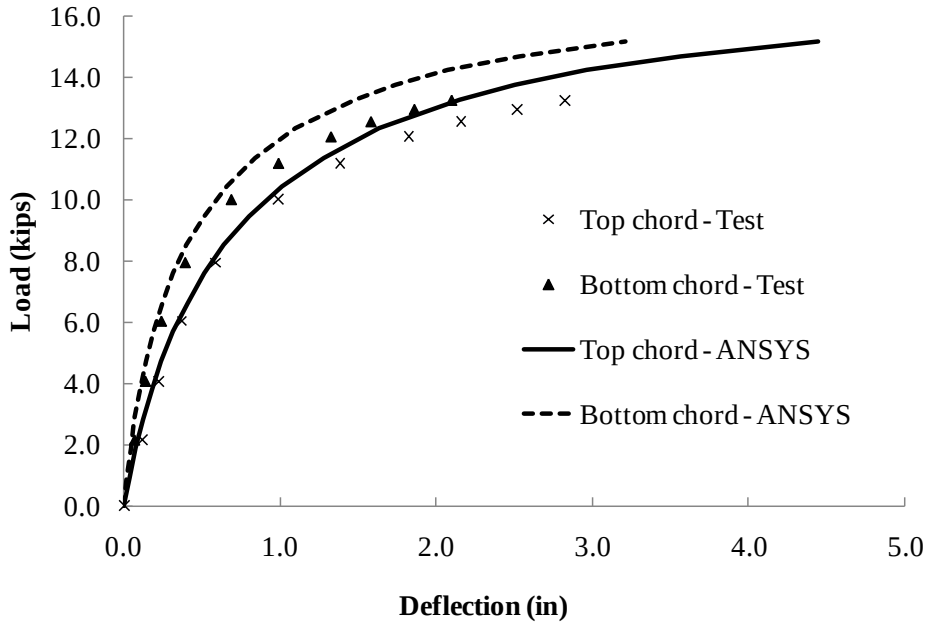

Figure 5.20 Midspan lateral deflection of truss with 2 large torsional braces at top chord with brace connection stiffener

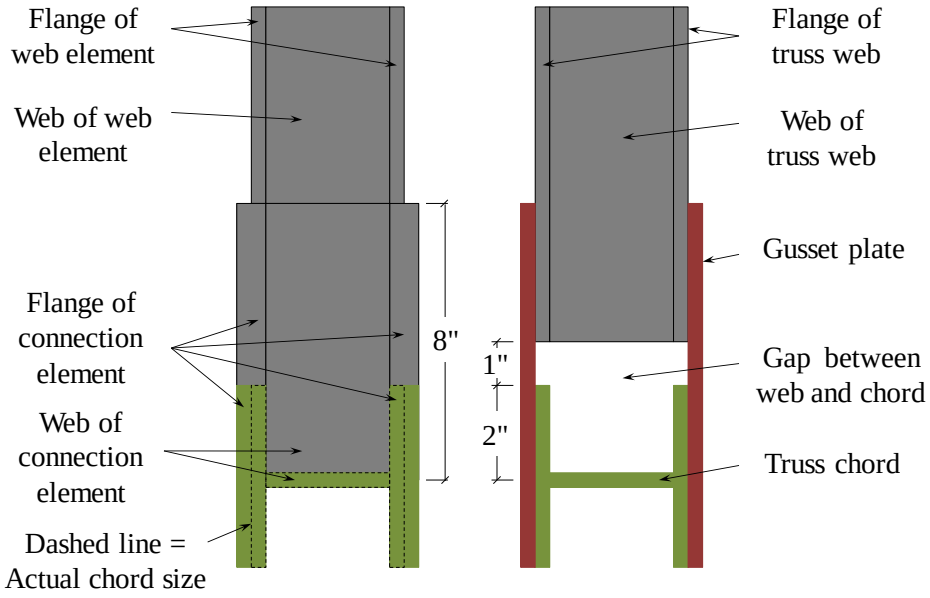

Figure 5.21 Comparison of idealize and actual connections

Even though the cross section distortion of the truss chord was prevented by the use of the connection stiffener, it is possible that a cross section distortion occurred on the gusset plate at the brace connection. Figure 5.22 shows the rotation at 48 feet of truss with 3 large torsional braces at the bottom chord with the connection stiffeners included. The rotation of the torsional brace was different from the rotation of the truss cross section. This indicated that there was the cross section distortion at the brace connections. Figure 5.23 shows the rotation at 52 feet of truss with 2 large torsional braces at the top chord with the connection stiffeners included. The rotation of the torsional brace was different from the rotation at the top chord (TC); however, was only slightly different from the top web (TW) and mid web (MW). This indicated less connection distorsion and more uniform cross section distorsion which can be captured by the truss model and resulted in less difference between the test results and the FEA model than in the bottom chord bracing case.

In the FEA model with wide flange section as the gusset plate model, the gusset plate model could transfer the shear very well to the torsional brace, which results in a

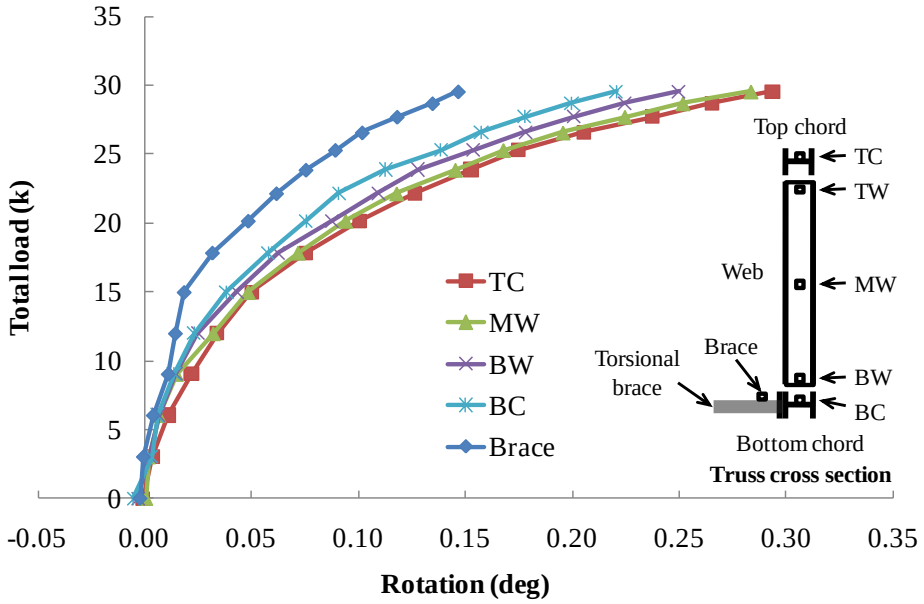

Figure 5.22 Cross section rotation at 48 feet of truss with 3 large torsional braces at bottom chord

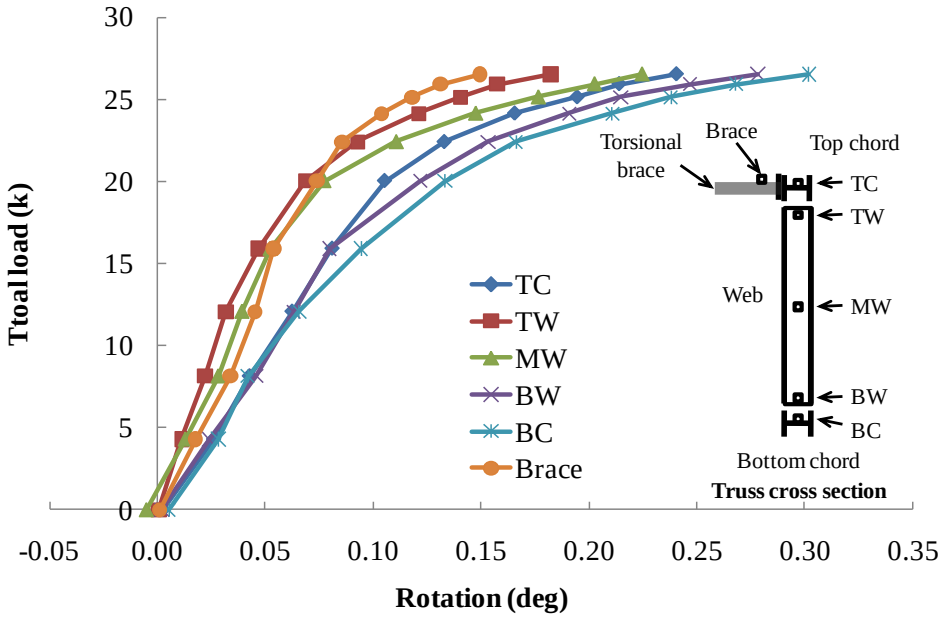

Figure 5.23 Cross section rotation at 52 feet of truss with 2 large torsional braces at top chord

stiffer system in the FEA model compared to the actual truss. Although the FEA model did not have good correlation with the test results (primarily for the bottom chord bracing), the model was still deemed to provide a reasonably good model for use in the parametric studies since most of the torsional braces that were used in the parametric studies were full depth cross frames. As a result, the gusset plate flexibility was not as much of a concern. The FEA model for the parametric studies is discussed more in Chapter 6.

5.4.4 Brace Force

One of the advantages of the BEAM44 elements is that the brace forces in the elements of the truss and the torsional braces were able to be obtained in the specific locations that conform with the actual strain measurement locations. For the torsional brace, the strains were obtained at the quarter points on the four sides of the braces. The gages labeled North and South represent the warping stresses in the brace, while the gages labeled Top and Bottom represent the torsional bracing moments. Selected comparisons of the brace stresses are shown below and are representative of the results from all of the tests. Additional results are provided in Appendix A. For the case of three small torsional braces (low brace stiffness) at the top chord, Figure 5.24 and Figure 5.25 show the stress at the quarter point on all four sides of the torsional brace. The stress from the analysis had good agreement with the test results on both the torsional and warping moments. However, when the truss was approached the buckling capacity, the difference between the test results and the analysis increased.

For the case of the two large top chord torsional braces, Figure 5.26 shows the stress at the three quarter point of the North brace of the truss with two large top chord torsional braces. Figure 5.27 shows the results at the quarter point on the South brace of the truss with three large bottom chord torsional braces. The analysis demonstrated a very good agreement with the case of top chord bracing as illustrated by the fact that the stress from the analysis matched to the test results very well. However, the result of the analysis was totally off for the case of the truss with three large torsional braces at the

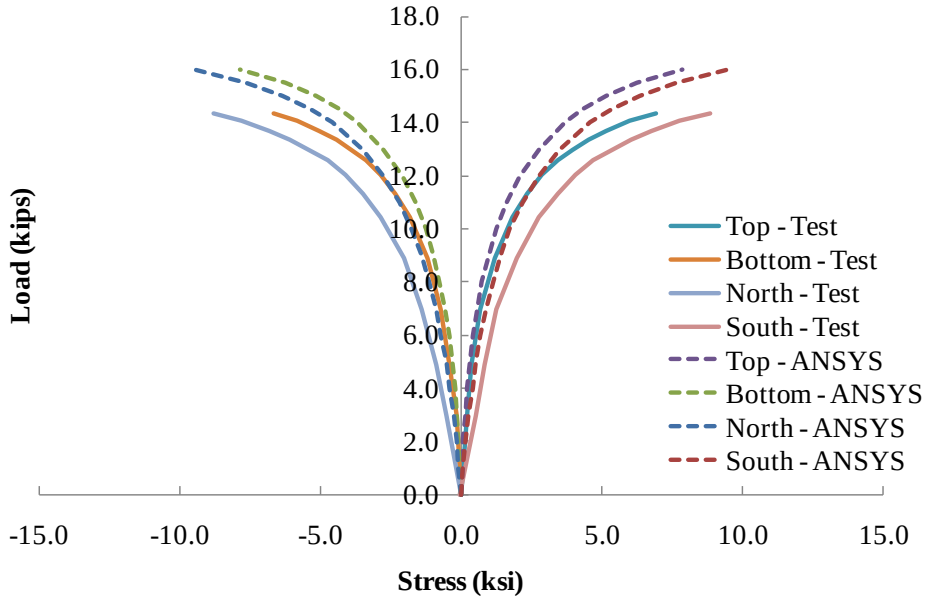

Figure 5.24 Strain in North brace at quarter point of truss with 3 small torsional braces at top chord

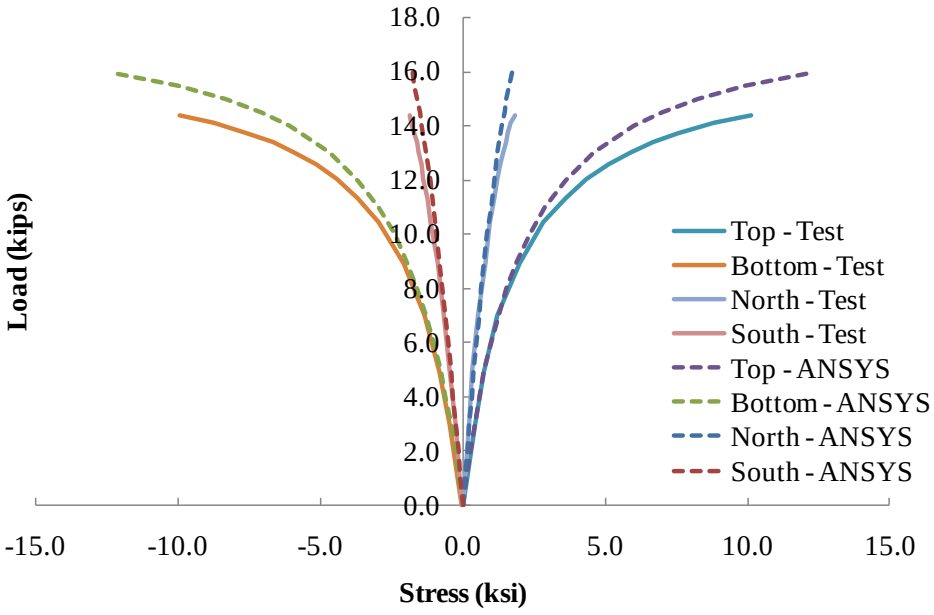

Figure 5.25 Strain in midspan brace at quarter point of truss with 3 small torsional braces at top chord

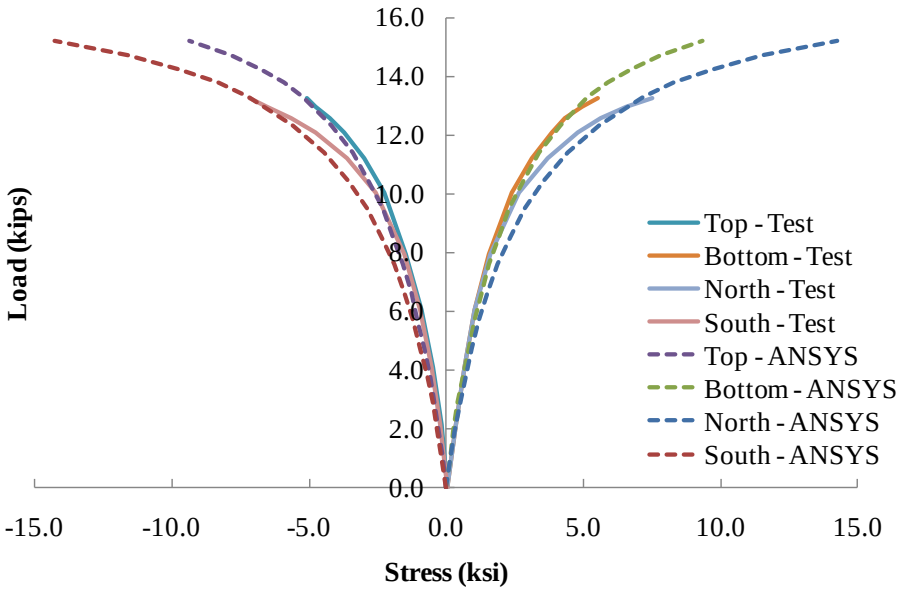

Figure 5.26 Strain in North brace at three quarter point of truss with 2 large torsional braces at top chord

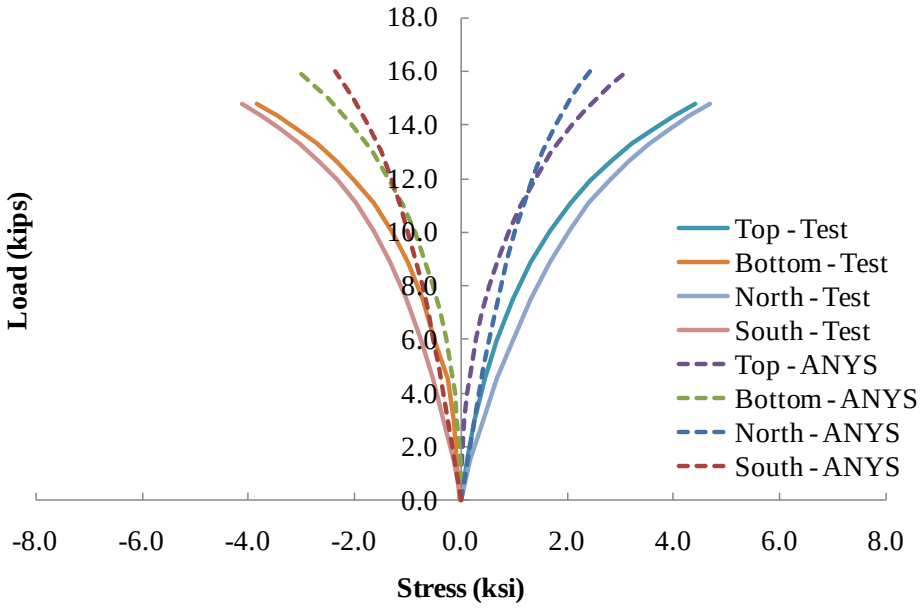

Figure 5.27 Strain in South brace at quarter point of truss with 3 large torsional braces at bottom chord

bottom chord. As mentioned earlier on the midspan lateral deflection that the model worked well for the case of two large torsional brace at top chord and did not work well for the cases of three torsional brace at bottom chord. It seem like the effect was also valid with the stress in the brace. The lateral deflection of the truss with three large torsional braces at the bottom chord was about two third of the model. Since the stress in the brace was a little better than lateral deflection, it is likely that the degree of agreement between the analysis and the test results regarding to the stress in the brace was similar to that of the lateral deflection.

5.5 SUMMARY

The truss model was developed by using the line element model with the BEAM44 elements. The gusset plate connections were modeled as short wide flange section. In order to correctly verify the truss behavior, the initial imperfection of the model needed to be set the same as in the test. According to the self weight on the truss, the modeled initial imperfection was adjusted to simulate the same conditions under which the truss imperfection was modeled. The model showed a good agreement with the test results of the lateral stiffness both with and without the lateral stop of the regular and inverted trusses. The model worked well in comparison of the midspan lateral and vertical deflection on buckling tests of truss without bracing. Cross section distortion in the truss without stiffeners at the brace connection had a significant effect on the buckling behavior. The FEA model was much stiffer than the test results where the cross section distortion was not taken into account. The models with the connection stiffeners had better agreement with FEA model. The models still had distortions in the gusset plate connections that were difficult to model. The agreement between the torsional bracing FEA models and the laboratory test results was better for trusses with torsional brace at the top chord compared to the bottom chord. This effect was observed in both the applied load versus the lateral deformation behavior and also in the torsional brace forces.

Although the FEA model did not exactly model the connection flexibility, the correlation was good enough so that trends in the behavior would likely be possible. In

addition, aside from pony truss systems, most bracing systems for trusses are much deeper and therefore connection flexibility is not as much of a concern between the brace and the gusset plate. For example, most of the parametric studies that are presented in Chapter 6 made use of full depth cross frames for the torsional braces. The truss model was therefore deemed sufficiently accurate to provide a good indication of the behavior of torsional braces in truss systems. The FEA model for the parametric studies is discussed more in Chapter 6.

CHAPTER 6
Parametric Study of Truss Buckling Behavior

6.1 INTRODUCTION

The laboratory tests provided valuable data for demonstrating the behavior of bracing systems for truss systems and validating the FEA models. The FEA models were then used to conduct parametric studies to further improve the understanding of the factors that affect the torsional bracing behavior so that design methodologies can be developed for the bracing. In addition to using the laboratory test data, the ANSYS model was also verified using the finite element program MASTAN2 (Ziemian and McGuire, 2007). The parametric studies were done on the truss with torsional bracing consisting of flexural members that framed into one of the chords similar to the laboratory experiments and also using full depth cross frames. The difference between these two brace types is that cross sectional distortion is not generally an issue with full-depth cross frames. This allowed the study to eliminate cross sectional distortions so that other factors could be focused on in the absence of distortion. Although analyses were conducted using the beam elements for the braces, most of the solutions presented in this chapter focus on the use of full depth cross frames since those solutions were used to develop the design methodologies presented later in the chapter. Comparisons are made between models with cross frames and models with flexural braces with very stiff web elements to minimize cross sectional distortion. The effects of cross sectional distortion are still under study and that work is discussed in more detail in the subsection on future work in Chapter 8.

6.2 CRITERIA OF THE ANALYSIS AND ASSUMPTIONS

6.2.1 Chord and Web Size

The size of the vertical and diagonal web members were selected to be less than or equal in depth and area of the chord members. Figure 5.1 showed the FEA model that was used for the trusses and the braces. The connection elements that were used to simulate the gusset plates were selected so that the ratio of moments of inertia of the main member and the connection elements were approximately 0.288 and 0.150 for I_x and I_y respectively. The larger stiffness of the connection element was to model the stiffening effects of the gusset plates, which overlap the main members. The sections that were selected for the web members consisted of sections from the AISC Manual (AISC, 2005a) and were the "W4x13", "W8x24", and the "W12x26". Another member that was used that is not available on the market is the "W3x8", which was generated so that the "W4x13" truss chord had a smaller web than chord. Figure 6.1 shows the sections that were used for the web members and will be referred to as either A) Very flexible, B) Flexible, C) Moderate, and D) Stiff. There were three sections used for the chords which include the "W4x13", "W8x24" and "W12x50". As indicated in Figure 6.1, the corresponding chord members will be referred to as A) Flexible, B) Moderate, and C) Stiff. The section properties of the chords and webs are provided in Appendix B. The wide range of sections that were used was primarily used so that the design expressions that are developed in Chapter 7 are based upon the variability that might occur between the stiffness of the chord and the stiffness of the web elements.

There were several analyses that were done on the truss with axial only web elements (simplified webs) connected to the beam element chord. For these cases, the axial only elements were set to have the same cross section areas as the normal web elements. Since most trusses are idealized as consisting of pin-ended members, the simplified webs were selected to obtain an indication of the effect of joint restraint on the member behavior. In reality, most trusses will have a significant amount of joint restraint, depending on the nature of the connections at the joints. Although extensive

analyses were conducted with the different web and flange members, select results are shown in this chapter to demonstrate the general behavior. The remainder of the results are provided in the Appendix B.

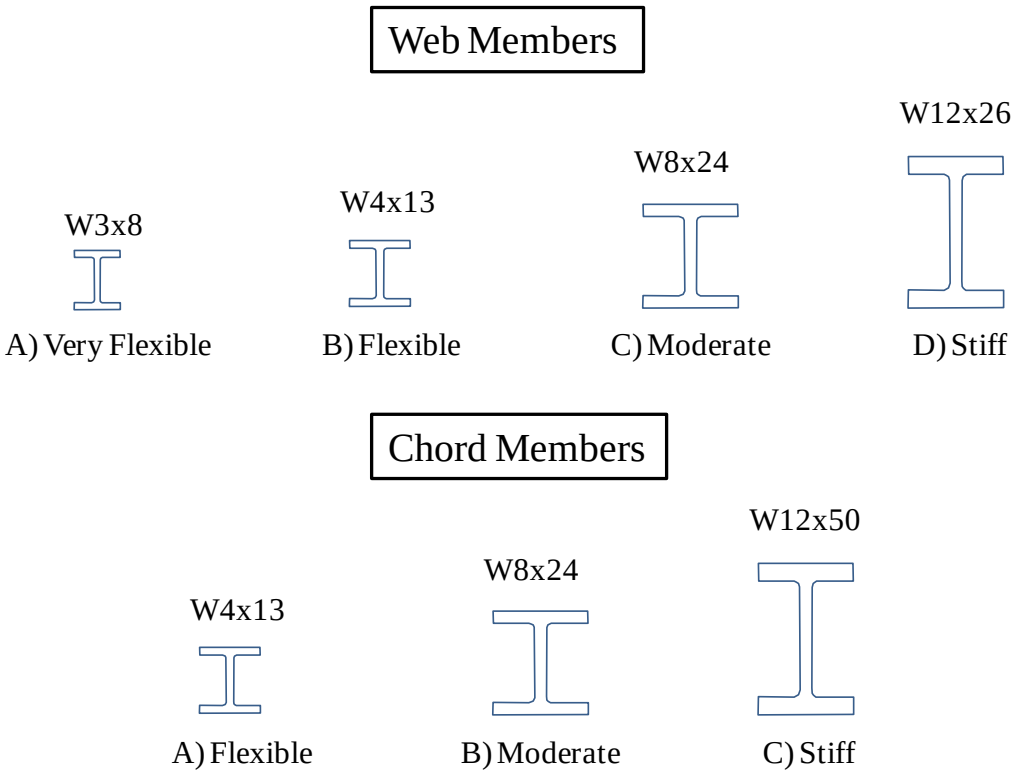

Figure 6.1 Chord and web sections used in the analysis

6.2.2 Torsional Braces

6.2.2.1 Beam Elements

As noted earlier in the chapter, two different types of torsional braces were used: beam elements that framed into the truss joints and full depth cross frames. The sizes of each of these different types of braces were varied. In the analysis with beam elements used for the torsional braces, the braces were not coupled in the warping direction so that the braces only restrained torsional deformations of the trusses and not warping deformations. Since warping restraint is rarely relied upon, this modeling assumption is consistent with common design practice. The sizes of the connection elements for the

brace were varied by maintaining the ratio of the I_x and I_y of the brace to the connection element. This created some of the unusual shapes of the connection elements (very narrow and steep wide flange sections). Since this is numerical analysis, the shapes of the connection elements should not affect the analysis. The stiffness values of the braces were varied for the wide range to cover the possible cases. Steel tubes were used for the torsional braces and the sizes ranged from 3.0"x1.5" to 1.4"x12.0" into 11 brace sizes. The major axis moment of inertias ranged from 0.62 to 82.0 in^4. The ratio of the major and minor axis moment of inertia between the brace and the connection elements were all kept the same which were about 0.335 and 0.185, respectively. The details of the brace used in the analysis are provided in Appendix B. In cases that a higher brace stiffness was required, the brace sizes were maintained and the modulus of elasticity of 20 times, 580,000 k/in^2, the original value was used.

6.2.2.2 Cross frame

Full depth cross frames were utilized so that cross sectional distortion was not a factor in the problem. Tension-only cross frames were used in the analysis. In practice, most tension-only cross frames consist of two struts and two diagonals, with one diagonal in tension and one in compression; however the compression diagonal is conservatively neglected since the buckling strength is often small. Computationally, a single diagonal can provide either tension or compression; however the stiffness of the cross frame is identical to the tension-only system. The area of the cross frame members was varied from 0.00025 in^2 to 35.0 in^2. A total of 80 different cross frames sizes were used in the analysis. The cross frame size was varied to determine the stiffness required to reach full bracing, which consisted of reaching a load corresponding to buckling between the brace points. In some cases where the full bracing was not reached, the brace cross section areas were limited to 35.0 in^2.

6.2.3 Analysis assumptions and scope for parametric study

A number of assumptions were made during the parametric studies. The goal of the studies was to determine the stiffness requirements for the torsional bracing systems using eigenvalue buckling analyses. The following assumptions and modeling decisions were made throughout the investigation.

- No truss self weight was considered in the analysis
- Uniform loads were applied as concentrated forces applied at the joints
- The loads were applied concentrically at the joints with no eccentricities
- The initial imperfection was not considered for the eigenvalue buckling analysis due to the minimal impact on the solution.
- Truss spans of 48, 72, and 96 feet were considered with span to depth ratios ranging from 8 to 32
- The truss depths considered in the analyses were 3 and 6 feet
- Pinned (referred to as simplified webs) and restrained connections were used for the web members
- To develop a solution for torsional bracing, the study focused on trusses with a single brace at midspan. Work is ongoing focusing on the behavior of systems with several intermediate braces, however to formulate a solution the study focused on the case with a single brace. Some results are shown with multiple braces.

6.2.4 Model verification with structural analysis program of single truss

In addition to using the experimental data, the ANSYS model was also verified with a model created in MASTAN2 (Ziemian and McGuire, 2007). Eigenvalue buckling analyses were done on both models on only selected cases with joint loads resulting from uniform load applied at the top chord. The MASTAN2 model was developed using rigid connections at the joint. An Eigenvalue buckling analysis was conducted as well as a large displacement analysis. The model of the 72-ft span truss with 6-ft depth with stiff

chords subjected to uniform load at top chord is shown in Figure 6.2. The corresponding results for the ANSYS and MASTAN2 models are provided in Table 6.1.

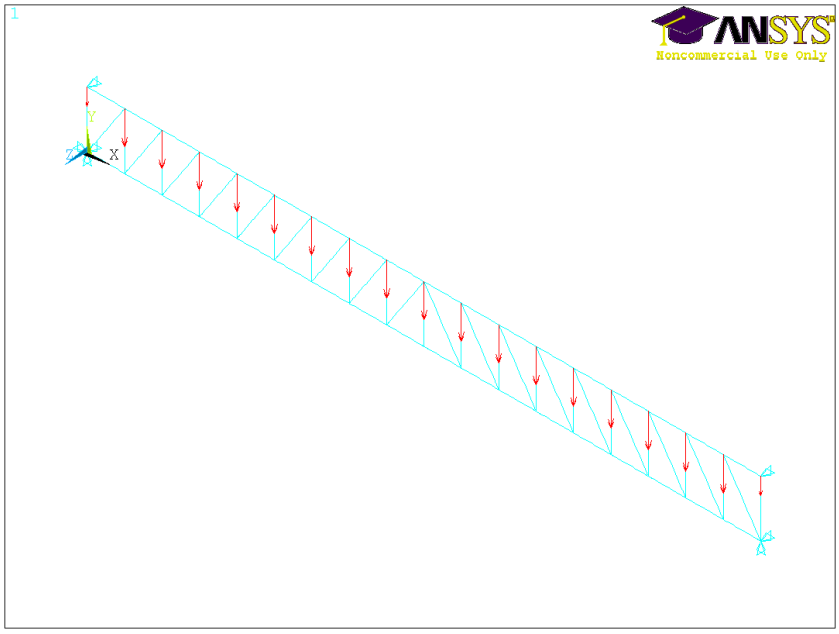

Figure 6.2 72-ft span truss with 6-ft depth and uniform load at top chord

Table 6.1 Comparison of buckling capacity from ANSYS and MASTAN2 models

Vertical Web Section	Diagonal Web Section	P_{cr} (kips)		Percent Different (%)
		ANSYS	MASTAN2	
Flexible	Flexible	7.58	6.55	15.7
Moderate	Flexible	8.39	7.17	17.0
	Moderate	16.15	13.83	16.8
Stiff	Flexible	8.47	7.25	16.8
	Moderate	17.83	15.31	16.5
	Stiff	24.31	20.81	16.8

It can be seen that the results from the ANSYS model were consistently higher than the MASTAN2 results by approximately 16%. This can be explained by the effect

of the inclusion of the gusset plates model at the connections. The connection composed of the stiffer element than the chord element due to the addition of the gusset plates to the chord. Including the gusset plate into the ANSYS models by using the connection elements shorten the member effective length and increase the stiffness of the system, which leads to the higher buckling capacity in the ANSYS model. To verify this explanation, additional analyses of selected cases were conducted on the truss in MASTAN2. The gusset plates were modeled in MASTAN2 by adding the connection elements with the same sizes and lengths at the same locations as in ANSYS model. The results are shown in Table 6.2.

Table 6.2 shows the eigenvalue for the 72-ft span truss with 6-ft depth and a uniform load at either the top (TC) or the bottom (BC) chord. The conditions of the gusset plate model were varied from the simplified rigid connection model to the models with the gusset plate simulated a) web only and b) web and chord members. The simplified model yielded the lowest buckling capacity. Adding the gusset plate model only the web did not significantly change the buckling capacity, which is likely due to the relatively small deformation between the joint and the web members. Including the gusset plate model into all connections improved the buckling capacity and there was good agreement between the MASTAN2 and ANSYS solutions. Although the two software packages provided similar solutions, ANSYS was selected for the parametric studies since the software offered more options for potentially modifying the model during the parametric study as well as the ability to use the ANSYS Parametric Design Language (APDL) to facilitate the study.

Some of the studies on the torsional bracing were conducted with the Vierendeel truss configuration so that a single web member framed into a joint. The more simple layout was selected in an attempt to minimize the complexity of the problem. In the Vierendeel truss, the first mode eigenvalue buckling capacity and mode shape of truss when using ANSYS model were often different from those of the MASTAN2 model. For the MASTAN2 model with the simulated gusset plate, the first mode shape of the Vierendeel truss was a half-sine mode shape with a buckling capacity that was lower than

Table 6.2 Comparison of P_{cr} from ANSYS and MASTAN2 with gusset plate model

Chord Section	Web Section	Load Location	P_{cr} ANSYS (kips)	P_{cr} MASTAN2 (kips)		
				w/o gusset	w gusset on web only	w gusset on web + chord
Flexible	Flexible	BC	1.147	0.960	1.016	1.138
Moderate	Flexible	BC	4.28	3.623	3.787	4.29
Stiff	Moderate	BC	22.98	19.42	20.41	22.99
Moderate	Moderate	TC	16.15	13.83	14.86	16.35

the case with same truss with a small web diagonal. The second mode was the local buckling of the truss vertical web at the support which buckled into full sine shape with a buckling capacity higher than the case with the same truss with small diagonal web. However, for the ANSYS model, the first mode shape and buckling capacity were different from the MASTAN2 model. Although the first mode had the same half-sine buckled shape, the buckling capacities were different and in some cases were higher than the buckling capacity of the same truss with a small diagonal web. For example, for the case of a 72-ft span Vierendeel truss with stiff chord and stiff web with bottom chord loading, the buckling capacity of the truss from MASTAN2 for the respective cases of first and second modes were 10.1 kips with half sine mode shape and 26.9 kips with local buckling at support web. The first mode buckling capacity for the same truss in ANSYS was 26.68 kips with the half sine mode shape, as shown in Figure 6.3. The buckling capacities of the same truss in ANSYS with a flexible diagonal web were 15.5 kips and 13.0 (from basic model) kips for the ANSYS and MASTAN2 models, respectively. Theoretically, the buckling capacity of the Vierendeel truss should be less than that of the same truss with the diagonal web. This indicated that there was some difficulty when using the ANSYS model for predicting the buckling capacity of the Vierendeel truss.

The ANSYS and MASTAN2 model comparison mentioned above and the lab test results comparison have indicated that the model worked fine for regular truss. However,

additional studies were conducted to check for the correctness of the model by conducting large displacement analyses. The analyses were done on the 96-ft span regular truss with the stiff chords, stiff vertical web elements and the very flexible diagonal web elements compared to the Vierendeel truss with the same chord and vertical web elements. The trusses had a straight bottom chord and a half-sine initial imperfection on the top chord with a maximum displacement at midspan of L/1000. The respective results of the lateral deflection at the top and bottom chord from ANSYS are shown in Figure 6.4 and Figure 6.5 for the respective cases with bottom chord loading and top chord loading. As expected, the Vierendeel truss had less out-of-plane stiffness than the regular truss and the effect was more explicit in the top chord loading case. For the case with bottom chord loading, the Vierendeel truss deflected in the same direction with larger deformations when compared to the regular truss at the same load level. This indicated that the buckling capacity of the Vierendeel truss was lower than that of the regular truss with small diagonal web elements. For the case with top chord loading, the Vierendeel truss buckled in a mode where the chords deflected in opposite directions while the chords in the regular truss deflected in a mode in the same direction; however the bottom chord was nearly straight. The Vierendeel truss still had lower buckling capacity in this case. This seemed to be a reasonable behavior. The behavior of the ANSYS model followed the expected behavior in the large displacement analyses and was therefore used in the parametric studies.

6.3 CALCULATION OF TRUSS IN-PLANE MOMENT OF INERTIA

A discussion of the impact of the in-plane stiffness (β_g) of beams sections on the torsional bracing behavior was provided in Chapter 2. The evaluation of the in-plane stiffness of truss systems is complicated since there is not a general solution available to calculate the in-plane moment of inertia of the truss. To develop a suitable expression, the solution for a beam subjected to the uniform bending moment as shown in Figure 6.6 was investigated. For a given moment level (M = Fh, where F is the chord force and h is the truss depth), the in-plane moment of inertia of truss was calculated by using Equation

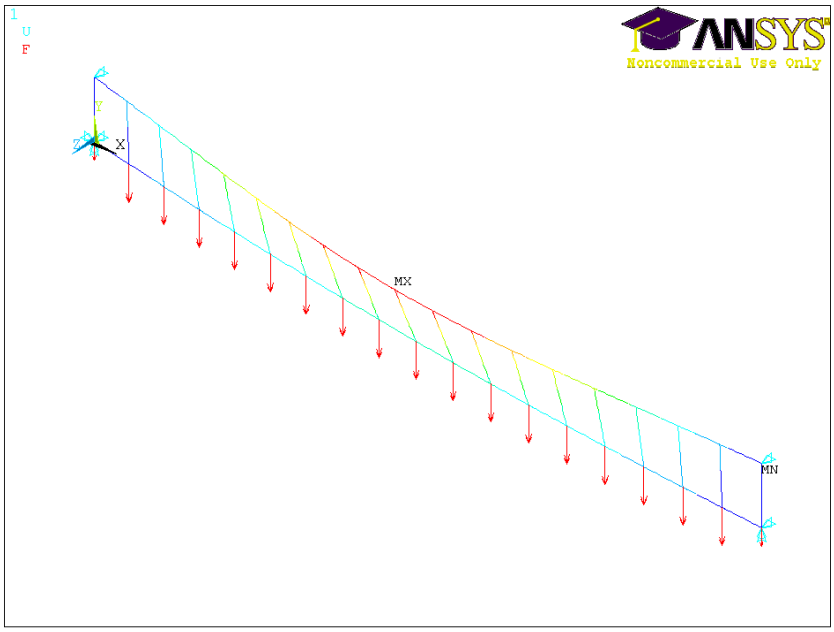

Figure 6.3 Buckling mode shape for Vierendeel truss with stiff chord and stiff web with bottom chord loading

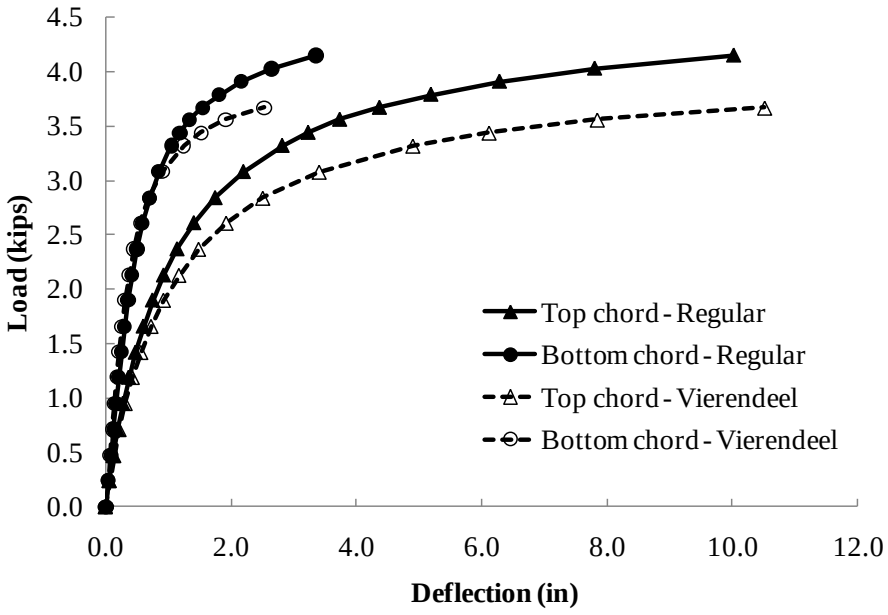

Figure 6.4 Large displacement analysis of truss with stiff chord and stiff vertical web with and without very flexible diagonal web with bottom chord loading

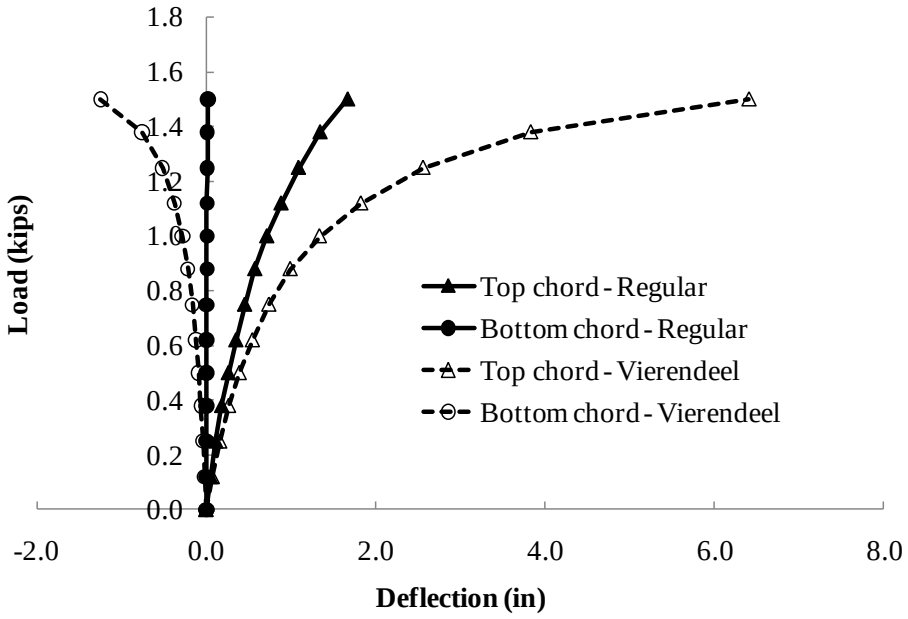

Figure 6.5 Large displacement analysis of truss with stiff chord and stiff vertical web with and without very flexible diagonal web with top chord loading

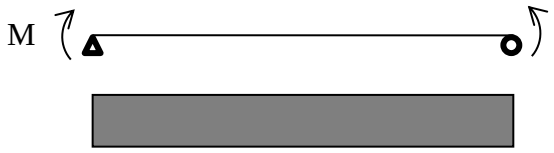

Bending moment diagram

$$\Delta = \frac{ML^2}{8EI_x}$$

Figure 6.6 Calculation of truss in-plane moment of inertia

(6.1). The resulting values are provided in Table 6.3 for selected cases of the truss subjected to uniform bending moment. The results from the ANSYS static analysis are compared to the calculation of the chord moment of inertia at the midheight by using parallel axis theorem. For the cases of the truss with the same chord but different webs, the results showed that the in-plane moment of inertia (I_x) were equal. There were three

pairs of chord sizes in the analysis. Each pair had the same chord size but different webs. From Table 6.3, it can be seen that the I_x of the truss was directly related to the chord in-plane moment of inertia but it was independent of the web and diagonal members.

$$I_x = \frac{ML^2}{8E\Delta} \tag{6.1}$$

The truss was composed of the several small wide flange sections, which the moment of inertia cannot be calculated directly by just using the basic equation ($I = I_o+Ad^2$) for each individual chord. If the basic equation is used to calculate the moment of inertia and transfer to the midheight, the results are indicated in Table 6.3. The values of I from the basic equation were slightly lower than the actual values from ANSYS. However, the differences were approximately the same for all truss combinations. The basic equation yielded about 12-13% lower stiffness than the actual value. The extra moment of inertia might come from the contribution of the web elements in some term other than the in-plane stiffness of the individual vertical and diagonal elements. The calculation of the inertia by using basic equation seemed to be on the conservative side in estimating the deflection and calculating the in-plane stiffness (β_g) if the contribution of the web to the moment of inertia is neglected.

Table 6.3 Calculation of in-plane stiffness of 6-ft depth truss

	Span (ft)	72 ft			96 ft		
Chord	Web	ANSYS	$I=I_o+Ad^2$	% diff	ANSYS	$I=I_o+Ad^2$	% diff
W4x13	W3x8	11393	9935	-12.8	11392	9935	-12.8
W4x13	W4x13	11392	9935	-12.8	11392	9935	-12.8
W8x20	W3x8	20948	18388	-12.2	20944	18388	-12.2
W8x20	W4x13	20945	18388	-12.2	20942	18388	-12.2
W12x50	W3x8	43279	37956	-12.3	43250	37956	-12.2
W12x50	W4x13	43255	37956	-12.3	43236	37956	-12.2
W12x50	W8x24	43238	37956	-12.2	43228	37956	-12.2
W12x50	W12x26	43234	37956	-12.2	43225	37956	-12.2

According to the lab test results and lateral stiffness analyses, it was found that the lateral stiffness of the truss was not the same in both the top and bottom chords. In the lateral load tests of regular (Howe) truss, with the same applied load on the top and bottom chords, the top chord usually deflected more than the bottom chord. This shows that the truss might behave similar to the singly symmetric girder where the centroid is not at midheight. Since the truss deflected at the top chord more than the bottom chord, it might be assumed that the top chord had a smaller effective out-of-plane moment of inertia. The truss had the same top and bottom chord sizes, implying that the centroidal axis should locate somewhere below the midheight. The moment of inertias of the truss might be able to be calculated based on the offset of the distance from the midheight. The moment of inertias of the truss were back-calculated to replicate a singly-symmetric girder and to determine the locations that provide better correlation with the effective moment of inertia obtained from ANSYS. The results are shown in Table 6.4. It can be seen that the centroidal axis were similar for the same depth and were about 11.2 and 22.5 inches from the bottom chord for the cases of the 3 and 6-ft depth trusses, respectively. These values were about 60-65 % of the midheight. The equation to calculate the in-plane truss moment of inertia was not further developed since it is beyond the scope of this dissertation. Instead an approximation of the effective moment of inertia can be made simply using the parallel axis theorem about midheight and will provide reasonable results that are slightly conservative. To obtain the in-plane stiffness component for the bracing problems, the in-plane moment of inertia in the remainder of this dissertation was obtained directly from the ANSYS analysis by subjecting the truss to uniform bending moment.

6.4 BUCKLING BEHAVIOR OF TRUSS WITH RIGID WEB AT BRACE POINT

The use of a beam element allows the torsional brace to be positioned at either the top or bottom chord. These types of braces are frequently used in pony truss applications; however the web elements must have suitable stiffness to control cross sectional distortion. Although studies are underway focusing on the cross sectional

distortion of the web, studies were also done with a relatively rigid web element at the brace location to control the distortion. The stiffness of the web at the brace location was increased by providing a large modulus of elasticity for the individual web vertical. The analyses were done only on the cases of truss with single torsional bracing at midspan.

Table 6.4 Calculation of equivalent centroidal axis of 96-ft span truss

Truss depth		3 feet		6 feet	
Chord	Web	Centroid	% of midheight	Centroid	% of midheight
W4x13	W3x8	11.07	61.50	22.20	61.67
W4x13	W4x13	11.07	61.50	22.20	61.67
W8x20	W3x8	11.23	62.39	22.57	62.69
W8x20	W4x13	11.23	62.39	22.57	62.69
W12x50	W3x8	11.21	62.28	22.53	62.58
W12x50	W4x13	11.21	62.28	22.55	62.64
W12x50	W8x24	11.21	62.28	22.57	62.69
W12x50	W12x26	11.21	62.28	22.57	62.69

The results of eigenvalue buckling analysis of a truss with a rigid web vertical at the brace location are shown in Figure 6.7 and Figure 6.8 for the respective cases of a moderately chord and a stiff chord with flexible web. In Figure 6.7 with the moderately stiff truss chord, both top and bottom chord loading were considered and the brace was also positioned at both the top and bottom chord loading. Top chord loading resulted in a lower capacity than bottom chord loading; however the brace position did not affect the solution. In Figure 6.8, the results are shown for bottom chord loading on a truss with a stiff chord. The brace was positioned at both the top and bottom chords and the brace location had no impact on the buckling behavior. This was also valid for the uniform moment cases, indicating that the buckling capacity is independent of the brace locations if the truss web is rigid elements. For systems with a flexible web, the brace location did have an impact on the behavior with top chord bracing often being more effective

compared to bottom chord loading. The behavior with flexible webs is still under study. There was no sign of the truss to buckle into the full sine mode buckle shape within the analysis range for the uniform loading cases. There were some cases with uniform moment approached or reached the full sine mode case at very high brace stiffness. When the web was small compared to the chord size, such as stiff chord with very flexible or flexible web, the truss tended to buckle in asymmetric buckling mode shape, which can be expected in the beam bracing. This leads to the lower buckling capacity with the same brace size. It is worth mentioning that this large chord small web is not practical in truss design and can be eliminated by increasing the web size to moderate or stiff.

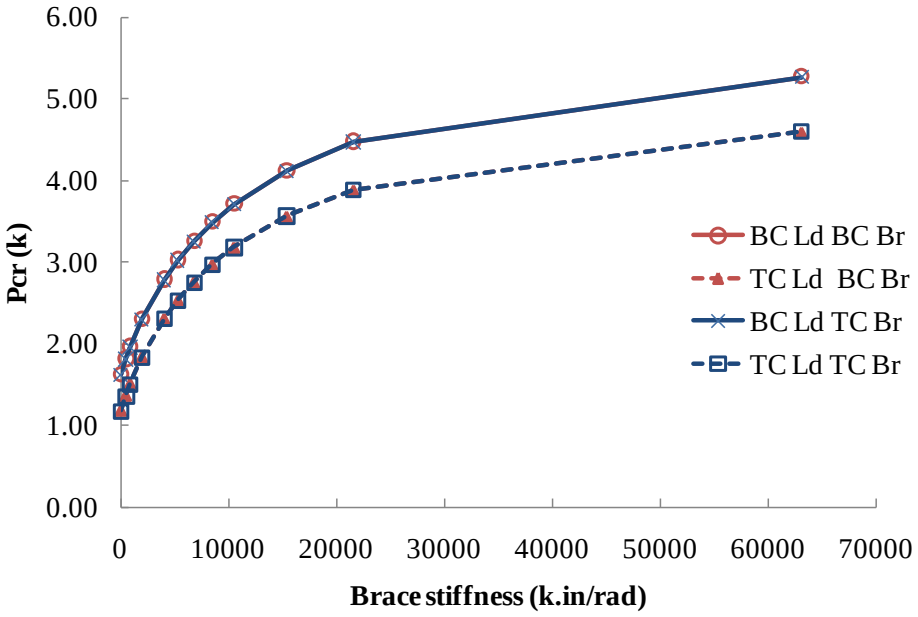

Figure 6.7 Buckling capacity of 96-ft moderate chord and flexible web truss with rigid web at midspan

6.5 TRUSSES WITH CROSS FRAME BRACING

As noted earlier, much of the parametric studies focused on trusses with full-depth cross frame braces. Since these trusses control the deformation of the top chord relative to the bottom chord, cross sectional distortion does not impact the problem.

These bracing system are frequently used in structural applications such as roof trusses. A typical tension-only cross frame attached to a truss is depicted in Figure 6.9. From a stability bracing perspective, one of the diagonals will be in compression while the other will be in tension. Since relatively light members are often used for the braces, the buckling strength of the compression diagonal is often conservatively neglected and the tension diagonal is sized to provide sufficient stiffness. For example, the dashed diagonal in Figure 6.9 would often be neglected.

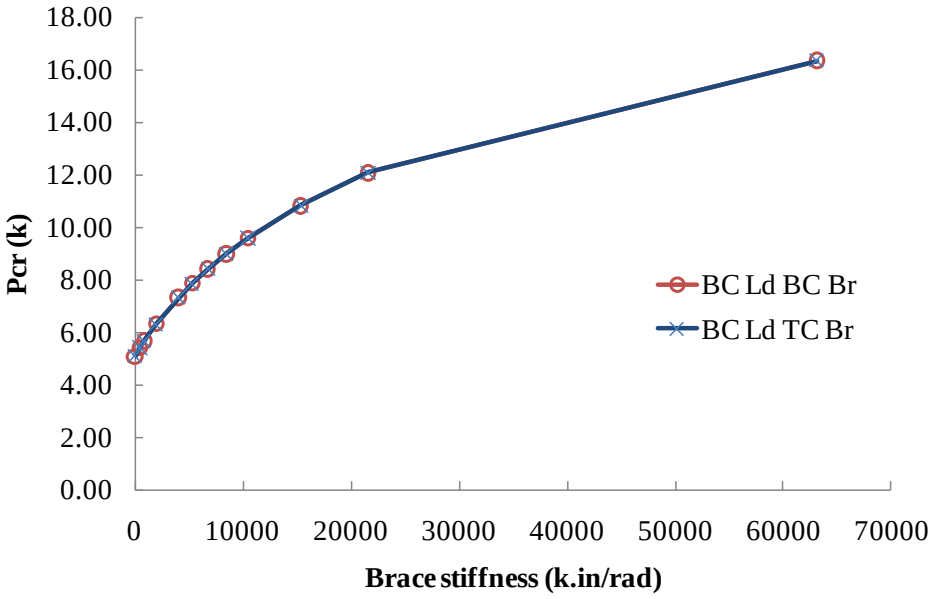

Figure 6.8 Buckling capacity of 96-ft stiff chord and flexible web truss with rigid web at midspan

The stiffness of a tension-only cross frame can be calculated by using the following expression provided by Yura (2001):

$$\beta_b = \frac{ES^2h_b^2}{\frac{2L_c^3}{A_c} + \frac{S^3}{A_b}} \tag{6.2}$$

Where, β_b is the torsional brace stiffness, E is the modulus of elasticity of the cross frame material, and A_c and A_b are the respective areas of the diagonal and strut members. The other terms are defined in Figure 6.9. The cross frame was attached at

midspan for cases with 1 cross frame and at quarter points for cases with 3 cross frames. A graph of the nodal buckling capacity versus the brace stiffness is provided in Figure 6.10 for a 96-ft span with the moderately stiff chord and flexible web. The 6-ft deep truss subjected to a uniformly distributed load applied at the top chord. Results are shown for the case of a single brace at midspan as well as three braces distributed equally along the length (quarter points and at midspan. The truss with the single brace reached the full sine mode of buckling, while the truss with three braces stayed in the half-sine mode shape.

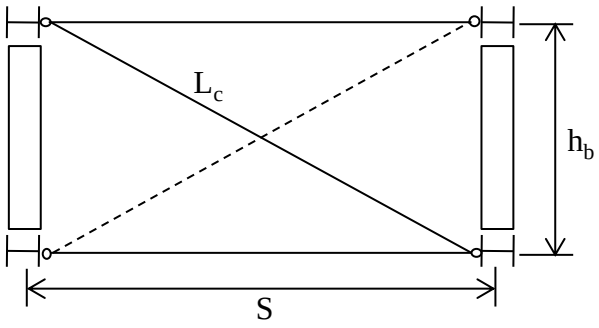

Figure 6.9 Truss cross section at midspan with tension only cross frame

For the truss with single cross frame, it was difficult to reach the full sine mode buckle shape and required very large cross frame stiffness for the cases where the web was large compared to the chord, especially for the cases with uniform moment, as shown in Figure 6.11. The truss did reach the full sine mode but required a relatively large brace stiffness. It was difficult to identify the ideal brace stiffness in the graph since the graph was flat and transitioned smoothly from the half-sine mode to the full-sine mode. Many of the trusses that were studied experienced the system mode of buckling that was discussed in Chapter 2. These systems will not generally reach the load level corresponding to buckling between the brace points and often stay in the half-sine mode. The system mode of buckling can generally be identified provided the in-plane stiffness of the truss, β_g, as discussed in Chapter 2 is considered.

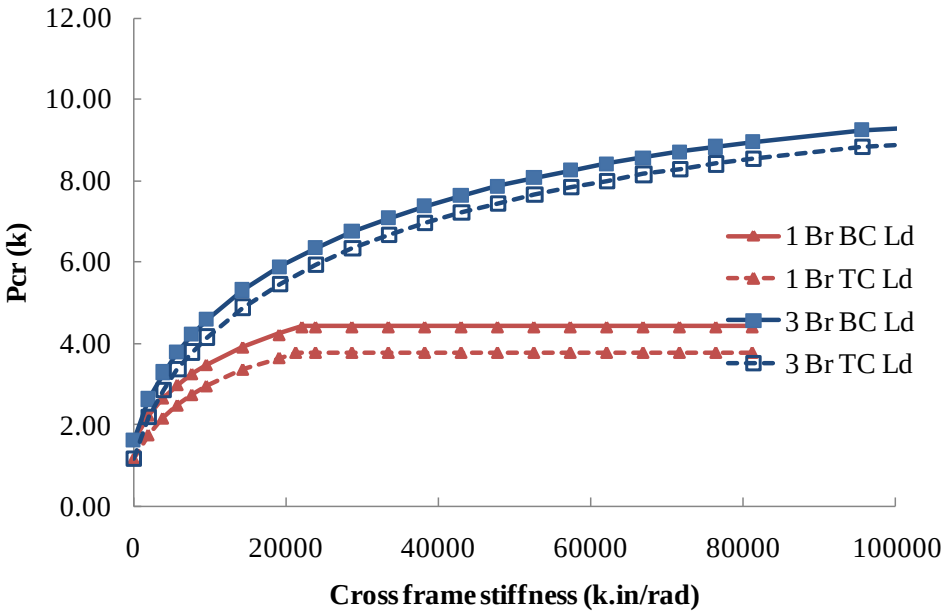

Figure 6.10 Buckling capacity of 96-ft span with 6-ft depth moderate chord and flexible web truss with cross frame

The effectiveness of the cross frames were not generally sensitive to the load locations on the truss cross section. To demonstrate this effect, the contribution of the bracing to the truss buckling capacity can be determined by subtracting the buckling capacity of the truss with no bracing from the capacity with bracing. For example, subtracting the capacity with zero cross frame stiffness from the results in Figure 6.10 produces the graphs Figure 6.12. The curves are nearly coincident for a given number of braces along the length. This demonstrates that the contribution from the bracing is not sensitive to top or bottom chord loading.

6.5.1 Comparisons of Bracing Behavior for Cross Frames and Beam Element Torsional Braces

Comparisons were made between the bracing behavior of the trusses with both cross frames and the beam element torsional braces. For the beam element systems, results are shown for both the rigid web as well as the regular webs used throughout.

Therefore, the rigid web and the cross frame results are not affected by cross sectional distortion, while the beam element brace with the regular web is affected by cross sectional distortion.

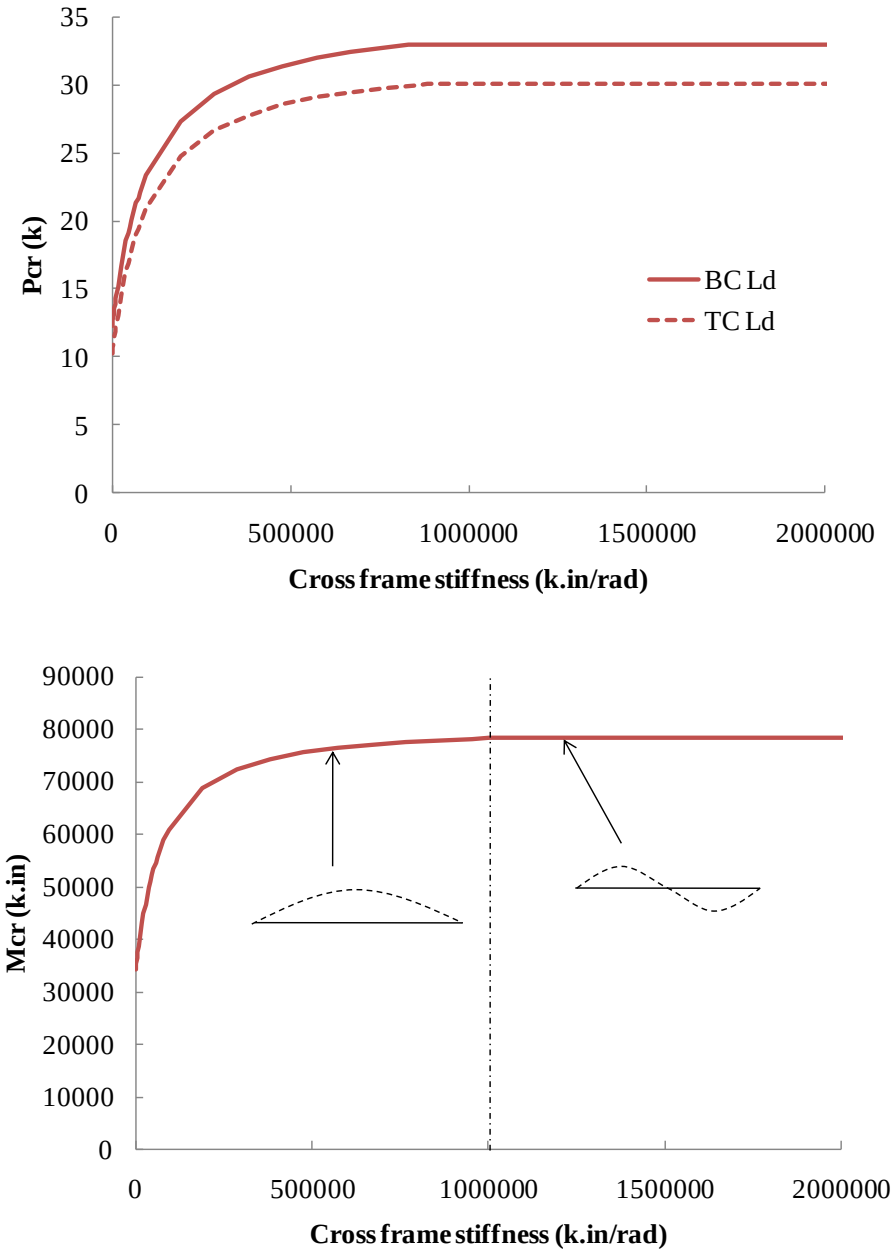

Figure 6.11 Buckling capacity of 96-ft span stiff chord and flexible web truss with one cross frame at midspan (above – uniform load, below – uniform moment)

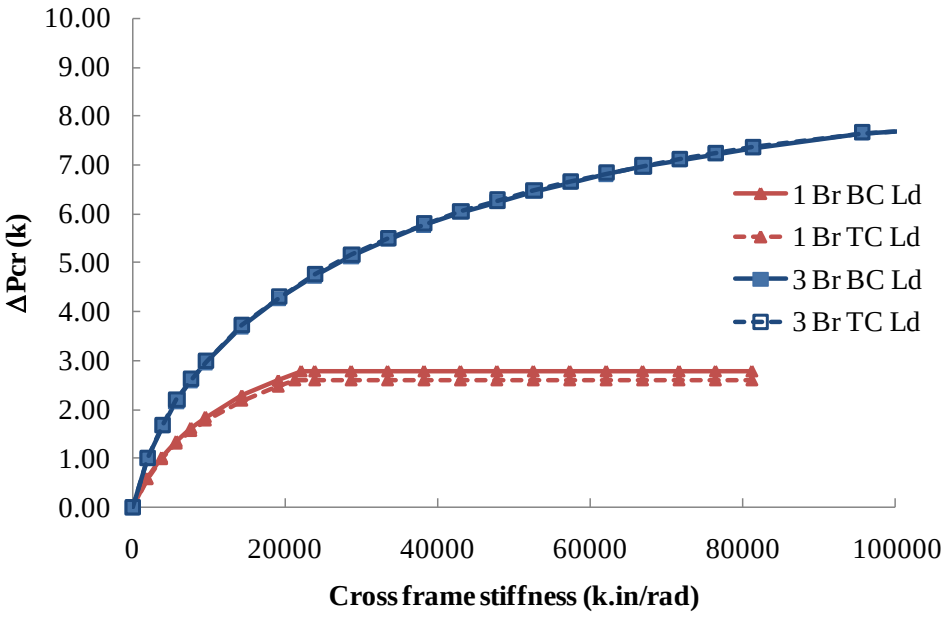

Figure 6.12 Increase in buckling capacity due to the addition of the cross frame of moderate chord and flexible web 96-ft span truss

Figure 6.13 shows the results for uniform moment loading on the 96-ft span truss with a 6-ft depth. The moderately stiff chord was used with the flexible web. The results of the same configuration but with the stiff chord and stiff web are shown in Figure 6.14. For both cases, it clearly shows that the truss with rigid web had the highest buckling capacity throughout the stiffness range, while the regular web with torsional bracing at the bottom chord yielded the lowest buckling capacity. The trusses with the flexural brace and the rigid web at the brace point buckled in the half-sine mode for all stiffness values. The reason for the truss with rigid web did not buckle into the half sine shape came from the high torsional stiffness of the very stiff vertical web at the brace point forced the truss to stay in the half sine curve. The cross frame results graphed very close to the flexural brace with the rigid web until there was a change in mode shape. The cross frame system in Figure 6.13 buckled into the full sine mode.

The truss with regular web and a flexural member for the torsional bracing had the lowest buckling capacity due to the effects of cross sectional distortion. There also

was a difference in the bracing effectiveness for top and bottom chord bracing for the truss with web distortion. Bracing at top chord was more efficient than bracing at the bottom chord for the regular truss with single brace at midspan which relate to the elements connected at brace point.

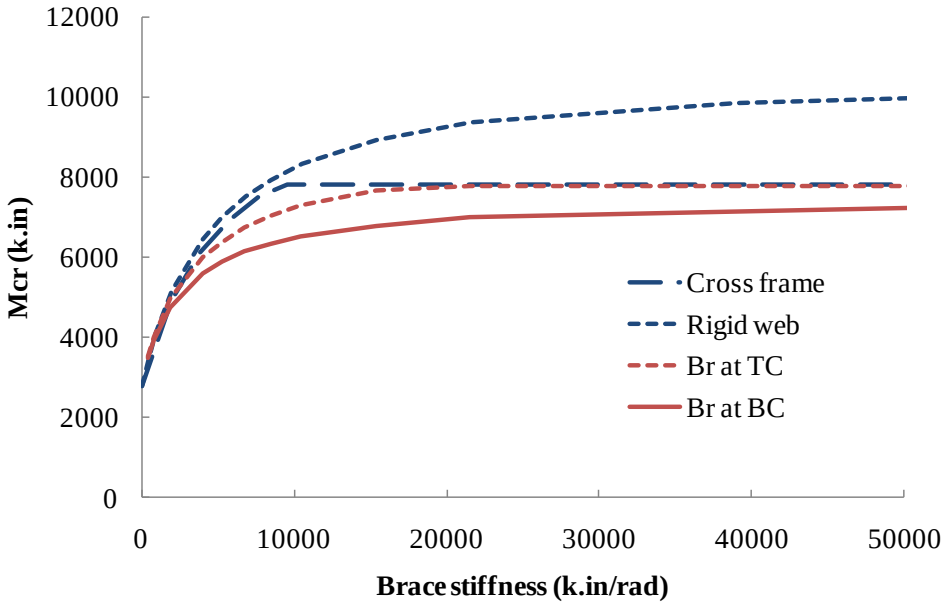

Figure 6.13 Comparison of buckling capacity of 96-ft span moderate chord and very flexible web truss with uniform moment

6.5.2 Comparison of Buckling Capacity of Trusses with Multiple Intermediate Braces

6.5.2.1 Uniform Moment Cases

As mentioned earlier, the difference between the uniform moment and uniform load cases is that uniform moment does not create the axial forces in the web since the shear is zero and the axial force in the chords is the same throughout the span length. Conversely, the uniform load creates variability in the chord forces and web forces. The maximum chord force occurs at midspan and decreases to zero at the support while the

web members have the maximum force at the supports and the minimum near midspan. The variability in the forces may have an effect on the buckling behavior. To investigate the effects of the force distribution, two different truss geometries were investigated: a) 48-ft span and b) 96-ft span. For the 48-ft span, a single cross frame was placed at midspan to create an unbraced length of 24 feet. To create the same unbraced length for the 96-ft span, 3 intermediate braces were used and positioned at the two quarter points and midspan.

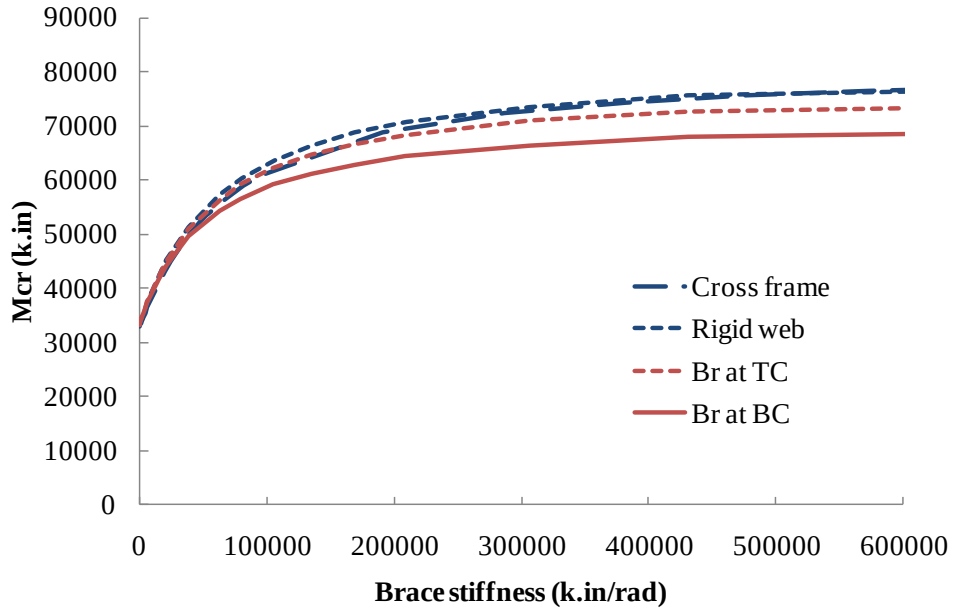

Figure 6.14 Comparison of buckling capacity of 96-ft span stiff chord and web truss with uniform moment

A comparison of the two different truss geometries buckling capacity of the 6-ft depth trusses with moderate chords and flexible web members with the uniform moment are shown in Figure 6.15. The graphs show the buckling moment on the vertical axis and the stiffness of a single cross frame on the horizontal axis. Additional analyses were done on the 3-ft depth truss. As expected, with uniform moment loading, the buckling capacities were about the same when full bracing was reached. The buckling mode with

full bracing is shown in Figure 6.16 for the system with 3 intermediate braces. For lower values of the stiffness the trusses buckled in the half-sine curve mode shape.

The truss with three braces required a larger stiffness to reach a given moment level than the truss with a single brace. The effectiveness of the bracing also was less for the case with three braces, which is evidenced by the larger separation between the two curves for higher values of the stiffness.

Buckling capacities of the similar case to Figure 6.15 of 3-ft deep truss with flexible chord and flexible web are shown Figure 6.17. The truss with three intermediate braces remained in the half sine buckle mode shape and never reached the buckling capacity of truss with single cross frame. The mode shape in this case had very little twist and was dominated by lateral deformation.

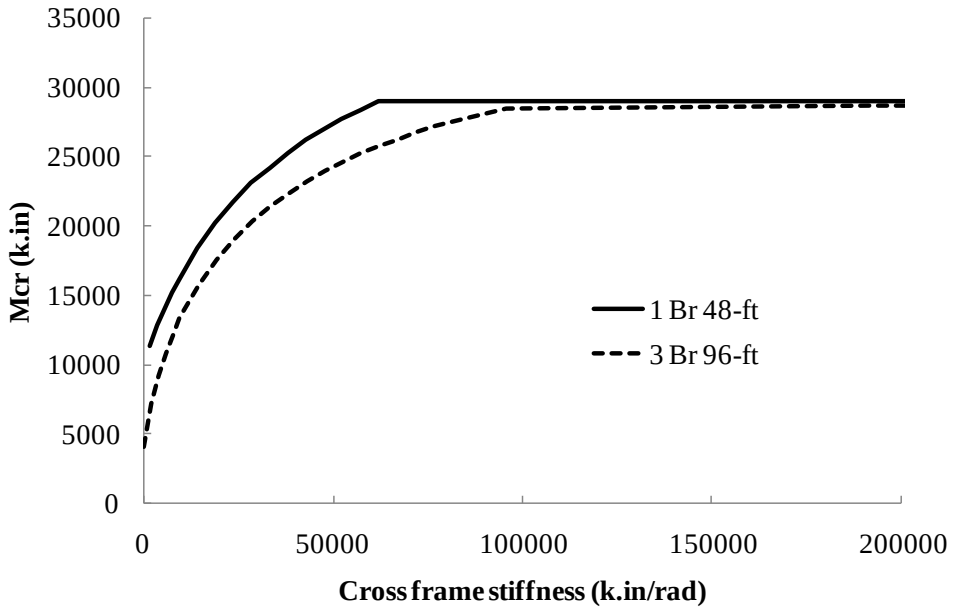

Figure 6.15 Buckling capacity of moderate chord and flexible web truss with 24-ft unbraced length with uniform moment

The buckling solutions for torsionally braced beams often make use of an equivalent continuous torsional stiffness by expressing the bracing as a stiffness per unit

length using the expression: $\bar{\beta} = n\beta/L$, A graph of the equivalent torsional stiffness for the two different cases of a single brace and three braces is shown in Figure 6.18. Based upon the effect on the curves, it doesn't appear that such a simple approach is directly applicable to truss systems. Work is still underway on the torsional bracing requirements for trusses with several braces along the length. The solutions that are developed in Chapter 7 focus on the stiffness requirements for trusses with a single brace at midspan.

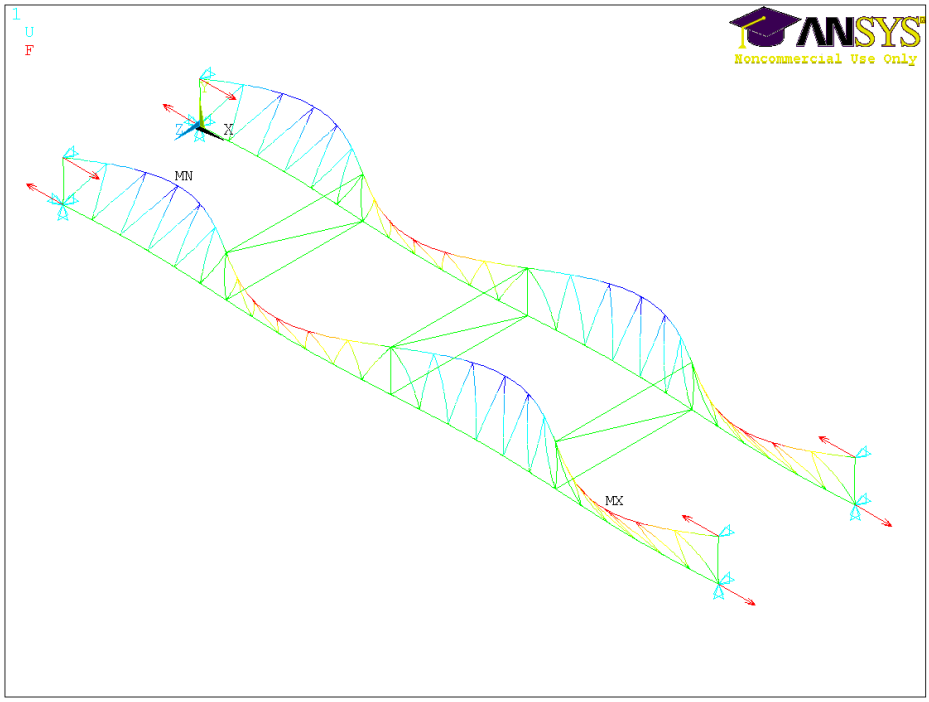

Figure 6.16 Buckle between the brace point of truss with three cross frames

6.5.2.2 Uniform Load Cases

The buckling behavior of trusses with different spans and the same spacing between the braces were also investigated for the case of a uniformly distributed load. Similar to the last section, trusses with a span of 48 feet and a single brace were compared to trusses with a span of 96 feet and three intermediate braces. Figure 6.19 shows a comparison of the behavior of the trusses with moderately stiff chords and a

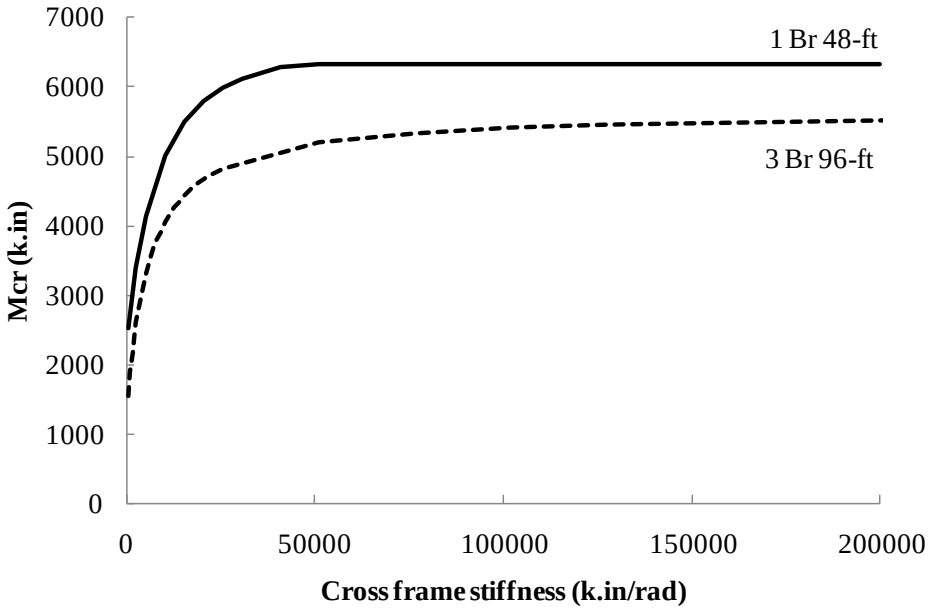

Figure 6.17 Buckling capacity of flexible chord and flexible web truss with 24-ft unbraced length with uniform moment

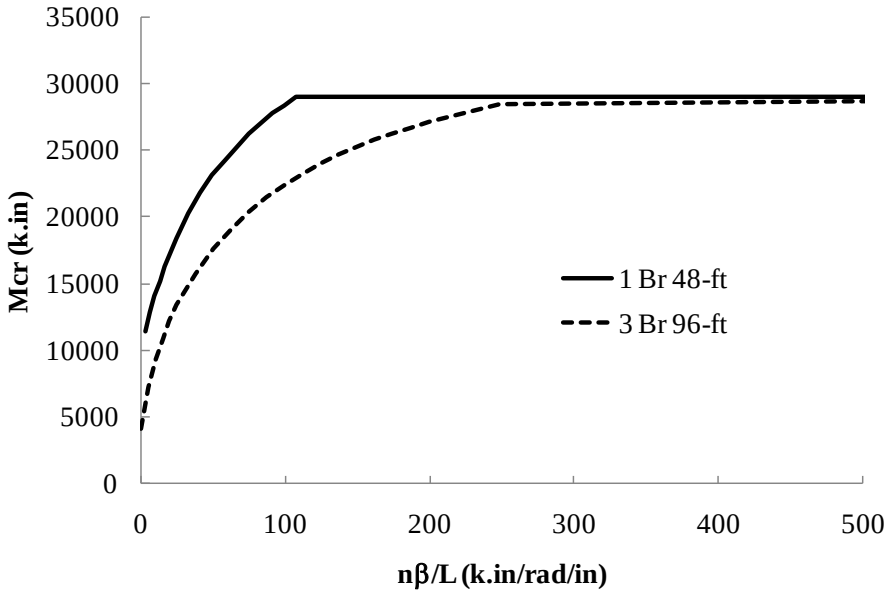

Figure 6.18 Buckling capacity of moderate chord and flexible web truss with 24-ft unbraced length with brace stiffness per linear length with uniform moment

flexible web. The behavior was different than was observed for the case with uniform moment. The buckling capacity of the truss with multiple cross frames and the longer span was significantly below the cases with a single cross frame and a shorter span for both top and bottom chord loading cases. The truss with the longer span was not sensitive to whether the load was at the top or bottom chord and the trusses buckled into a complicated mode shape. The top chord tended to buckle between the brace points while the bottom chord tended to buckle into the full sine mode shape as shown in Figure 6.20. The cross frame area for the buckled shape shown was 10.0 in^2.

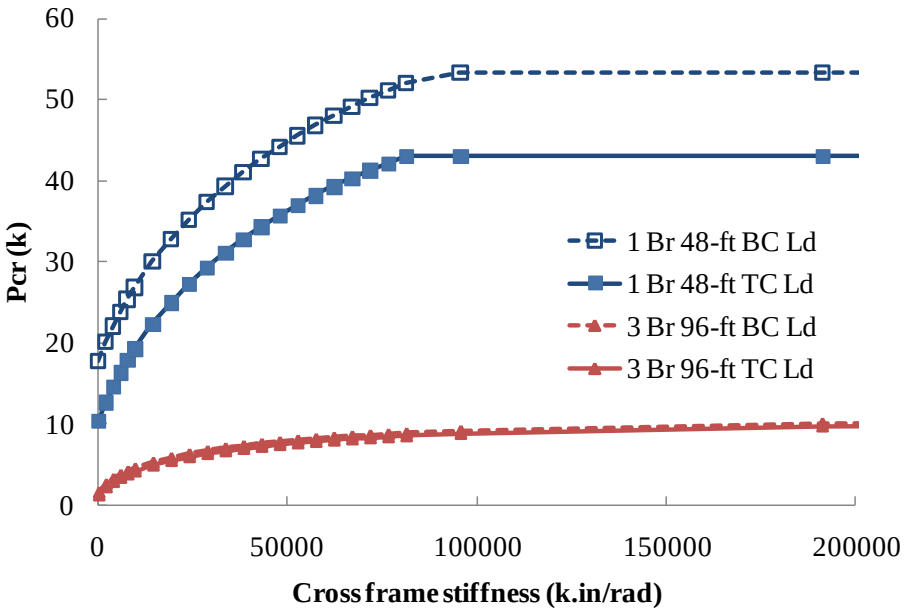

Figure 6.19 Buckling capacity of moderate chord and flexible web truss with 24-ft unbraced length with uniform load

The reason that the truss with 3 cross frame has a significantly lower buckling capacity is due to a combination of several factors. The first factor is the span length. The cross frame is effective in controlling the twist, but not the lateral deflection. When the span becomes longer, the lateral mode dominate the buckling mode since the system is sensitive to the system mode of buckling discussed in Chapter 2. Similar to behavior

observed in beams (Yura et al., 2008) when the system mode of buckling controls possible solutions are to add lateral bracing or to change the geometry of the truss system. Increasing the stiffness of the torsional braces or decreasing the spacing between the braces is relatively ineffective in these cases. The system mode of buckling is still being studied and is discussed in more detail in the section on future work in Chapter 8.

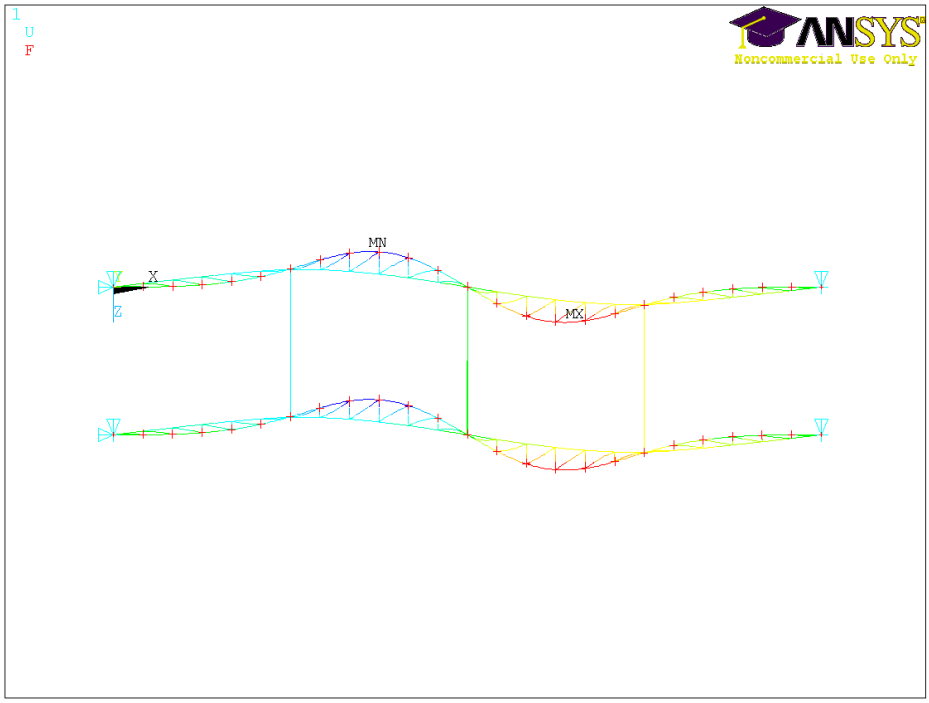

Figure 6.20 Buckled mode shape of truss with high stiffness cross frame

Another factor affecting the behavior of the longer span truss is the moment gradient at the brace point. For truss with a single cross frame at midspan, the chord force varies from zero load at one end and maximum load at another end. However, for the cases with 3 cross frames, the unbraced length near midspan carry the maximum load at one end as well as a sizeable chord force at the other end, which is a more critical problem than the single cross frame case.

Similar to the case with uniform moment, the effectiveness of the brace point is also the factor that affects the buckling capacity. The cross frames located further away from the midspan where the maximum deflection and rotation occur are less effective in

providing the bracing effect since the twist in these regions is significantly smaller than at midspan.

The last reason is the ratio of applied load to the maximum chord force. This could have the most significant impact on lower bucking capacity of the truss with three cross frames compared to the truss with one cross frame. The maximum bending moment calculated by using the beam equation with uniform load of the 96-ft span truss chord was about 4 times higher than the 48-ft span truss chord at the same applied load level. This also indicates that the axial force in the truss chords will be 4 times higher in the longer span truss compared to the short span truss. According to the analysis results for the truss with the moderately stiff chord and the flexible web, the buckling capacity from the case with one cross frame was about 53.3 kips while the three cross frames was 10.2 kips with a cross frame stiffness of about $1x10^6$ k.in/rad. The ratio was about 5 which is close to the moment ratio of four discussed above. Therefore, the truss buckled at a comparable axial load level in the chord, suggesting that the truss might exhibit behavior similar to columns. This behavior was not observed in the cases with uniform moment since the trusses were subjected to uniform axial force throughout the span length at the same applied moment level in both cases of different truss spans.

6.6 BEHAVIOR OF TRUSSES WITH SIMPLIFIED WEB CONNECTIONS

Trusses are typically idealized as systems composed of axially loaded members that are pinned at the joints. The actual connections of the trusses usually have some restraints from the gusset plates. To investigate the behavior of the idealized connection behavior versus the as-built system, two different models were used for the web connections. The as-built system utilizes the system discussed in Chapter 5. The simplified system consisted of modeling the web members with pinned ends. Figure 6.21 and Figure 6.22 show the comparison of the buckling capacity with the two different configurations of the web connections for the 96-ft span truss with 3-ft and 6-ft depth, respectively, with various chord and web sections for uniform moment loading.

The major difference of using the simplified web is that the bending stiffness of the web is neglected. The stiffness of the web does contribute to the buckling capacity. By neglecting the web stiffness, the buckling capacity of the truss is independent of the web size, as demonstrated in the graph that the buckling capacity of trusses with the simplified webs are equal within the same chord size. As expected, for the trusses with the flexible web sections, the buckling capacity of the truss with the simplified web connections is close to the regular web case. With larger web sizes, the difference between the regular and simplified webs increases. The simplified connection model is likely to be reasonably accurate for trusses with Tee sections for the chords and angles for the web members. For trusses with wide flange connections for the flanges and chords, the simplified connection would underestimate the truss stiffness.

For the respective cases of top chord and bottom chord loading, Figure 6.23 and Figure 6.24 show the corresponding results for the case with uniform distributed loads. The trusses have spans of 96-ft span and a 6–ft depth. The results for the other span lengths and depths were also similar in behavior and also similar to the bending moment case. In addition to the uniform bending moment case, the difference between the regular and simplified web was higher for the top chord loading case than the bottom chord loading case.

Another factor that was compared between the regular and simplified web connections was the in-plane moment of inertia of the truss. The comparison of the in-plane moment of inertia is shown Figure 6.25. Apparently, the simplified web did not affect the in-plane moment of inertia of the truss due to the same axial behavior of the truss web elements.

6.7 SUMMARY

Parametric studies were conducted on the trusses using three dimensional finite element models. The verification of the truss model with MASTAN2 indicated that there were some limitations when using the ANSYS model to estimate the eigenvalue of Vierendeel truss systems. A variety of models were considered including trusses with

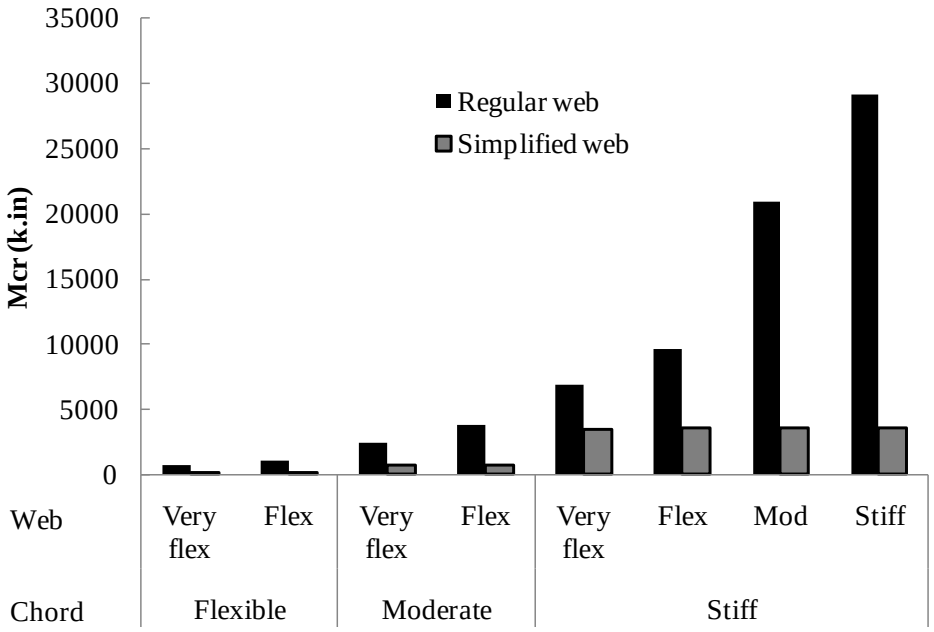

Figure 6.21 Buckling capacity of 96-ft span 3-ft depth truss with regular and simplified web

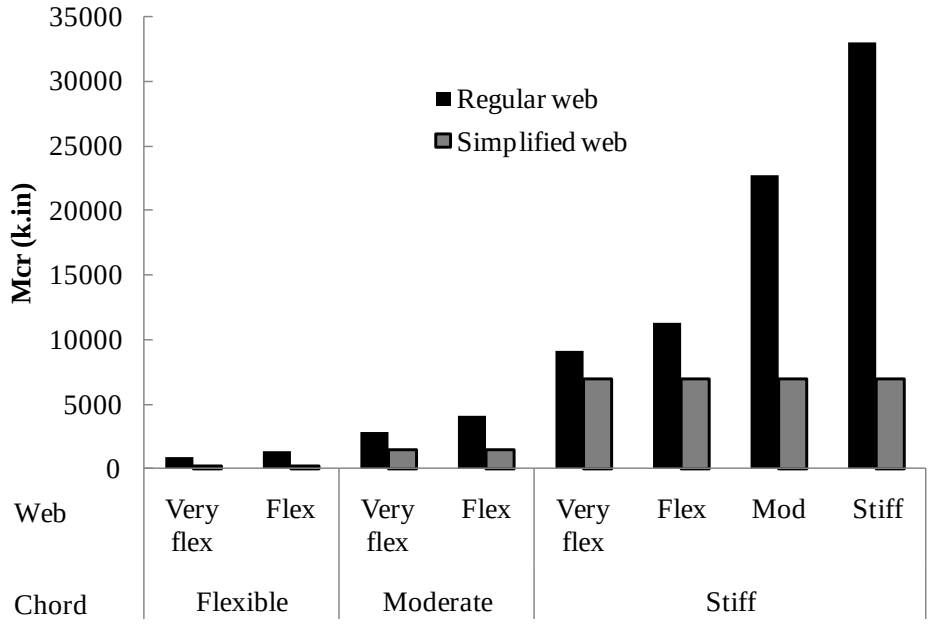

Figure 6.22 Buckling capacity of 96-ft span 6-ft depth truss with regular and simplified web

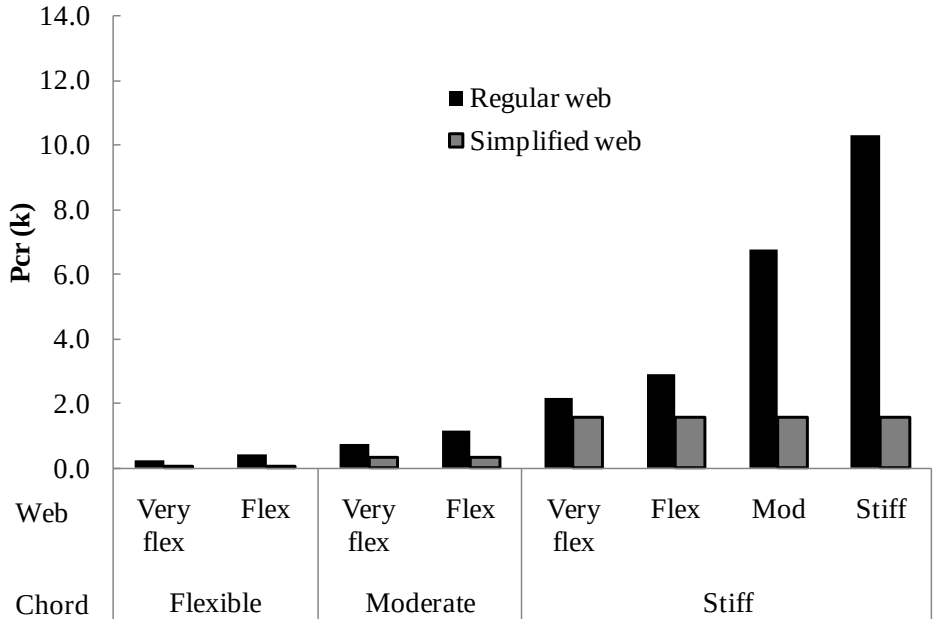

Figure 6.23 Buckling capacity of 96-ft span 6-ft depth truss with regular and simplified web with top chord loading

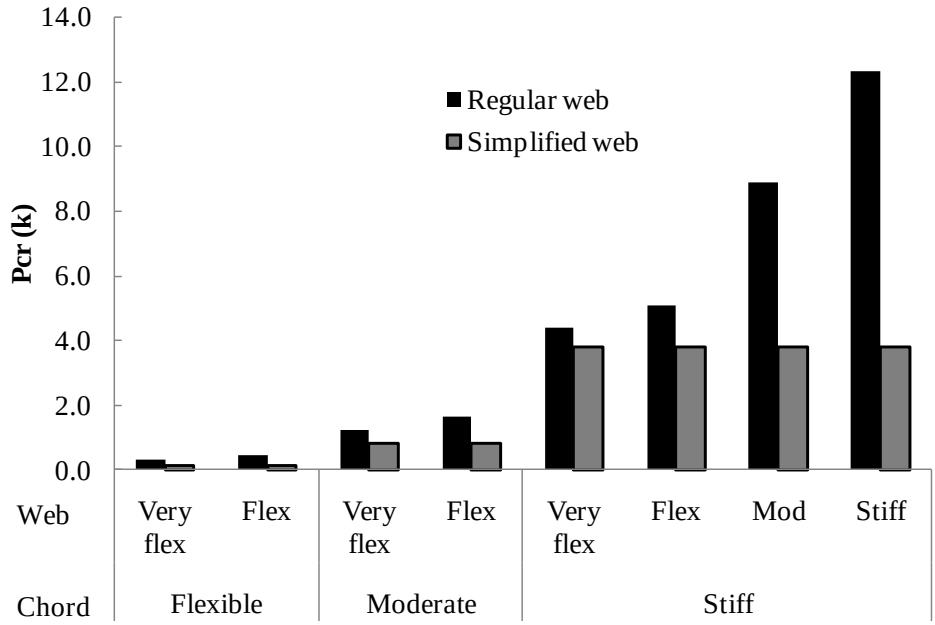

Figure 6.24 Buckling capacity of 96-ft span 6-ft depth truss with regular and simplified web with bottom chord loading

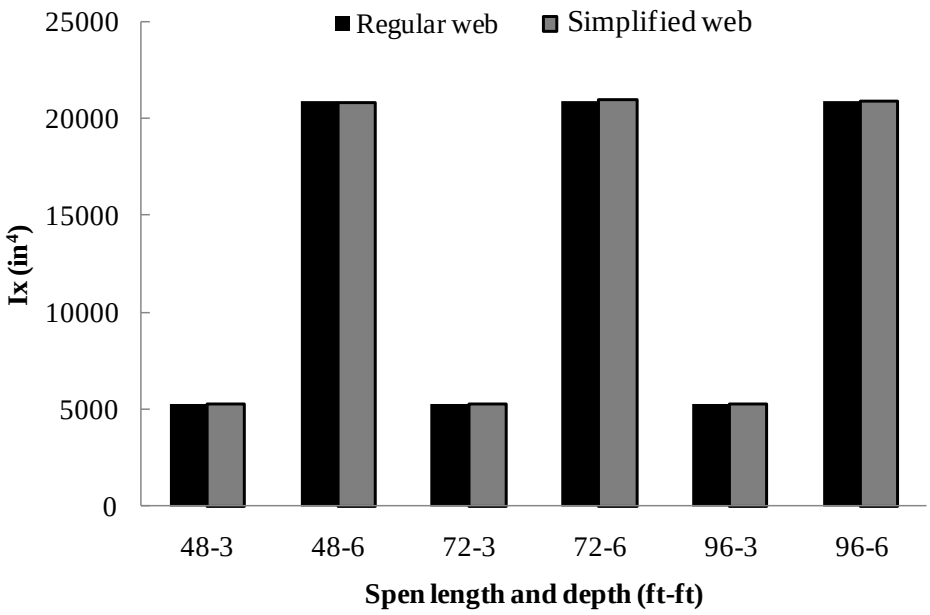

Figure 6.25 Comparison of truss in-plane moment of inertia

torsional braces consisting of flexural members that attached to the chords and full depth cross frames. The systems with the full depth cross frames are not sensitive to cross sectional distortion. Models were checked using flexural braces that connected to trusses with rigid web verticals at the brace location as well as webs that did experience cross sectional distortion. The buckling capacity of the truss with rigid web with torsional bracing provided highest buckling capacity; however the system did not reach a point where the truss buckled between the brace points. The trusses with cross frame, had good agreement with the trusses that used the flexural braces and the rigid web verticals up until the truss with the cross frame buckled between the brace points. The buckling capacity of truss with the regular web had a lower buckling capacity than the other systems due to cross sectional distortion. The buckling behavior of the truss is sensitive to the type of connections of the web elements. Trusses with the simplified web connections had a lower buckling capacity. The simplified web connections are conservative and in some instances may provide a practical approach for developing design expressions.

CHAPTER 7
Stiffness Requirements for Torsional Bracing of Truss Systems

7.1 INTRODUCTION

To develop the torsional bracing requirements for truss systems, analyses were conducted on trusses using three different sections for the chords and four different sections for the web members. The same size sections were used for the verticals and diagonals of the webs. Although a most of the analyses was conducted using a prismatic layout of the sections, selected cases of were also considered using a configuration where the diagonal web elements near the supports were larger than the sections near midspan to account for the larger shear demand. The analyses were divided into two categories that are referred to as 1) the regular truss and 2) the simplified truss. In the simplified truss, the interior web elements were axial-only (LINK8) element without the connection elements modeling the connection region. The simplified truss serves as the idealized model of the truss system where the members are modeled as pin ended. Such a model is likely a reasonable model for trusses with relatively flexible web connections such as systems with T-shaped chords and angle sections for the webs. In trusses with wide flange sections for the web elements, such as the trusses in the laboratory tests, the gusset plates can provide significant joint restraint for which the regular truss system is a more accurate model; however the simplified model is a conservative approximation for these systems.

To determine the stiffness requirements, eigenvalue buckling analyses were conducted. Comparisons were made with the brace stiffness requirements that have been established for column and beam systems. The later part of this chapter focuses on the development of an expression for estimating the buckling capacity of a truss with a

torsional brace at midspan. Two load cases are considered, uniform moment and a uniformly distributed load. The analysis was conducted using a full depth cross frame for the torsional brace. The simplified truss with the pin ended webs was used in the analysis to develop the stiffness requirements; however analyses were also done using the regular truss with restrained web elements.

7.2 BUCKLING CAPACITY AND IDEAL CROSS FRAME STIFFNESS OF TRUSS WITH ONE CROSS FRAME AT MIDSPAN

The truss analyses were conducted on the truss with a single cross frame at midspan. The cross frames were composed of truss elements (LINK8) that resist only axial force. The eigenvalue analyses were performed with various stiffness values of the cross frame. The cross frame was modeled as a tension-only system for which the brace stiffness is given by the following expression:

$$\beta_b = \frac{ES^2h_b^2}{\frac{2L_c^3}{A_c} + \frac{S^3}{A_b}} \tag{7.1}$$

Where, E is the modulus of elasticity of the cross frame material, S is the truss spacing, h_b is the depth of the cross frame (full truss depth was used), L_c is the length of the cross frame diagonal, A_c is the area of the diagonal, and A_b is the area of the strut of the cross frame. For simplicity, the same sizes were used for the struts and diagonals of the cross frame. The stiffness of the cross frame was changed in the analysis by simply altering the area of the diagonal and struts.

As mentioned in Chapter 2 that the total brace stiffness is the combination of the stiffness from several component. The equation for the total brace stiffness calculation, including the in-plane stiffness, is shown here again for convenience.

$$\frac{1}{\beta_{tot}} = \frac{1}{\beta_{br}} + \frac{1}{\beta_{sec}} + \frac{1}{\beta_g} \tag{7.2}$$

The cross frame was full depth and connected directly to the top and bottom chord so that there was no cross sectional distortion and the β_{sec} is eliminated. Therefore, since there was no cross sectional distortion, the stiffness of the brace and the in-plane truss stiffness are the components for establishing the stiffness requirements for the truss. Because the trusses had a relatively large spacing as well as significant in-plane stiffness, the in-plane stiffness effects did not significantly impact the behavior of the truss system with relative low brace stiffness. However, for the stiff torsional brace, the effect of the in-plane stiffness would be noticeable in reduction of the total brace stiffness. The effects of cross sectional distortion will be addressed in future research and are discussed in the summary chapter.

7.2.1 Regular Truss Model

Table 7.1 provides a summary of the eigenvalue (P_{cr}) and the corresponding ideal brace stiffness for the case of the 72-ft span regular truss a with 6-ft depth. The truss spacing was 20 feet.

Table 7.1 Eigenvalue and ideal brace stiffness of truss with uniform load

Chord	Web	Bottom chord loading		Top chord loading	
		P_{cr} (kips/joint)	β_{Ideal} (kips.in/rad)	P_{cr} (kips/joint)	β_{Ideal} (kips.in/rad)
W4x13	W3x8	2.25	10063	1.96	9773
	W4x13	3.32	31047	3.03	30835
W8x24	W3x8	10.10	22149	8.08	20729
	W4x13	12.14	36952	10.11	34840
W12x50	W3x8	38.65	75499	31.39	74828
	W4x13	44.29	100957	35.03	91257
	W8x24	62.72	219895	53.30	215926
	W12x26	84.15	693404	74.69	699129

In general, when the web sizes become larger, the effectiveness of the bracing tends to decrease. An example of this can be observed by comparing the bracing required for the W4x13 web versus the W12x26 web of truss with W12x50 chord. The larger chord had buckling capacities for both top and bottom chord loading that were approximately twice that for the smaller chord (bottom chord: 84.15k versus 44.29k; top chord loading: 74.69k versus 36.03k). Although the buckling capacity was roughly doubled, the larger chord ideal brace stiffness required was approximately 7 times the larger than required for the smaller chord. This was possible due to the truss with larger chord had the higher cross section stiffness which results into less twist. This led to the lateral dominated lateral torsional buckling mode and results in reduction in the effectiveness of the brace and required higher stiffness to reach the full sine buckling mode shape.

For the case with uniform moment loading on the trusses with regular web, the eigenvalue results were graphed in Figure 7.1 with the ratio of the axial force in the compression chord due to the applied moment to the unbraced length, F_{cr}/L, where $F_{cr} = M_{cr}/h$, on the vertical axis versus the ideal stiffness required. The ratio F_{cr}/L relates the bracing behavior to the stiffness requirements for both relative and discrete bracing systems for columns. For a column, the ideal stiffness for a relative brace is F_{cr}/L, while the ideal stiffness for a discrete brace would be $2F_{cr}/L$ (single brace). In the legend the first term represents the span of the truss while the second represents the depth of the truss (ie. 48' x 36" is for a 48-ft span and a truss depth of 36 inches). Each legend represents the results from the mixture of truss chord and web geometry used in the analysis with the same span length and depth. From the graph there is no clear relationship between the ratio F_{cr}/L and the ideal stiffness required. A similar graph was observed for the case with uniform load. Therefore, the torsional bracing requirements are more likely to be similar to the bracing requirements for beam systems.

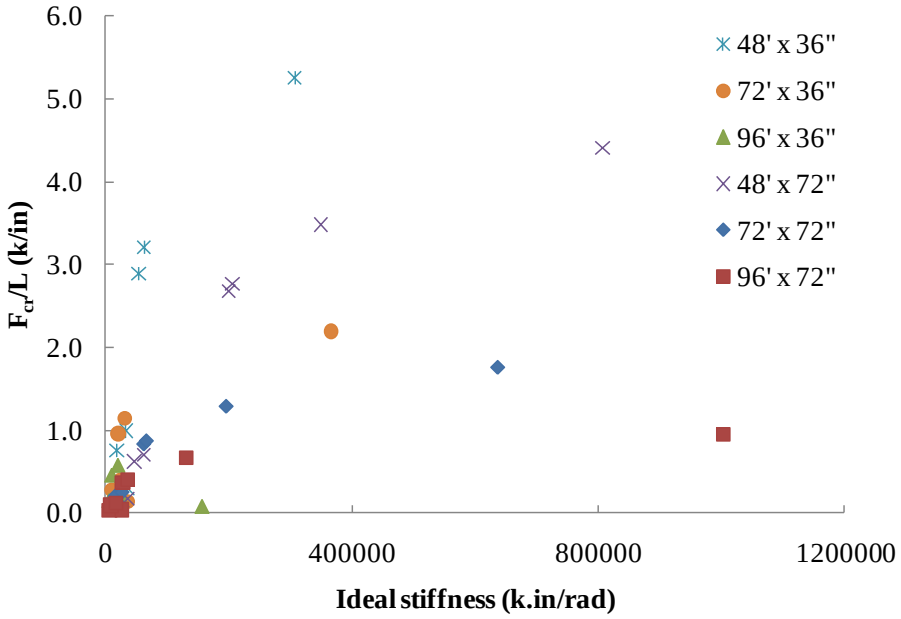

Figure 7.1 Stiffness requirement by using column formula for truss with regular web and uniform bending moment

The stiffness requirements for beam systems were derived from a continuous bracing formulation that neglects the contribution of the beam with no bracing. The expression that is given in the AISC Specification (AISC, 2005a) is as follows:

$$\beta_T = \frac{2.4LM_f^2}{\Phi nEI_{eff}C_{bb}^2} \tag{7.3}$$

The terms in Equation 7.2 were defined in Chapter 2. Neglecting constant terms in Eq. 7.2 and changing I_{eff} to I_{chord} Leads to the following expression (note C_b=1.0 for uniform moment):

$$\beta_T = \frac{LM_f^2}{I_{chord}} \tag{7.4}$$

To use Eq. 7.3 for truss systems the maximum moment, M_f, needs to be replaced with the chord force multiplied by the truss depth: $F_{cr}h$. The results from the eigenvalue analyses on the truss systems can therefore be graphed using Eq. 7.3 versus the ideal

stiffness required as shown in Figure 7.2 for the 6-ft deep truss. Aside from a few outliers, the data showed a relatively linear relationship. The outliers were for the cases where the web was large compared to the chord which made the truss require very large brace stiffness. The behavior was also the same for other cases with bottom chord loading and also with the 3-ft depth truss. The case of truss with the uniform moment also exhibited similar behavior as the uniform load case. Since the case with larger webs had a lot higher buckling capacity than the small web, the consequence was that the truss in-plane stiffness became more significant. Therefore, the in plane stiffness need to be taken into account.

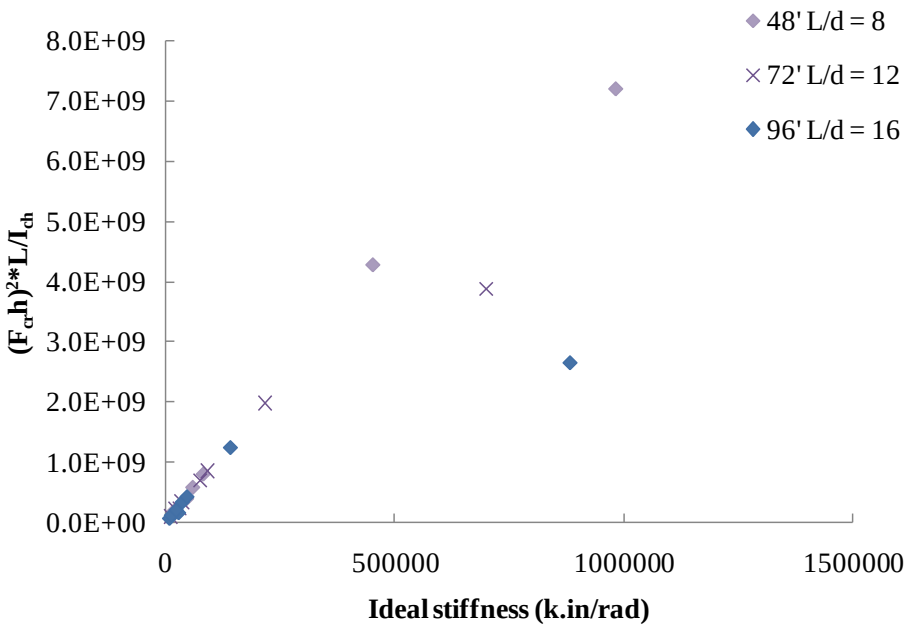

Figure 7.2 Stiffness requirement by using beam formula for truss with regular web and top chord loading

The results of the plot of the stiffness requirement and the total stiffness are shown in Figure 7.3. Including the truss in-plane stiffness pulled the two outliers closer to the rest of the data that exhibited a linear relationship. This is also valid for the cases with 3-ft depth with either the top or bottom chord loading and the case with uniform

moment. Figure 7.4 shows the similar case of 3-ft deep truss with uniform load. The 3-ft depth case did not show as good agreement as the cases with 6-ft depth. This could be explained by the fact the 3-ft depth truss had higher L/d ratios, up to 32, which is relatively large for a truss system and would not likely be used very frequently in design. Trusses with higher L/d ratios may often have relatively small angles for the diagonals, which were not considered as a variable in this study. The trusses in this study had diagonal angles in the range of 36.9 to 56.3 degree. Figure 7.5 shows the similar case of 3-ft deep truss with uniform moment. For the case with uniform moment, the relationship was not as linear as the case with uniform load; however the agreement was still reasonable.

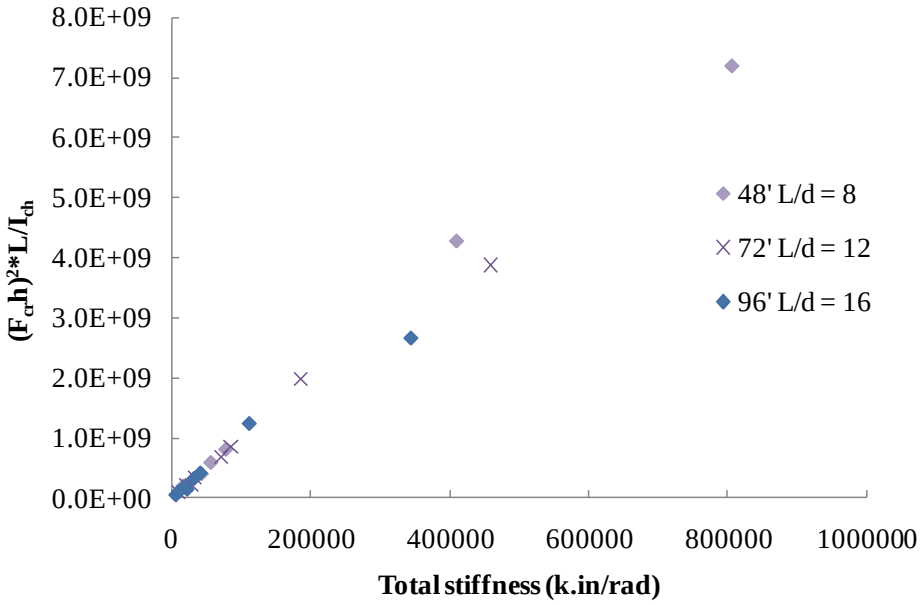

Figure 7.3 Total stiffness requirement by beam equation of 6-ft depth truss with regular web and uniform load at top chord

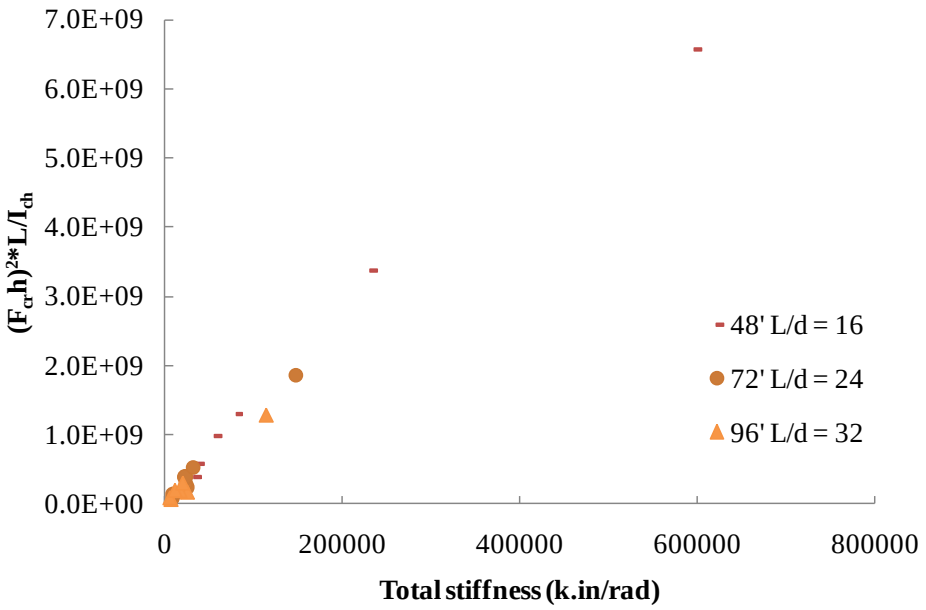

Figure 7.4 Total stiffness requirement by beam equation of 3-ft depth truss with regular web and uniform load at bottom chord

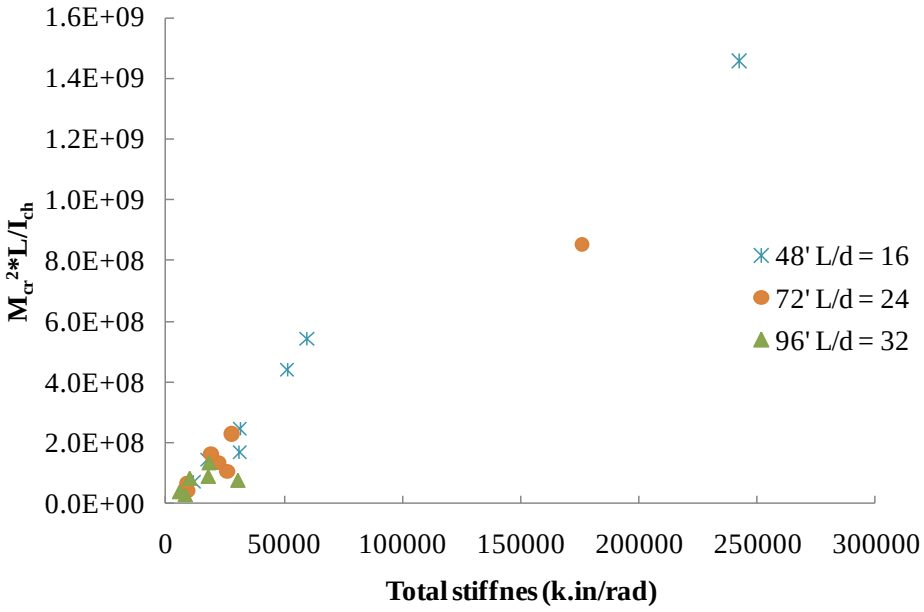

Figure 7.5 Total stiffness requirement by beam equation of 3-ft depth truss with regular web and uniform moment

Because the shear is larger near the supports, many trusses might have larger diagonal sizes in these regions. To investigate the impact of variable diagonals sizes on the behavior, selected cases were considered using the 72-ft span truss with a 6-ft depth. The sizes of the diagonal webs of first three panels near the supports were increase to one size larger than the diagonal web members near midspan. For example, if the diagonal web at midspan was W3x8, the diagonal web near support was W4x13. The detail of the web size and the buckling capacity of 72-ft span truss are indicated in Table 7.2. The eigenvalue and the ideal brace stiffness were both increased in most of the cases except with the W12x50 chord with W12x26 web where the ideal stiffness slightly decreased which probably indicated the better control of the lateral deflection of truss with large torsional brace and resulted in increasing in the efficiency of the brace. To compare with the regular web, Figure 7.6 shows the plot of the cases indicated in Table 7.1 and Table 7.2 for the top chord loading case. Even though the larger diagonal web near the support had a higher ideal brace stiffness, the corresponding eigenvalues also increased. Again, aside from a few outliers, the data exhibited a relatively linear behavior.

Table 7.2 Eigenvalue and ideal brace stiffness of truss with larger web near supports with uniform load

Chord	Web		Bottom chord loading		Top chord loading	
	Mid span	Support	P_{cr} (kips/joint)	β_{Ideal} (kips.in/rad)	P_{cr} (kips/joint)	β_{Ideal} (kips.in/rad)
W4x13	W3x8	W4x13	2.41	10784	2.14	10517
	W4x13	W8x24	3.69	33795	3.42	33760
W8x24	W3x8	W4x13	10.58	24552	8.56	21995
	W4x13	W8x24	13.48	41522	11.51	39741
W12x50	W3x8	W4x13	42.66	88637	33.43	80977
	W4x13	W8x24	47.51	107073	37.99	99161
	W8x24	W12x26	66.57	232217	57.40	228400
	W12x26	W12x40	86.68	683178	77.40	698311

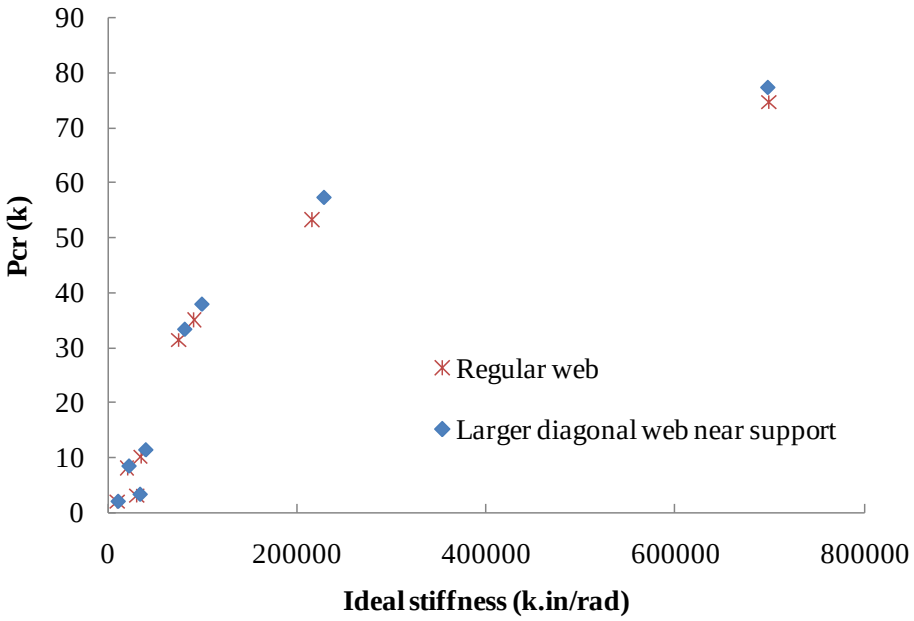

Figure 7.6 Comparison of eigenvalue for truss with larger diagonal near support and regular truss

7.2.2 Simplified Truss Model

This section presents the data of the behavior of the simplified trusses with the pin ended web members. The model was modified by changing the web element from the BEAM44 element to LINK8 where the element would carry only axial force. The web connection elements were also removed. The chord was kept same as the regular model and was continuous along the truss length. In addition, the vertical web elements at the support were kept the same to maintain geometric stability of the chord along the length. The results of the cases of the trusses with 72-ft span and a 6-ft depth are provided in Table 7.3.

The major difference between the simplified and regular trusses was that the web did not affect the buckling capacity and the ideal brace stiffness with the simplified system. Without the bending stiffness contribution of the web to the chord, the buckling capacities and ideal brace stiffness values were similar for those with the same chord size. The decrease in the buckling capacity and ideal brace stiffness using the pinned

web connections for the cases with larger webs was significant. The buckling capacity was reduced by approximately 50% in some cases and the required ideal brace stiffness was decreased to one tenth for the cases with the W12x50 chord and W12x26 web. For a given chord size, the difference of ideal brace stiffness with different web sizes was insignificant. The results of eigenvalue solutions are graphed in the same manner as the cases with beam web elements and shown in Figure 7.7.

Table 7.3 Eigen value and ideal brace stiffness of truss with simplified web

Chord	Web	Bottom chord loading		Top chord loading	
		P_{cr} (kips/joint)	β_{Ideal} (kips.in/rad)	P_{cr} (kips/joint)	β_{Ideal} (kips.in/rad)
W4x13	W3x8	1.25	2409	0.96	2123
	W4x13	1.25	2414	0.96	2146
W8x24	W3x8	8.93	17343	6.86	15501
	W4x13	8.93	17287	6.86	15449
W12x50	W3x8	41.55	91744	31.91	79338
	W4x13	41.49	89584	31.87	77553
	W8x24	41.43	87831	31.83	75835
	W12x26	41.43	87694	31.83	75726

The graphs of the buckling capacity of the trusses with the pinned web elements exhibited a linear relationship using the beam stiffness formulation discussed in the last section. The one outliner on the graph corresponded to the case with the W12x50 chord and the W3x8 web. Due to the extremely small web compared to the chord, this data point can be neglected. The relationship was also very good for the cases with uniform moment and with the truss depths of 3 and 6-ft as depicted in Figure 7.8 and Figure 7.9 for the respective cases on 3-ft deep truss with uniform load at top chord and 6-ft deep truss with uniform moment. Since the beam formulation for the bracing requirement had good agreement with the eigenvalue solutions, the next step was to determine the constants necessary for the equation to be used in design.

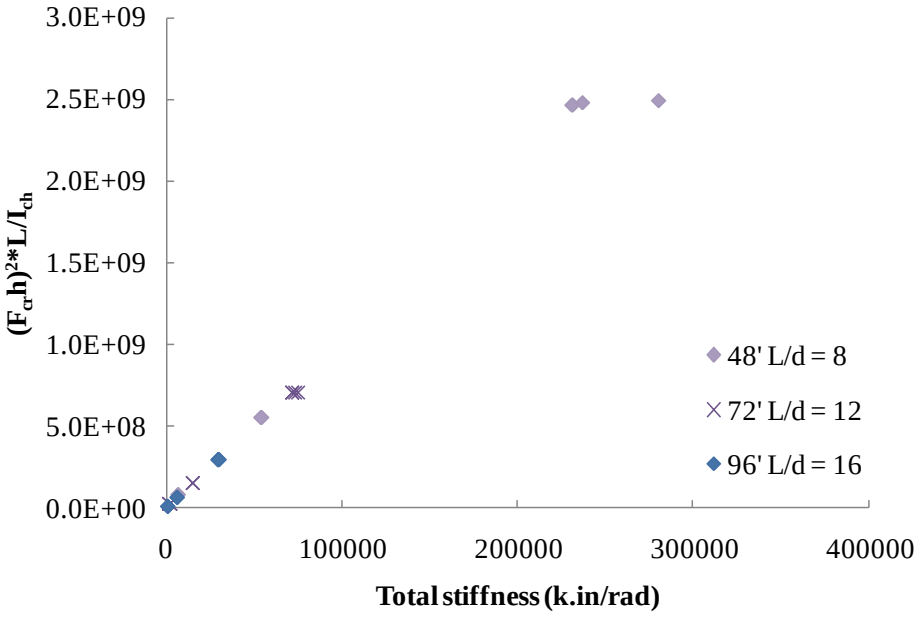

Figure 7.7 Stiffness requirement by using beam formula for 6-ft deep truss with pinned web and top chord loading

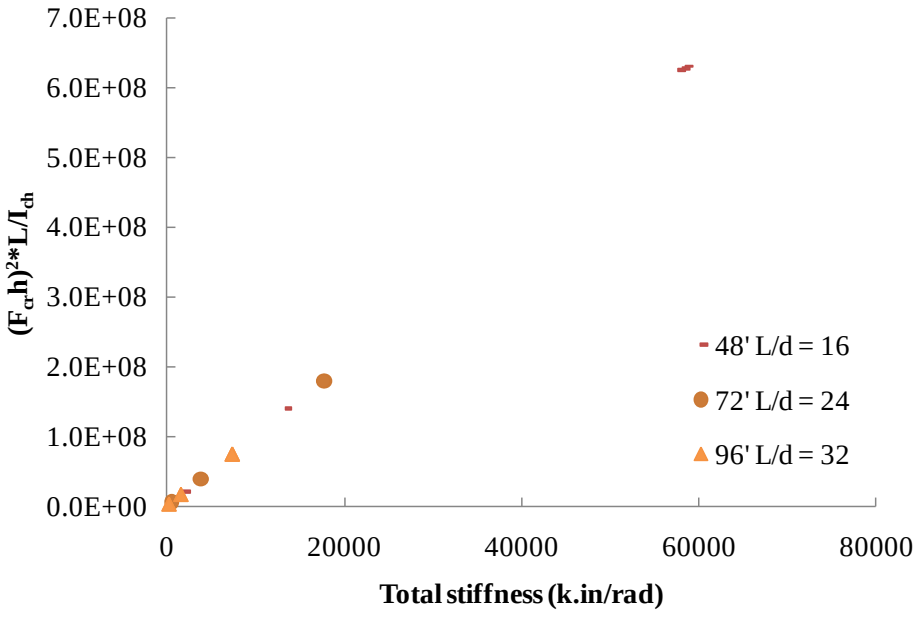

Figure 7.8 Stiffness requirement by using beam formula for 3-ft deep truss with pinned web and top chord loading

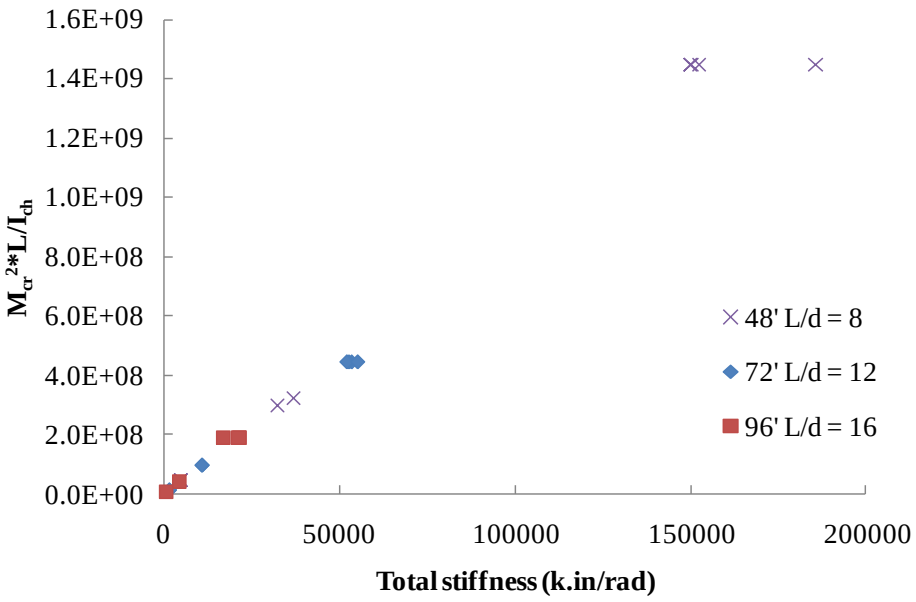

Figure 7.9 Stiffness requirement by using beam formula for 6-ft deep truss with pinned web and uniform moment

Comparisons were also made between the truss solutions with the regular webs versus the simplified webs. The results for both top and bottom chord loading were combined into a single graph. The results for the truss with regular web are shown in Figure 7.10. The corresponding data for top chord loading and bottom chord loading are each relatively linear with the exception of four data points for each load type that fall below the linear trend. The four data points that were out of trend were the cases with the largest chord and web, W12x50 chord and W12x26 web. These cases required higher brace stiffness to reach the full bracing; however, they were still in the practical range. The other consideration is that the applied load at the full bracing would results in the inelastic range which may not be practical sections for full bracing.

Figure 7.11 shows a graph of all of the combined data for the trusses with both the regular and simplified webs disregarded the four points for each load locations mentioned previously with uniform load. The graph resulted in the good agreement between the regular and simplified web in both top and bottom chord loading cases. However, the

graphs were not match in the cases of uniform moment where the simplified web case had about 20 percent higher slope than the regular web truss as shown in Figure 7.12.

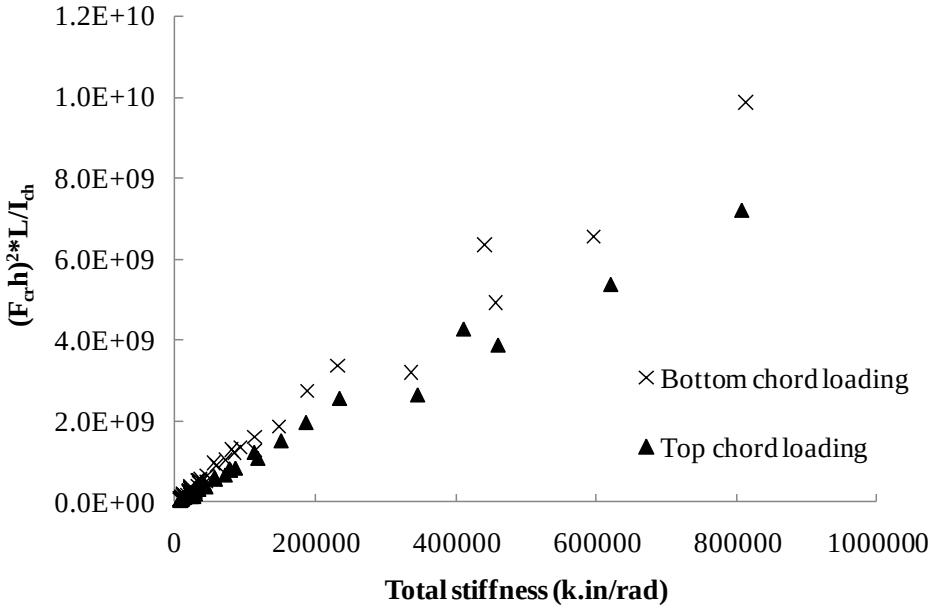

Figure 7.10 Stiffness requirement for combine plot of truss subjected to uniform load

The coincident of the cases of truss with simplified web and regular web indicated that the stiffness requirement largely depends on the buckling capacity of the truss rather than the truss's web configuration, especially for the truss with small web. However, the truss's web configuration did affect the buckling capacity of the truss. For the moment cases where the load pattern was different from the uniform load, the truss web configuration did affect the stiffness requirement, however, within 20 percent range. In general, the stiffness requirement for the beam usually be 3 to 4 times the ideal brace stiffness due to the large deflection at the buckling load when the brace stiffness was equal to ideal brace stiffness. The higher required brace stiffness should cover all of the outlier data in the studied range.

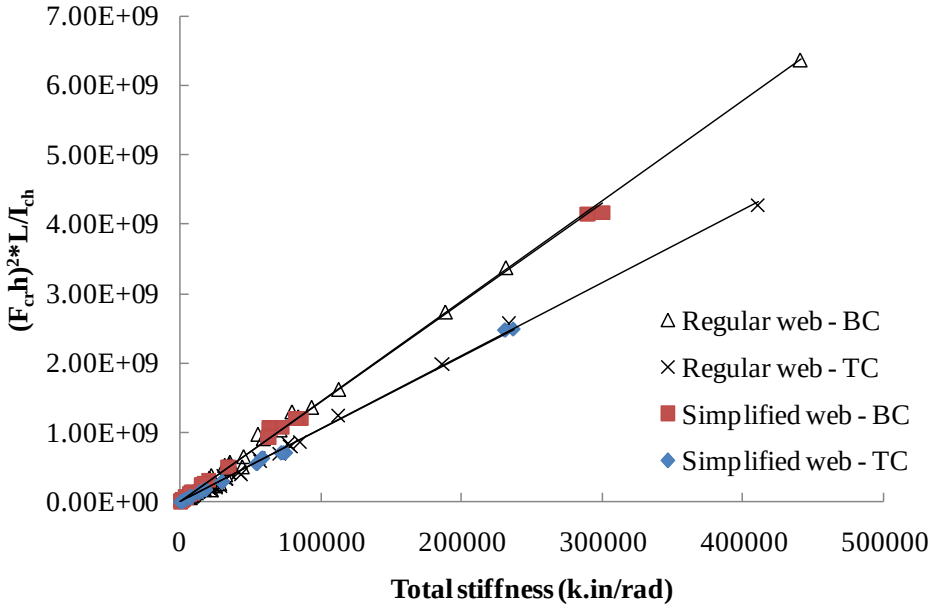

Figure 7.11 Comparison of stiffness requirement of simplified web and regular web truss subjected to uniform load (exclude outlier)

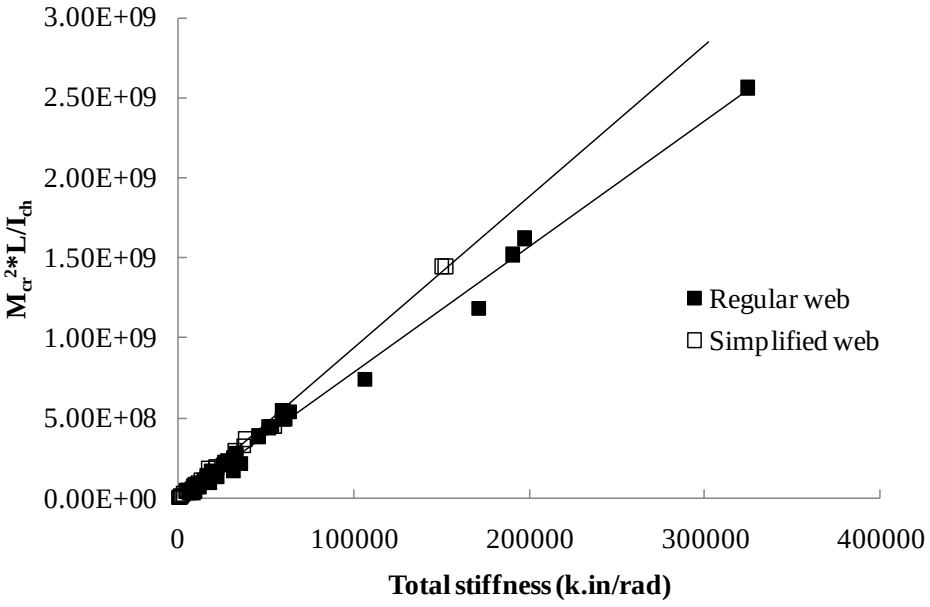

Figure 7.12 Comparison of stiffness requirement of simplified web and regular web truss subjected to uniform moment (exclude outlier)

7.3 DEVELOPMENT OF THE STIFFNESS REQUIREMENT FOR THE TRUSS WITH SINGLE CROSS FRAME AT MIDSPAN

By using Figure 7.11, the stiffness requirement can be developed using the equation for each graph. The equations for the bottom chord loading case and for the top chord loading case are shown in equations (7.5) and (7.6), respectively.

$$\frac{(F_{cr}h)^2 L}{I_{chord}} = 14300\ \beta_{i\_tot} \tag{7.5}$$

$$\frac{(F_{cr}h)^2 L}{I_{chord}} = 10500\ \beta_{i\_tot} \tag{7.6}$$

Where F_{cr} = Maximum axial force in chord (kips)

h = Truss depth (in)

L = Span length (ft)

I_{chord} = Out-of-plane moment of inertia of compression chord (in^4)

By taking the ratio of the two constants in the equations, the load height effect is 1.36. Assuming the material for the trusses are steel (E=29000 ksi) and adjusting the span length unit to be consistent with the system, Eqs. (7.5) and (7.6) can be modified to the following expressions for the stiffness requirements for bottom and top chord loading:

$$\beta_{i\_tot} = \frac{2.0(F_{cr}h)^2 L}{12EI_{chord}} \tag{7.7}$$

$$\beta_{i\_tot} = \frac{2.8(F_{cr}h)^2 L}{12EI_{chord}} \tag{7.8}$$

A single equation can be developed by incorporating a factor, B, to account for load height on the cross section. The resulting expression is as follows:

$$\beta_{i\_tot} = \frac{2.8(F_{cr}h)^2 L}{12EI_{chord}B} \tag{7.9}$$

Where B = Load height factor

= 1.0 for top chord loading

= 1.4 for bottom chord loading

For the cases with uniform moment loading, the results from the analysis of trusses with the simplified webs model were used. The resulting equation is as follows:

$$\frac{M_{cr}^2 L}{I_{chord}} = 9400\beta_{tot} \tag{7.10}$$

The term M_{cr} is the term F_{cr}*h in the case with uniform load. Comparing this equation to equation (7.6) from the top chord loading of the uniform load case, this yielded the C_b for the uniform moment of 10,500/9400 = 1.12. The equation was modified to:

$$\beta_{tot} = \frac{M_{cr}^2 L}{4EI_{chord}C_b B} \tag{7.11}$$

Where M_{cr} = Critical moment in uniform moment (kip.in)

= F_{cr}h for uniform load (kip.in)

F_{cr} = Maximum axial force in chord (kip)

h = Truss depth (in)

L = Span length (in)

I_{chord} = Out-of-plane moment of inertia of compression chord (in^4)

B = Load height factor

= 1.0 for top chord loading

= 1.4 for bottom chord loading

C_b = 1.0 for uniform moment

= 1.12 for uniform load

The proposed equation was then used to compare to the stiffness requirement of the analysis. Figure 7.13 and Figure 7.15 show the comparison of the proposed equation for the cases of top and bottom chord loadings, respectively. Figure 7.14 and Figure 7.16 show the plot of the same cases but with only the low stiffness range. The proposed

equation shows the good agreement with the analyses data especially for the simplified web model.

For the comparison of the uniform moment case, the proposed equation was plotted with the regular truss and shown in Figure 7.17 for all data range. Figure 7.18 shows the same results at the low required brace stiffness range. The proposed equation show good agreement with the simplified web model, but did not show a good result as the cases with uniform load with the regular web model. However, in over all, this equation is still in good agreement with the analysis results.

In addition to the proposed equation, the required brace stiffness is normally 2-3 times larger than the ideal brace stiffness for controlling of the lateral deflection and accounting for the effect of initial imperfection. Together with the load factor in the design, this equation provides reasonable required total stiffness to the truss system.

7.4 ESTIMATING THE BUCKLING CAPACITY OF TORSIONALLY BRACED TRUSS

7.4.1 Truss Subjected to Uniform Load

Chapter 2 outlined the bracing behavior of column and beams systems. For torsionally braced beams, the following expression was presented for a beam subjected to uniform moment with torsional braces along the length:

$$M_{cr} = \sqrt{M_o^2 + \bar{\beta}_T^2 E I_y} \tag{7.12}$$

Where, M_{cr} is the buckling capacity of the torsionally braced beam (uniform moment), M_o is the buckling capacity of the beam with no intermediate bracing, $\bar{\beta}_T$ is the equivalent continuous torsional brace stiffness (k-in/rad/in), E is the modulus of elasticity of the beam material, and I_y is the weak axis moment of inertia. According to Equation (7.12), there are two primary terms involved in the buckling capacity of the torsional braced beam: 1) the first term under the radical represents the capacity of the beam with no bracing, and 2) the second term under the radical represents the contribution of the bracing.

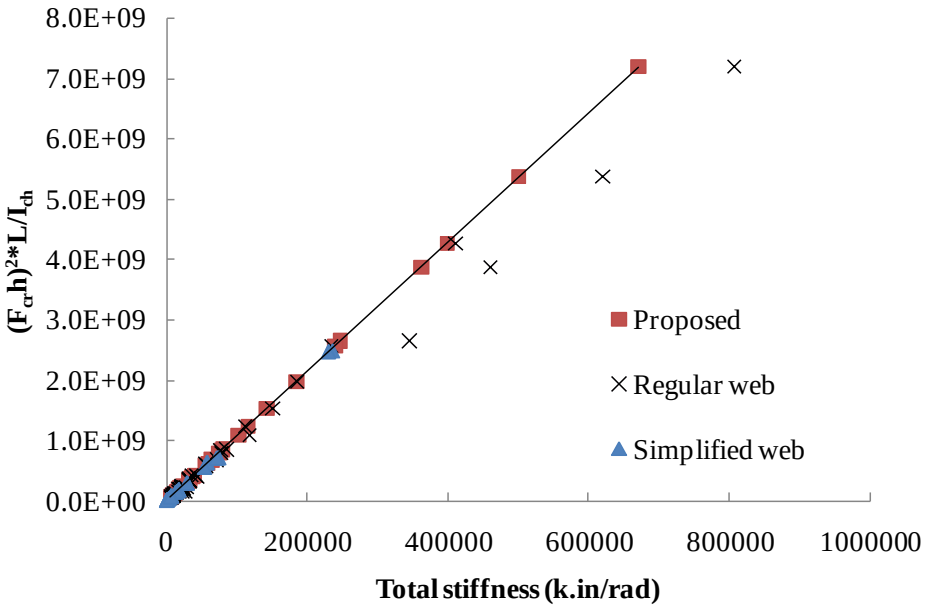

Figure 7.13 Stiffness requirement of proposed equation compared to the analysis – top chord loading

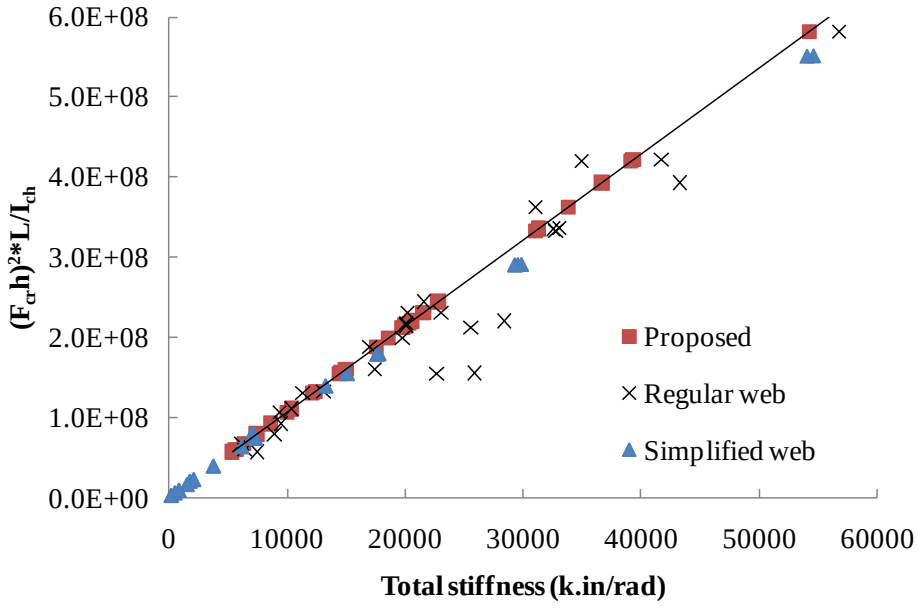

Figure 7.14 Stiffness requirement of proposed equation compared to the analysis at low stiffness value – top chord loading

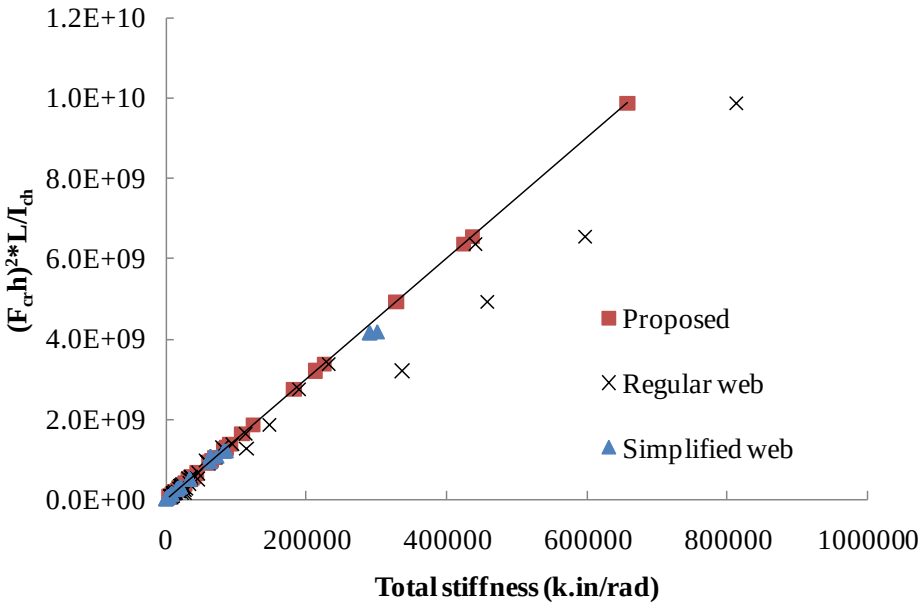

Figure 7.15 Stiffness requirement of proposed equation compared to the analysis – bottom chord loading

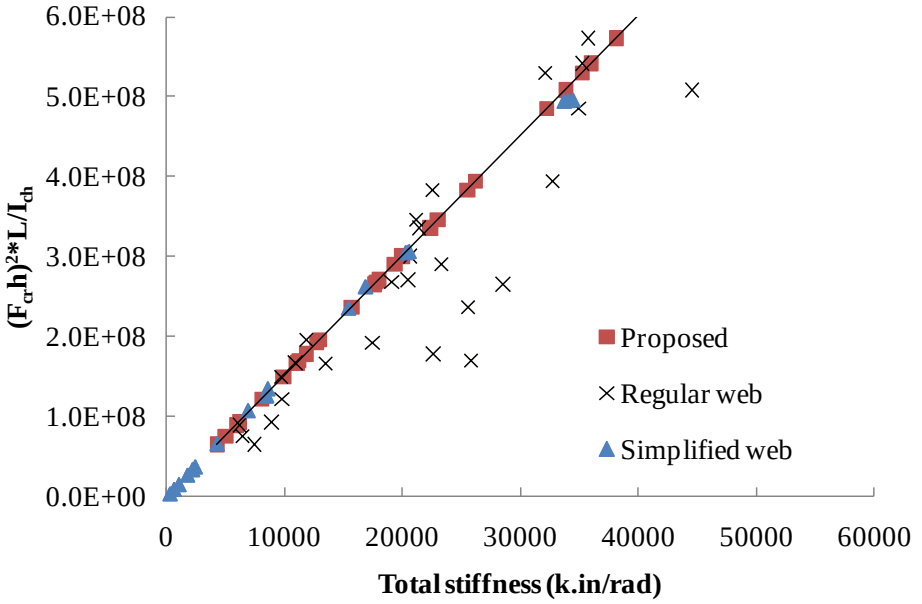

Figure 7.16 Stiffness requirement of proposed equation compared to the analysis at low stiffness value – bottom chord loading

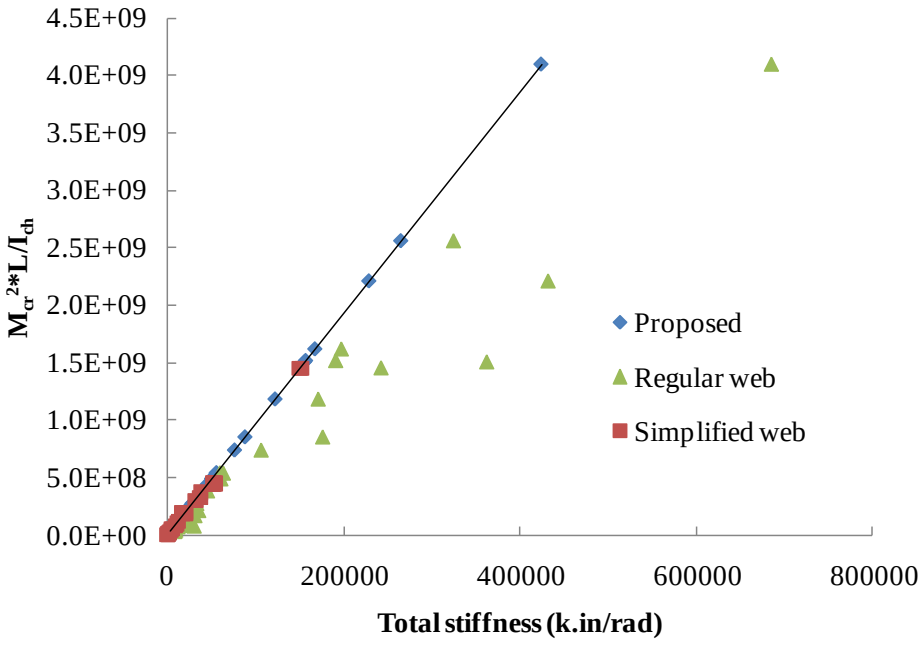

Figure 7.17 Stiffness requirement of proposed equation compared to the analysis – uniform moment

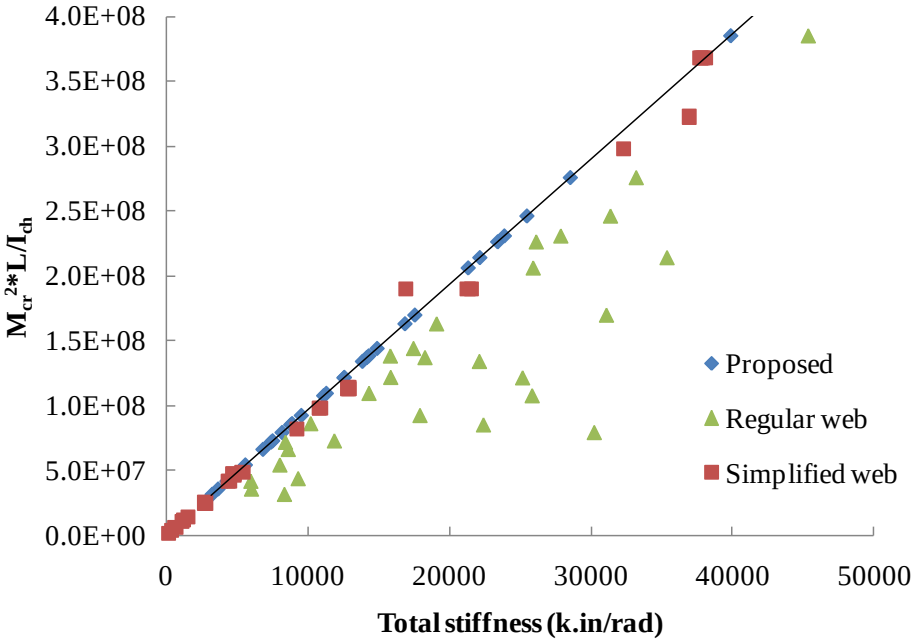

Figure 7.18 Stiffness requirement of proposed equation compared to the analysis at low stiffness values – uniform moment

For truss systems, the results presented so far indicate that the truss configuration has an effect on the buckling capacity and buckling behavior. For the purposes of developing a buckling solution for torsional braced trusses, systems with the simplified web connections were used (pin ended members). Using Eq. (7.13) as a starting point, the studies on the bracing behavior demonstrated that value of the unbraced buckling capacity (M_o) can be replaced by the product of the axial force in the chord and the depth of the truss ($f_o h$). For the latter term, it was found that the total stiffness of the truss bracing was too high with the square term, so the square was eliminated. Based upon comparisons with FEA solutions, it was found that the following expression provided reasonable estimates of the capacity for trusses with bottom chord loading:

$$\Delta P_{cr} \;=\; \Delta W_{cr} S_p \;=\; \sqrt{(f_o h)^2 + \;(1000)\beta_T} - \; f_o h \tag{7.13}$$

Where ΔP_{cr} is the increment in the load carrying capacity at each joint of the truss along the length with a uniform distributed load, ΔW_{cr} is increment in buckling capacity of braced truss per unit length and S_p is panel length. The relationship of Equation (7.13) is graphed in Figure 7.19 for the case of the 96-ft span truss with 6-ft depth from zero to ideal stiffness range. Assuming the linear relationship from of the increment of the load carrying capacity at the zero brace stiffness to the load carrying capacity at the ideal brace stiffness is slightly under estimate but conservative. The slope of the linear line was obtained. This slope together with the slope from the different span lengths and the chord out-of-plane moment of inertia that were considered are graphed in Figure 7.20.

The slopes of Figure 7.20 were linear; however, the Y-intercepts were slightly greater than zero. Assuming zero origin, the slopes of the linear relationships were obtained. With this linear relationship, it was found that the relationship could be approximated with the following expression:

$$\Delta P_{cr} \;=\; \Delta W_{cr} S_p \;=\; \left[\frac{E I_{chord}}{L^3}\right]\left(\sqrt{(f_o h)^2 + \;(1000)\beta_T} - \; f_o h\right) \tag{7.14}$$

Substituting the ΔP_{cr} into the relationship of

$$P_{cr} \;=\; P_o + \; \Delta P_{cr} = \;\; (W_0 + \Delta W_{cr}) S_p \tag{7.15}$$

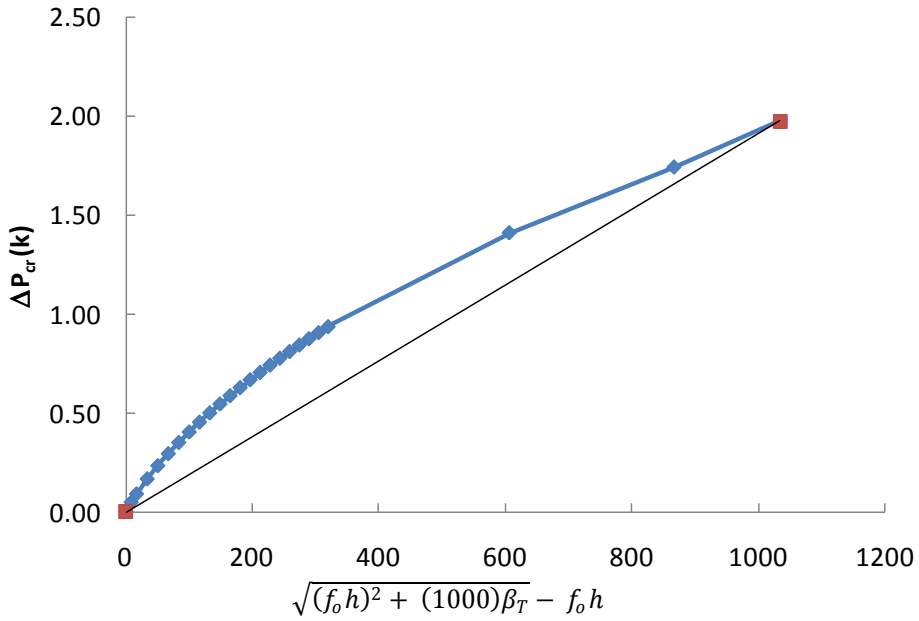

Figure 7.19 Additional buckling capacity of 96-ft span truss with 72-in depth

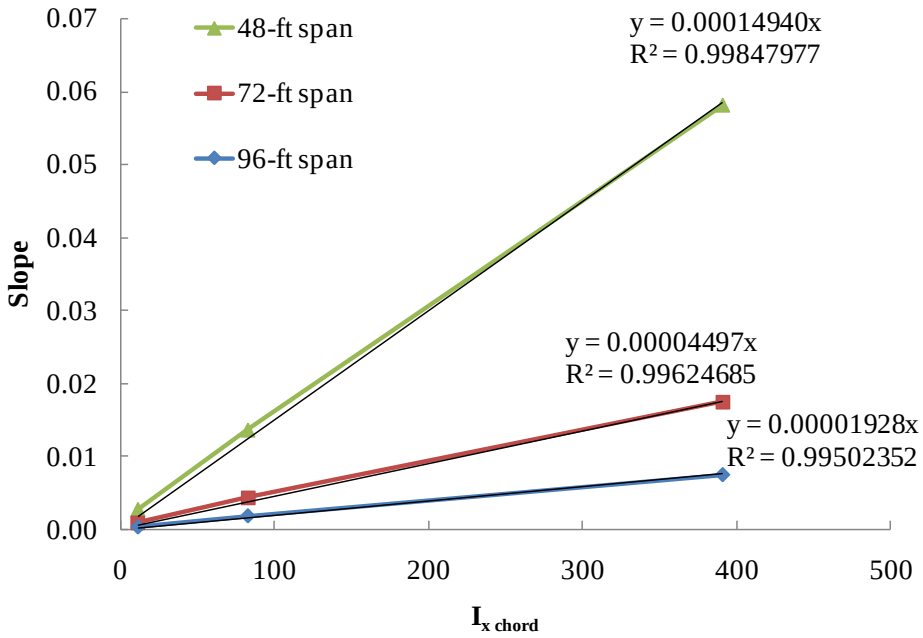

Figure 7.20 Span length adjustment

The equation has turned into

$$P_{cr} = P_o + \left[\frac{EI_{chord}}{L^3}\right]\left(\sqrt{(f_o h)^2 + (1000)\beta_T} - f_o h\right) \quad (7.16)$$

With the adjustment of the non-zero origin in Figure 7.20 and the load location, the final equation is

$$P_{cr} = P_o + \left[\frac{B^2 EI_{chord}}{2L^3}\right]\left(\sqrt{(F_o h)^2 + \left(\frac{2E}{B^4 I_{chord}} + 1000\right)\beta_T} - f_o h\right) \quad (7.17)$$

Where P_{cr} = Buckling capacity of braced truss per joint (kips/joint)

= $W_{cr}S_p$

P_o = Buckling capacity of unbraced truss (kips)

= W_oS_p

β_T = Total brace stiffness (k.in/rad)

W_{cr} = Buckling capacity of braced truss per unit length (kips/ft)

W_o = Buckling capacity of unbraced truss per unit length (kips/ft)

S_p = Panel spacing (ft)

F_o = Maximum unbraced chord axial force (kips)

h = Truss depth (in)

L = Span length (in)

I_{chord} = Out-of-plane moment of inertia of compression chord (in^4)

B = Load height factor

= 1.0 for top chord loading

= 1.4 for bottom chord loading

Comparison of the proposed equation to the analysis results for the cases of 72-ft span with 6-ft depth with W4x13 chord, W 8x24 chord and W12x50 chord are shown in Figure 7.21, Figure 7.22 and Figure 7.23. The graphs were plot between the total stiffness on the X-axis and the critical load at each joint on the Y-axis. The comparisons of the other cases are provided in Appendix C.

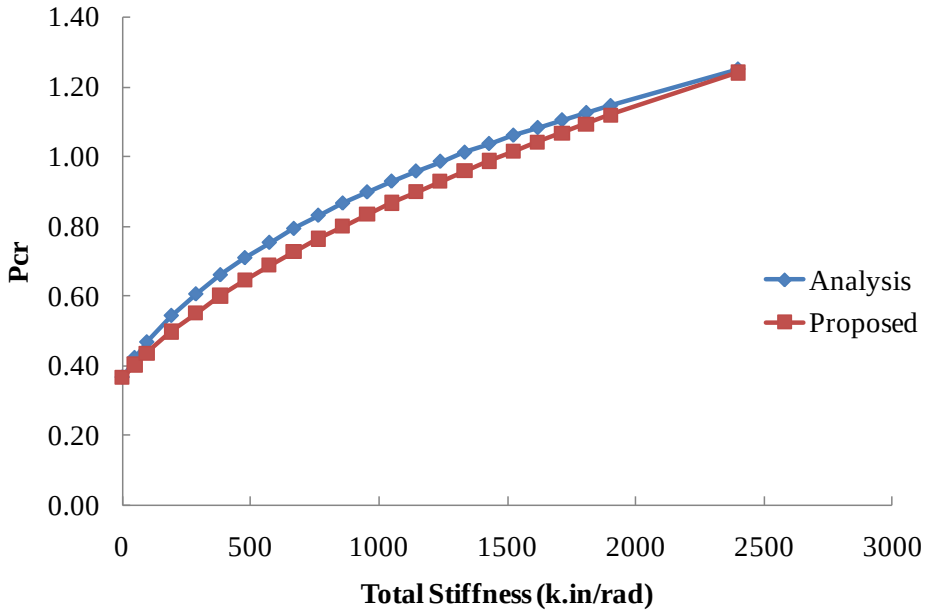

Figure 7.21 Comparison of 72-ft span truss with 6-ft depth – W4x13 chord with bottom chord loading

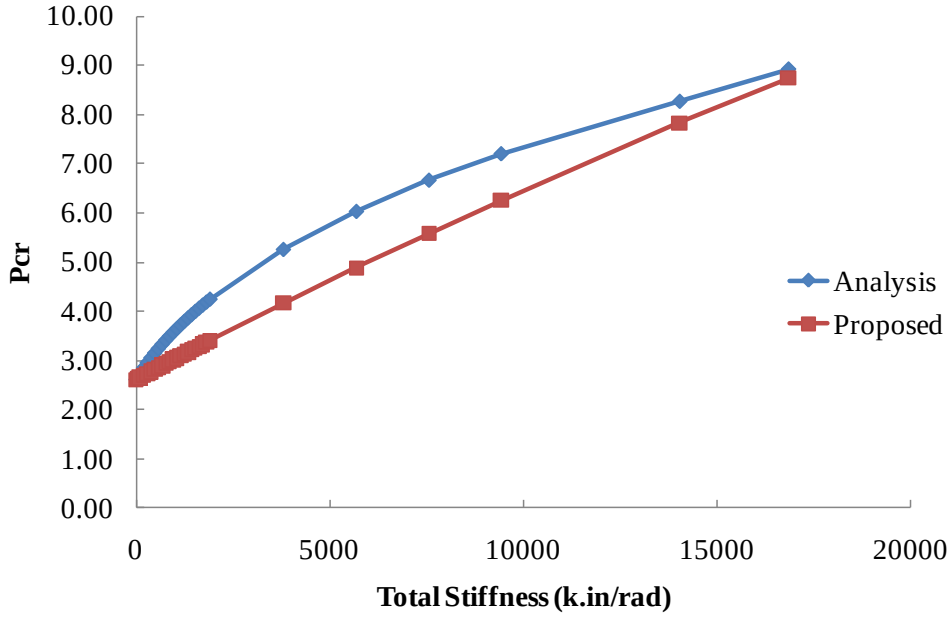

Figure 7.22 Comparison of 72-ft span truss with 6-ft depth – W8x24 chord with bottom chord loading

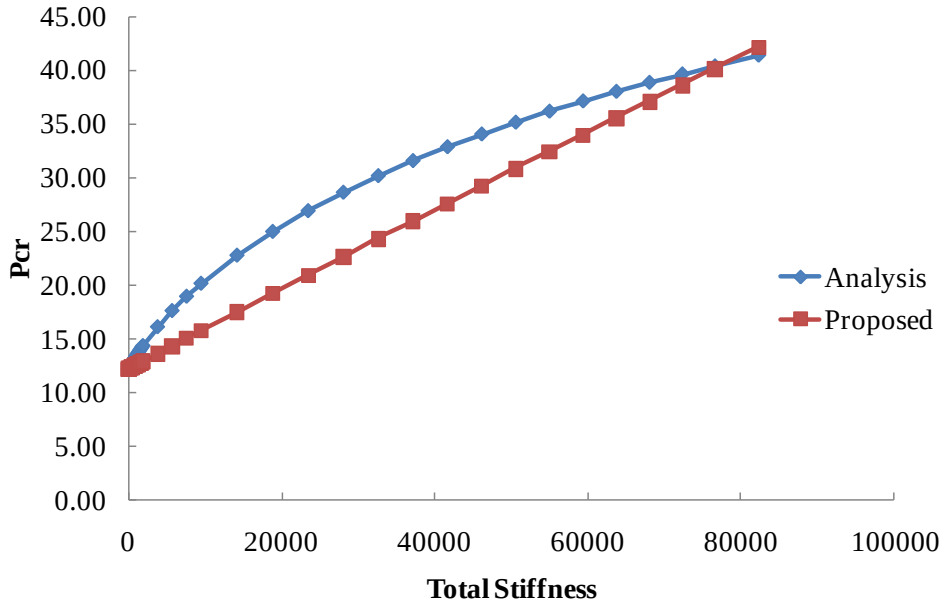

Figure 7.23 Comparison of 72-ft span truss with 6-ft depth – W12x50 chord with bottom chord loading

7.4.2 Truss Subjected to Uniform Bending Moment

Based on the graph of the uniform moment cases, a linear relationship of the buckling capacity and the total stiffness between truss without intermediate bracing and at the ideal stiffness value was established, for example of the case with 48-ft span and 6-ft depth in Figure 7.24. The slope of the straight line for any chord size for the truss with the same span length and depth were approximately the same as indicated in Table 7.4.

The slope seemed to be approximately constant with both the 3 and 6-ft depth trusses. When plotting the average slope against the span length, shown in Figure 7.25, it can be assumed that the relationship of the slope plots were straight line with zero origin. By implementing this relationship with the truss depth, the relationship of the buckling capacity of truss under uniform moment can be defined as:

$$M_{cr} = M_o + \frac{0.6L\beta_T}{h} \tag{7.18}$$

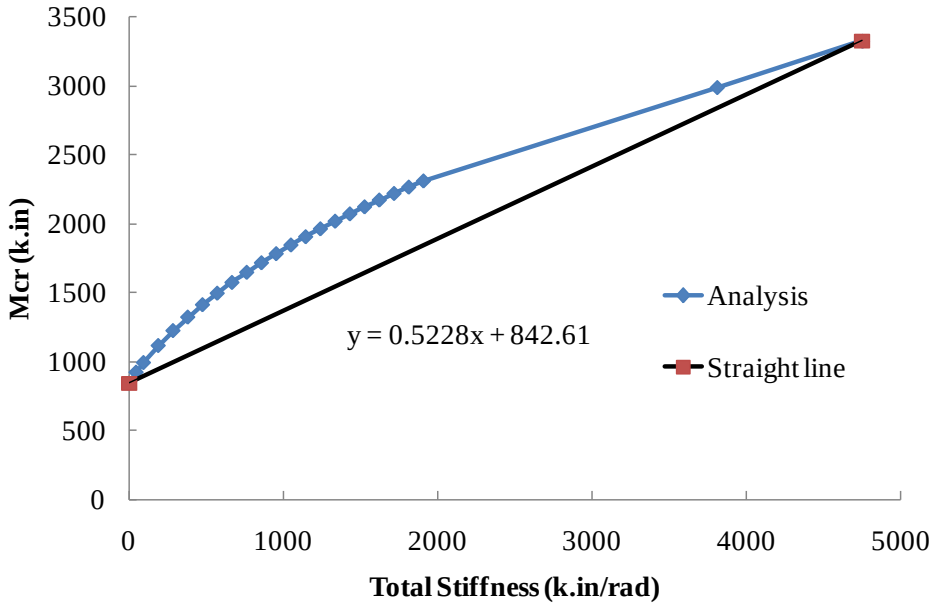

Figure 7.24 Buckling capacity of 48-ft span truss with 6-ft depth with uniform moment.

Table 7.4 Slope of the straight line between unbraced and fully braced buckling capacity

Chord I_x (in^4)	Truss span length (in)		
	576	864	1152
11.3	0.523	0.713	0.966
82.7	0.516	0.731	1.015
391.0	0.539	0.667	0.978
Average	0.526	0.704	0.986

The comparison of the buckling capacity for the analysis to the proposed equation (7.18) of truss under the uniform bending moment of the 72-ft span truss with 6-ft depth with W4x13 chord, W8x24 chord and W12x50 chord are shown in Figure 7.26, Figure 7.27 and Figure 7.28 respectively. The comparisons for the other cases are provided in Appendix C. This indicated that the simplify proposed equation (7.18) might be on conservative side in estimating the buckling capacity of the truss with single cross frame

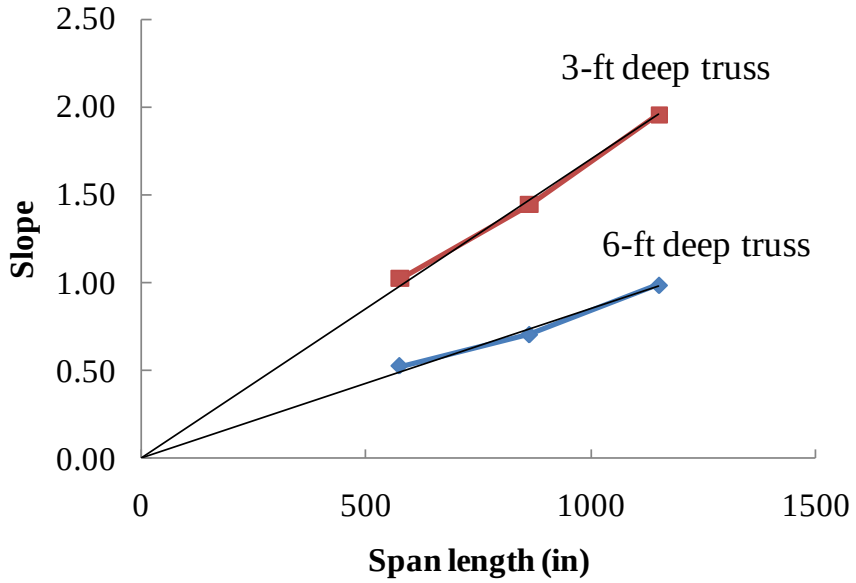

Figure 7.25 Slope plot of truss with uniform moment

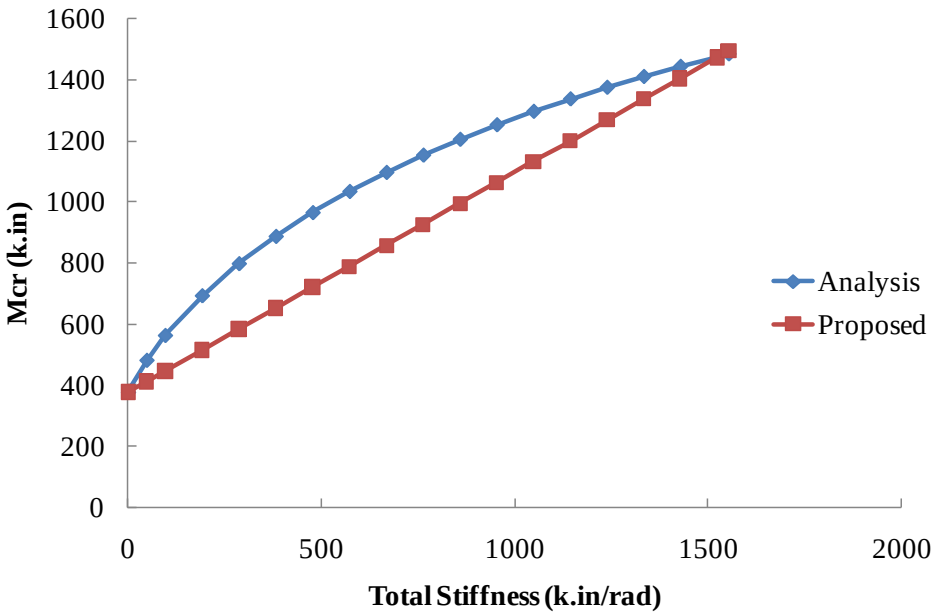

Figure 7.26 Comparison of buckling capacity of 72-ft span truss with 72-in depth – W4x13 chord

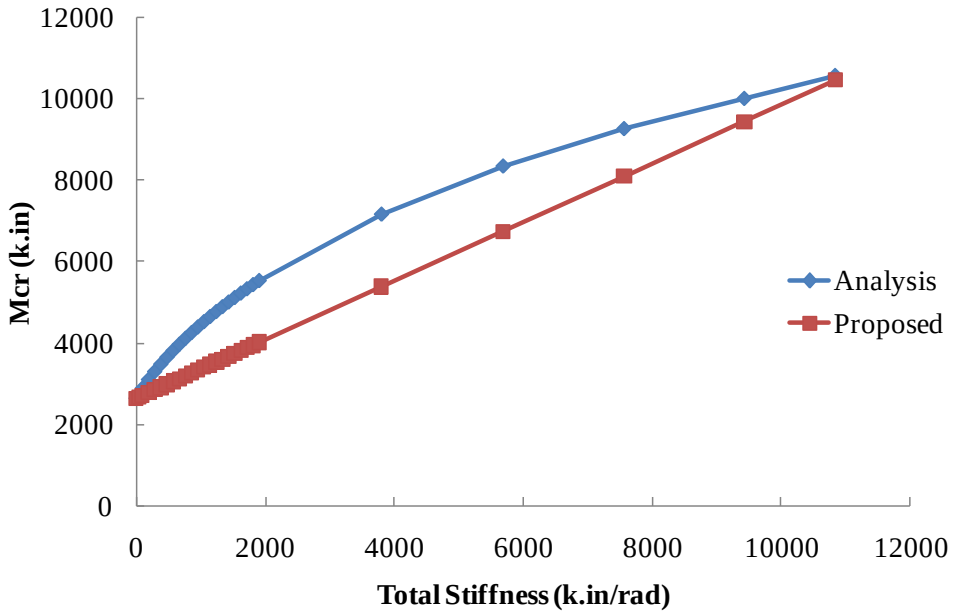

Figure 7.27 Comparison of buckling capacity of 72-ft span truss with 72-in depth – W8x24 chord

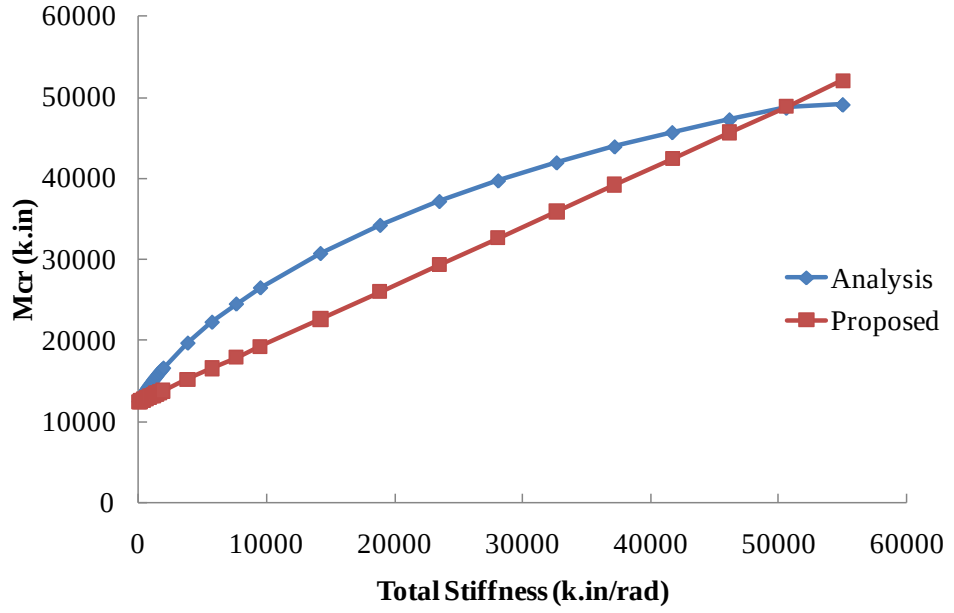

Figure 7.28 Comparison of buckling capacity of 72-ft span truss with 72-in depth – W12x50 chord

at midspan with total stiffness between zero and the ideal brace stiffness. However, this can be used to simply estimate the buckling capacity of the truss.

7.5 SUMMARY

Buckling capacity and ideal brace stiffness of regular truss with regular and simplified webs were determined by using the ANSYS model. It was found that the truss with larger chord near supports had slightly higher buckling capacity than the truss with the same web size throughout the span length; however, the difference was insignificant. The truss with simplified web yielded lower buckling capacity and required lower ideal brace stiffness than the truss with regular web. After eliminating the outlier, the buckling capacity of the regular and simplified web truss subjected to uniform load have the same relationship, while there was 20% different in the truss subjected to the uniform moment cases by using the beam bracing requirement relationship. The stiffness requirement of the truss was then developed. The estimation of the buckling capacity of the truss with cross frame was developed based on the truss with simplified web due to the fact that this is the most conservative case. This was to cover various types of truss connection in the regular truss. It was found that the truss subjected to uniform load and uniform moment behaved differently in terms of increasing in buckling capacity. Therefore, the equation was developed separately.

CHAPTER 8
Conclusion and Recommendation

8.1 OVERVIEW

The stability bracing behavior of trusses were investigated using experimental testing and computational modeling. The laboratory experiments were conducted on the twin trusses with W4x13 sections for the chord and web members. The trusses had a 4-ft depth and total length of 72 feet. Spans of 48 and 72 feet were used in the tests that included both lateral load tests and buckling tests. The trusses were tested without intermediate braces as well as cases with either lateral or torsional braces along the length. Most of the tests were done on the regular (Howe) truss, except the lateral stiffness tests which were also done on the inverted truss.

The computational model was developed using the three-dimensional finite element program, ANSYS. A variety of models were used to simulate both as-built and idealized truss models. The model was verified by the laboratory test results.

The parametric investigations focused on twin truss systems constructed from wide flange sections; however a wide variety of sections were used to vary the relative stiffness between the chords and the web members. In addition, the web connections included both restrained and pin-ended connections. Based upon results from the parametric investigations, expressions were developed for determining the stiffness requirements for trusses with a torsional brace at midspan as well predicting the buckling capacity of a truss with bracing at midspan. The expressions provide reasonable estimates of the buckling capacity and bracing requirements. The remaining subsections summarize the findings and recommendations from the research study.

8.1.1 Truss Buckling Behavior

The experiments demonstrated that the buckling capacity of the truss with torsional bracing largely depended on the brace stiffness and the number of intermediate braces. The effectiveness of the brace generally decreased with the increase in the number of the braces. This was due to reduction in effectiveness of the brace when it was further away from mid span. Similar behavior was observed in the truss with lateral bracing.

Additionally, the laboratory test results revealed that the truss was susceptible to distortion of the chord at the torsional brace. The addition of web stiffeners on the braced chord at the brace location greatly reduced the impact of the distortions. Flexibility in the gusset plate at the brace location also affected the bracing behavior. Tests on the trusses with supports similar to pony truss applications showed that the buckling capacity of the pony truss was not much less than that of the regular truss with the same configuration. In the pony truss configurations, the top chord at the support displace significantly different than was observed in the regular truss configuration.

The lateral stiffness tests on the trusses demonstrated that the orientation of the diagonals impacted the lateral stiffness of the trusses. The Howe Truss that had the diagonals pointing towards the support (from the midspan location) had a lower stiffness than the inverted (Pratt) truss where the diagonals pointed towards midspan.

Differences in the imperfections between the two trusses caused some measurable axial forces in the torsional braces indicating lean-on behavior. Tests were also done by offsetting the load to artificially increase the effective imperfection. As expected, offsetting the load point laterally from the axis of the chord tended to uniformly reduce the buckling capacity of the truss with torsional bracing. The effect was similar to the impact changing the magnitude of the imperfection observed in previous studies. Since the actual imperfections often differ from the critical imperfections found in practice, offsetting the load is sometimes desirable to create a scenario to match a critical condition that might be found in practice.

Although the cross frames effectively controlled the twist of the truss in the lateral-torsional mode, cases requiring very high values of the torsional brace stiffness are generally inefficient in long span trusses. The buckling modes often may be dominated by significant lateral deformation.

Parametric studies were conducted with torsional bracing provided by flexural members that connected to one of the chords with rigid web verticals at the brace point to prevent cross sectional distortions. The solutions were compared with analyses with full depth cross frames for which cross sectional distortion was also not a problem. The analysis results showed that the braces with the rigid webs provided an upper bound of the buckling capacity of the truss. The results demonstrated trusses with torsional braces that framed into one of the chords with flexible web members had significant cross sectional distortion in the truss web. The cross sectional distortion significantly reduced the effectiveness of the bracing.

8.1.2 Recommendation of Stiffness Requirement for Trusses with Midspan Torsional Brace

The stiffness requirements for torsional braces in trusses with a brace at midspan were developed. The recommendations were compared with trusses with both restrained and pin-ended web members. In developing the recommendations, the stiffness formulations for both column and beam systems were considered. The bracing systems tended have much better agreement with formulations similar to beam bracing instead of column bracing systems. The empirical expression was therefore developed based on the stiffness requirements for beams. The proposed stiffness requirement is:

$$\beta_{tot} = \frac{M_{cr}^2 L}{2EI_{chord}C_b B}$$

This equation is valid for the trusses subjected to both uniform bending moment and uniform distributed load. M_{cr} represents the maximum applied moment. For the truss, M_{cr} can be replaced with F_{cr}.h, where F_{cr} is the maximum force in the compression chord and h is the depth of the truss. The equation had reasonable agreement with both

load types, but had better accuracy with the uniformly distributed load cases, which is the case most commonly found in practice. Since this equation was developed based on the elastic eigenvalue solution, it is not valid when the trusses enter into the inelastic range.

8.1.3 Recommendation for Estimating the Buckling Capacity of Truss with Torsional Brace at Midspan

The development of an empirical equation to estimate buckling capacity of the truss with cross frame at midspan was based on a truss with pin-ended web members. The estimation of the buckling capacity of the truss was divided into two separate cases which were the uniform load and uniform moments cases. The solutions are similar to the form of the expression used to develop the buckling capacity of torsionally restrained beams. The proposed equation is:

$$P_{cr} = P_o + \left[\frac{B^2 E I_{chord}}{2L^3}\right]\left(\sqrt{(F_o h)^2 + \left(\frac{2E}{B^4 I_{chord}} + 1000\right)\beta_T} - f_o h\right)$$

This proposed equation has good agreement with the analytical results.

The above expression for the uniform distributed load did not work for the truss with uniform moment loading. Therefore, an alternate expression was developed for that load case. The proposed equation is:

$$M_{cr} = M_o + \frac{0.6 L \beta_T}{h}$$

The above equation is a linear expression and works well for low values of the brace stiffness and at the stiffness values near the ideal brace stiffness; however, the expression is conservative between these values.

8.2 RECOMMENDATION FOR FUTURE WORK

The tests and parametric studies reported in this dissertation have included a wide variety of bracing systems and truss configurations. The extensive testing provides valuable data for the stiffness and strength requirements for both torsional and lateral bracing of truss systems. Due to practical limitations, a comprehensive solution for all

bracing systems was not possible in this study. The data from the tests can therefore provide valuable data to continue the investigations of both torsional and lateral bracing systems for truss bracing. The study resulted in stiffness requirements for the case of a single cross frame at midspan of the trusses; however there are several areas in practice that require additional guidance. The stiffness formulations of the torsional braces need to be developed for the more general system where several braces exist along the length. In addition, the design recommendations focused on full depth cross frames for which cross sectional distortion is not a concern. Most truss systems in building construction actually make use of cross frame type braces for the torsional restraints. The effects of cross sectional distortion also need to be further considered. The most common system for which cross sectional distortion is a major concern is in the case of pony trusses. In addition, although the design recommendations from this study focused on stiffness requirements, general strength requirements must also be developed for the bracing systems. Besides the torsional bracing, additional work is necessary for developing the stiffness and strength requirements for lateral bracing

The experiments that are documented in this dissertation focused on trusses composed of wide flange cross sections for both the chords and the webs. These trusses have relatively stiff cross sectional elements. To provide additional information on the behavior of other truss configurations, tests on trusses with elements composed of other cross sectional shapes will provide improved understanding of the general behavior. Short and medium span trusses are often configured with Tee sections for the chords and angles for the webs. Tests on these types of truss systems would therefore provide insight into the behavior of sections with greater flexibility between the web and chord element connections. The tests also focused on torsional and lateral bracing systems. In practice there are several other types of bracing systems that are used; however very little research has been conducted on the behavior. Two types of bracing systems that are frequently used that warrant additional behavior are lateral bracing in the form of relative braces that control the relative lateral movement of two points along the length of the truss such as the braces for the plan view of the twin truss system shown in Figure 8.1.

Many trusses also make use of metal sheeting that behaves as a shear diaphragm. Although significant studies have been carried out on beam and column systems, no investigation has been conducted on trusses.

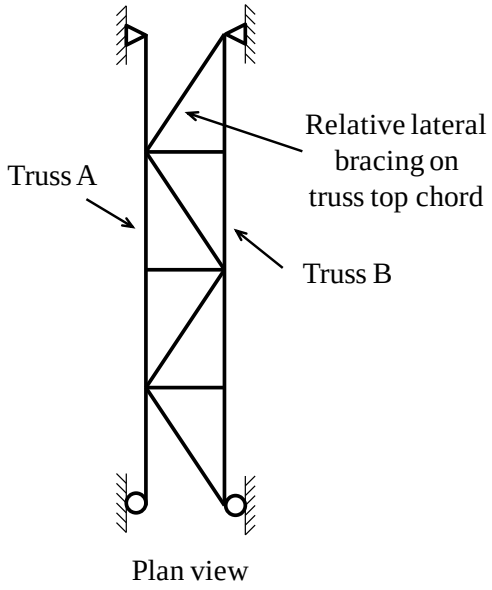

Figure 8.1 Relative lateral bracing in twin truss system

APPENDIX A

Test Results and Model Verification

The main chapters of this dissertation presented representative results from the laboratory tests and computational studies. This appendix contains supplementary results from the laboratory tests on the twin truss system as well as comparisons with the ANSYS finite element solutions.

A.1 LATERAL DEFLECTION OF LATERAL STIFFNESS TEST

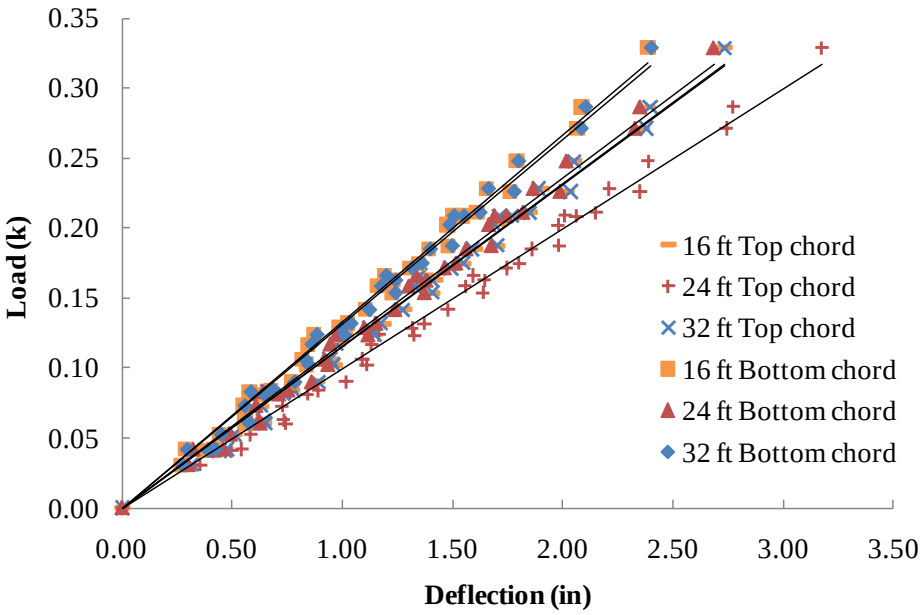

Figure A.1 48-ft regular truss - Top chord loading

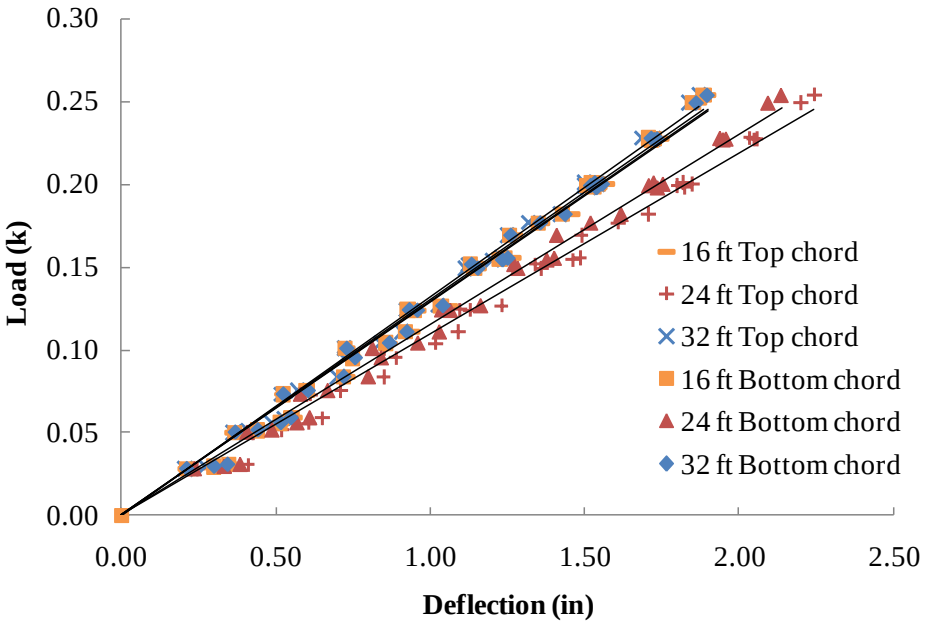

Figure A.2 48-ft regular truss - Bottom chord loading

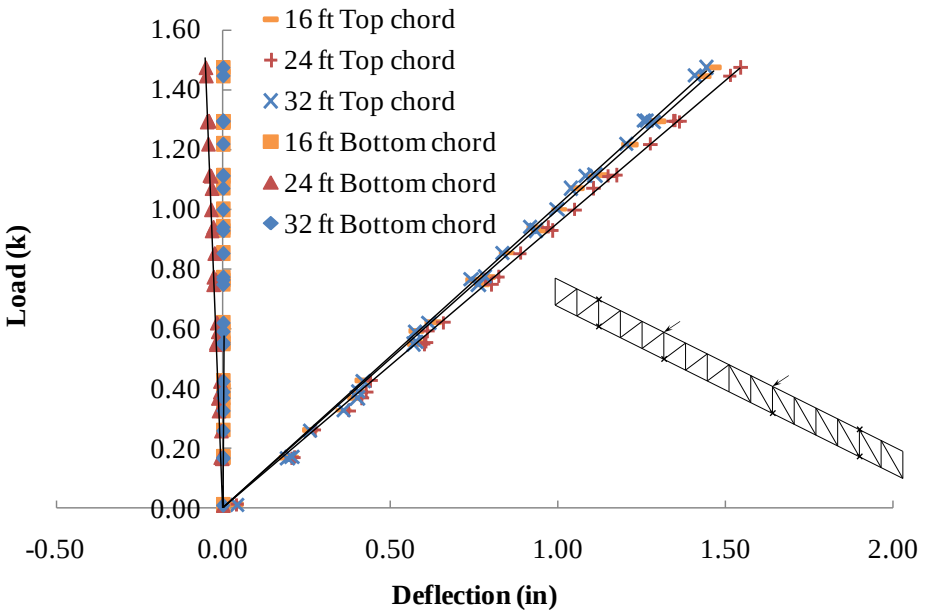

Figure A.3 48-ft regular truss - Top chord loading and bottom chord restrained

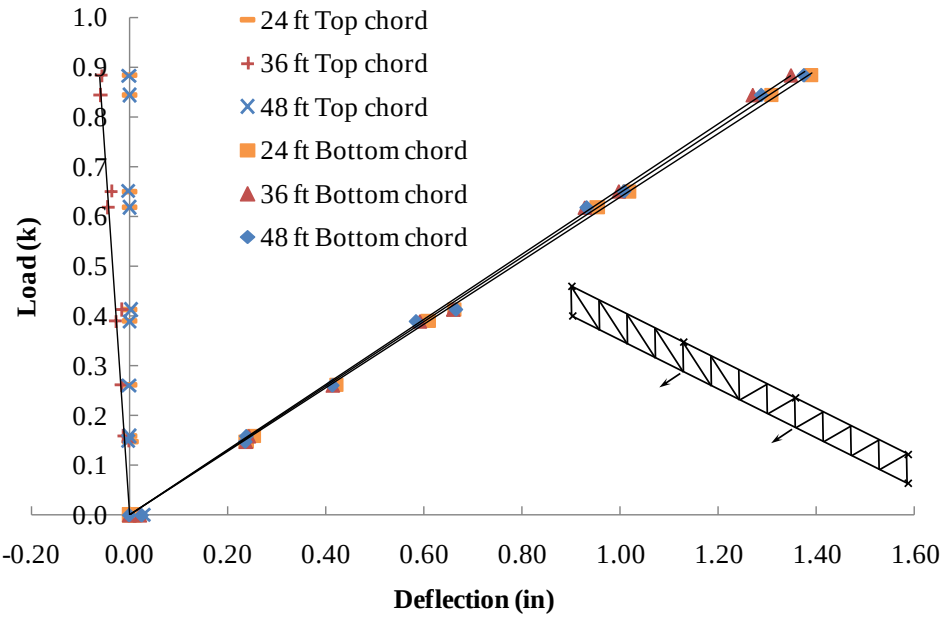

Figure A.4 72-ft inverted truss - Bottom chord loading and top chord restrained

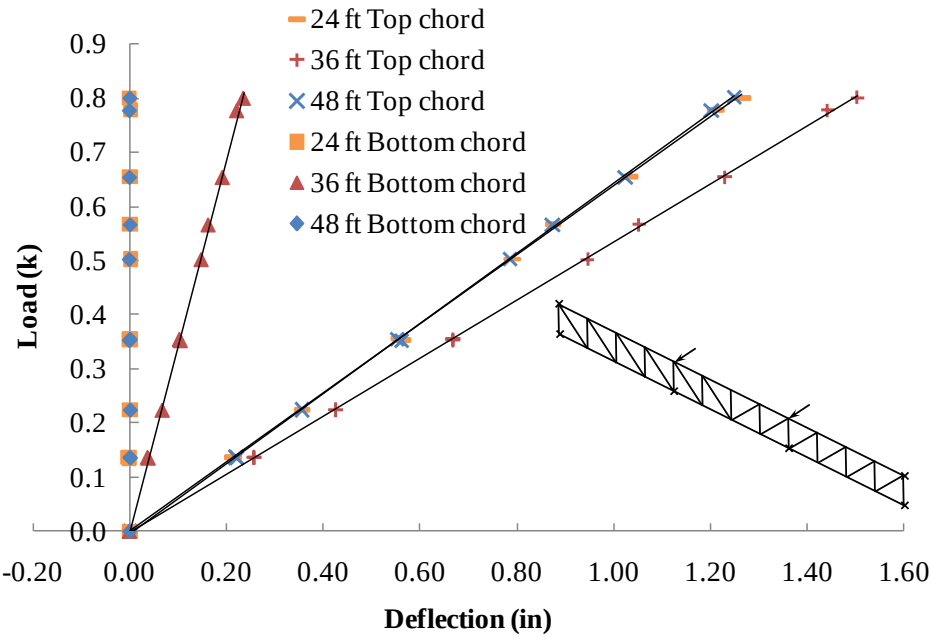

Figure A.5 72-ft inverted truss - Top chord loading and bottom chord restrained

A.2 LATERAL DEFLECTION OF BUCKLING TEST

A.2.1 Truss without Intermediate Bracing

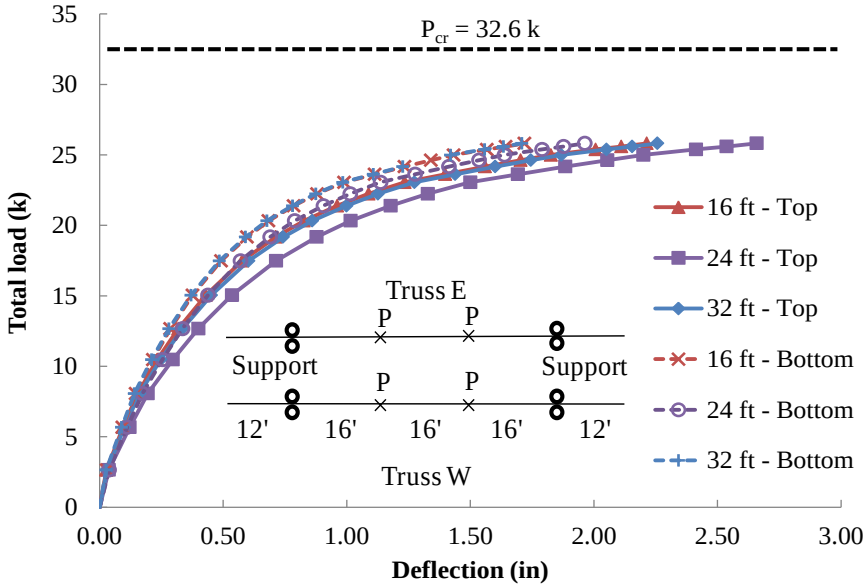

Figure A.6 48-ft span truss - Bottom chord loading

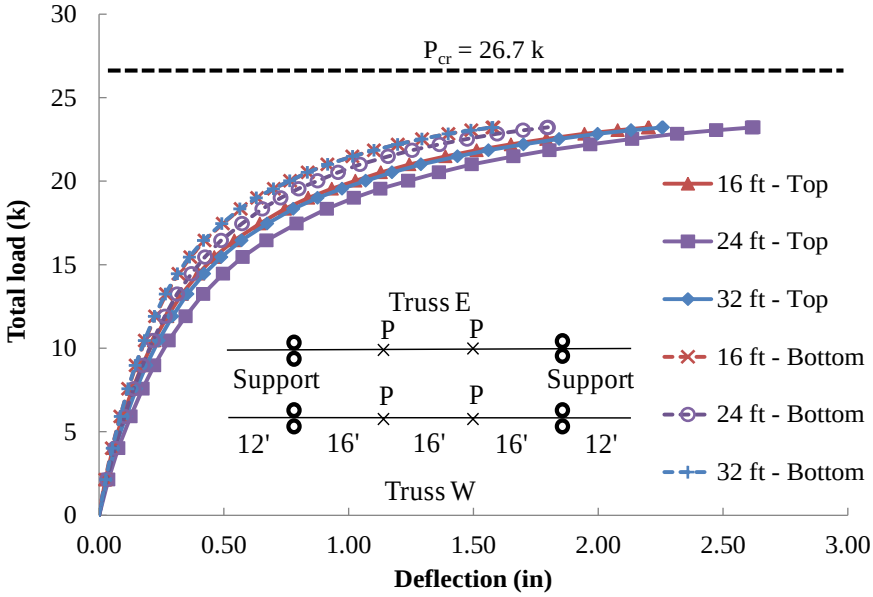

Figure A.7 48-ft span truss - Top chord loading

A.2.2 Truss with Top Chord Loading and Lateral Bracing

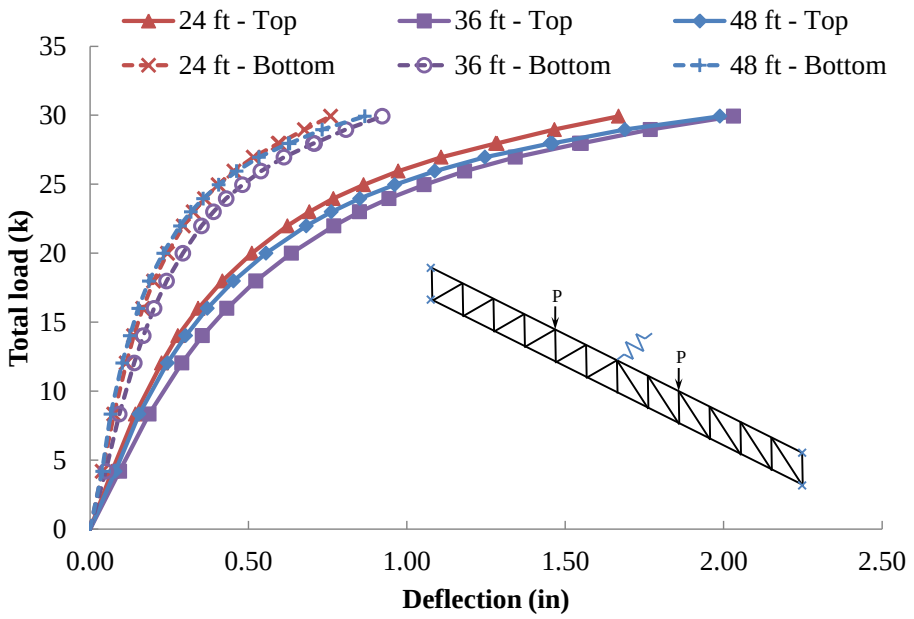

Figure A.8 Truss with single lateral brace - K = 0.50 k/in

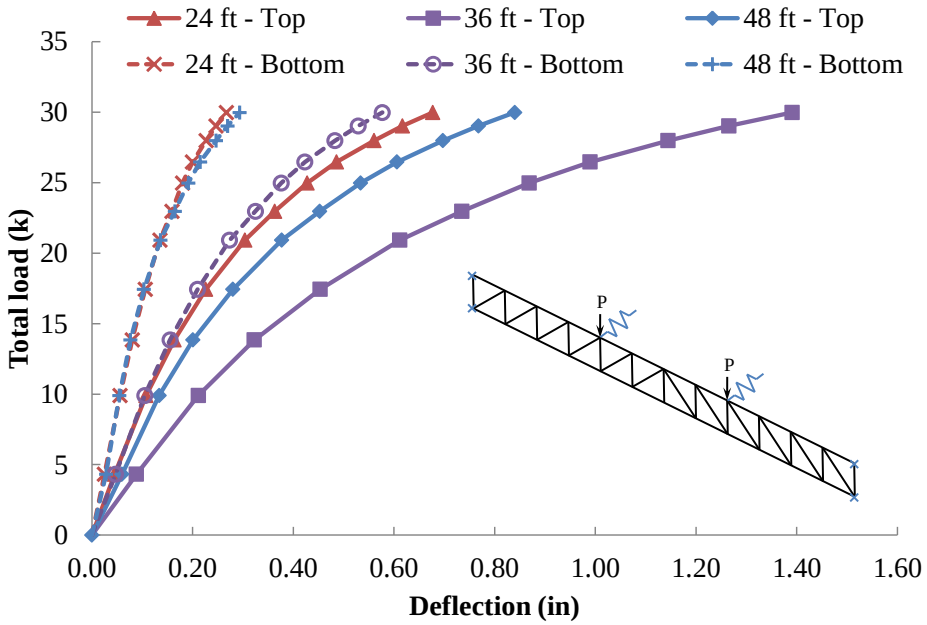

Figure A.9 Truss with 2 lateral braces - K = 0.50 k/in

A.2.3 Truss with Top Chord Loading and Torsional Bracing

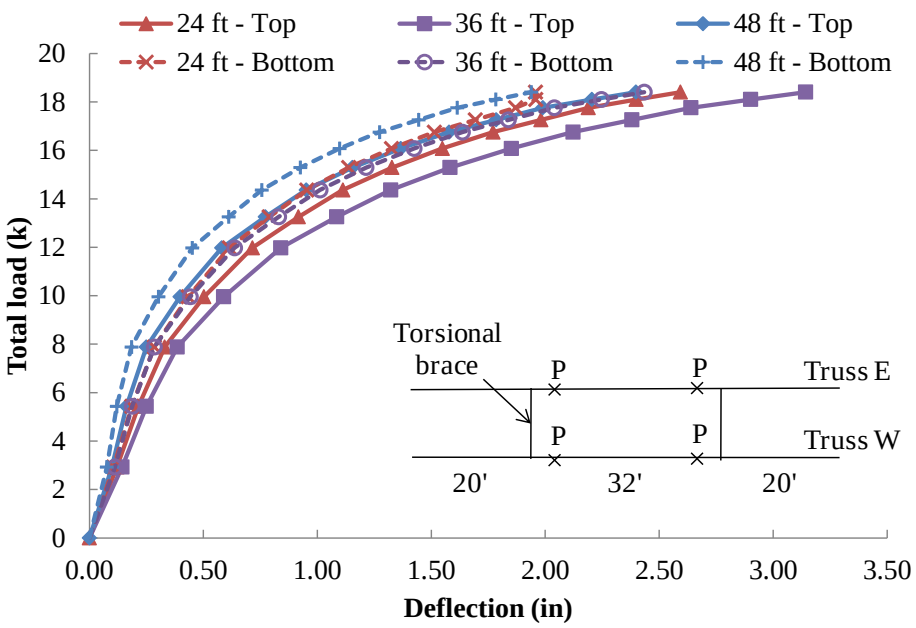

Figure A.10 Truss with 2 small torsional braces (with connection stiffener)

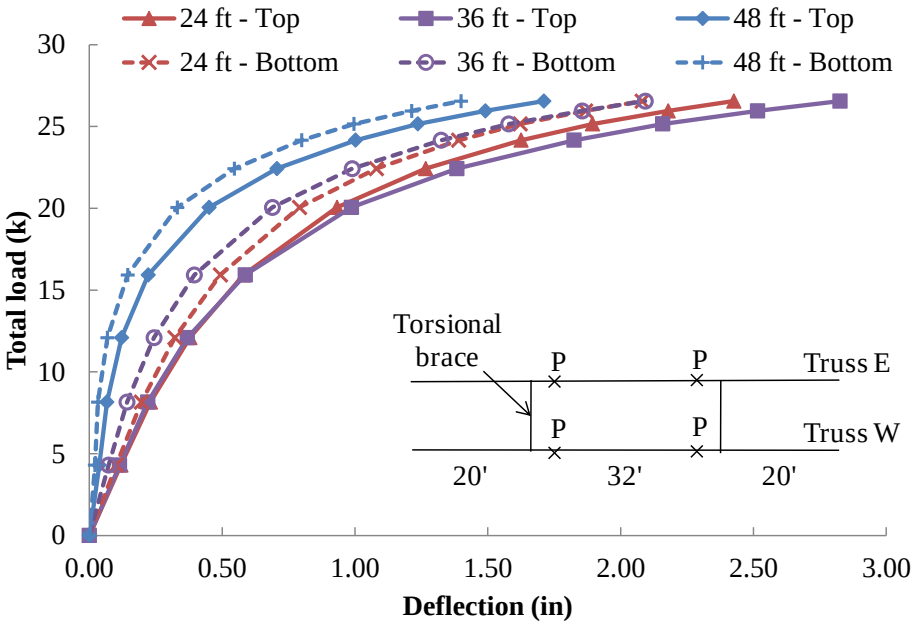

Figure A.11 Truss with 2 large torsional braces (with connection stiffener)

A.2.4 Truss with Bottom Chord Torsional Bracing and Loading

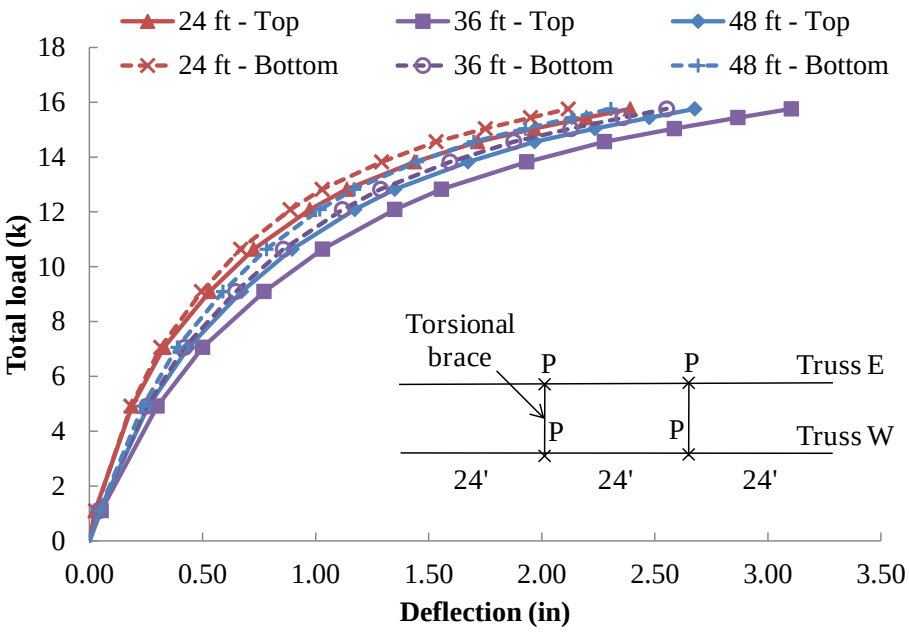

Figure A.12 Truss with 2 small torsional braces (without connection stiffener)

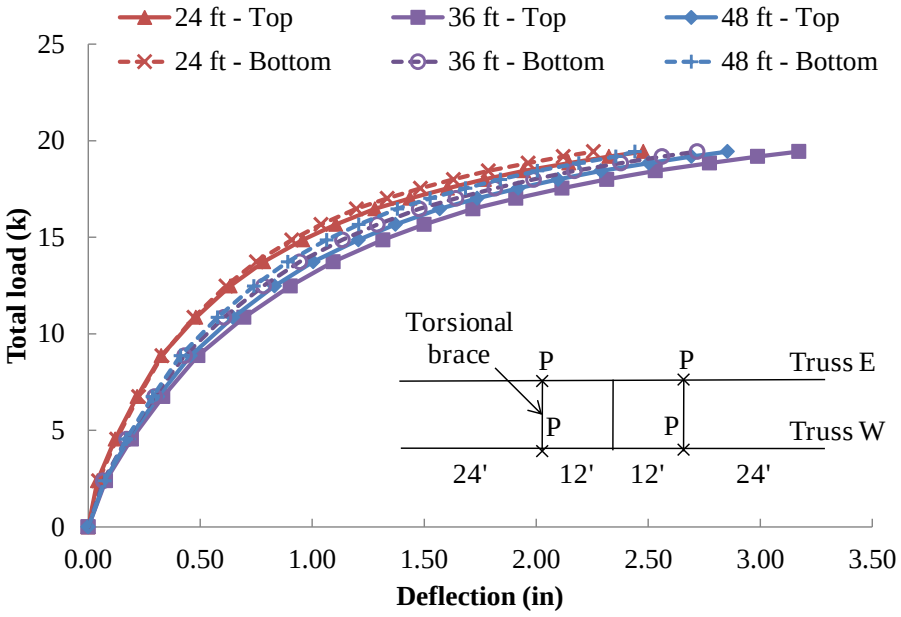

Figure A.13 Truss with 3 small torsional braces (without connection stiffener)

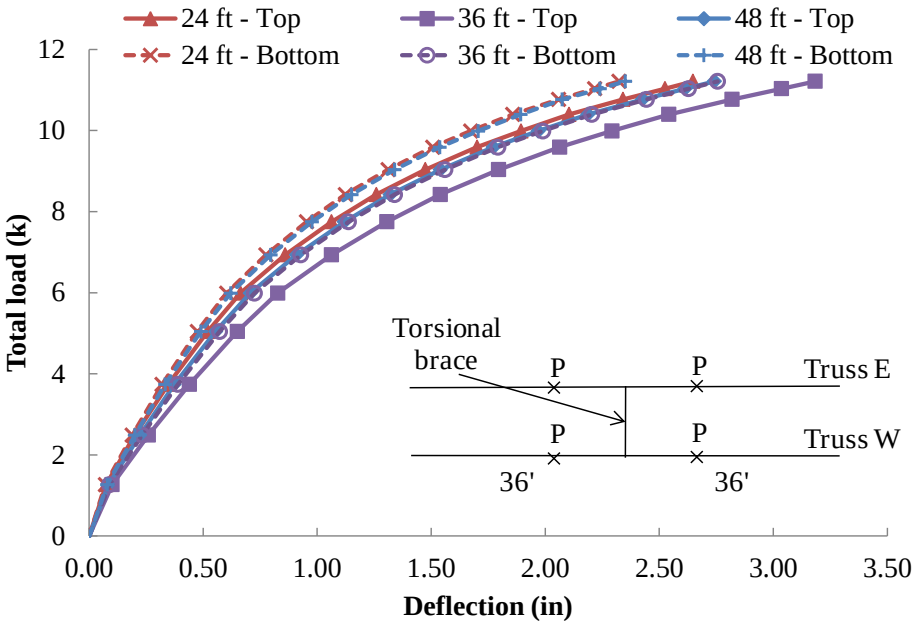

Figure A.14 Truss with single large torsional brace (without connection stiffener)

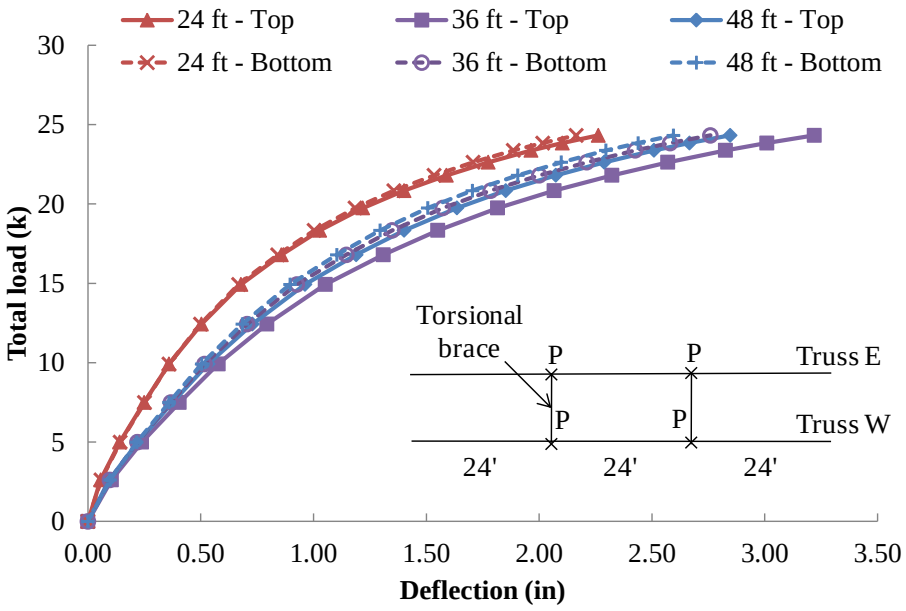

Figure A.15 Truss with 2 large torsional braces (with connection stiffener)

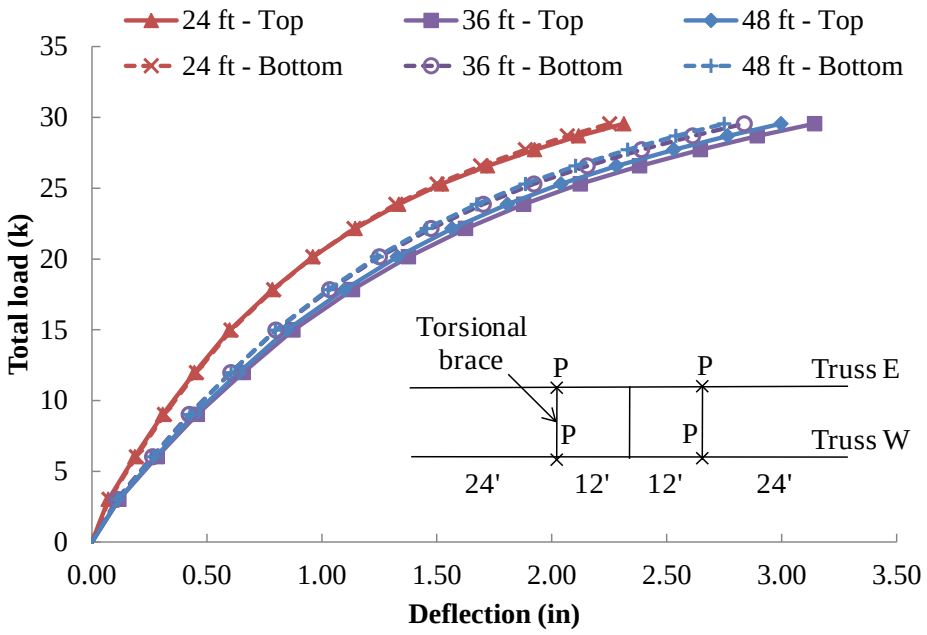

Figure A.16 Truss with 3 large torsional braces (with connection stiffener)

A.2.5 Pony Truss

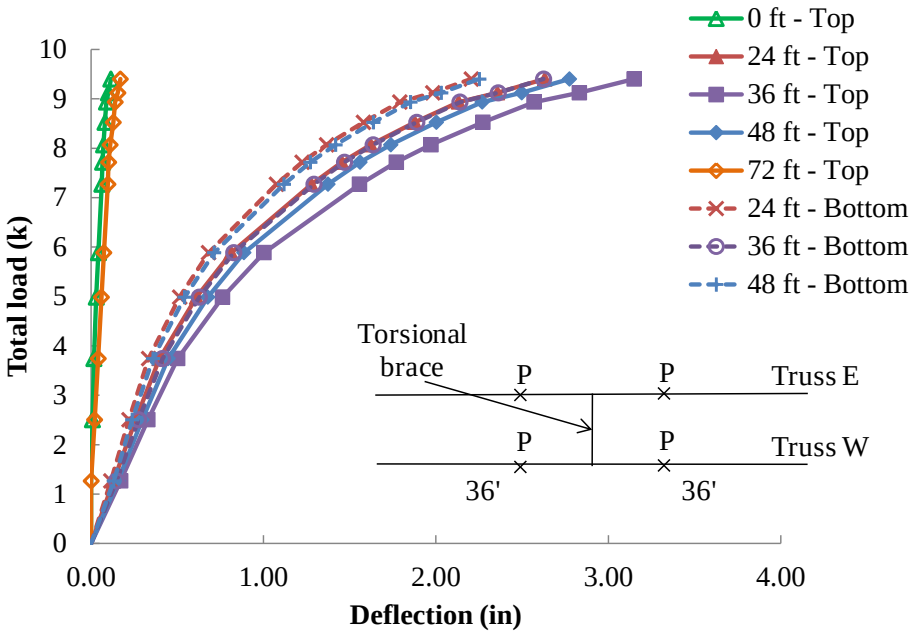

Figure A.17 Truss with single small torsional brace (without connection stiffener)

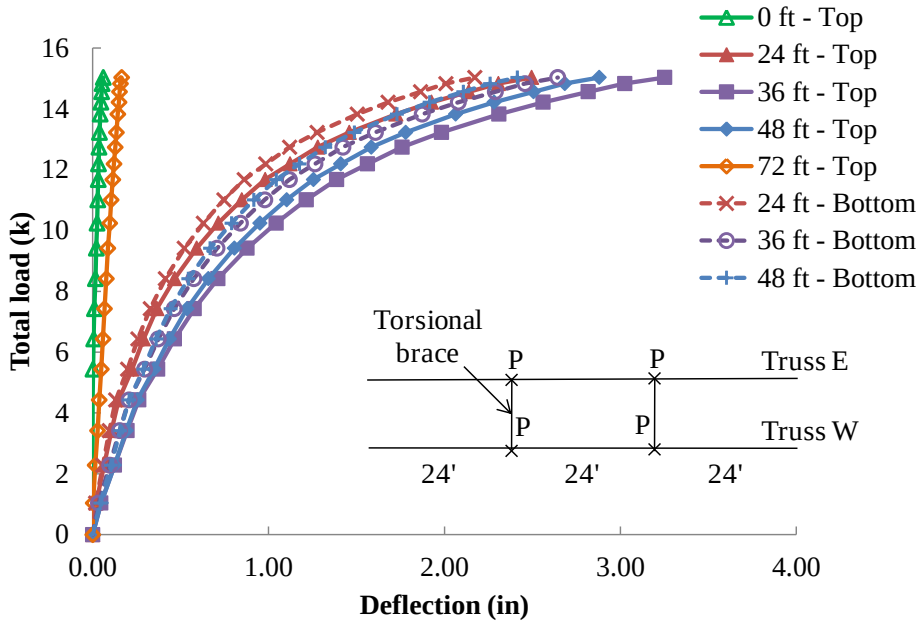

Figure A.18* Truss *with 2 small torsional braces (without connection stiffener)

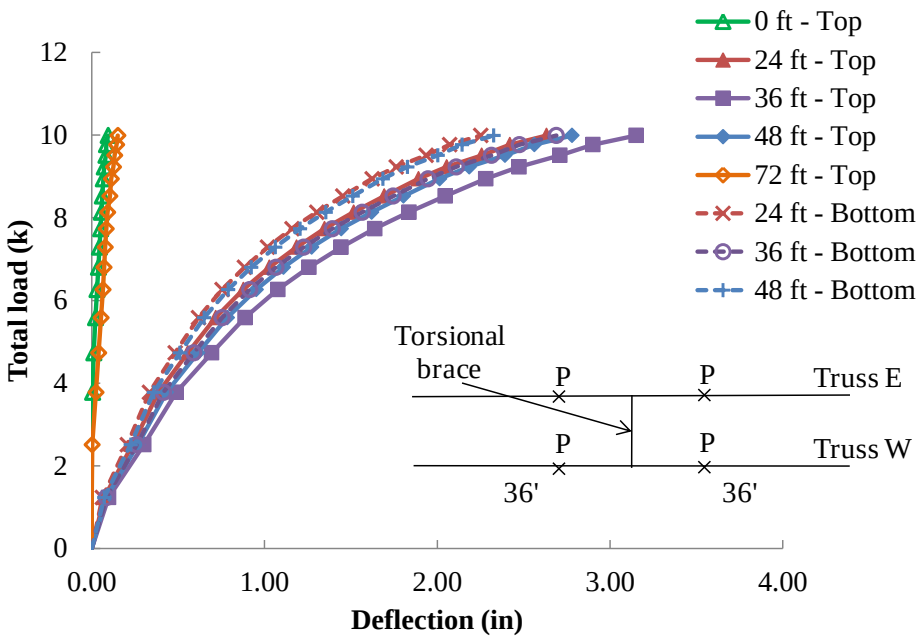

Figure A.19 Truss with single large torsional brace (without connection stiffener)

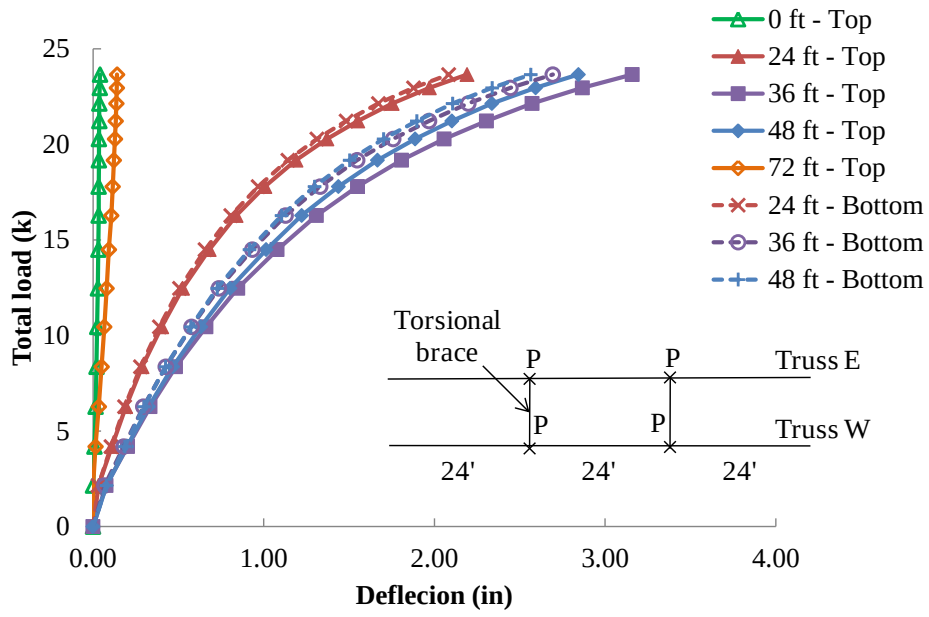

Figure A.20 Truss with 2 large torsional braces (with connection stiffener)

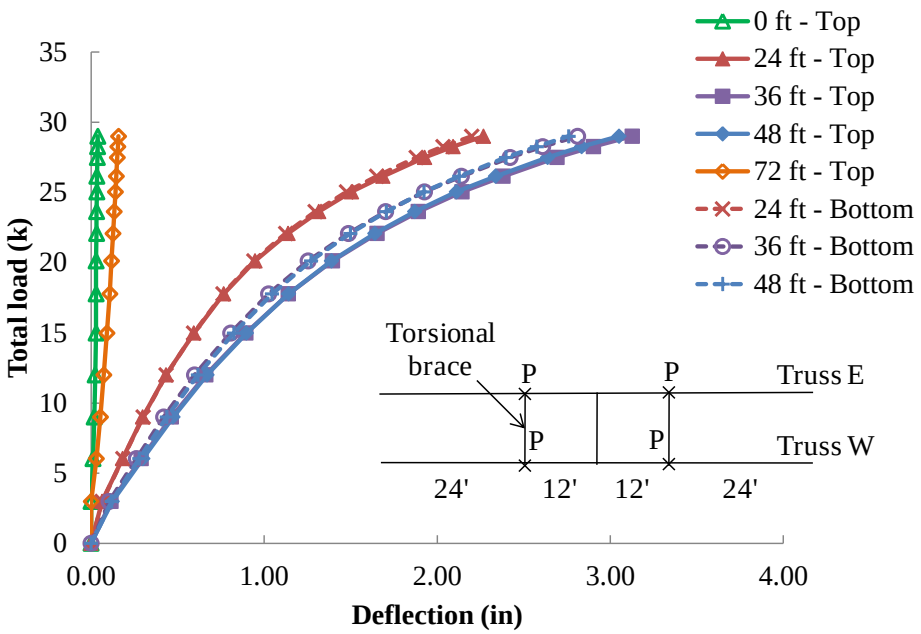

***Figure A.21* Truss with 3 large torsional braces (with connection stiffener)**

A.2.6 Comparison of Regular and Pony Truss

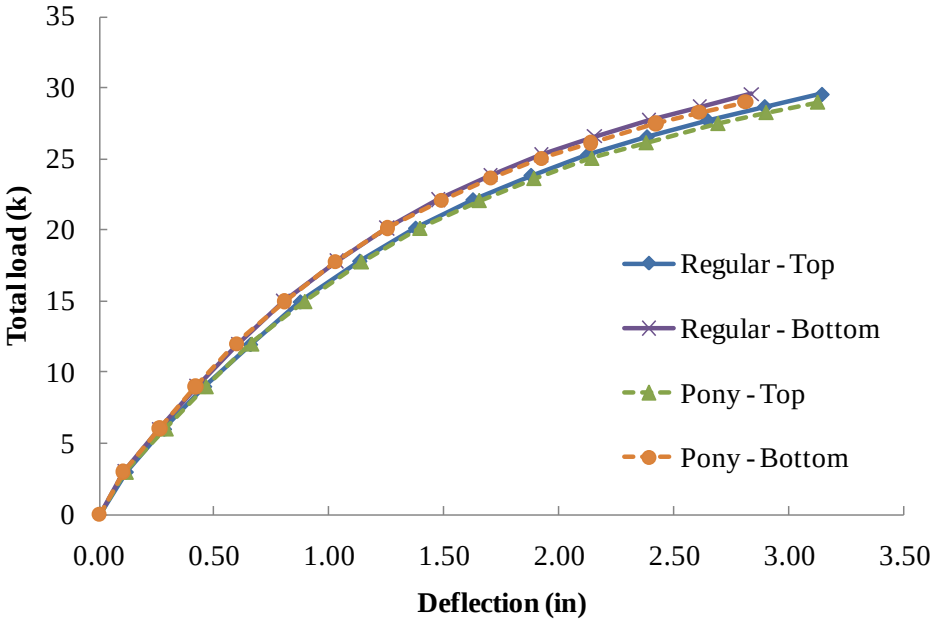

Figure A.22 Midspan lateral deflection of regular and pony truss with 3 large torsional braces at bottom chord (with connection stiffener)

A.2.7 Truss with Top Chord Torsional Bracing and Loading with Load Offset

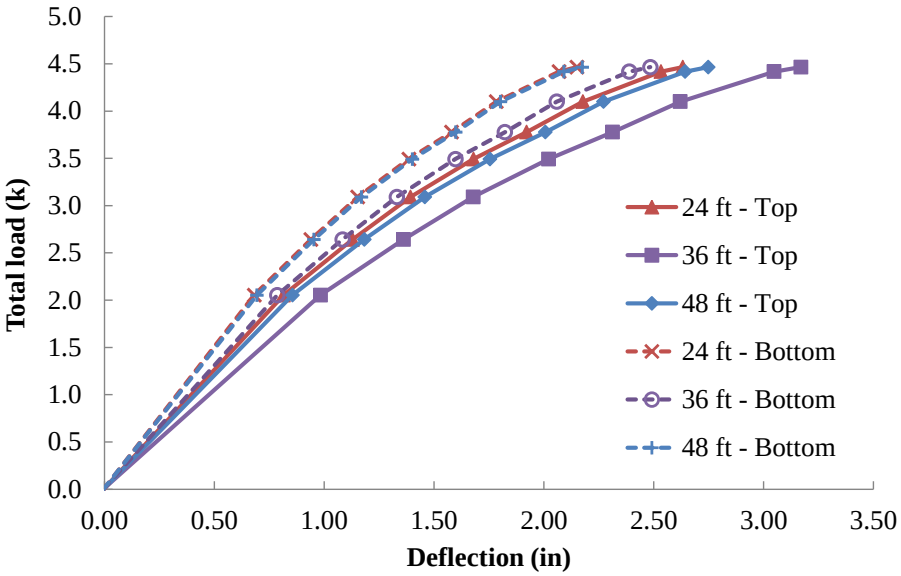

Figure A.23 Truss without intermediate bracing with 0.5" load offset (with connection stiffener)

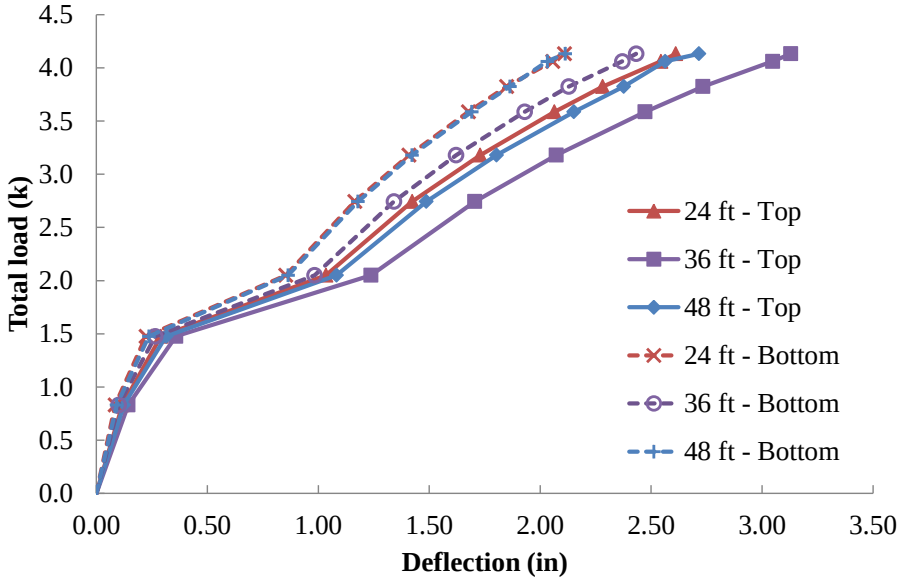

Figure A.24 Truss without intermediate bracing with 1.0" load offset (with connection stiffener)

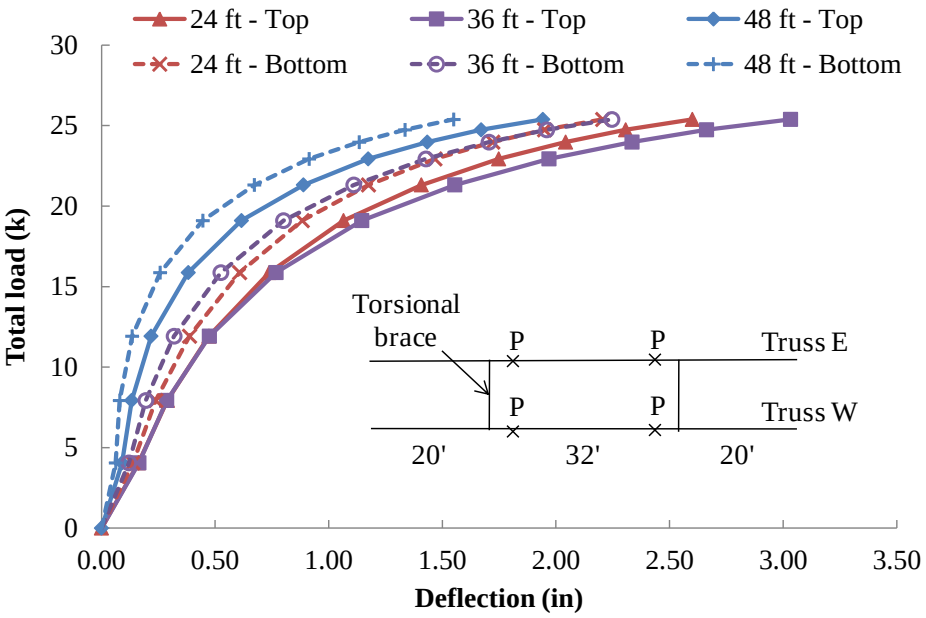

Figure A.25 Truss with 2 large torsional braces and 0.5" load offset (with connection stiffener)

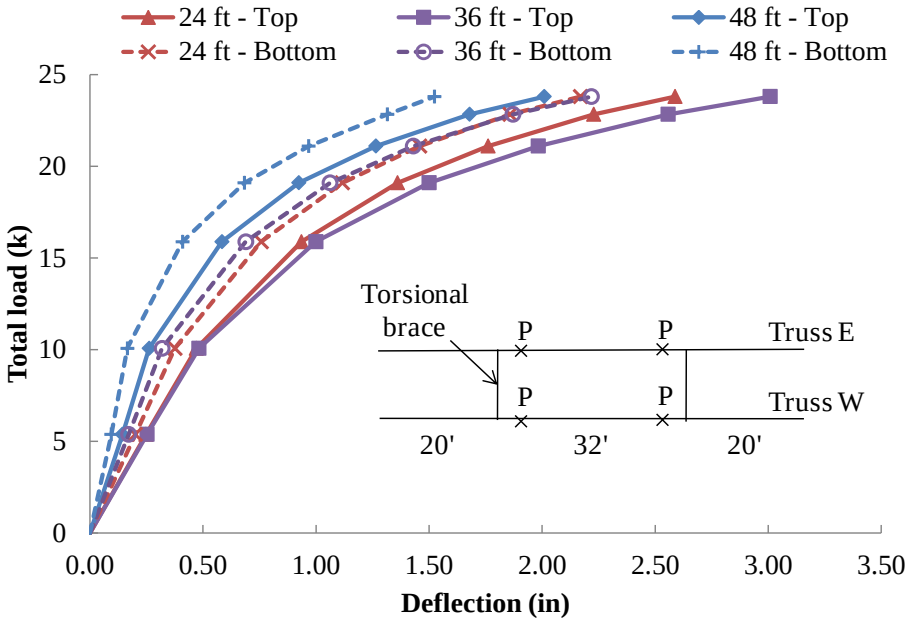

Figure A.26 Truss with 2 large torsional braces and 1.0" load offset at top chord (with connection stiffener)

A.3 Out-of-Plane Cross Section Rotation of Truss without Intermediate Bracing

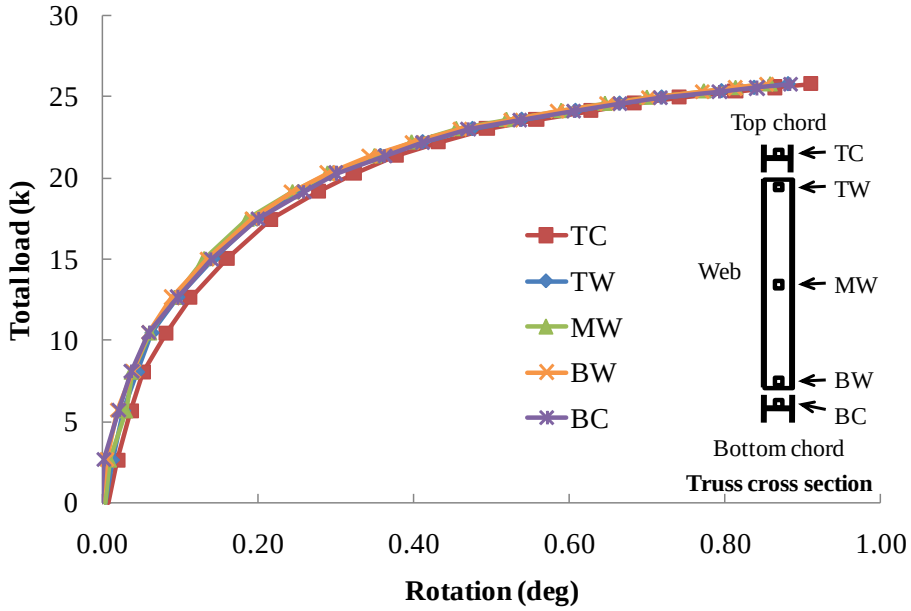

Figure A.27 Midspan rotation of 48-ft truss - Bottom chord loading

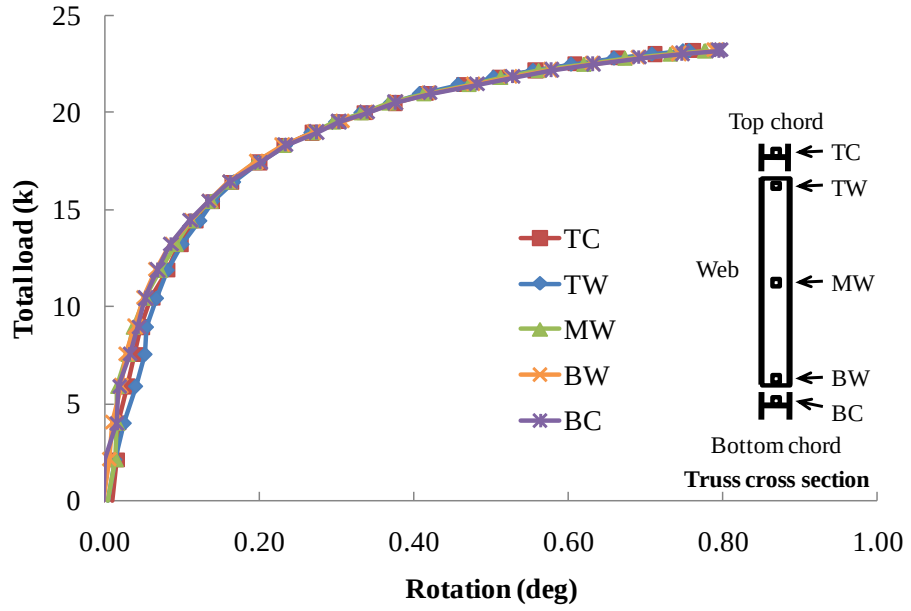

Figure A.28 Midspan rotation of 48-ft truss - Top chord loading

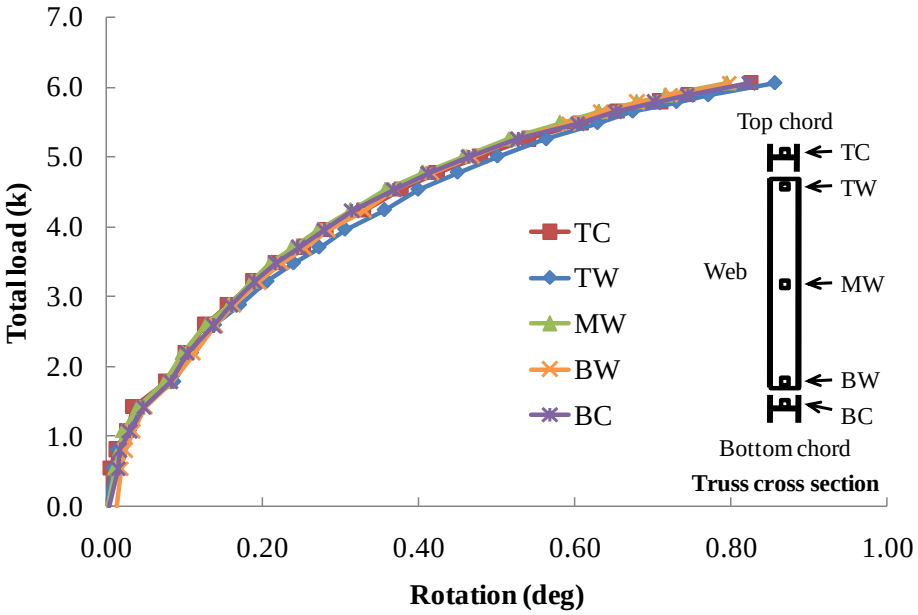

Figure A.29 Midspan rotation of 72-ft truss - Bottom chord loading

A.4 VERTICAL DEFLECTION OF TRUSS WITH LATERAL BRACING

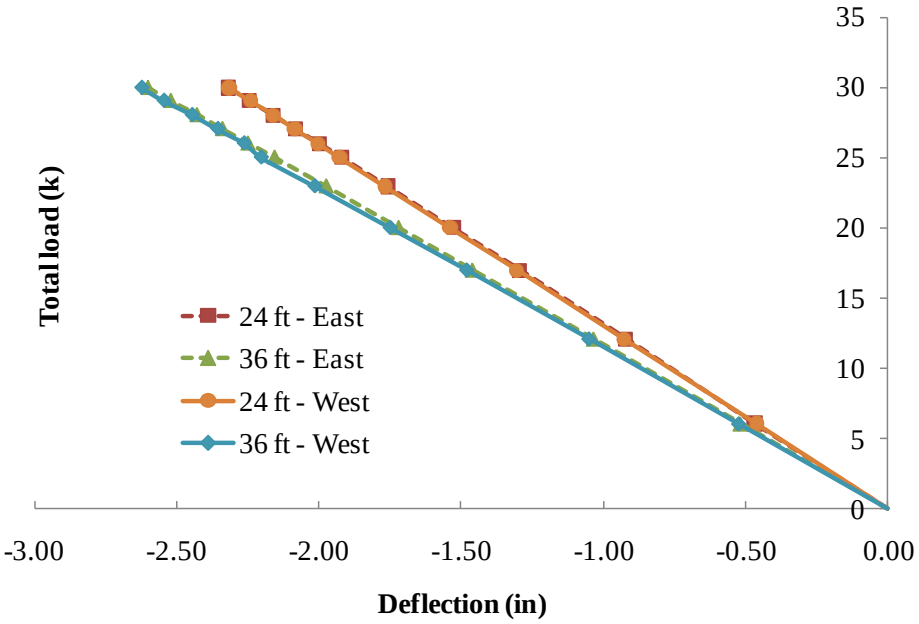

Figure A.30 Vertical deflection of 72-ft truss with single lateral brace – K = 0.8 kip/in

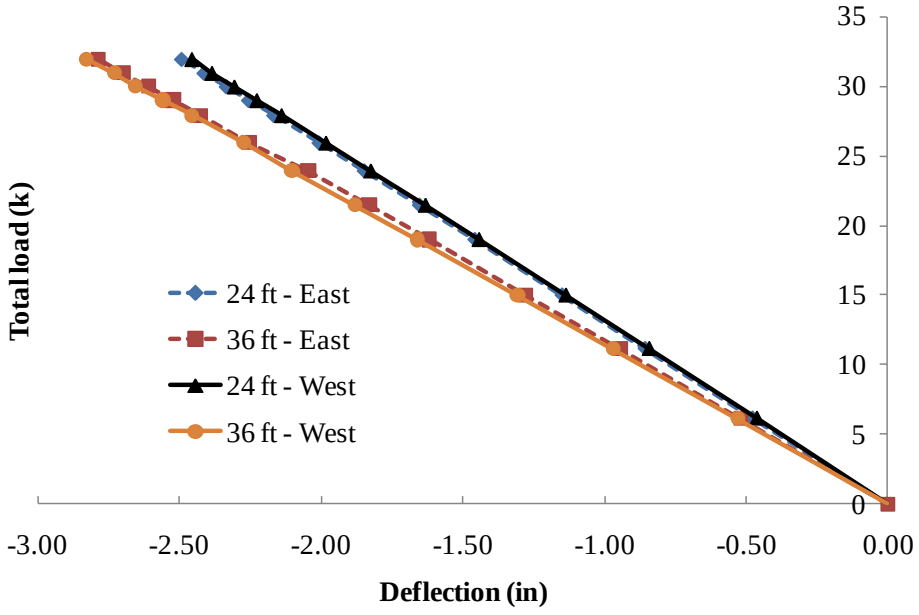

Figure A.31 Vertical deflection of 72-ft truss with 2 lateral brace – K = 0.8 kip/in

A.5 STRAIN IN TRUSS CHORD AT MIDSPAN

A.5.1 Truss without Intermediate Bracing

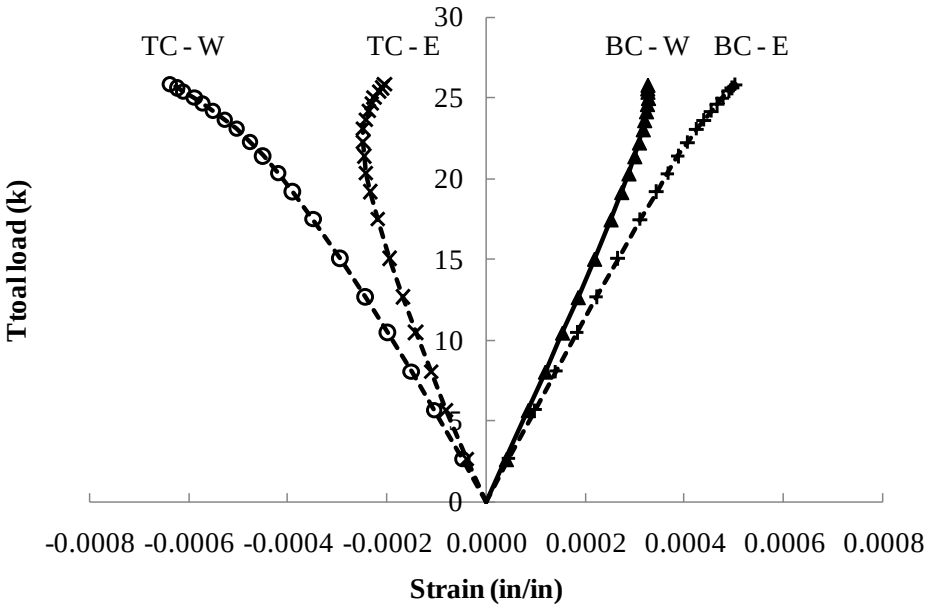

Figure A.32 Strain of 48-ft truss - Bottom chord loading

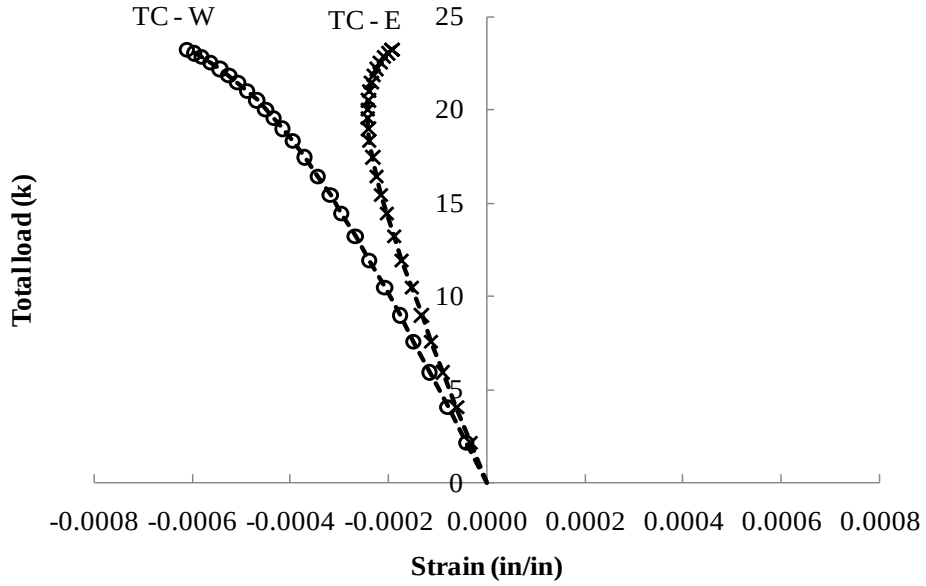

Figure A.33 Strain of 48-ft truss - Top chord loading

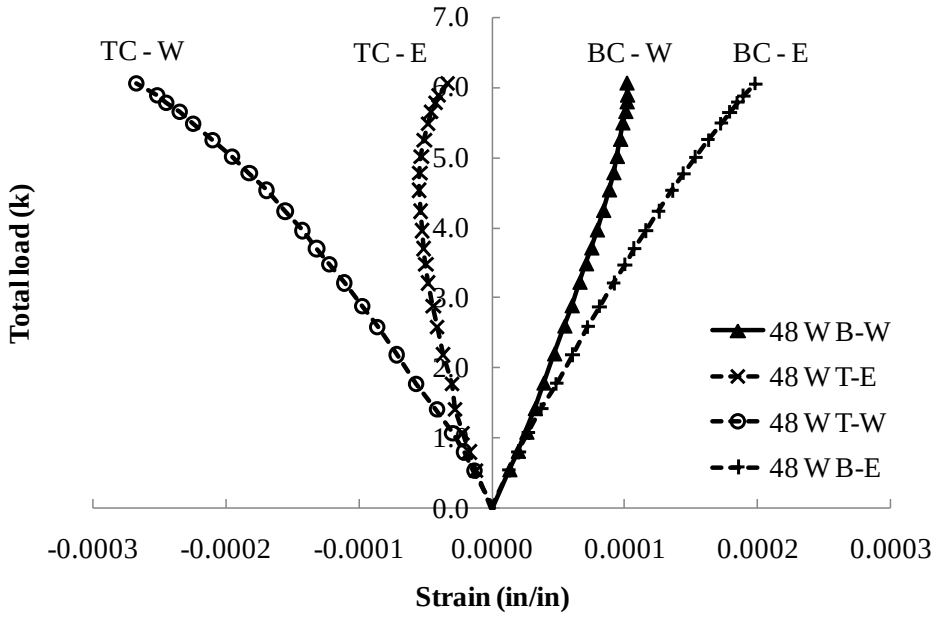

Figure A.34 Strain of 72-ft truss - Bottom chord loading

A.5.2 Truss with Lateral Bracing

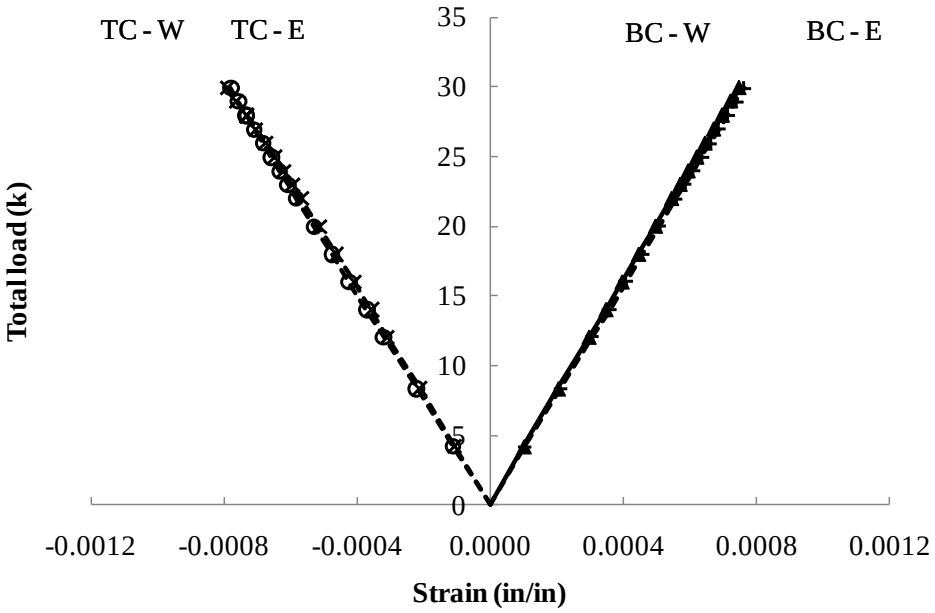

Figure A.35 Strain of 72-ft truss with single lateral brace - K = 0.5 k/in

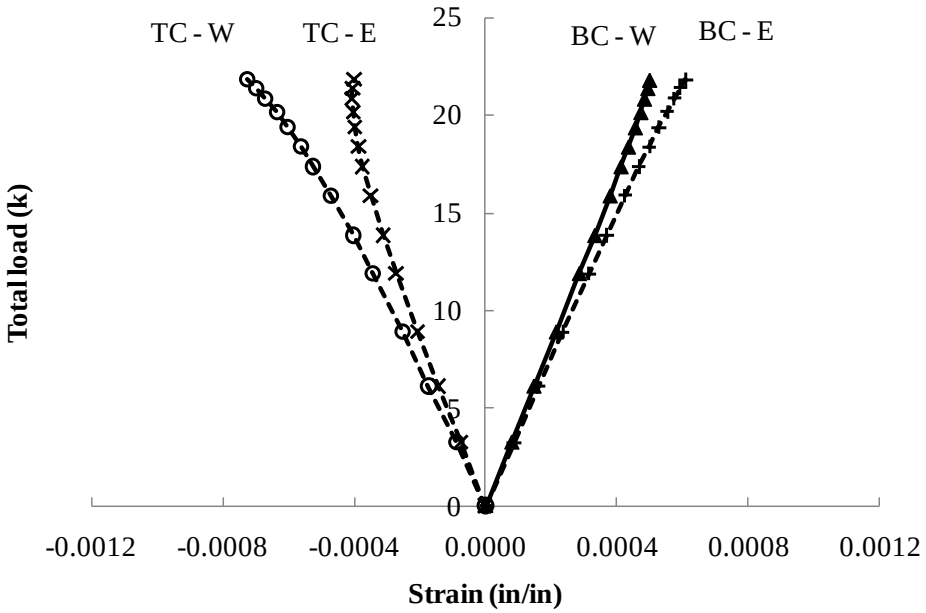

Figure A.36 Strain of 72-ft truss with 2 lateral braces - K = 0.2 k/in

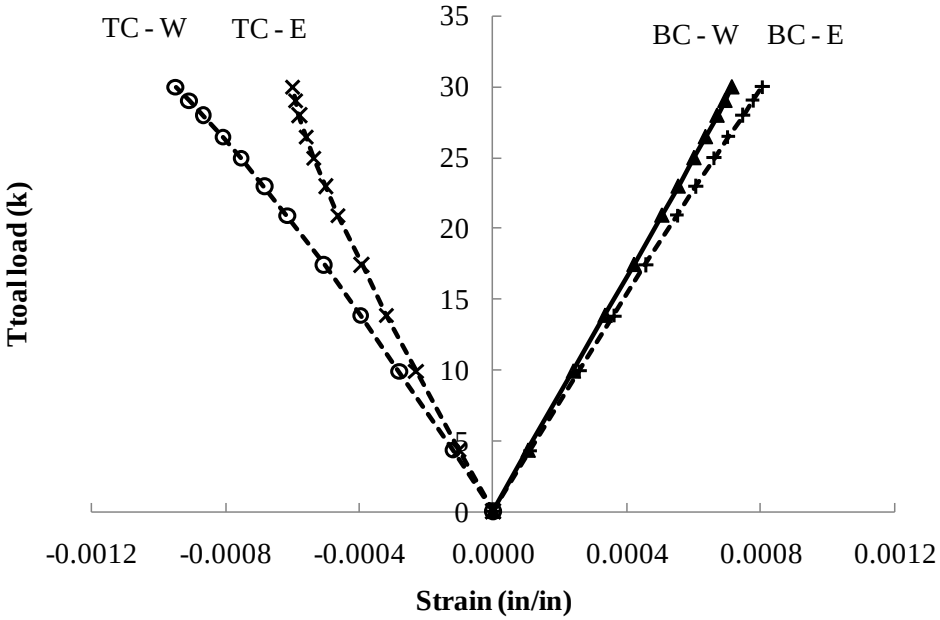

Figure A.37 Strain of 72-ft truss with 2 lateral braces - K = 0.5 k/in

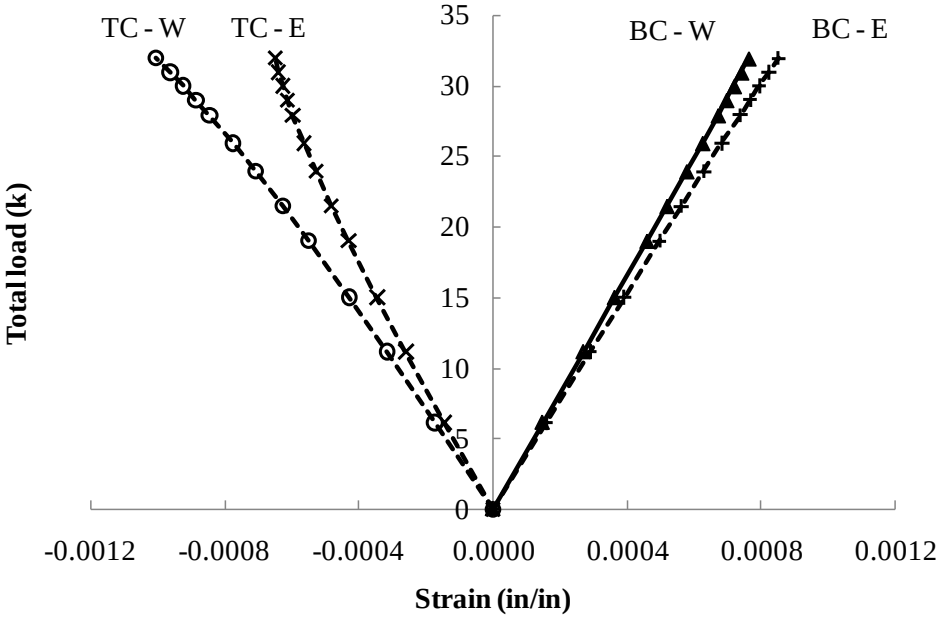

Figure A.38 Strain of 72-ft truss with 2 lateral braces - K = 0.8 k/in

A.5.3 Truss with Torsional Bracing

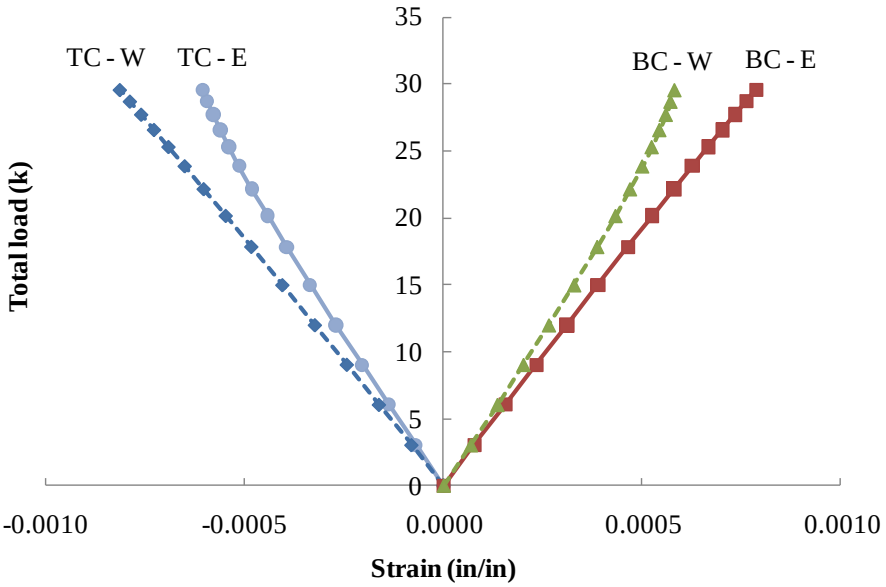

Figure A.39 Strain of 72-ft truss with 3 large torsional braces at bottom chord (with connection stiffener)

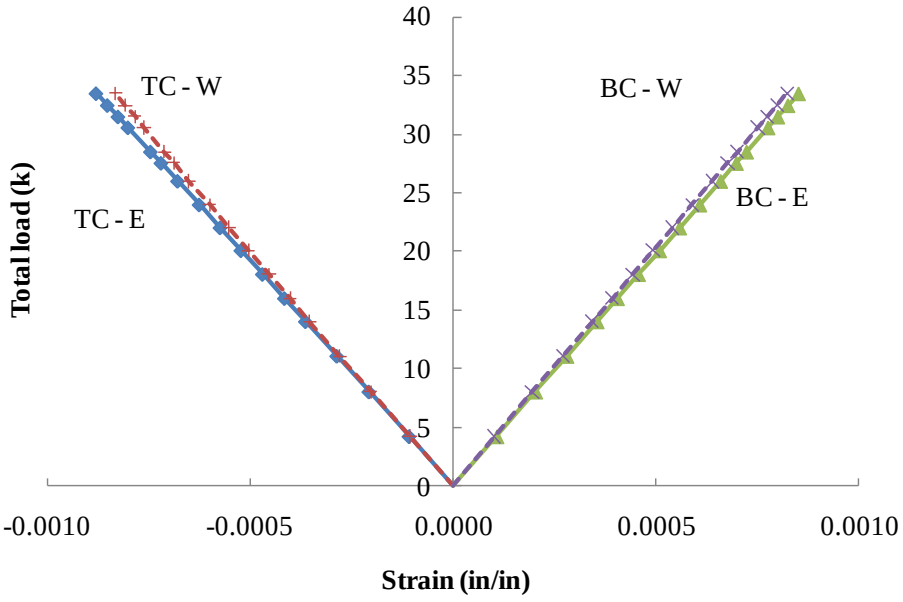

Figure A.40 Strain of 72-ft truss with 3 large torsional braces at top chord (with connection stiffener)

A.6 TORSIONAL BRACE AXIAL FORCE

A.6.1 Regular Truss

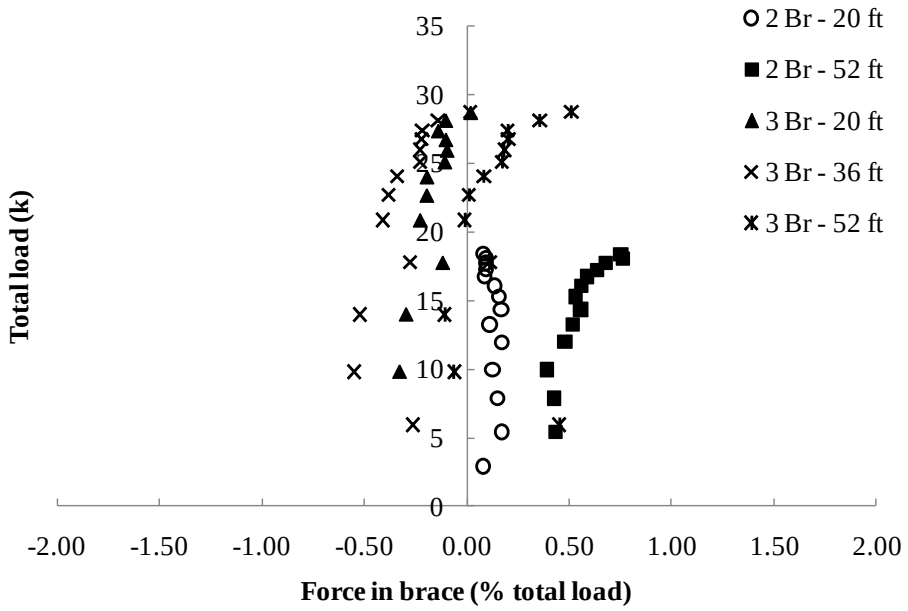

Figure A.41 Truss with small torsional braces at top chord

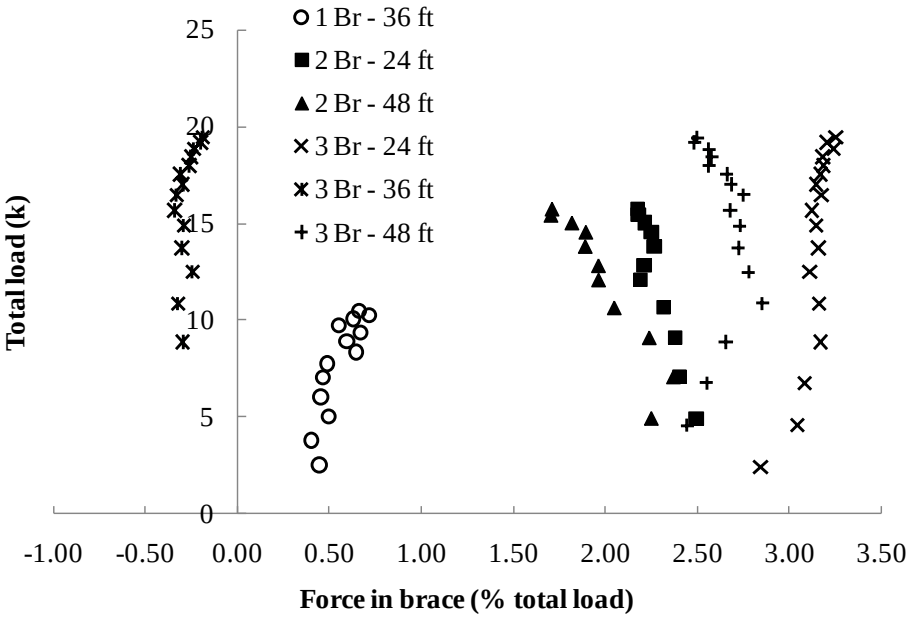

Figure A.42 Truss with small torsional braces at bottom chord

A.6.2 Pony Truss

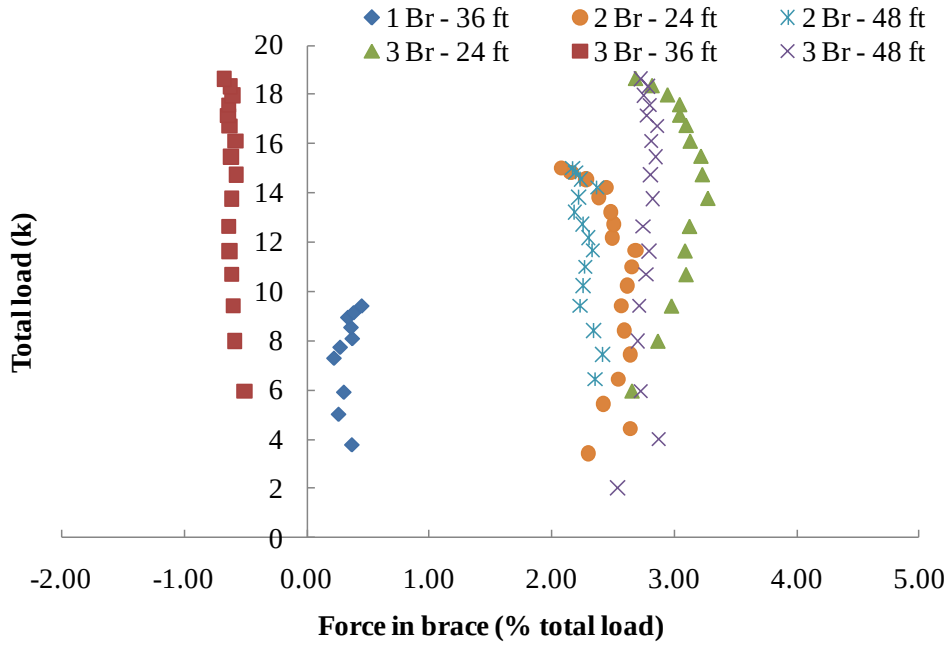

Figure A.43 Pony truss with small torsional braces

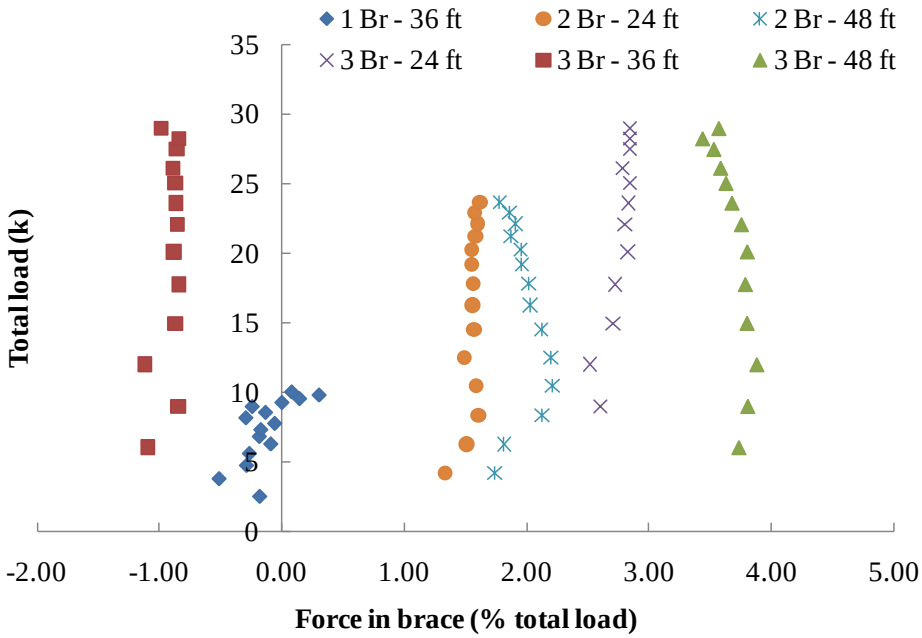

Figure A.44 Pony truss with large torsional braces

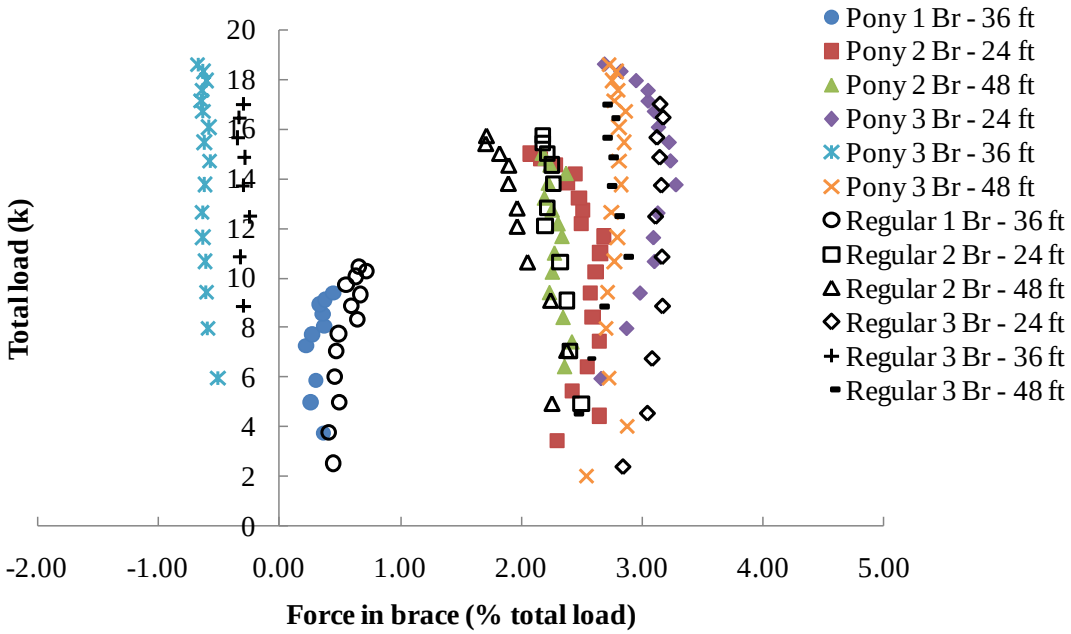

Figure A.45 Comparison of brace forces of truss with small torsional braces

A.7 COMPARISON BETWEEN BRACE STRAIN OF REGULAR AND PONY TRUSS

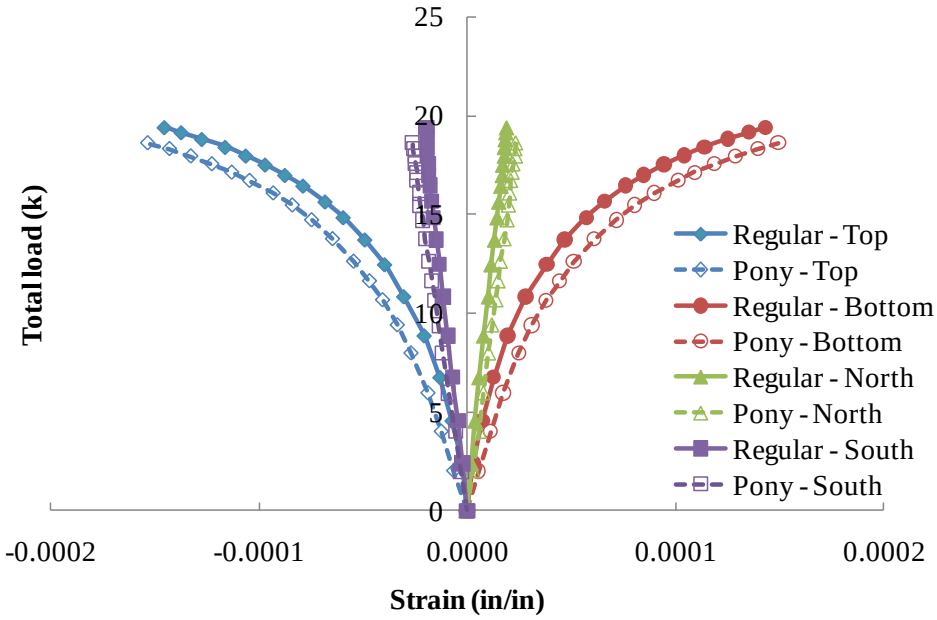

Figure A.46 Strain at 36 feet of truss with 3 small torsional braces

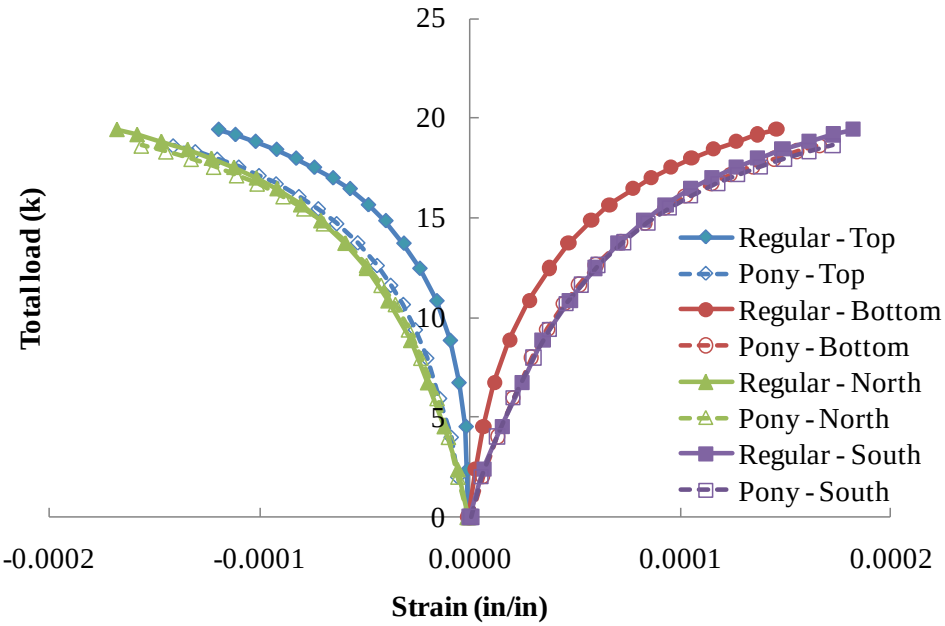

Figure A.47 Strain at 48 feet of truss with 3 small torsional braces

A.8 INITIAL IMPERFECTION

A.8.1 Initial Imperfection Component

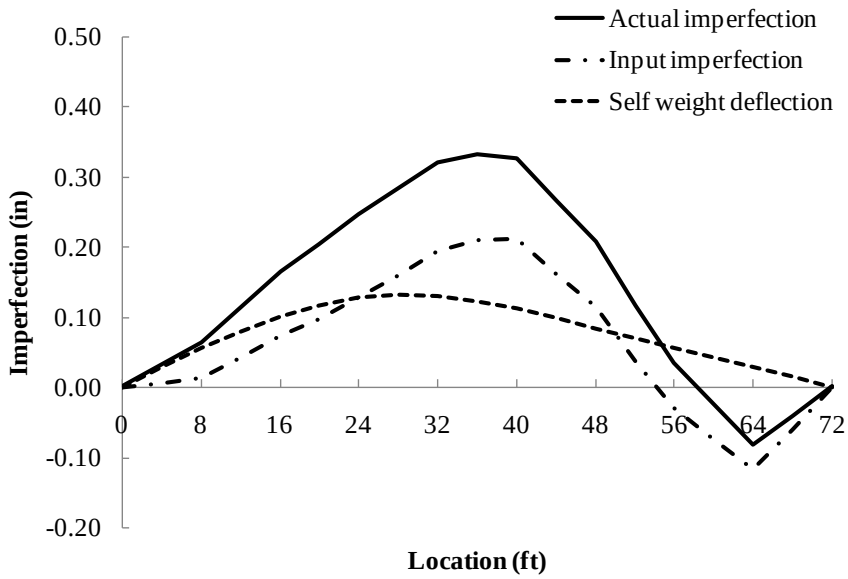

Figure A.48 Comparison of imperfection at top chord of truss with 3 small torsional braces at top chord - Top chord loading

A.8.2 Comparison of Initial Imperfections of Trusses without Intermediate Bracing

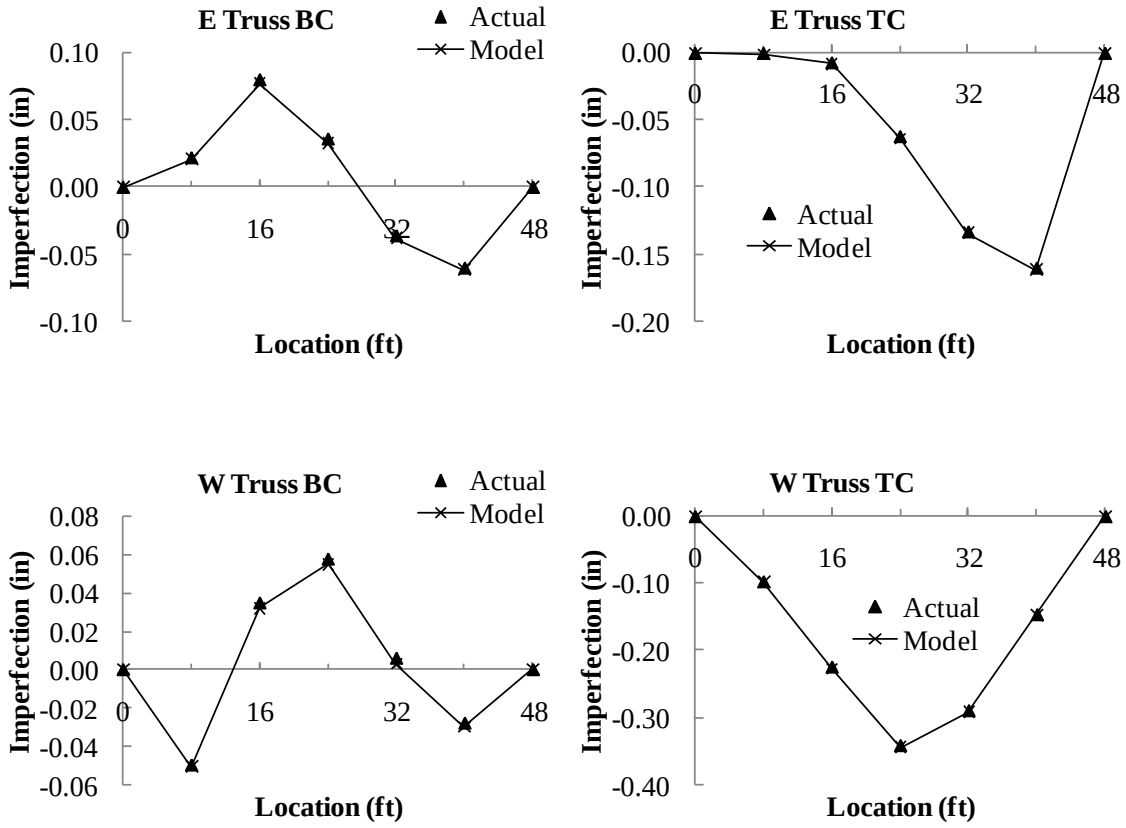

Figure A.49 48-ft truss - Bottom chord loading

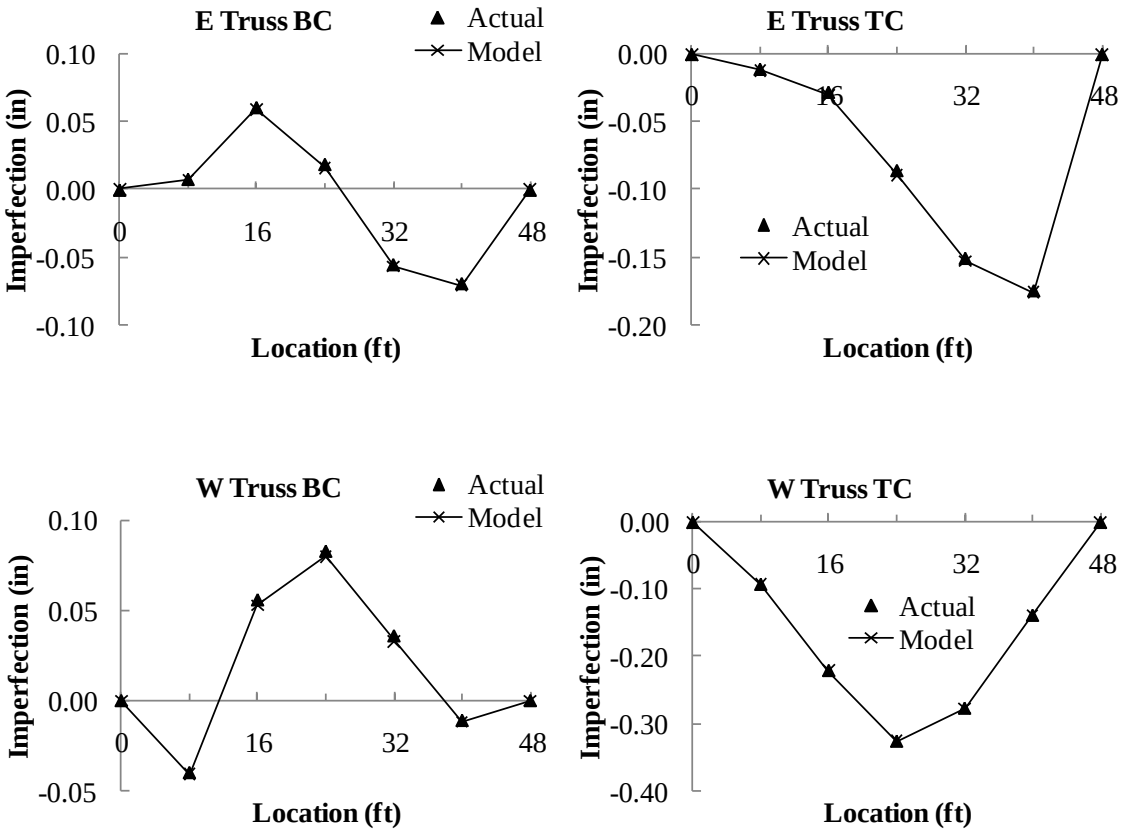

Figure A.50 48-ft truss - Top chord loading

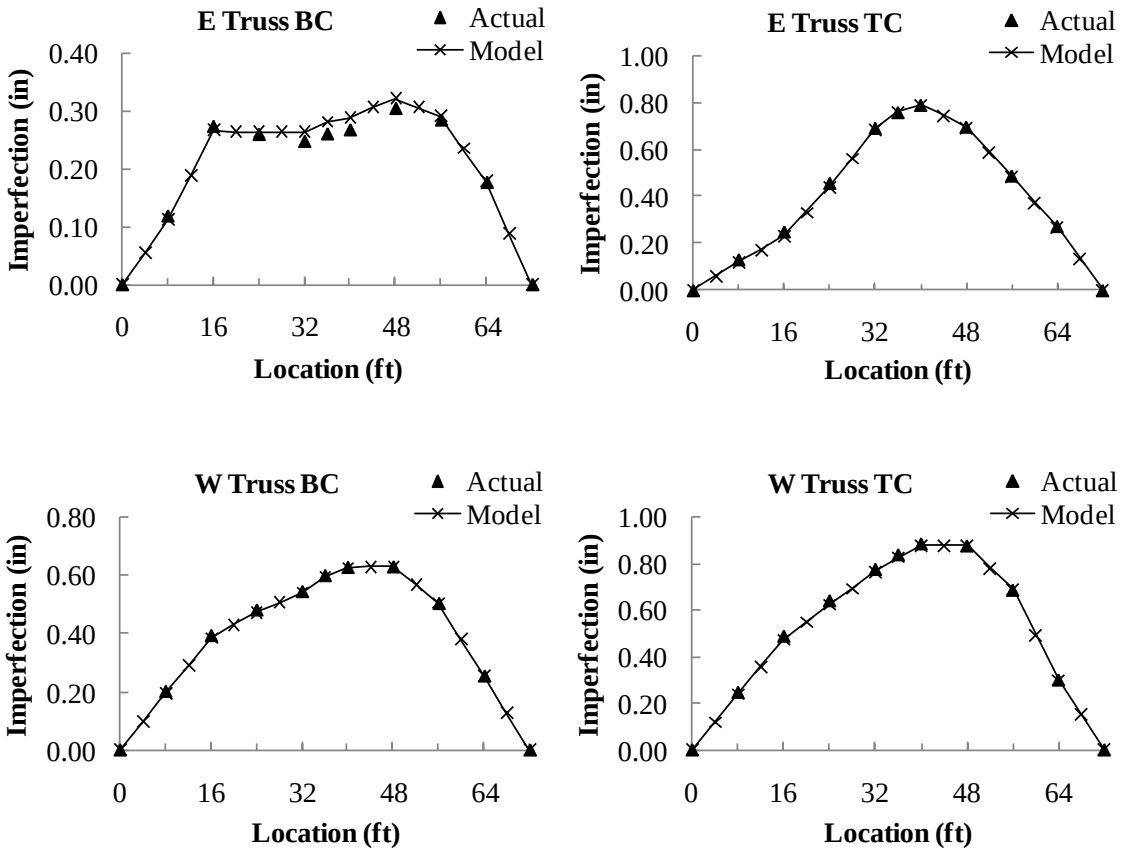

Figure A.51 72-ft truss - Top chord loading

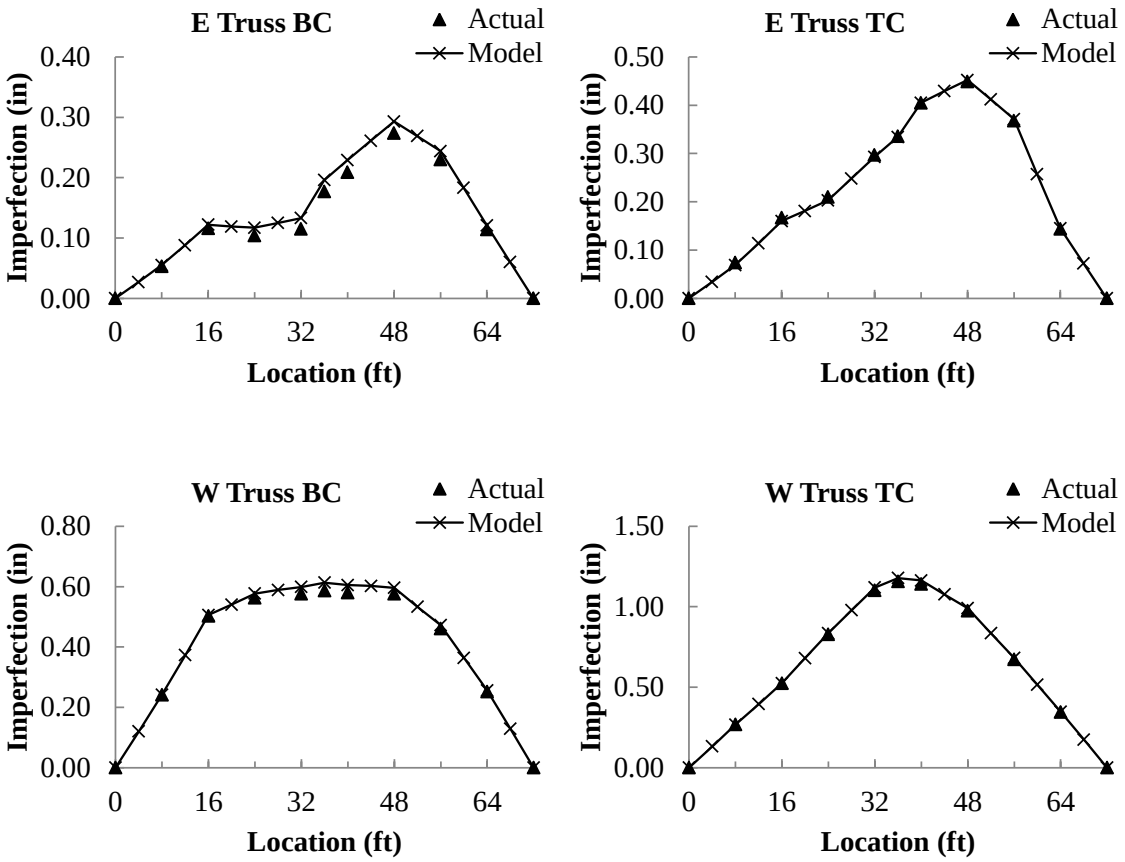

Figure A.52 72-ft truss - Bottom chord loading

A.8.3 Comparison of Initial Imperfections of Trusses with Torsional Bracing

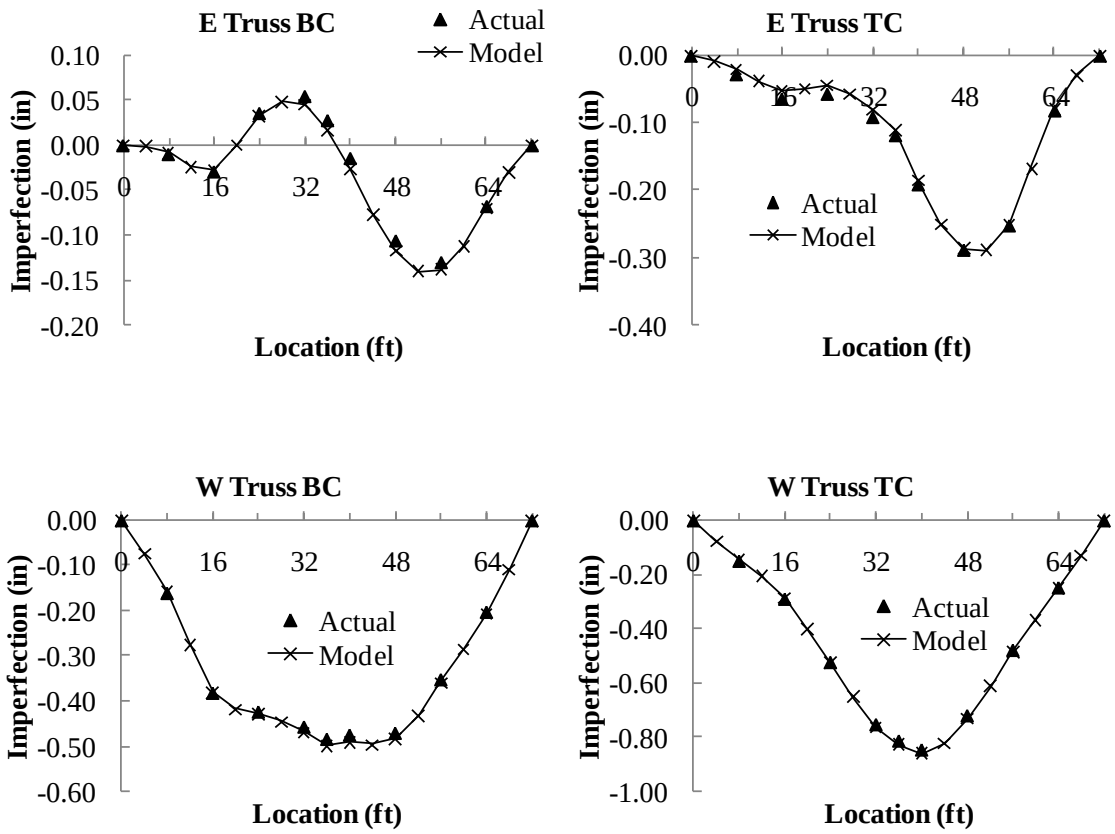

Figure A.53 72-ft truss with single small torsional brace at bottom chord - Bottom chord loading

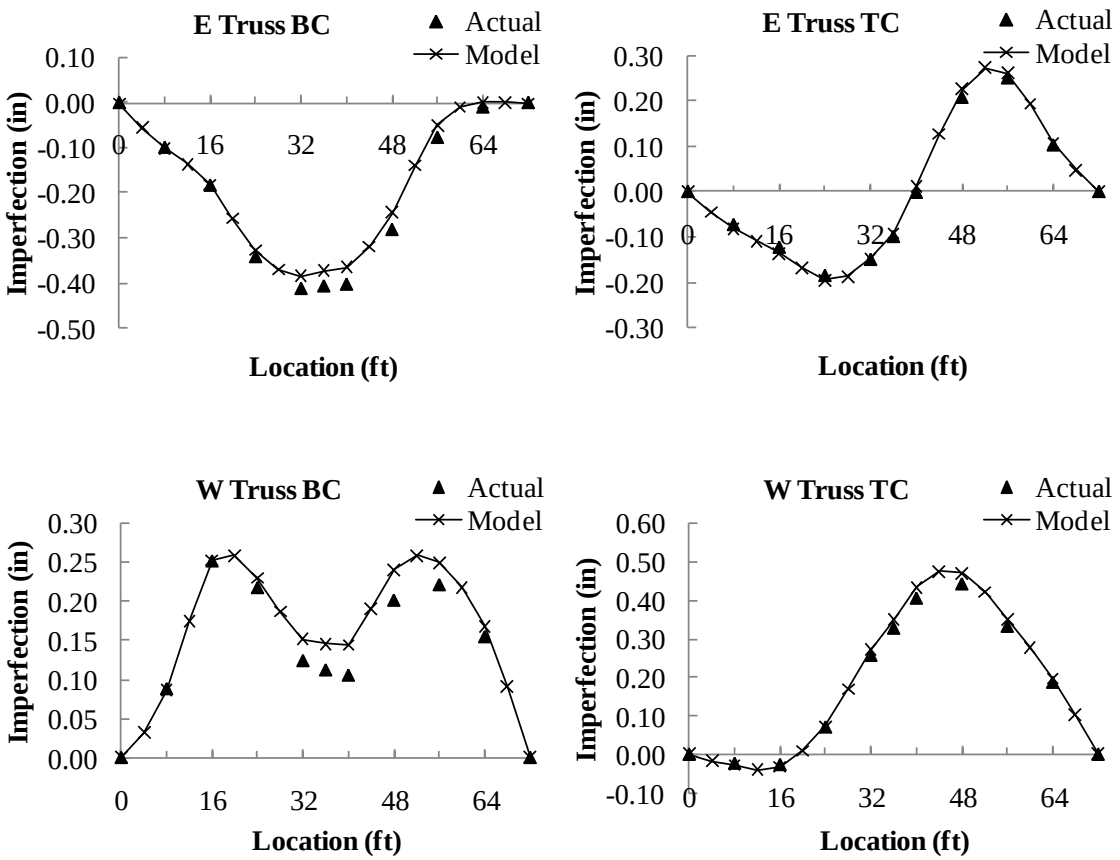

Figure A.54 72-ft truss with 2 large torsional braces at bottom chord - Bottom chord loading (with connection stiffener)

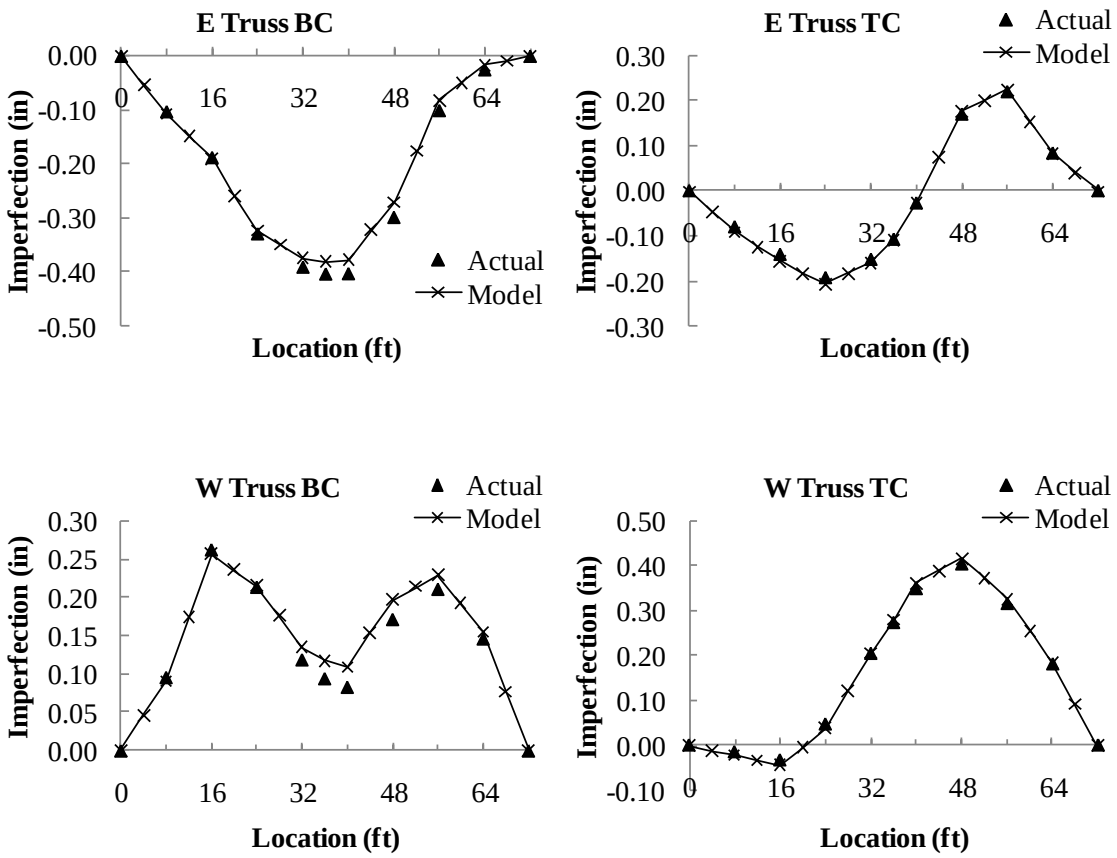

Figure A.55 72-ft truss with 3 large torsional braces at bottom chord - Bottom chord loading (with connection stiffener)

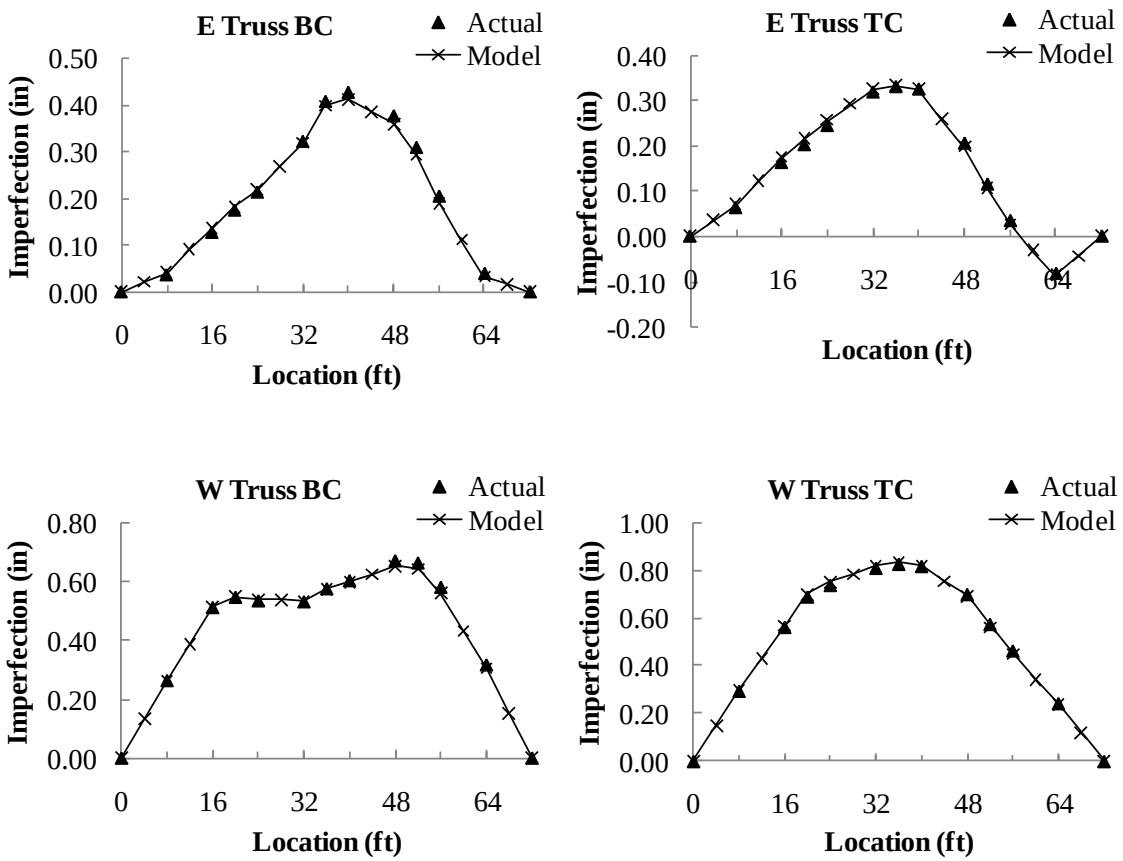

Figure A.56 72-ft truss with 3 small torsional braces at top chord - Top chord loading (with connection stiffener)

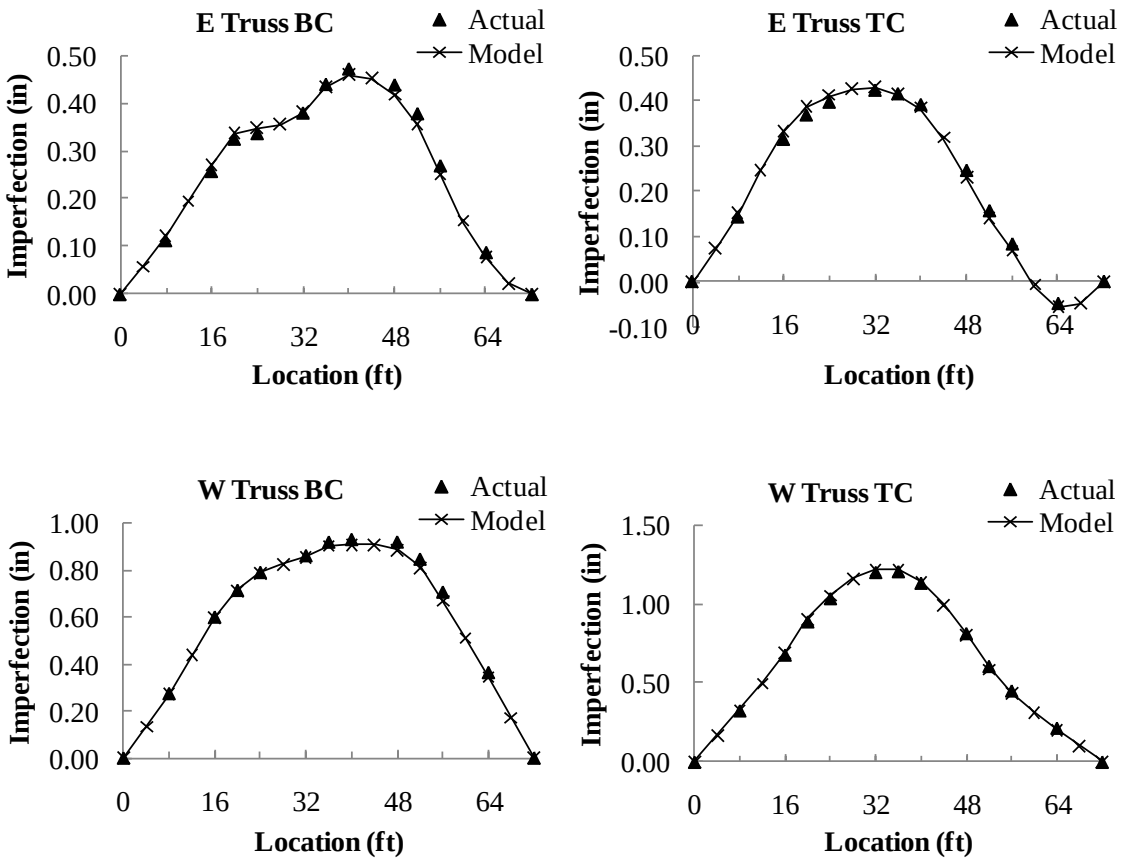

Figure A.57 72-ft truss with 2 large torsional braces at top chord - Top chord loading (with connection stiffener)

A.9 LATERAL STIFFNESS TEST VERIFICATION

A.9.1 48-ft Span Regular Truss without Lateral Restraint

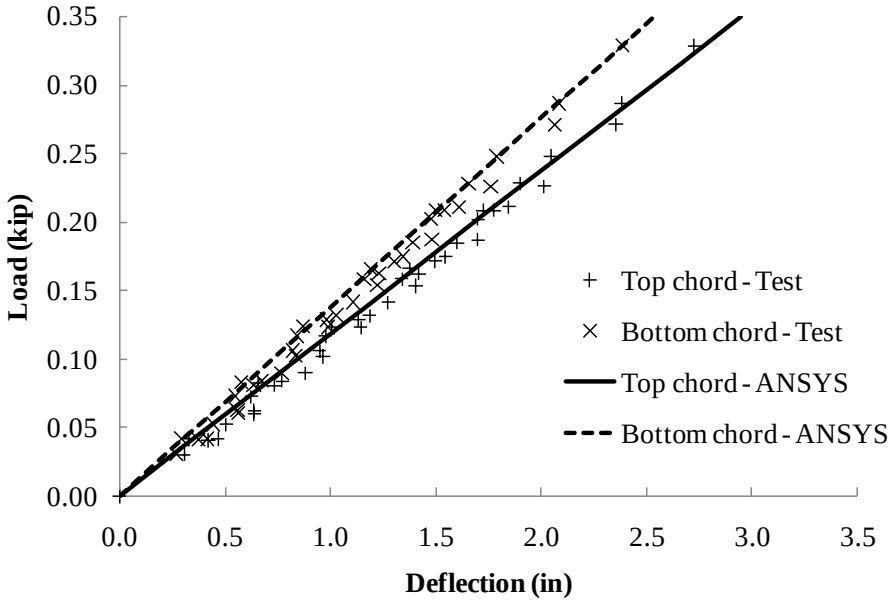

Figure A.58 Lateral deflection at 16 feet - Top chord loading

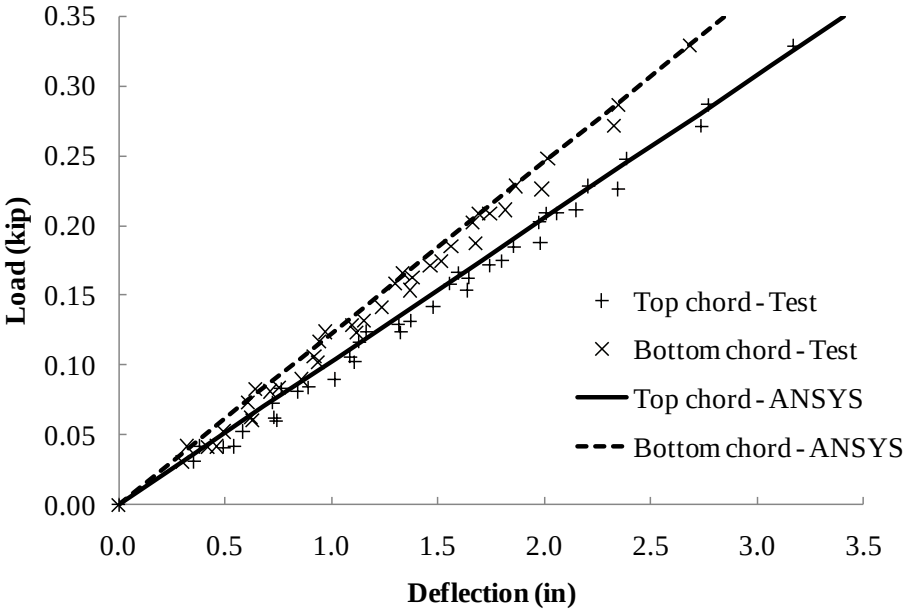

Figure A.59 Lateral deflection at midspan - Top chord loading

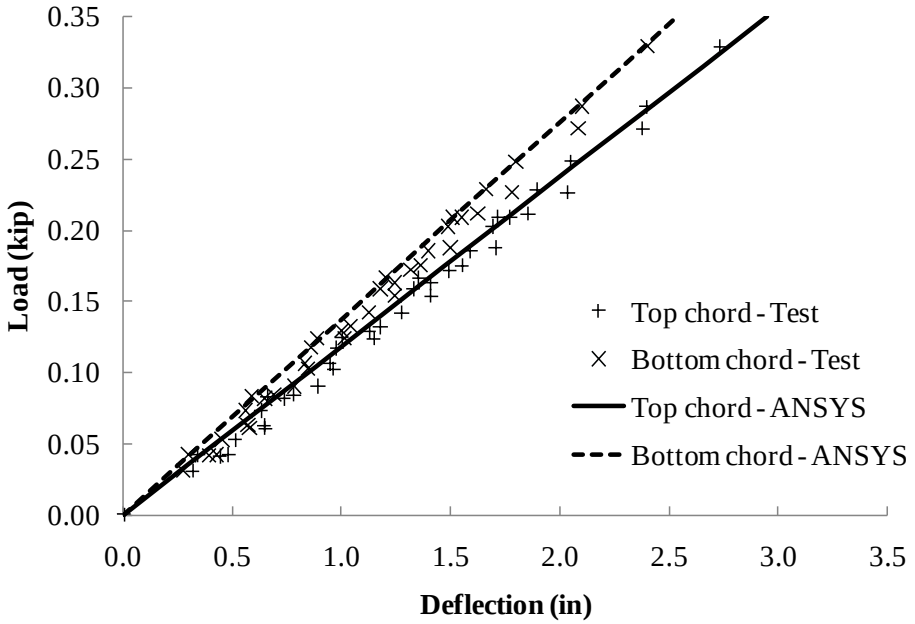

Figure A.60 Lateral deflection at 32 feet - Top chord loading

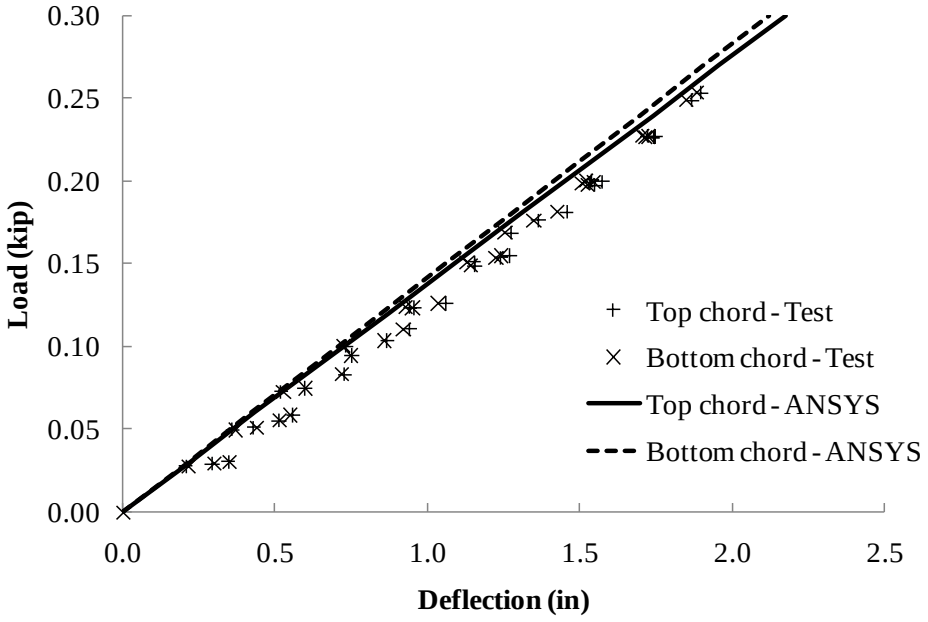

Figure A.61 Lateral deflection at 16 feet - Bottom chord loading

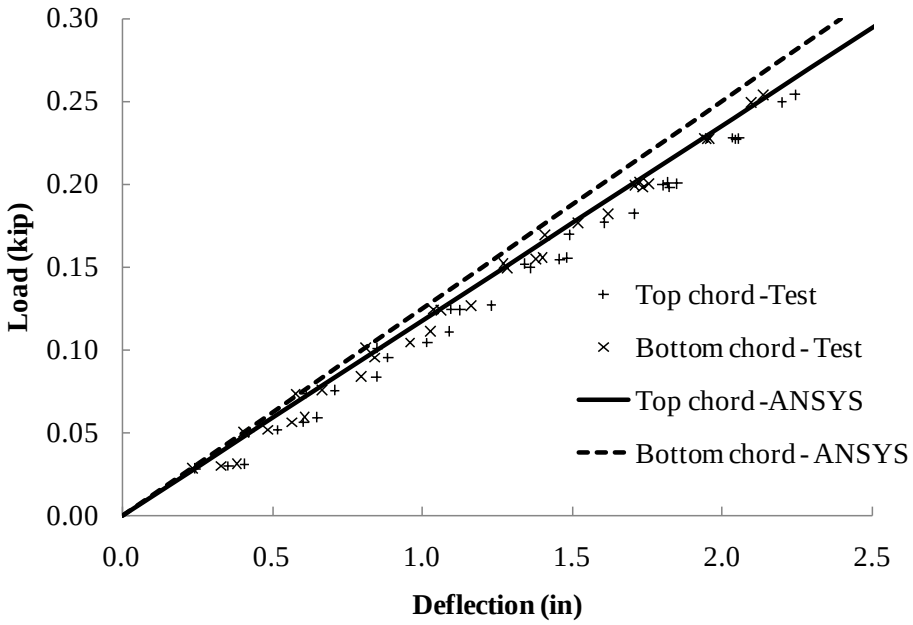

Figure A.62 Lateral deflection at midspan - Bottom chord loading

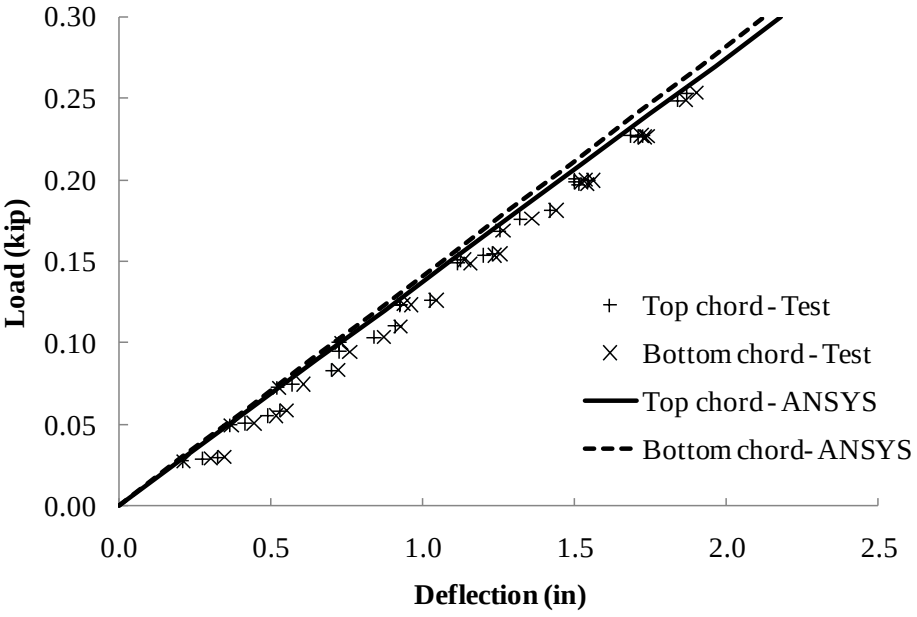

Figure A.63 Lateral deflection at 32 feet - Bottom chord loading

A.9.2 48-ft Span Regular Truss with Lateral Restraints

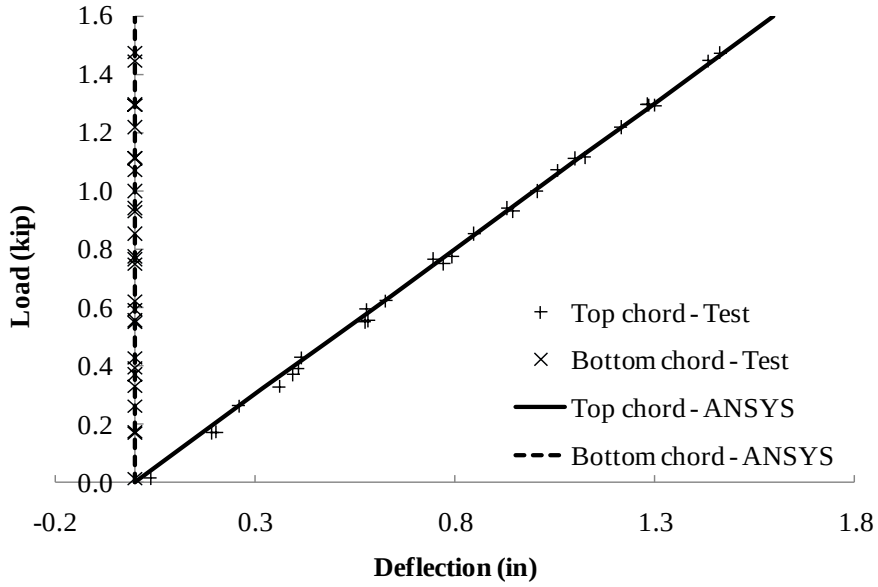

Figure A.64 Lateral deflection at 16 feet - Top chord loading and bottom chord restrained

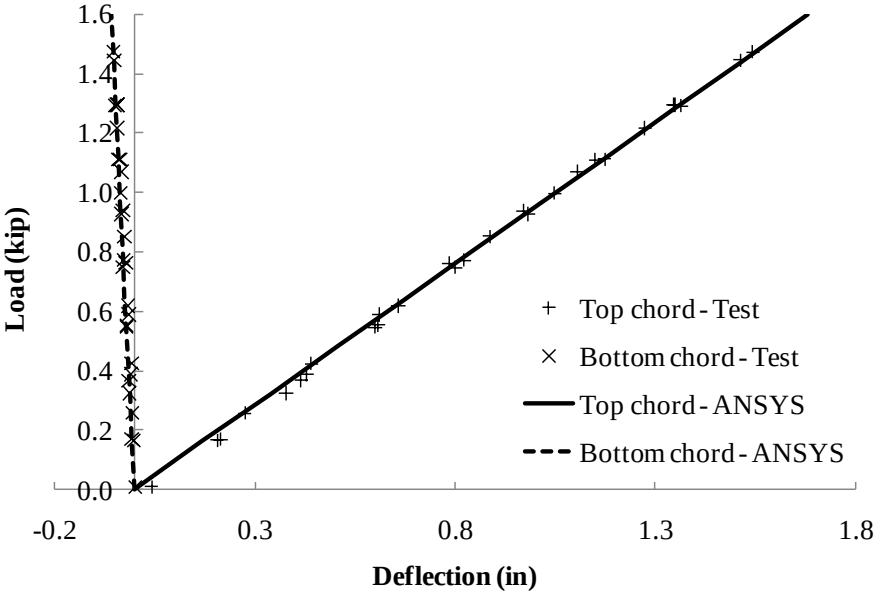

Figure A.65 Lateral deflection at midspan - Top chord loading and bottom chord restrained

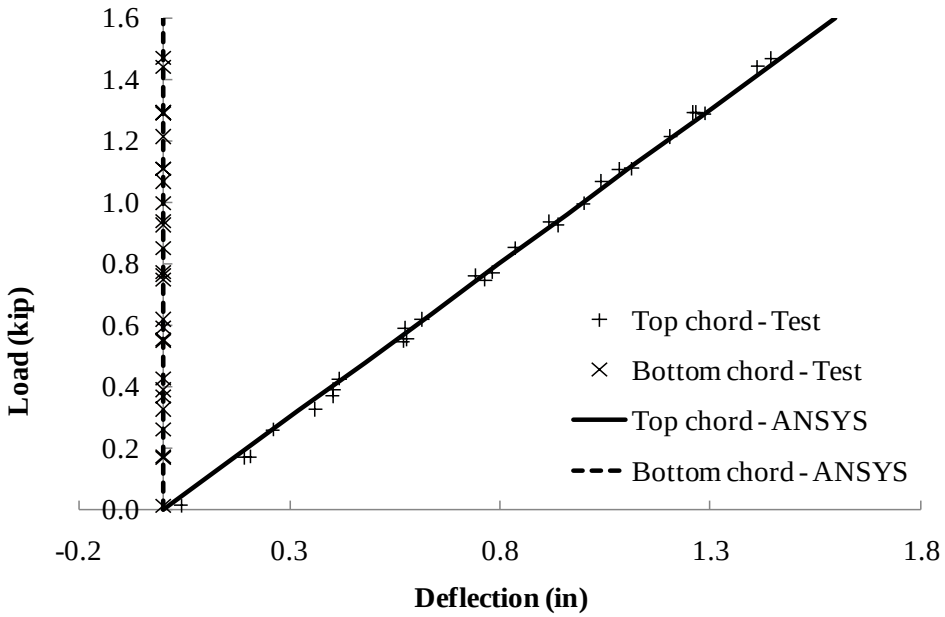

Figure A.66 Lateral deflection at 32 feet - Top chord loading and bottom chord restrained

A.9.3 72-ft Span Regular Truss without Lateral Restraint

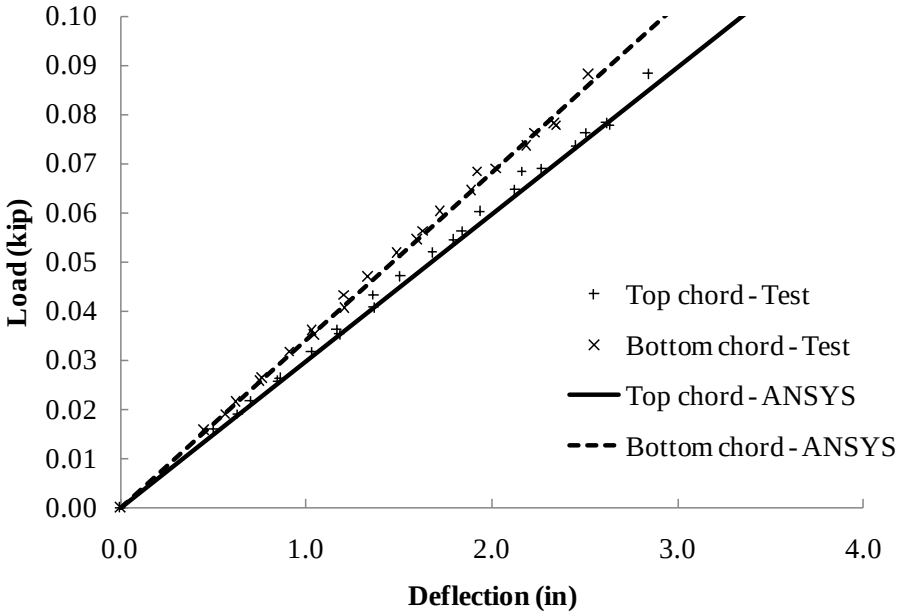

Figure A.67 Lateral deflection at 24 feet - Top chord loading

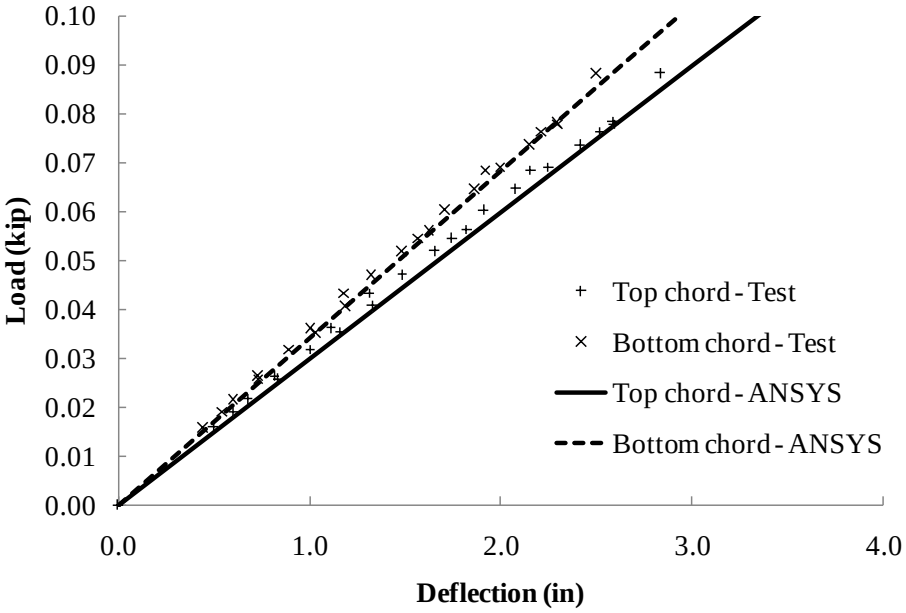

Figure A.68 Lateral deflection at 48 feet - Top chord loading

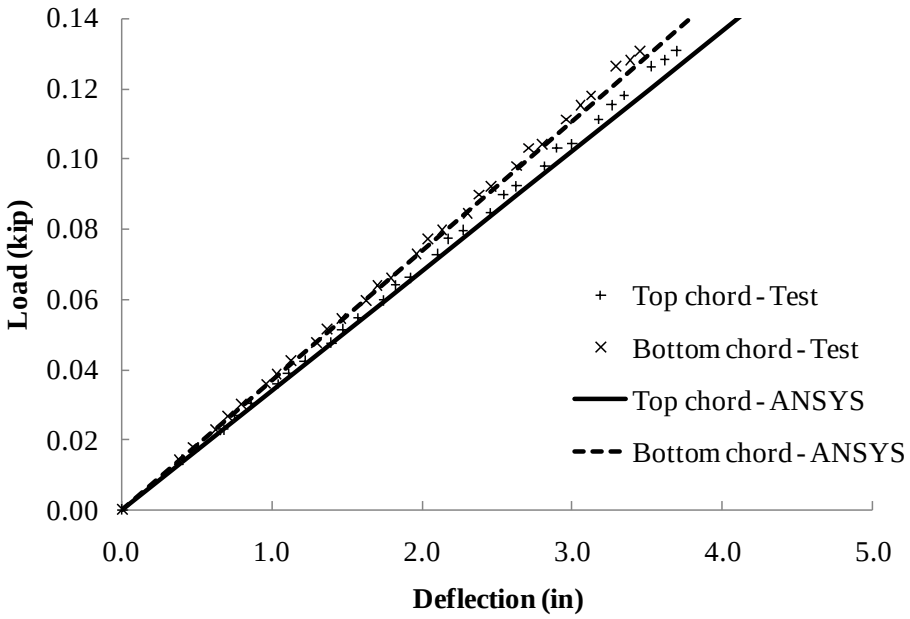

Figure A.69 Lateral deflection at 24 feet - Bottom chord loading

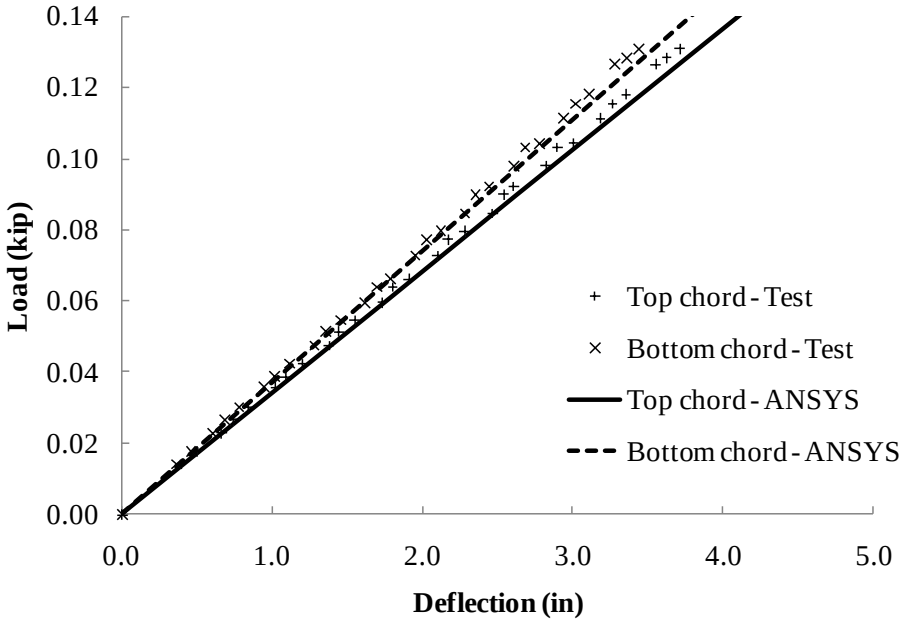

Figure A.70 Lateral deflection at 48 feet - Bottom chord loading

A.9.4 72-ft Span Regular Truss with Lateral Restraints

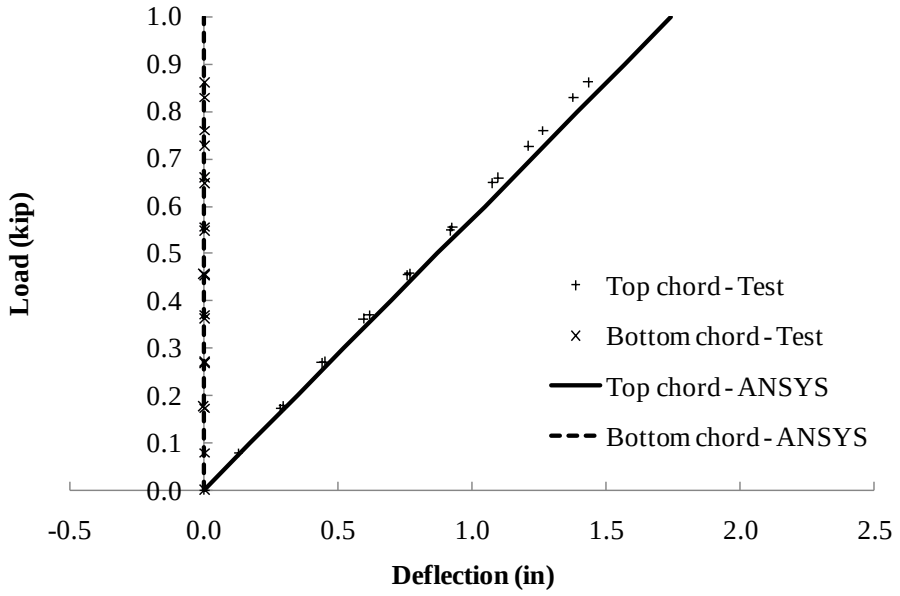

Figure A.71 Lateral deflection at 24 feet - Top chord loading and bottom chord restrained

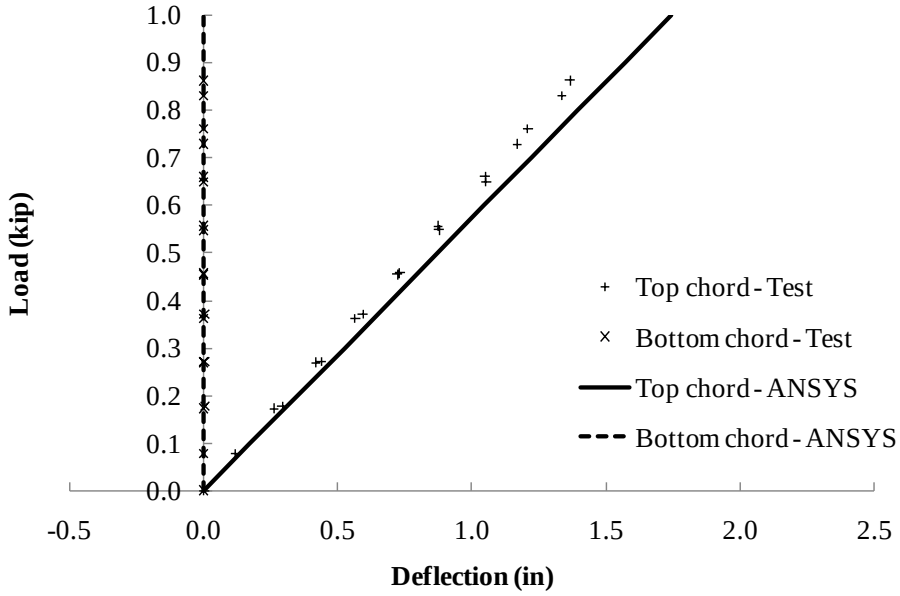

Figure A.72 Lateral deflection at 48 feet - Top chord loading and bottom chord restrained

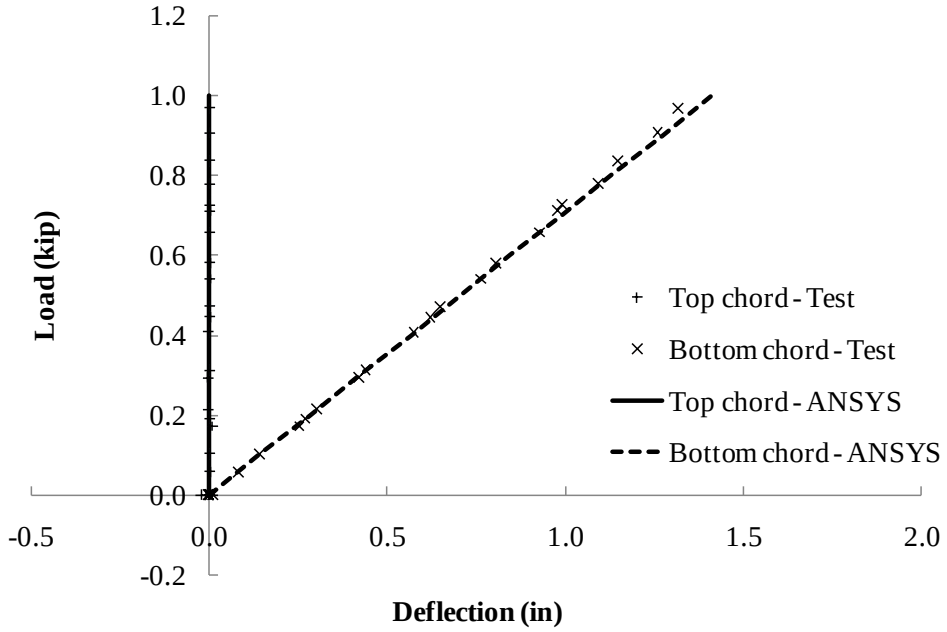

Figure A.73 Lateral deflection at 24 feet - Bottom chord loading and top chord restrained

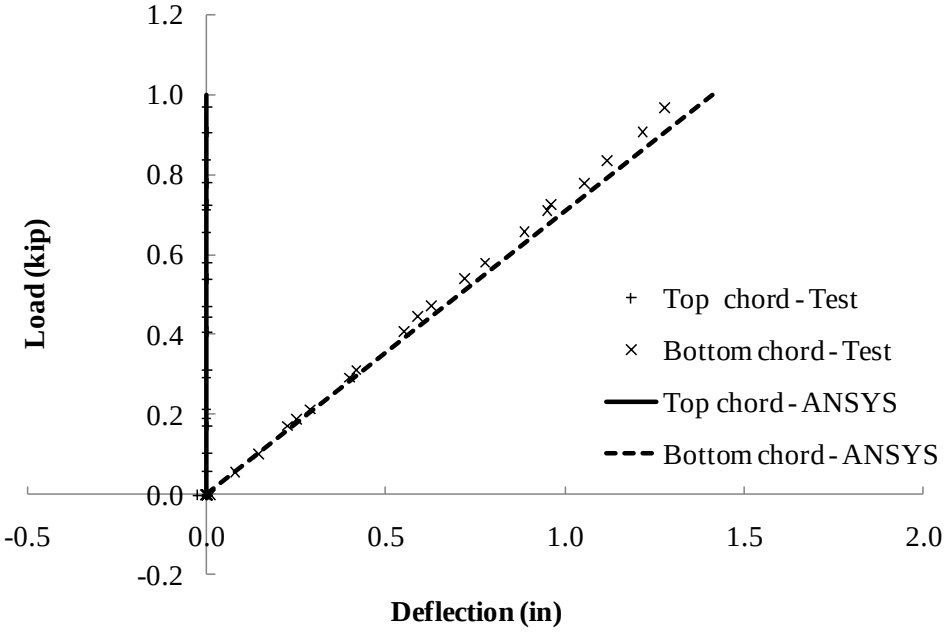

Figure A.74 Lateral deflection at 48 feet - Bottom chord loading and top chord restrained

A.9.5 72-ft Span Inverted Truss without Lateral Restraint

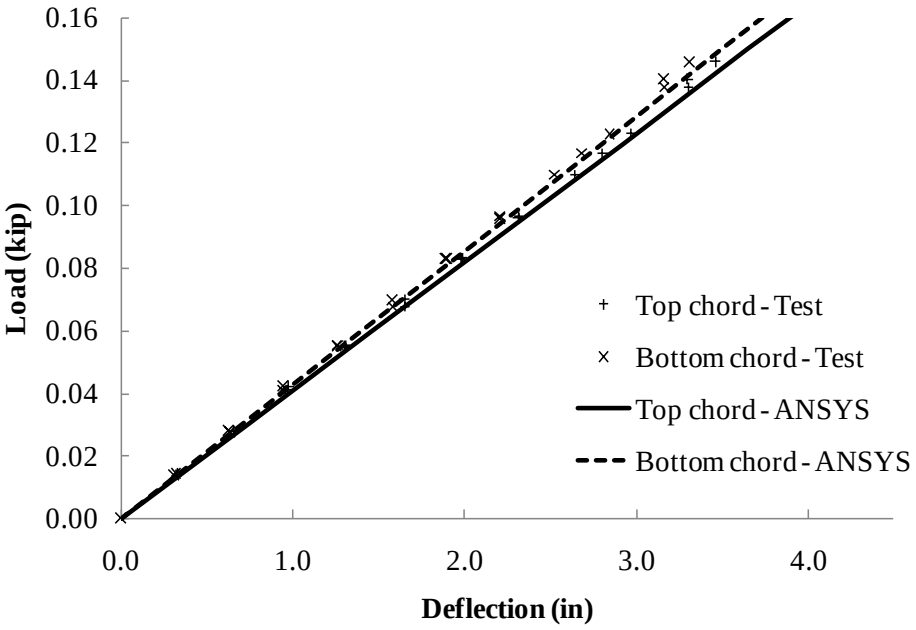

Figure A.75 Lateral deflection at 24 feet - Top chord loading

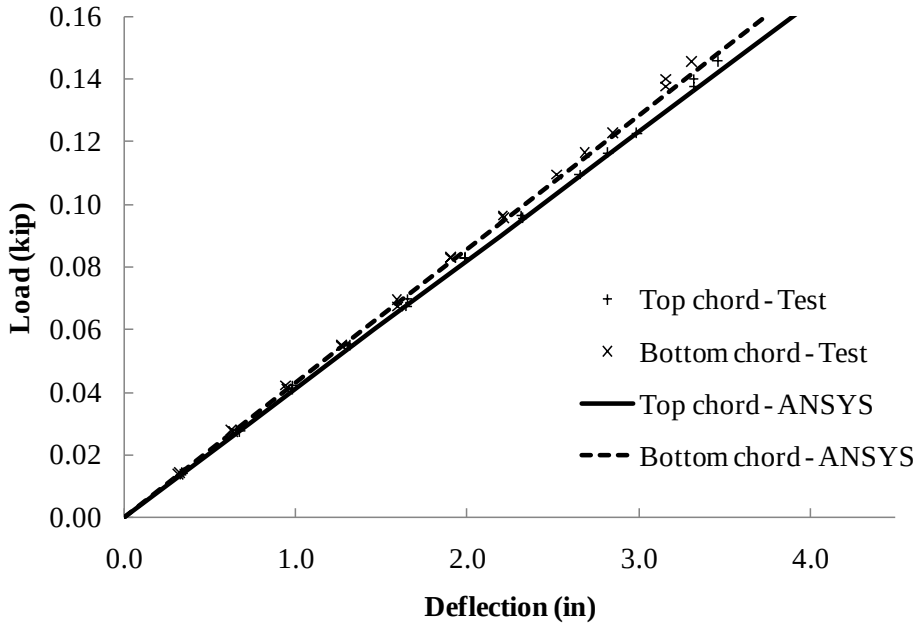

Figure A.76 Lateral deflection at 48 feet - Top chord loading

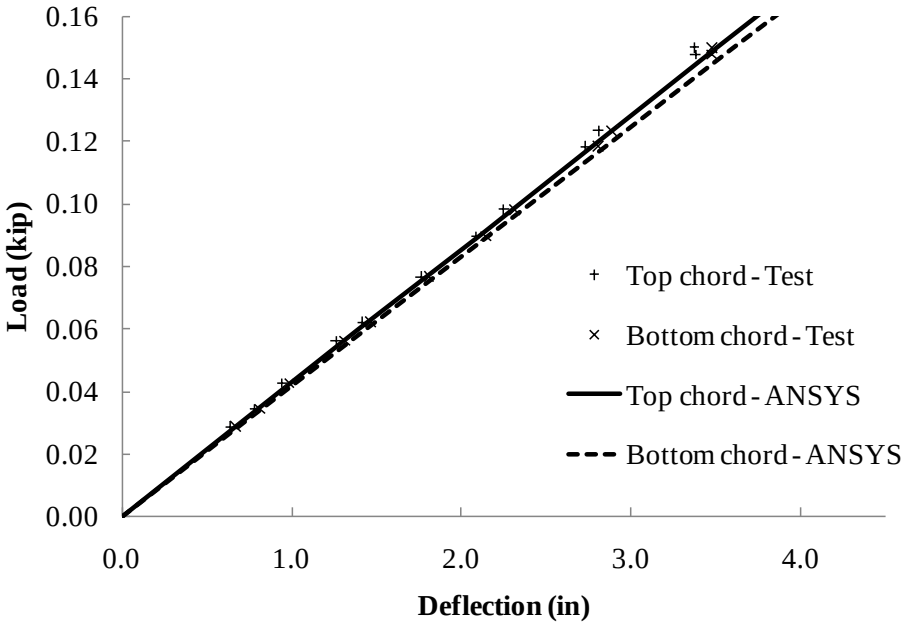

Figure A.77 Lateral deflection at 24 feet - Bottom chord loading

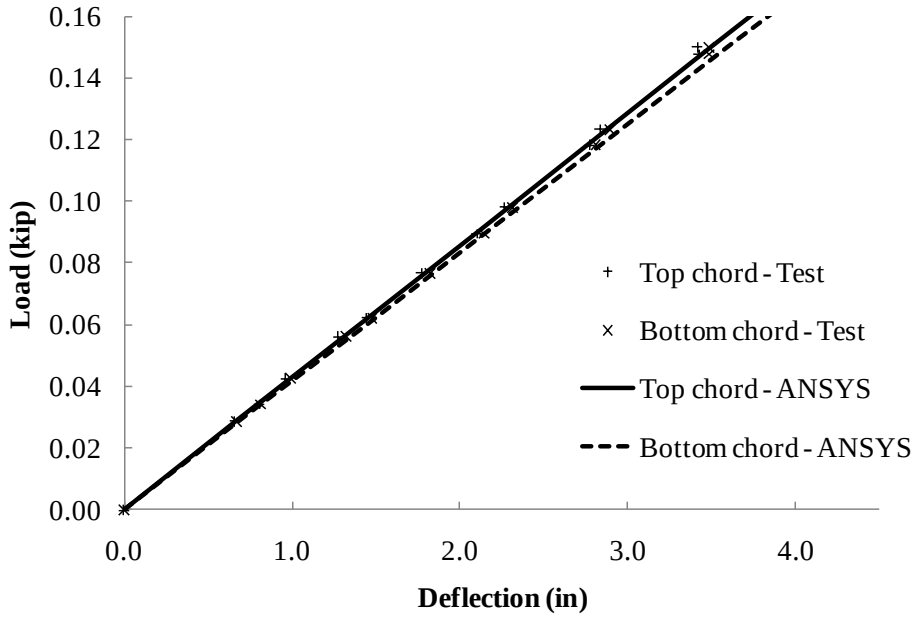

Figure A.78 Lateral deflection at 48 feet - Bottom chord loading

A.9.6 72-ft Span Inverted Truss with Lateral Restraints

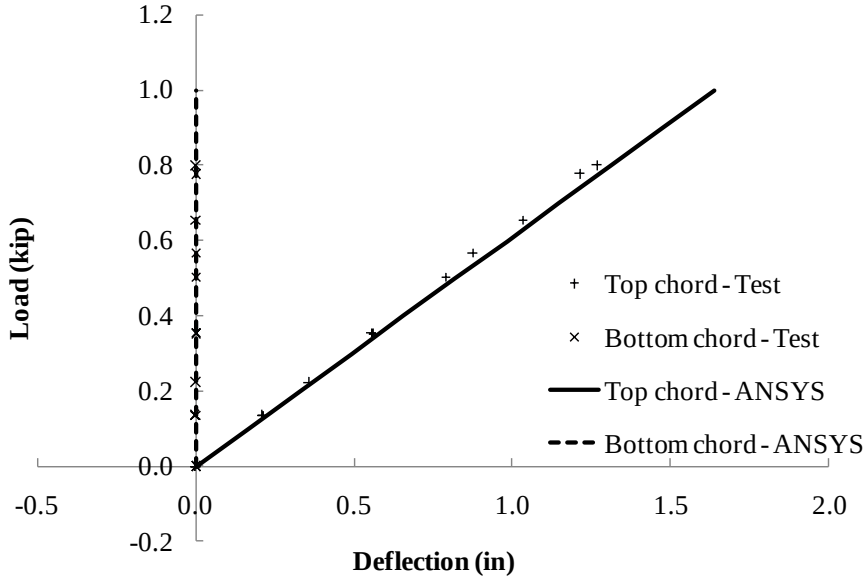

Figure A.79 Lateral deflection at 24 feet - Top chord loading and bottom chord restrained

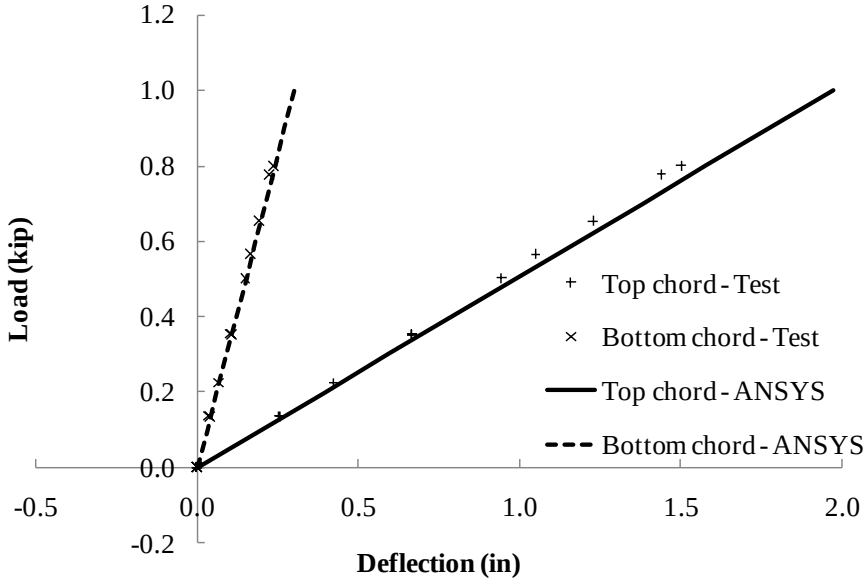

Figure A.80 Lateral deflection at midspan - Top chord loading and bottom chord restrained

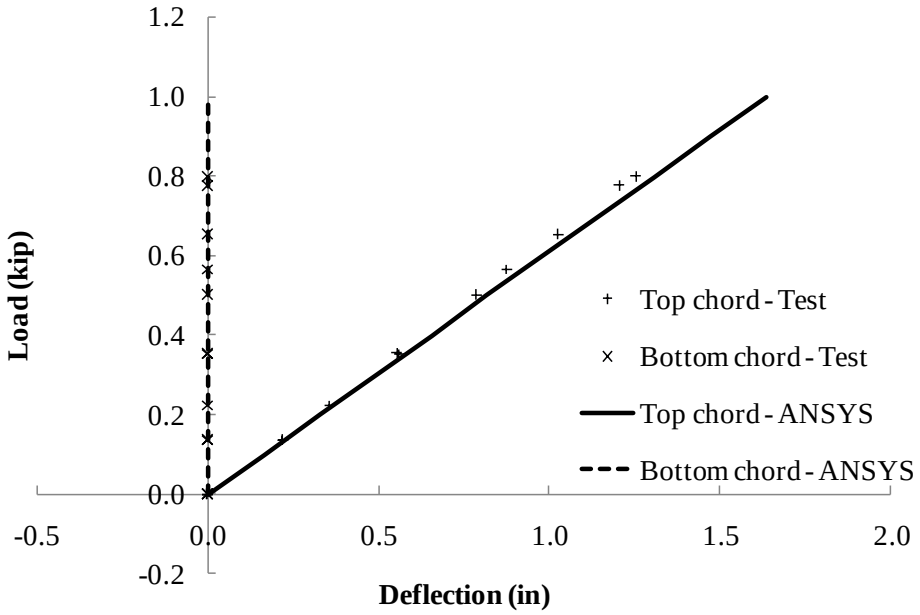

Figure A.81 Lateral deflection at 48 feet - Top chord loading and bottom chord restrained

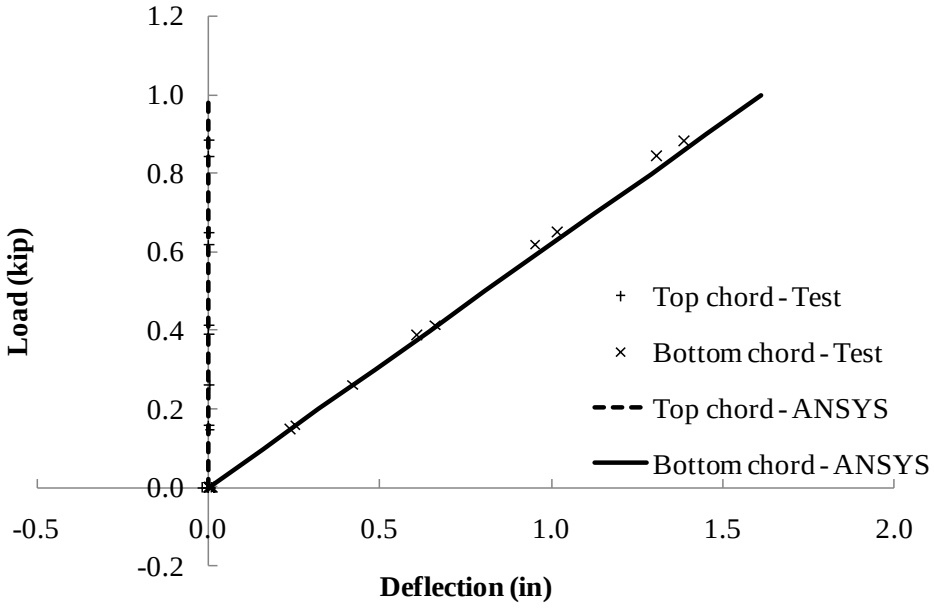

Figure A.82 Lateral deflection at 24 feet - Bottom chord loading and top chord restrained

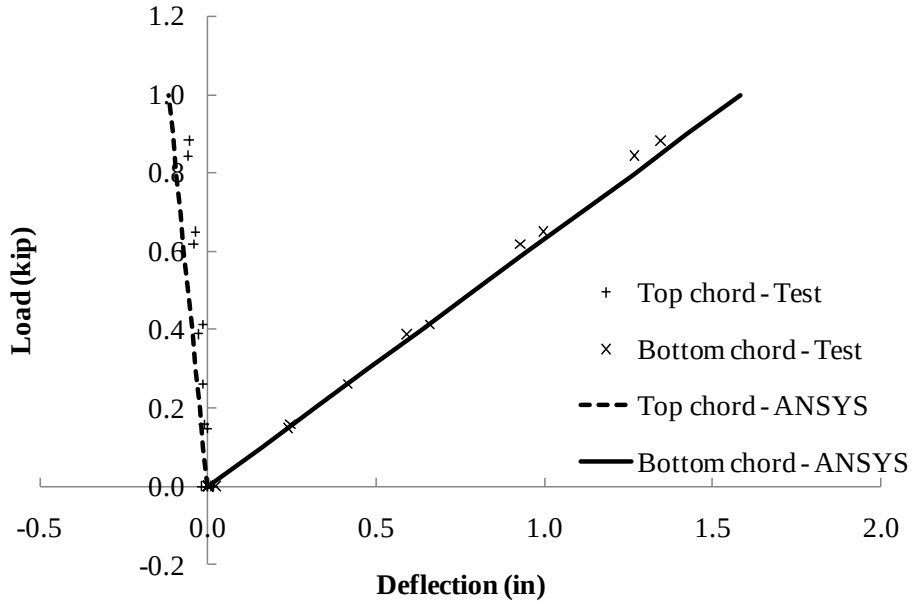

Figure A.83 Lateral deflection at midspan - Bottom chord loading and top chord restrained

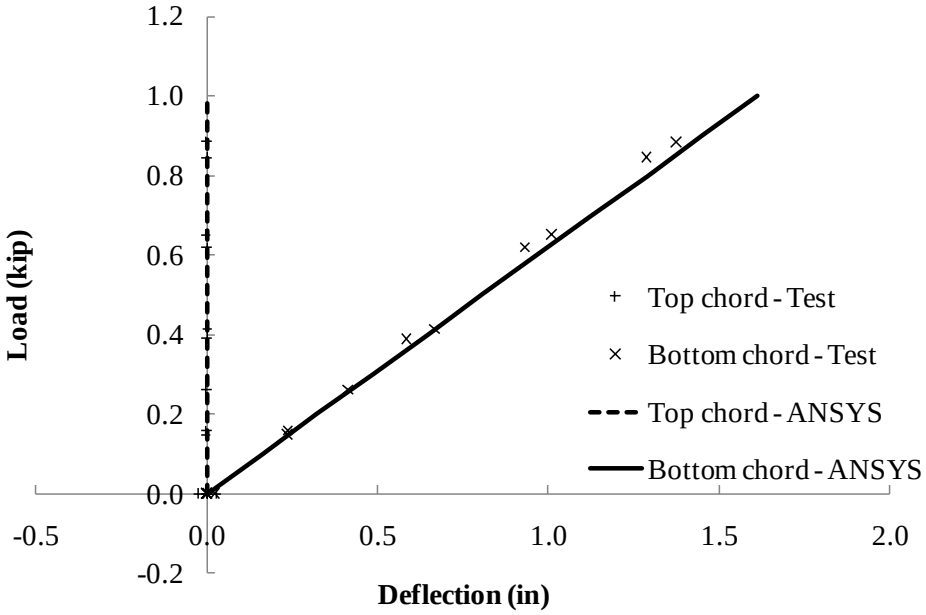

Figure A.84 Lateral deflection at 48 feet - Bottom chord loading and top chord restrained

A.10 MIDSPAN DEFLECTION VERIFICATION OF TRUSS WITHOUT INTERMEDIATE BRACING

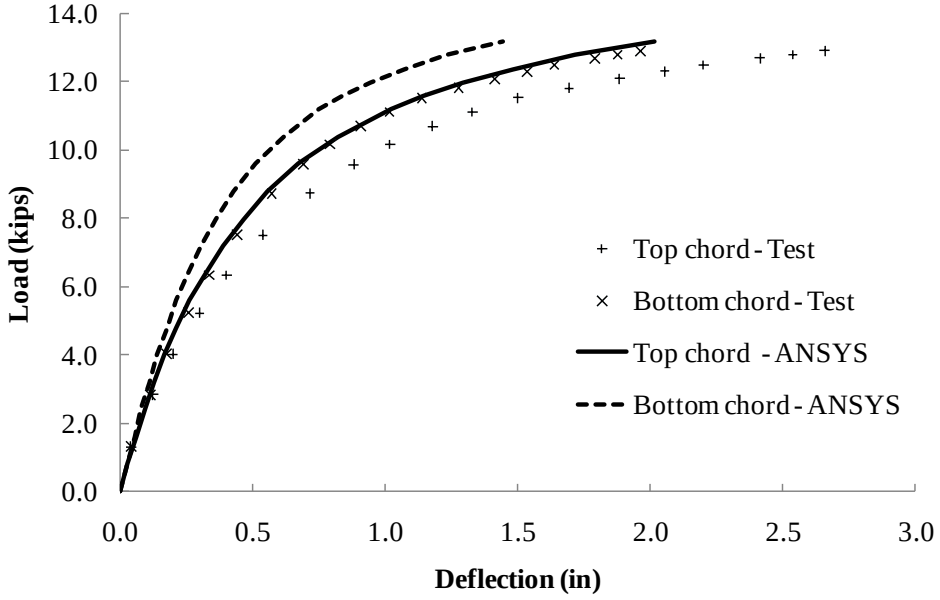

Figure A.85 Lateral deflection of 48 feet truss - Bottom chord loading

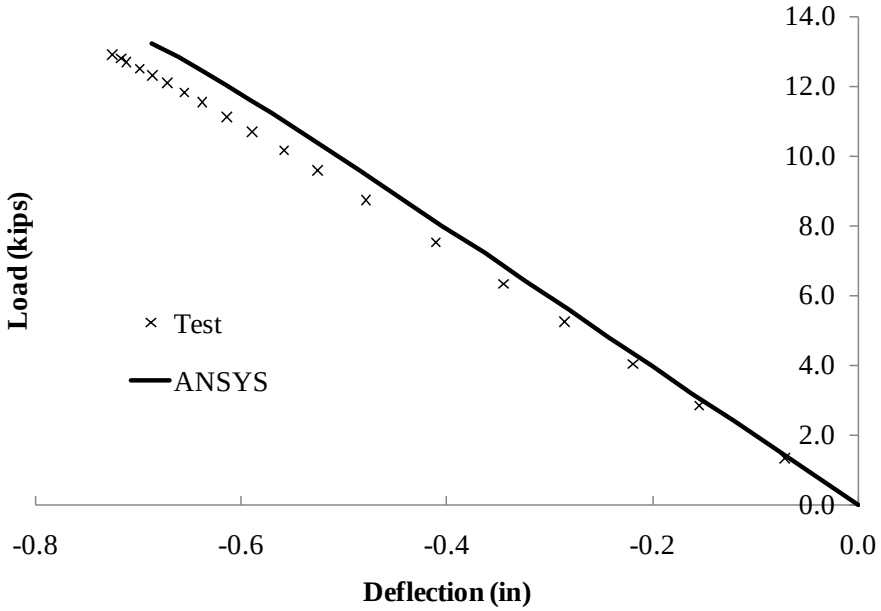

Figure A.86 Vertical deflection of 48 feet truss - Bottom chord loading

A.11 MIDSPAN DEFLECTION VERIFICATION OF TRUSS WITH TORSIONAL BRACING

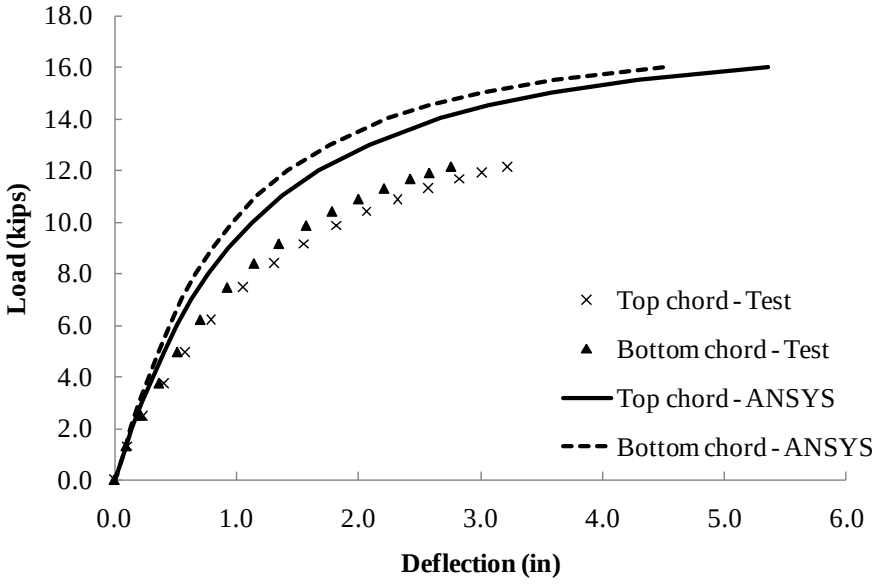

Figure A.87 Lateral deflection of truss with 2 large torsional braces at bottom chord (with connection stiffener)

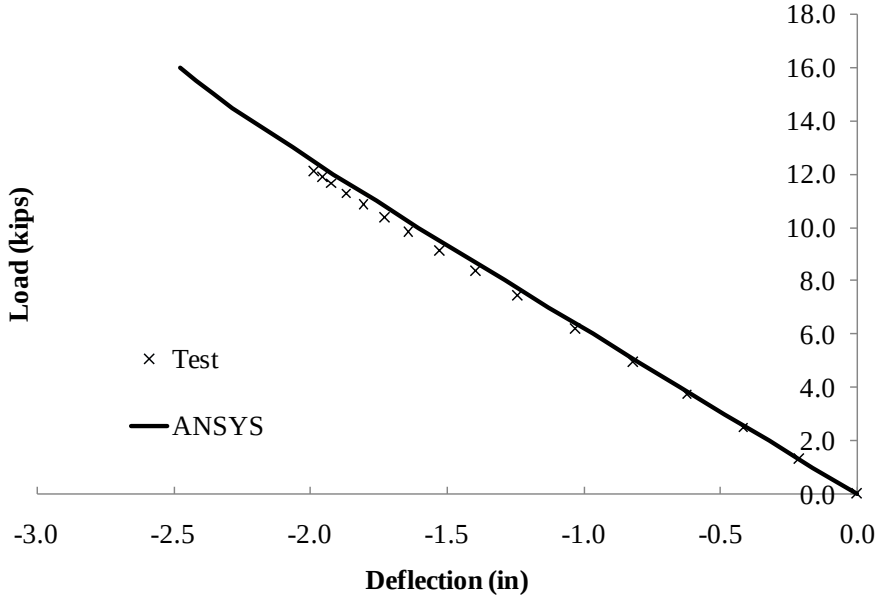

Figure A.88 Vertical deflection of truss with 2 large torsional braces at bottom chord (with connection stiffener)

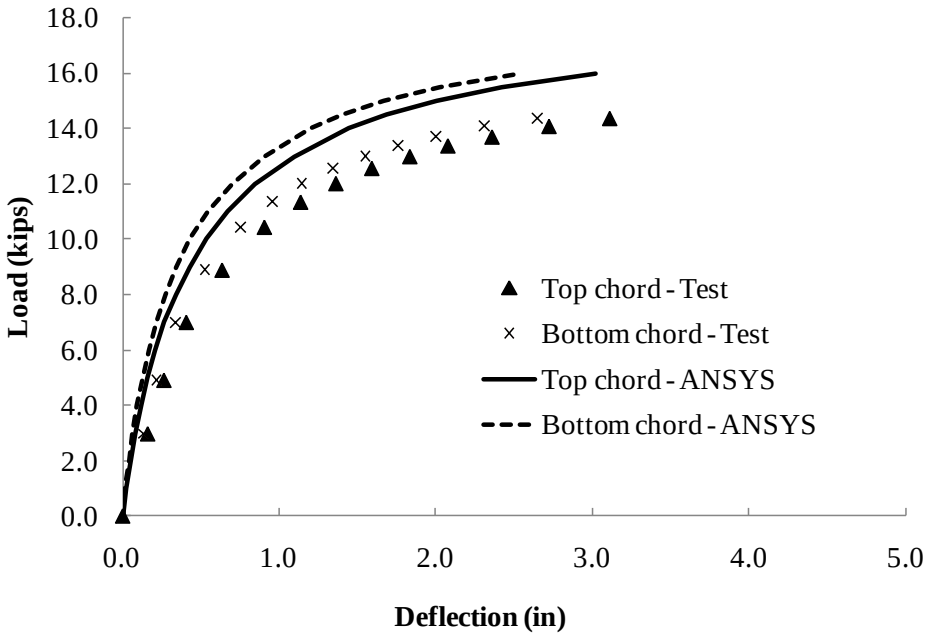

Figure A.89 Lateral deflection of truss with 3 small torsional braces at top chord (with connection stiffener)

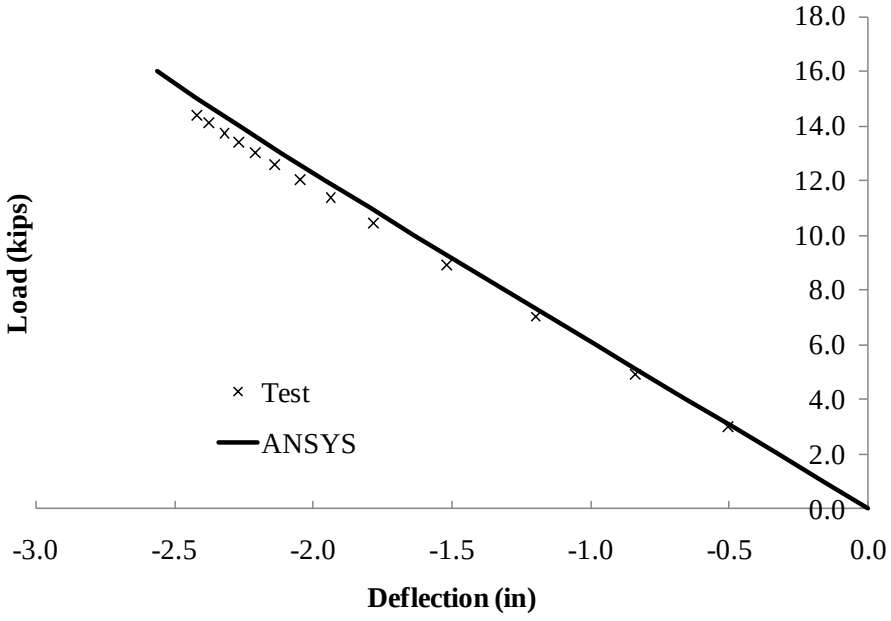

Figure A.90 Vertical deflection of truss with 3 small torsional braces at top chord (with connection stiffener)

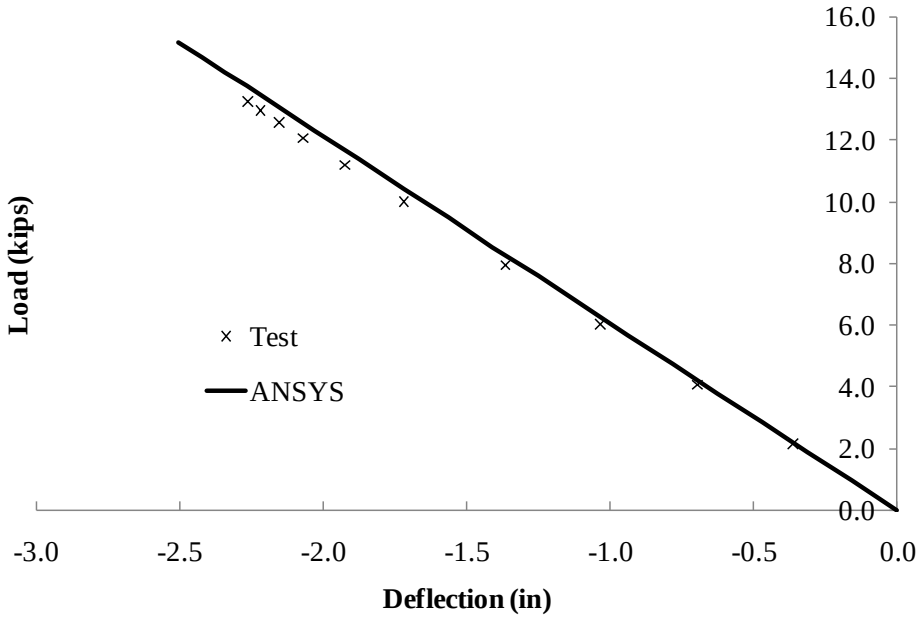

Figure A.91 Vertical deflection of truss with 2 large torsional braces at top chord (with connection stiffener)

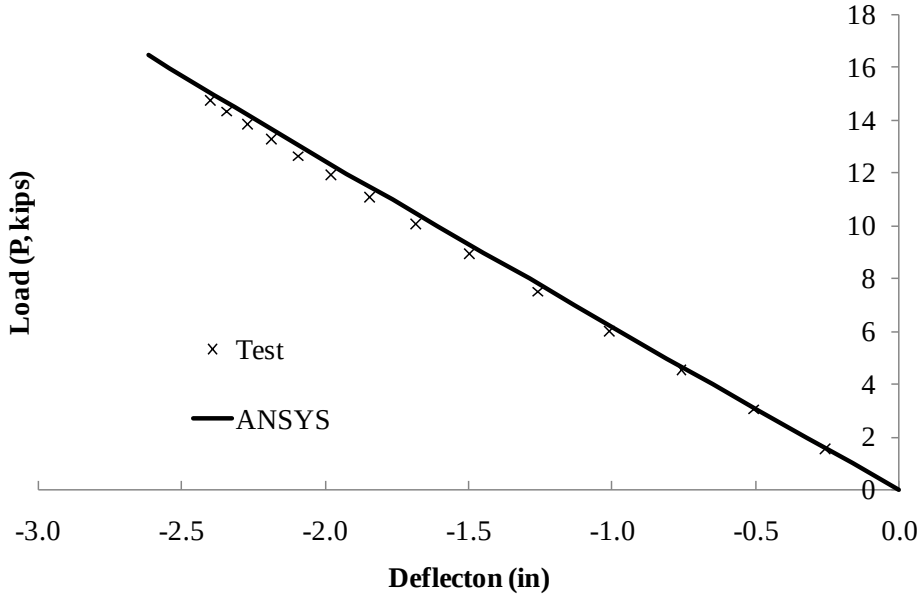

Figure A.92 Vertical deflection of truss with 3 large torsional braces at bottom chord (with connection stiffener)

A.12 VERIFICATION OF STRAIN IN TORSIONAL BRACES

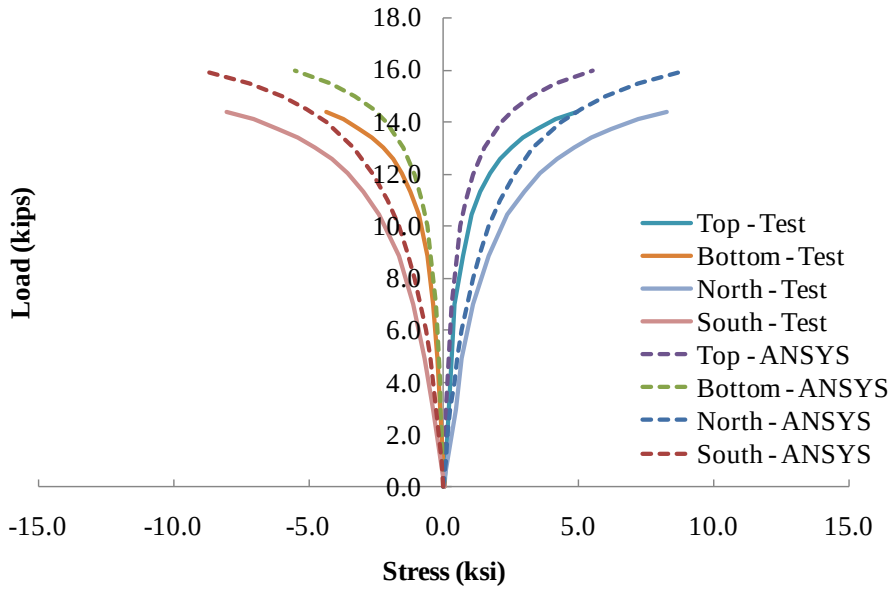

Figure A.93 Strain in South brace at quarter point of truss with 3 small torsional braces at top chord

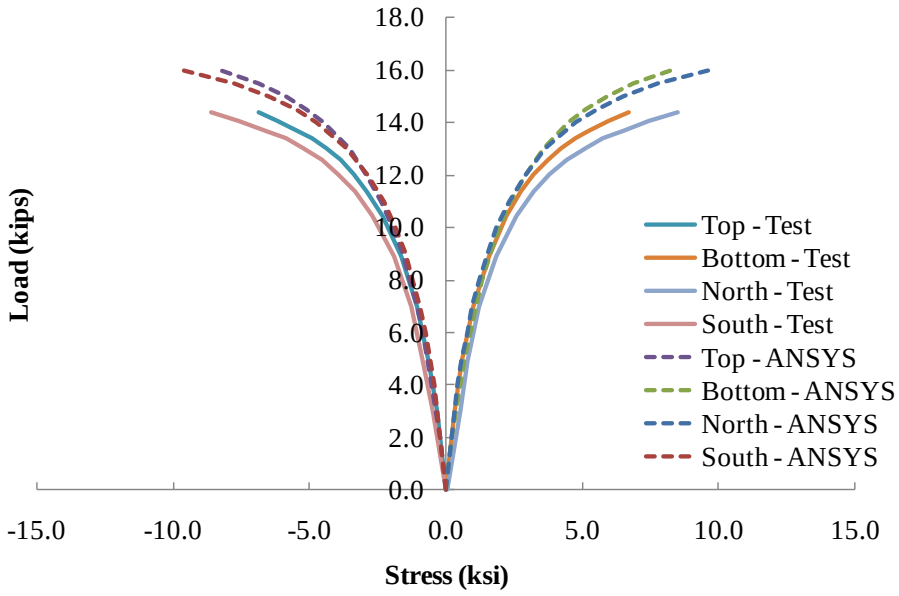

Figure A.94 Strain in North brace at three quarter point of truss with 3 small torsional braces at top chord

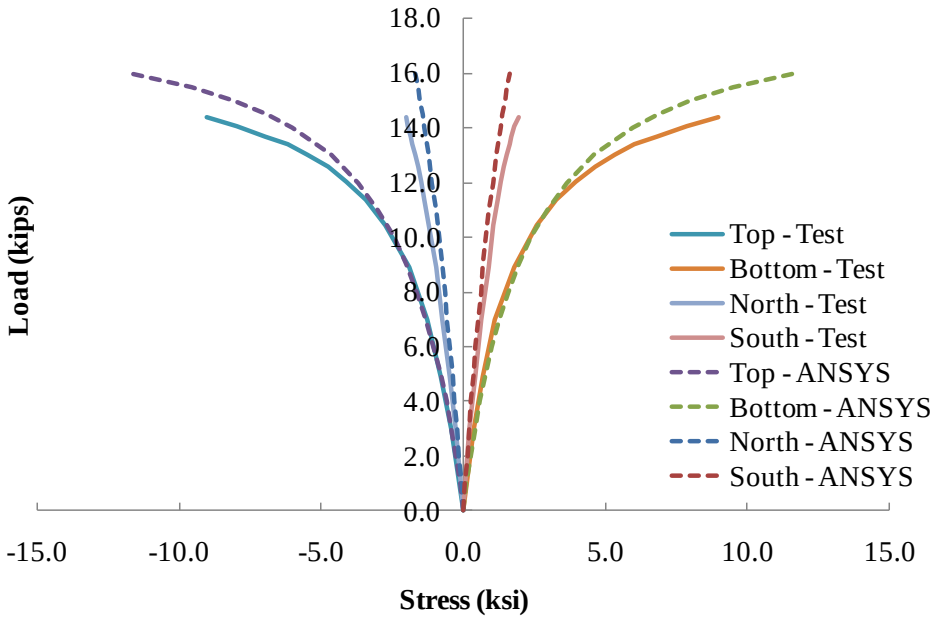

Figure A.95 Strain in midspan brace at three quarter point of truss with 3 small torsional braces at top chord

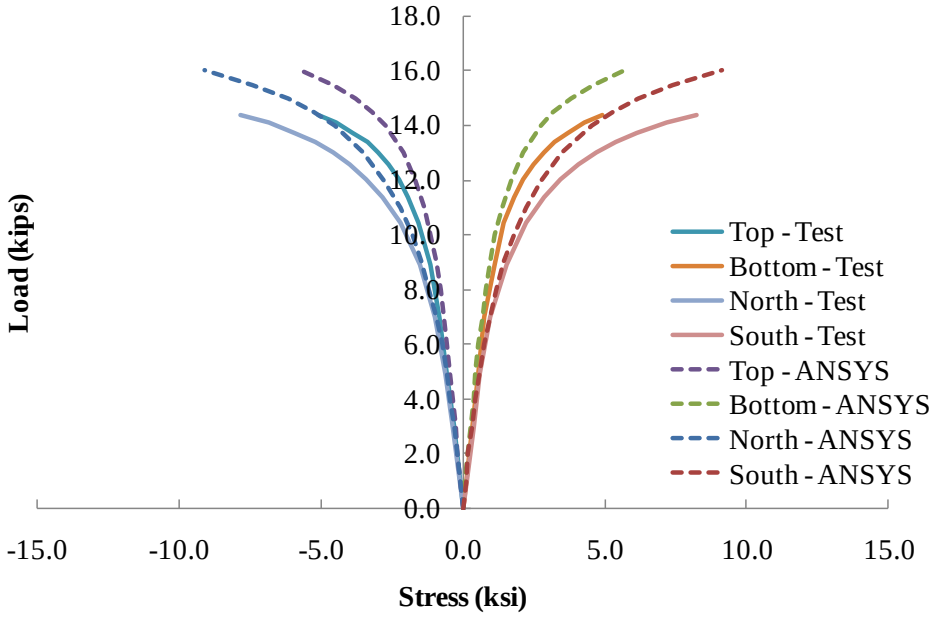

Figure A.96 Strain in South brace at three quarter point of truss with 3 small torsional braces at top chord

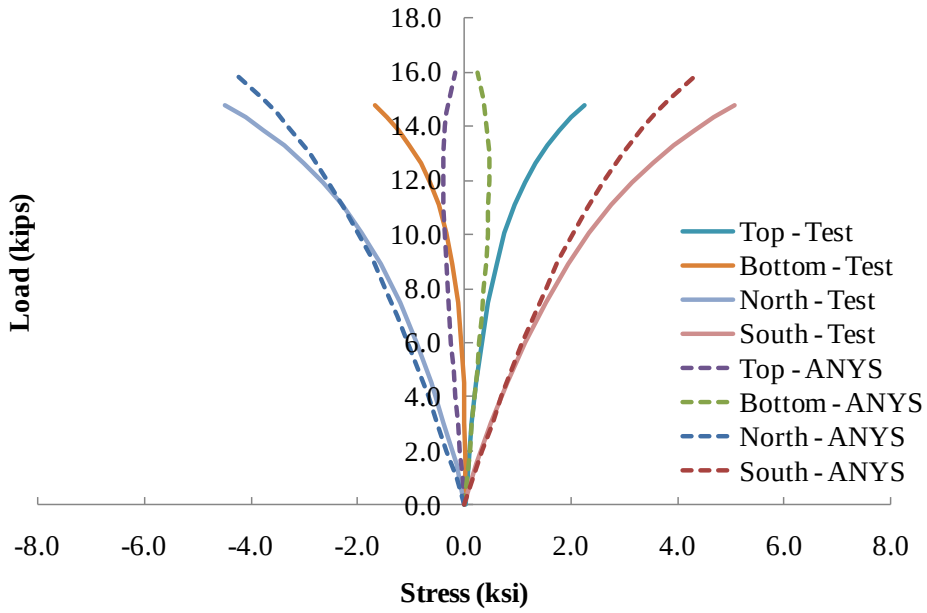

Figure A.97 Strain in North brace at quarter point of truss with 3 large torsional braces at bottom chord

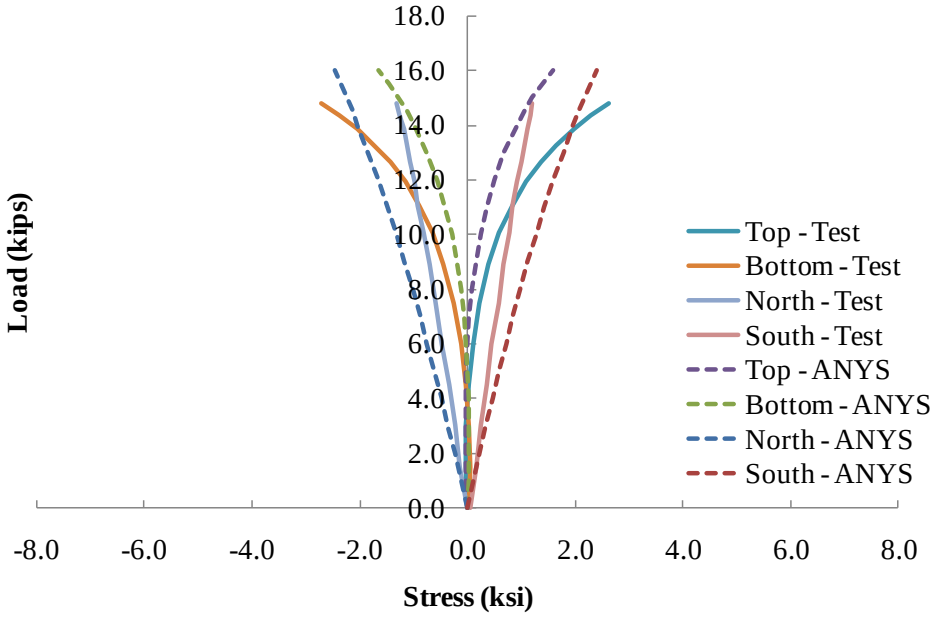

Figure A.98 Strain in midspan brace at quarter point of truss with 3 large torsional braces at bottom chord

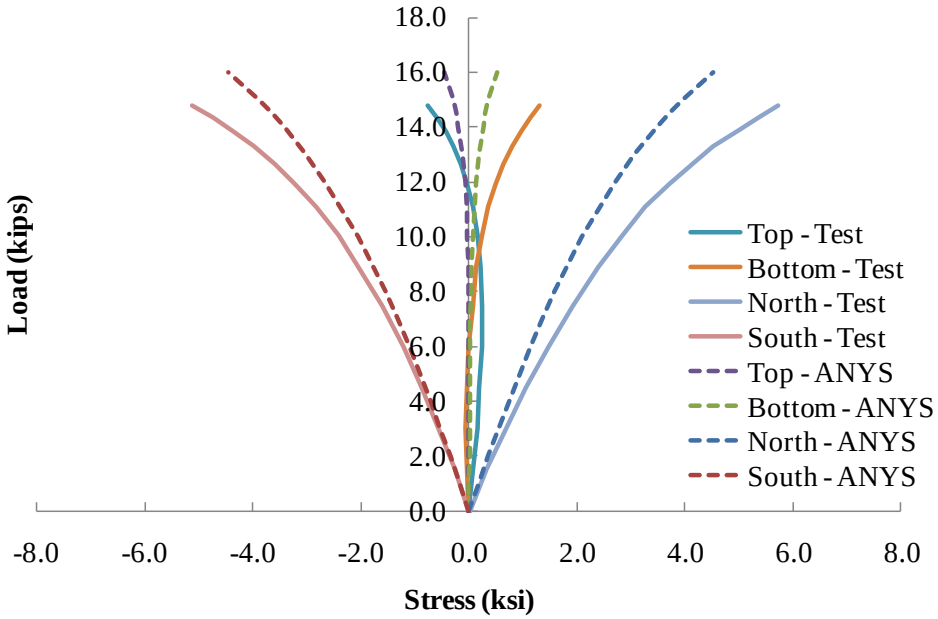

Figure A.99 Strain in North brace at three quarter point of truss with 3 large torsional braces at bottom chord

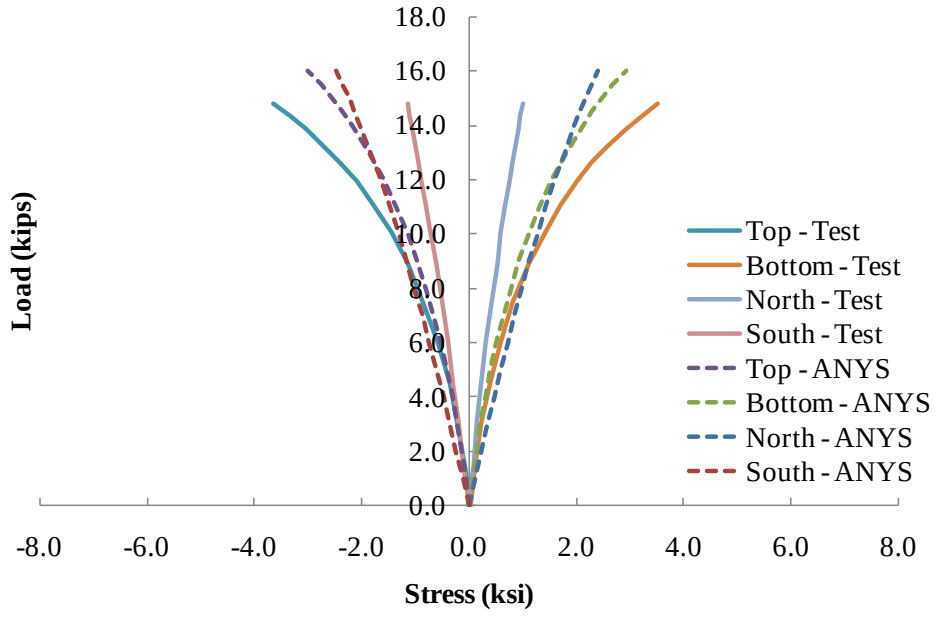

Figure A.100 Strain in midspan brace at three quarter point of truss with 3 large torsional braces at bottom chord

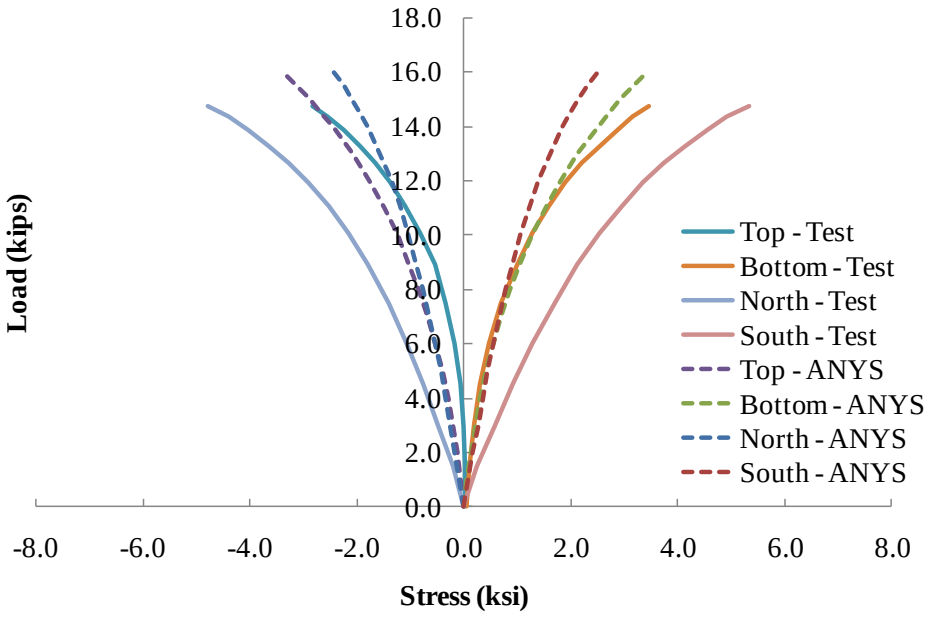

Figure A.101 Strain in South brace at three quarter point of truss with 3 large torsional braces at bottom chord

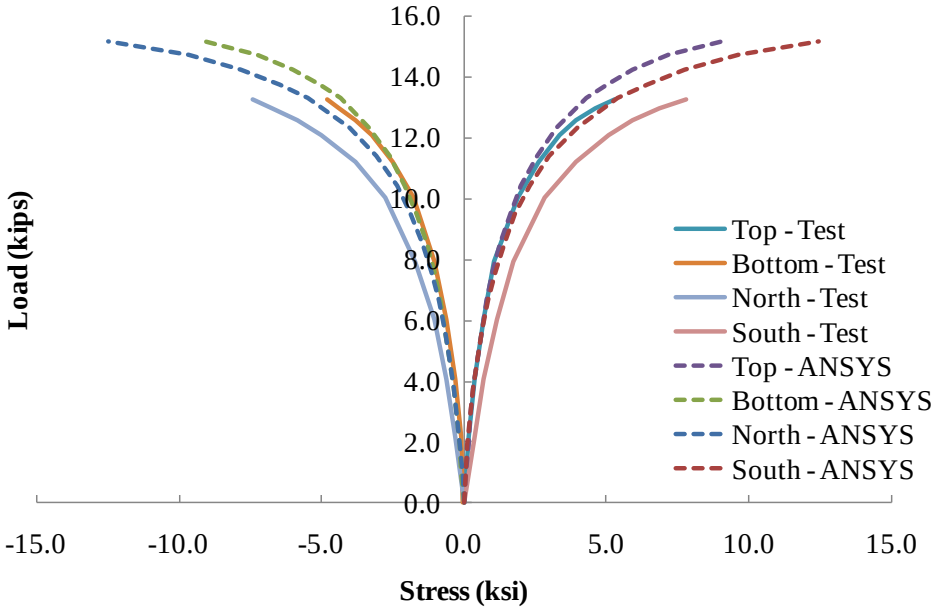

Figure A.102 Strain in North brace at quarter point of truss with 2 large torsional braces at top chord

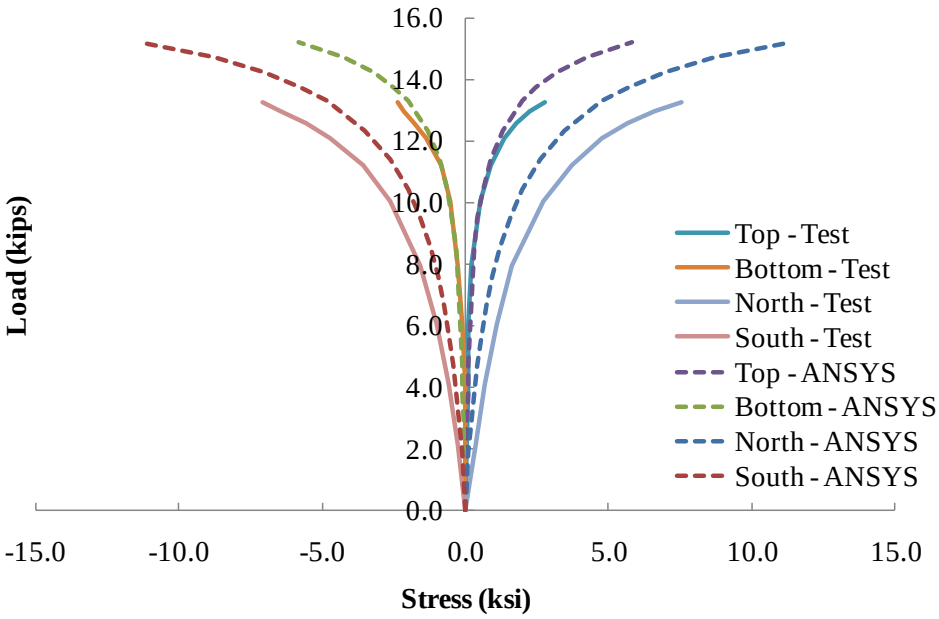

Figure A.103 Strain in South brace at quarter point of truss with 2 large torsional braces at top chord

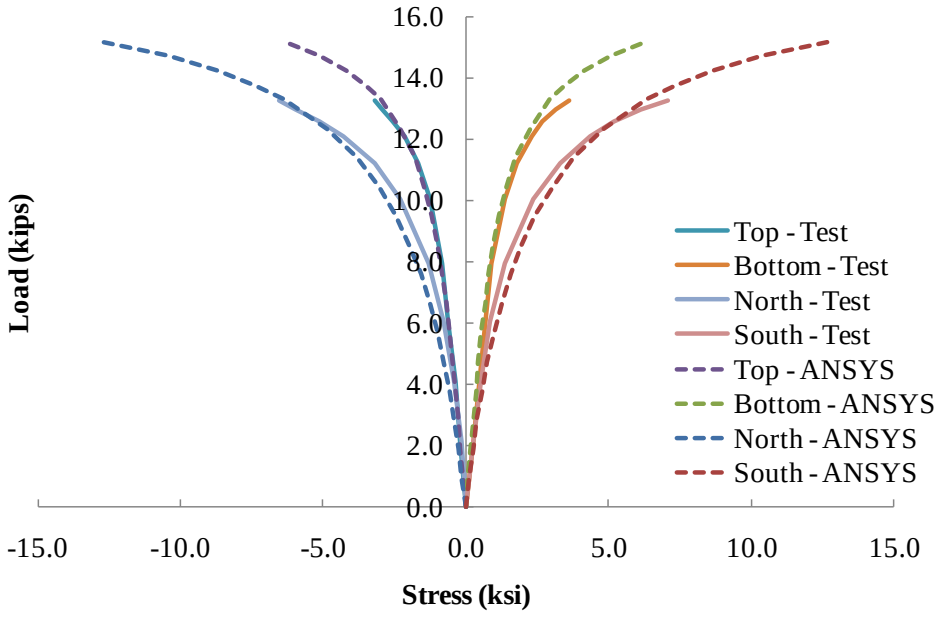

Figure A.104 Strain in South brace at three quarter point of truss with 2 large torsional braces at top chord

A.13 CALIBRATION OF LATERAL BRACES

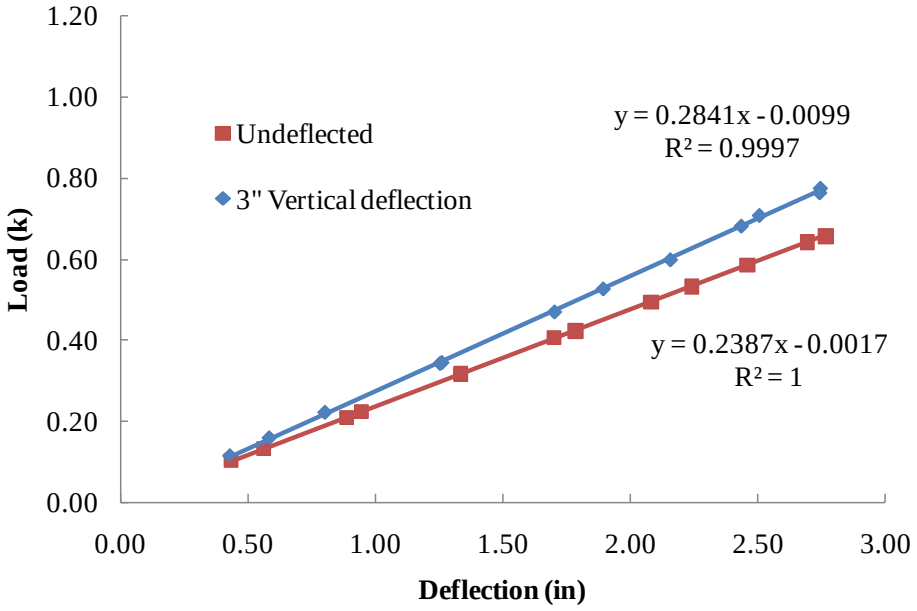

Figure A.105 Aluminum brace - K_{design} = 0.2 k/in

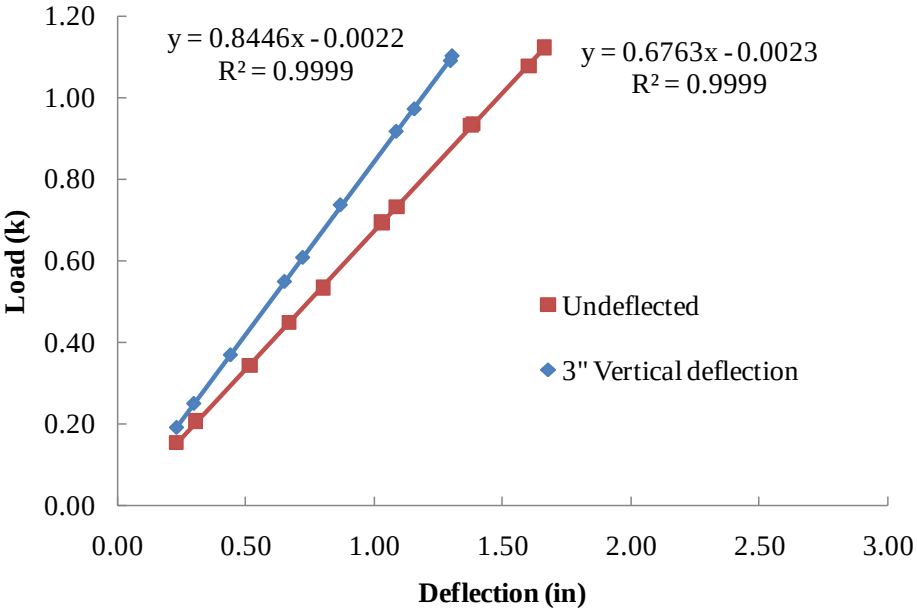

Figure A.106 Aluminum brace - K_{design} = 0.5 k/in

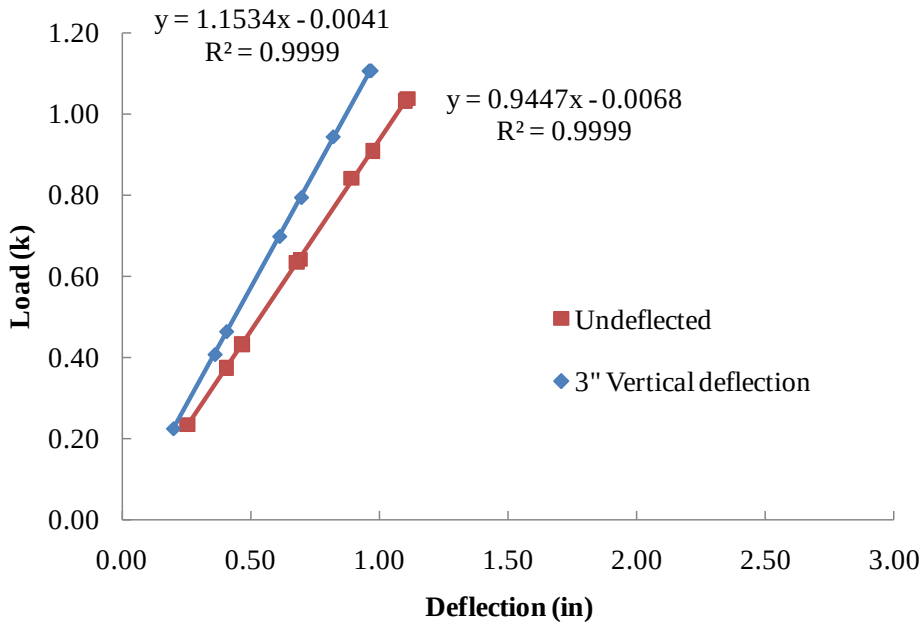

Figure A.107 Aluminum brace - K_{design} = 0.8 k/in

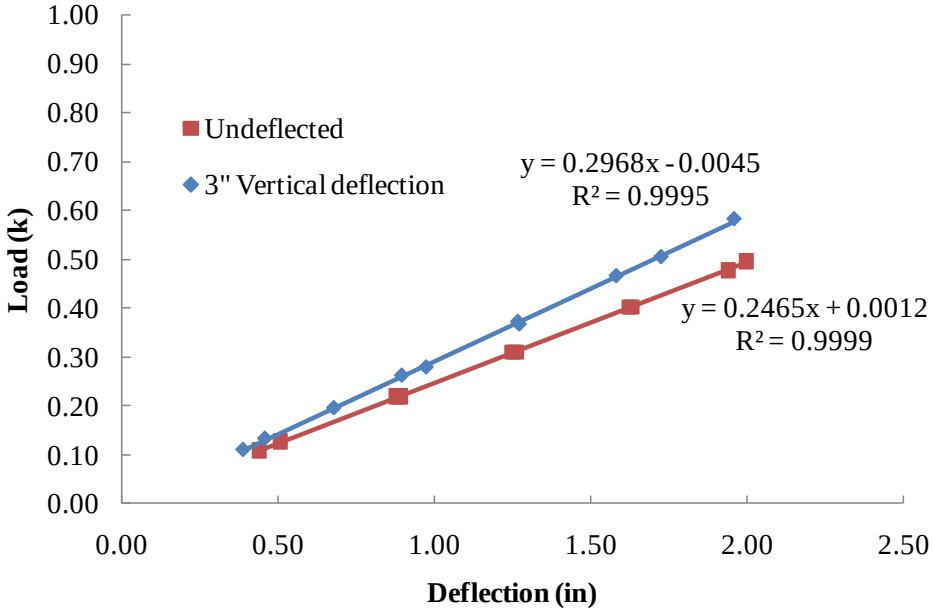

Figure A.108 Steel brace - K_{design} =0.2 k/in

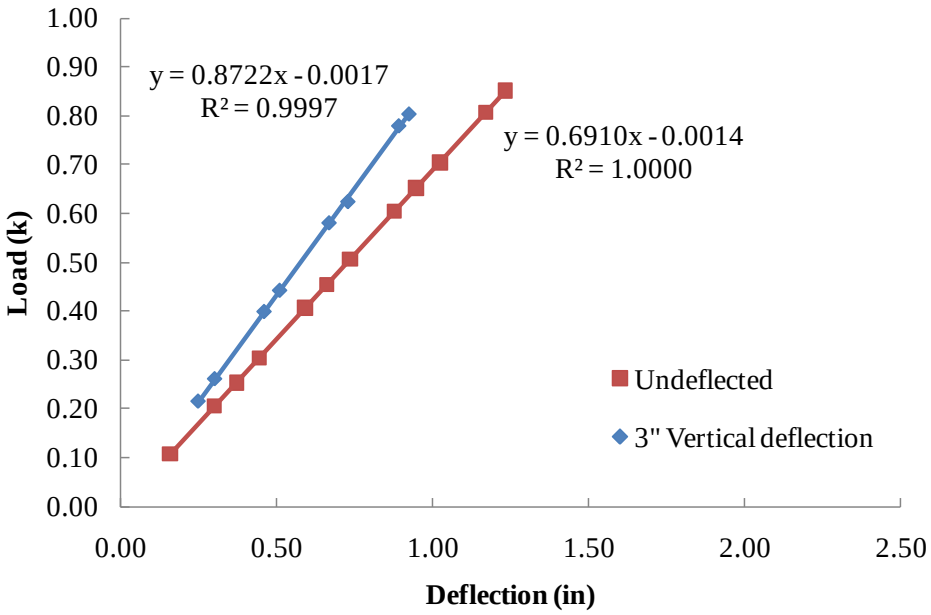

Figure A.109 Steel brace - K_{design} =0.5 k/in

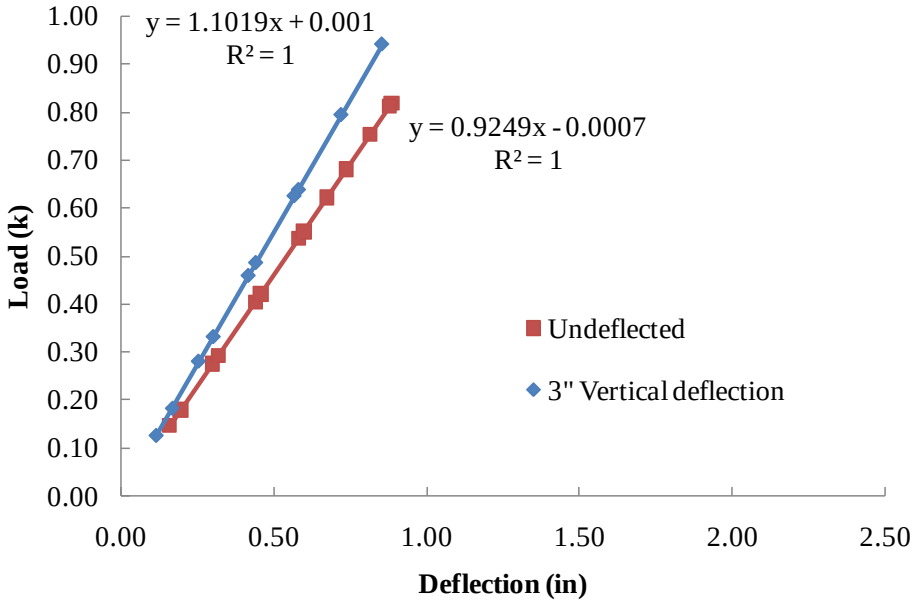

Figure A.110 Steel brace - K_{design} =0.8 k/in

APPENDIX B

Parametric Study Results

The main chapters of this dissertation presented representative results from the parametric studies that were conducted using the ANSYS finite element model. This appendix contains additional results from the parametric investigation.

B.1 SECTION PROPERTIES

Table B.1 Chord and web elements section properties

Name	Details	Width (in)	Depth (in)	Flg Thk (in)	Web Thk (in)
Very Flexible	W3x8	5.00	3.00	0.19	0.20
	Conn.	6.00	3.30	0.65	0.28
Flexible	W4x13	4.00	4.16	0.35	0.28
	Conn.	6.00	4.91	0.72	0.28
Moderate	W8x24	6.50	7.93	0.40	0.245
	Conn.	9.00	9.03	0.95	0.245
Stiff (Web)	W12x26	6.49	12.20	0.38	0.23
	Conn.	8.90	13.40	0.98	0.23
Stiff (Chord)	W12x50	8.08	12.20	0.64	0.37
	Conn.	11.40	13.92	1.50	0.37

Conn. = Connection element

Table B.2 Torsional brace section properties

No.	Element	Width (in)	Height (in)	Web Thk (in)	Flg Thk (in)
1	Brace	2.94	1.50	0.25	0.25
	Connection	4.40	1.90	0.75	0.25
2	Brace	2.70	2.00	0.25	0.25
	Connection	4.00	2.50	0.75	0.25
3	Brace	2.40	2.90	0.25	0.25
	Connection	3.50	3.50	0.75	0.25
4	Brace	2.13	4.00	0.25	0.25
	Connection	3.10	4.40	1.00	0.25
5	Brace	2.05	4.50	0.25	0.25
	Connection	3.00	4.85	1.00	0.25
6	Brace	1.96	5.00	0.25	0.25
	Connection	2.90	5.30	1.00	0.25
7	Brace	1.88	5.50	0.25	0.25
	Connection	2.82	5.75	1.00	0.25
8	Brace	1.82	6.00	0.25	0.25
	Connection	2.75	6.20	1.00	0.25
9	Brace	1.71	7.00	0.25	0.25
	Connection	2.65	7.00	1.00	0.25
10	Brace	1.62	8.00	0.25	0.25
	Connection	2.50	8.00	1.00	0.25
11	Brace	1.37	12.00	0.25	0.25
	Connection	2.20	11.60	1.00	0.25

B.2 Comparison of Truss with Regular and Rigid Web with Torsional Bracing and Cross Frame Subjected to Uniform Load

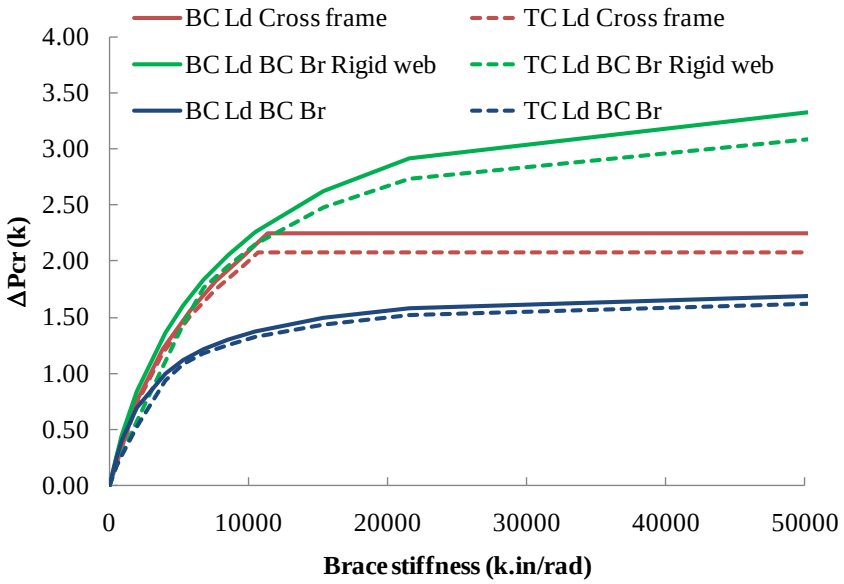

Figure B.1 Comparison of buckling capacity of 96-ft span moderate chord and very flexible web truss with uniform load and bottom chord bracing

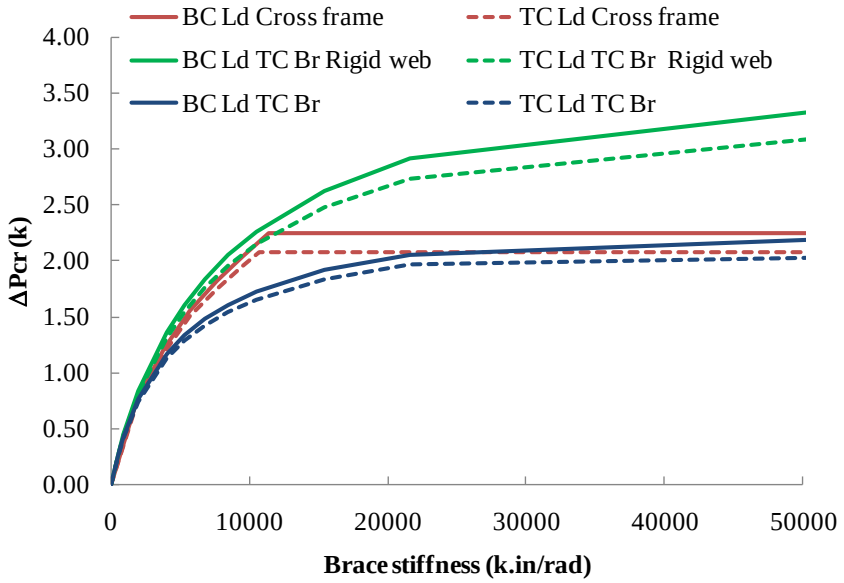

Figure B.2 Comparison of buckling capacity of 96-ft span moderate chord and very flexible web truss with uniform load and top chord bracing

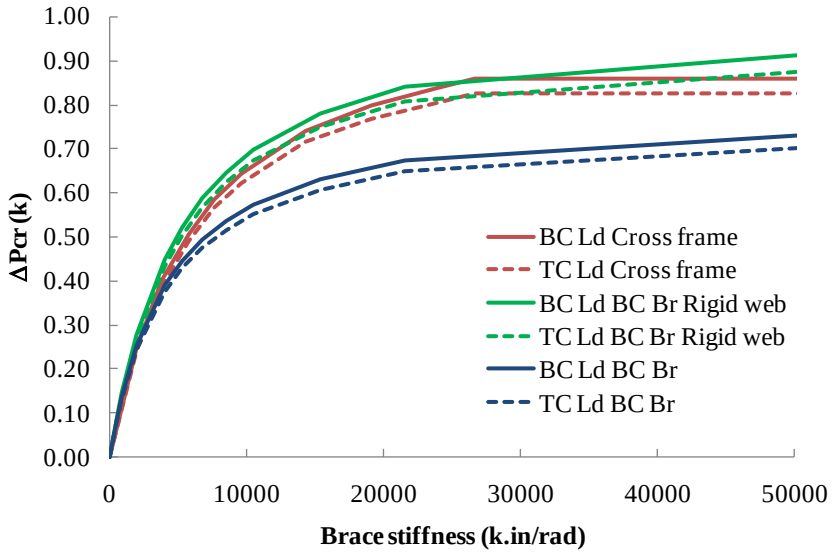

Figure B.3 Comparison of buckling capacity of 96-ft span flexible chord and flexible web truss with uniform load and bottom chord bracing

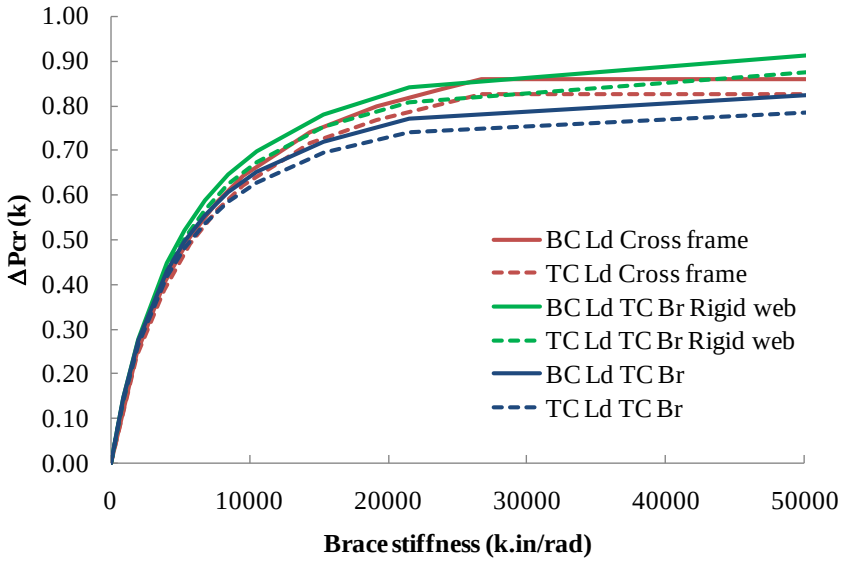

Figure B.4 Comparison of buckling capacity of 96-ft span flexible chord and flexible web truss with uniform load and top chord bracing

B.3 Comparison of the Buckling Capacity of Truss with the Same Unbraced Length with Stiffness per Unit Length

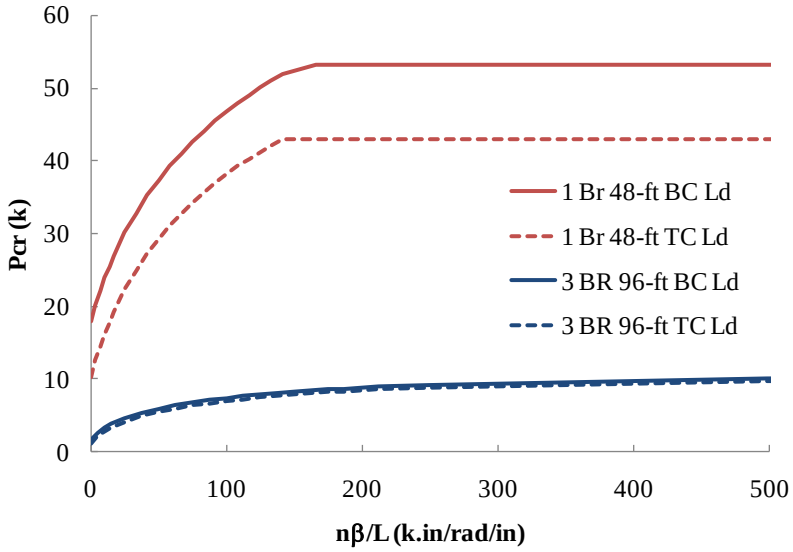

Figure B.5 Comparison of moderate chord and flexible web truss with 24-ft unbraced length

APPENDIX C

Stiffness Requirements for Torsional Bracing of Truss Systems

Chapter 7 of this dissertation made use of the finite element results to develop stiffness requirements for truss systems a torsional brace at midspan. Representative results were presented in Chapter 7. This Appendix presents supplementary results and comparisons with the proposed expressions.

C.1 Buckling Capacity (P_{cr}) and Ideal Stiffness (β_i) of Truss with Single Cross Frame at Midspan

C.1.1 Truss with Regular Web

Table C.1 48-ft span truss with 3-ft depth

Chord	Web	Unf Ld - BC		Unf Ld - TC		Unf moment	
		P_{cr} (k)	β_i (k.in/rad)	P_{cr} (k)	β_i (k.in/rad)	M_{cr} (k.in)	β_i (k.in/rad)
W4x13	W3x8	7.24	14116	6.47	13669	4126	12336
	W4x13	11.16	36781	10.30	36532	6317	34702
W8x24	W3x8	28.24	22001	23.06	20943	15729	18014
	W4x13	36.38	38277	31.13	37280	20583	33274
W12x50	W3x8	103.24	58592	82.65	58504	59978	53747
	W4x13	119.11	85927	95.64	82472	66456	62762
	W8x24	191.95	290870	167.47	293672	108923	307280
	W12x26	267.58	1245875	242.15	1352493	-	-

- = No full sine buckling mode shape

Table C.2 48-ft span truss with 6-ft depth

Chord	Web	Unf Ld - BC		Unf Ld - TC		Unf moment	
		P_{cr} (k)	β_i (k.in/rad)	P_{cr} (k)	β_i (k.in/rad)	M_{cr} (k.in)	β_i (k.in/rad)
W4x13	W3x8	9.19	19418	7.71	17216	5066	14472
	W4x13	12.67	46319	11.14	44891	7097	36467
W8x24	W3x8	45.92	61254	36.65	58305	25758	46339
	W4x13	53.27	87786	43.01	81310	29057	62267
W12x50	W3x8	*	*	*	*	111259	199182
	W4x13	*	*	*	*	114913	206190
	W8x24	263.59	488763	216.06	451554	144496	349518
	W12x26	328.43	991209	280.31	981909	182774	807269

* = Local buckling

Table C.3 72-ft span truss with 3-ft depth

Chord	Web	Unf Ld - BC		Unf Ld - TC		Unf moment	
		P_{cr} (k)	β_i (k.in/rad)	P_{cr} (k)	β_i (k.in/rad)	M_{cr} (k.in)	β_i (k.in/rad)
W4x13	W3x8	1.97	9920	1.82	9923	2602	10370
	W4x13	3.13	35906	2.97	35914	4102	36447
W8x24	W3x8	6.72	10353	5.70	9869	8683	9059
	W4x13	9.40	27158	8.38	26817	12387	25560
W12x50	W3x8	23.47	24188	18.75	23057	29718	20221
	W4x13	27.58	35476	22.84	34177	35380	30364
	W8x24	51.68	261768	46.85	270531	68129	365642
	W12x26	-	-	-	-	-	-

\- = No full sine buckling mode shape

Table C.4 72-ft span truss with 6-ft depth

Chord	Web	Unf Ld - BC		Unf Ld - TC		Unf moment	
		P_{cr} (k)	β_i (k.in/rad)	P_{cr} (k)	β_i (k.in/rad)	M_{cr} (k.in)	β_i (k.in/rad)
W4x13	W3x8	2.25	10063	1.96	9773	2902	8177
	W4x13	3.32	31047	3.03	30835	4359	27092
W8x24	W3x8	10.10	22149	8.08	20729	12581	16204
	W4x13	12.14	36952	10.11	34840	15374	26993
W12x50	W3x8	38.65	75499	31.39	74828	51734	62304
	W4x13	44.29	100957	35.03	91257	54134	66534
	W8x24	62.72	219895	53.30	215926	80208	195946
	W12x26	84.15	693404	74.69	699129	109631	636487

Table C.5 96-ft span truss with 3-ft depth

Chord	Web	Unf Ld - BC		Unf Ld - TC		Unf moment	
		P_{cr} (k)	β_i (k.in/rad)	P_{cr} (k)	β_i (k.in/rad)	M_{cr} (k.in)	β_i (k.in/rad)
W4x13	W3x8	0.80	9273	0.75	9297	1909	10685
	W4x13	1.29	83284	1.24	83657	3045	156550
W8x24	W3x8	2.53	6812	2.21	6707	5948	6497
	W4x13	3.72	23383	3.40	23369	8895	24167
W12x50	W3x8	8.16	12930	6.66	12262	18666	10953
	W4x13	10.12	24113	8.63	23338	23584	20930
	W8x24	20.85	564899	19.33	649743	-	-
	W12x26	-	-	-	-	-	-

- = No full sine buckling mode shape

Table C.6 96-ft span truss with 6-ft depth

Chord	Web	Unf Ld - BC		Unf Ld - TC		Unf moment	
		P_{cr} (k)	β_i (k.in/rad)	P_{cr} (k)	β_i (k.in/rad)	M_{cr} (k.in)	β_i (k.in/rad)
W4x13	W3x8	0.86	6743	0.77	6679	2031	6233
	W4x13	1.32	26669	1.23	26690	3157	26348
W8x24	W3x8	3.47	11367	2.83	10721	7829	8651
	W4x13	4.42	22122	3.79	21301	10220	16803
W12x50	W3x8	13.59	37631	10.66	34782	30335	27396
	W4x13	14.96	49525	11.99	45011	33501	35274
	W8x24	23.53	141369	20.58	139963	54910	130790
	W12x26	33.05	829919	30.10	882869	78386	1003980

C.1.2 Truss with Simplified Web

Table C.7 48-ft span truss with 3-ft depth

Chord	Web	Unf Ld - BC		Unf Ld - TC		Unf moment	
		P_{cr} (k)	β_i (k.in/rad)	P_{cr} (k)	β_i (k.in/rad)	M_{cr} (k.in)	β_i (k.in/rad)
W4x13	W3x8	3.27	2173	2.52	1812	1664	1215
	W4x13	3.28	2183	2.53	1821	1673	1220
W8x24	W3x8	23.33	15882	17.93	13644	11859	9353
	W4x13	23.33	15852	17.94	13625	11867	9344
W12x50	W3x8	108.04	77458	82.98	61735	54731	39379
	W4x13	107.77	67437	82.82	61261	54738	39185
	W8x24	107.42	66912	82.58	60789	54777	39048
	W12x26	107.42	66885	82.58	60763	54773	39032

Table C.8 48-ft span truss with 6-ft depth

Chord	Web	Unf Ld - BC		Unf Ld - TC		Unf moment	
		P_{cr} (k)	β_i (k.in/rad)	P_{cr} (k)	β_i (k.in/rad)	M_{cr} (k.in)	β_i (k.in/rad)
W4x13	W3x8	6.52	8624	5.02	7150	3318	4764
	W4x13	6.53	8629	5.03	7159	3327	4771
W8x24	W3x8	46.35	65230	35.70	56040	23580	37606
	W4x13	46.32	64489	35.69	55479	22658	32783
W12x50	W3x8	213.90	336433	164.87	298700	108552	193556
	W4x13	213.31	321629	164.46	250059	108560	157583
	W8x24	212.68	309643	163.99	243837	108582	155215
	W12x26	212.65	308670	163.97	243334	108579	155002

Table C.9 72-ft span truss with 3-ft depth

Chord	Web	Unf Ld - BC		Unf Ld - TC		Unf moment	
		P_{cr} (k)	β_i (k.in/rad)	P_{cr} (k)	β_i (k.in/rad)	M_{cr} (k.in)	β_i (k.in/rad)
W4x13	W3x8	0.63	610	0.48	533	742	388
	W4x13	0.63	603	0.48	536	748	392
W8x24	W3x8	4.50	4367	3.45	3888	5321	2776
	W4x13	4.50	4370	3.45	3888	5327	2777
W12x50	W3x8	20.99	21917	16.07	18818	24780	13393
	W4x13	20.96	21781	16.06	18724	24785	13347
	W8x24	20.94	21584	16.04	18634	24802	13317
	W12x26	20.93	21572	16.04	18626	24800	13313

Table C.10 72-ft span truss with 6-ft depth

Chord	Web	Unf Ld - BC		Unf Ld - TC		Unf moment	
		P_{cr} (k)	β_i (k.in/rad)	P_{cr} (k)	β_i (k.in/rad)	M_{cr} (k.in)	β_i (k.in/rad)
W4x13	W3x8	1.25	2409	0.96	2123	1479	1554
	W4x13	1.25	2414	0.96	2146	1485	1560
W8x24	W3x8	8.93	17343	6.86	15501	10578	11038
	W4x13	8.93	17287	6.86	15449	10584	11013
W12x50	W3x8	41.55	91744	31.91	79338	49129	55510
	W4x13	41.49	89584	31.87	77553	49135	54685
	W8x24	41.43	87831	31.83	75835	49146	54037
	W12x26	41.43	87694	31.83	75726	49145	57363

Table C.11 96-ft span truss with 3-ft depth

Chord	Web	Unf Ld - BC		Unf Ld - TC		Unf moment	
		P_{cr} (k)	β_i (k.in/rad)	P_{cr} (k)	β_i (k.in/rad)	M_{cr} (k.in)	β_i (k.in/rad)
W4x13	W3x8	0.20	255	0.15	220	418	163
	W4x13	0.20	255	0.15	220	422	165
W8x24	W3x8	1.40	1785	1.08	1598	3004	1140
	W4x13	1.41	1793	1.08	1598	3008	1141
W12x50	W3x8	6.57	9008	5.02	7761	14032	5589
	W4x13	6.57	8979	5.02	7741	14036	5580
	W8x24	6.56	8950	5.02	7722	14046	5576
	W12x26	6.56	8950	5.02	7722	14045	5574

Table C.12 96-ft span truss with 6-ft depth

Chord	Web	Unf Ld - BC		Unf Ld - TC		Unf moment	
		P_{cr} (k)	β_i (k.in/rad)	P_{cr} (k)	β_i (k.in/rad)	M_{cr} (k.in)	β_i (k.in/rad)
W4x13	W3x8	0.39	1011	0.30	883	833	646
	W4x13	0.39	1022	0.30	888	837	649
W8x24	W3x8	2.79	7067	2.14	6335	5970	4483
	W4x13	2.79	7057	2.14	6327	5974	4480
W12x50	W3x8	13.00	36752	9.97	31565	27814	22387
	W4x13	12.99	36286	9.96	31216	27818	17455
	W8x24	12.98	35908	9.96	30936	27825	22117
	W12x26	12.98	35876	9.96	30921	27824	22106

C.2 VERIFICATION OF THE ESTIMATION OF THE BUCKLING CAPACITY OF TRUSS WITH CROSS FRAME

C.2.1 Uniform Load Cases

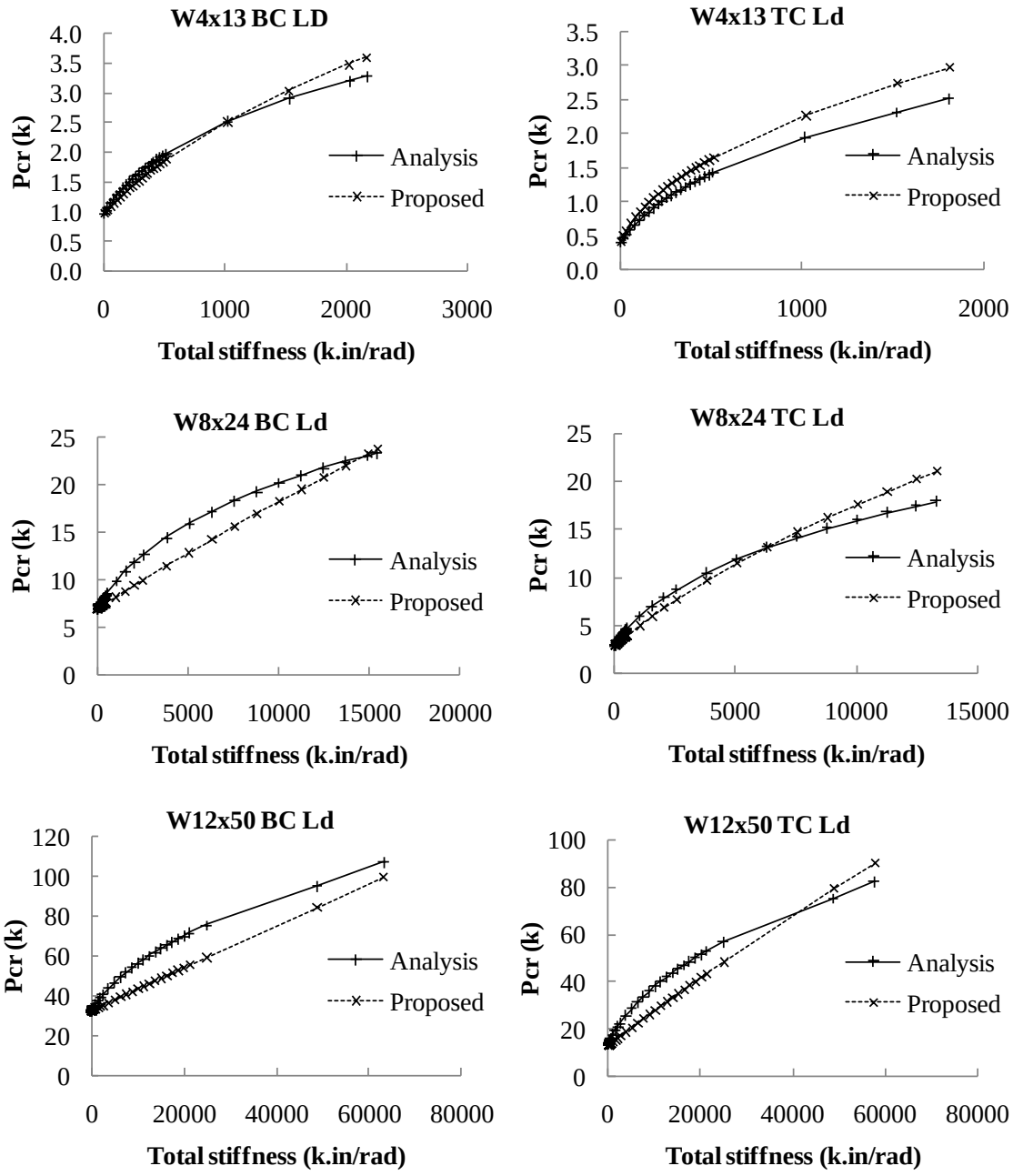

Figure C.1 48-ft span truss with 3-ft depth

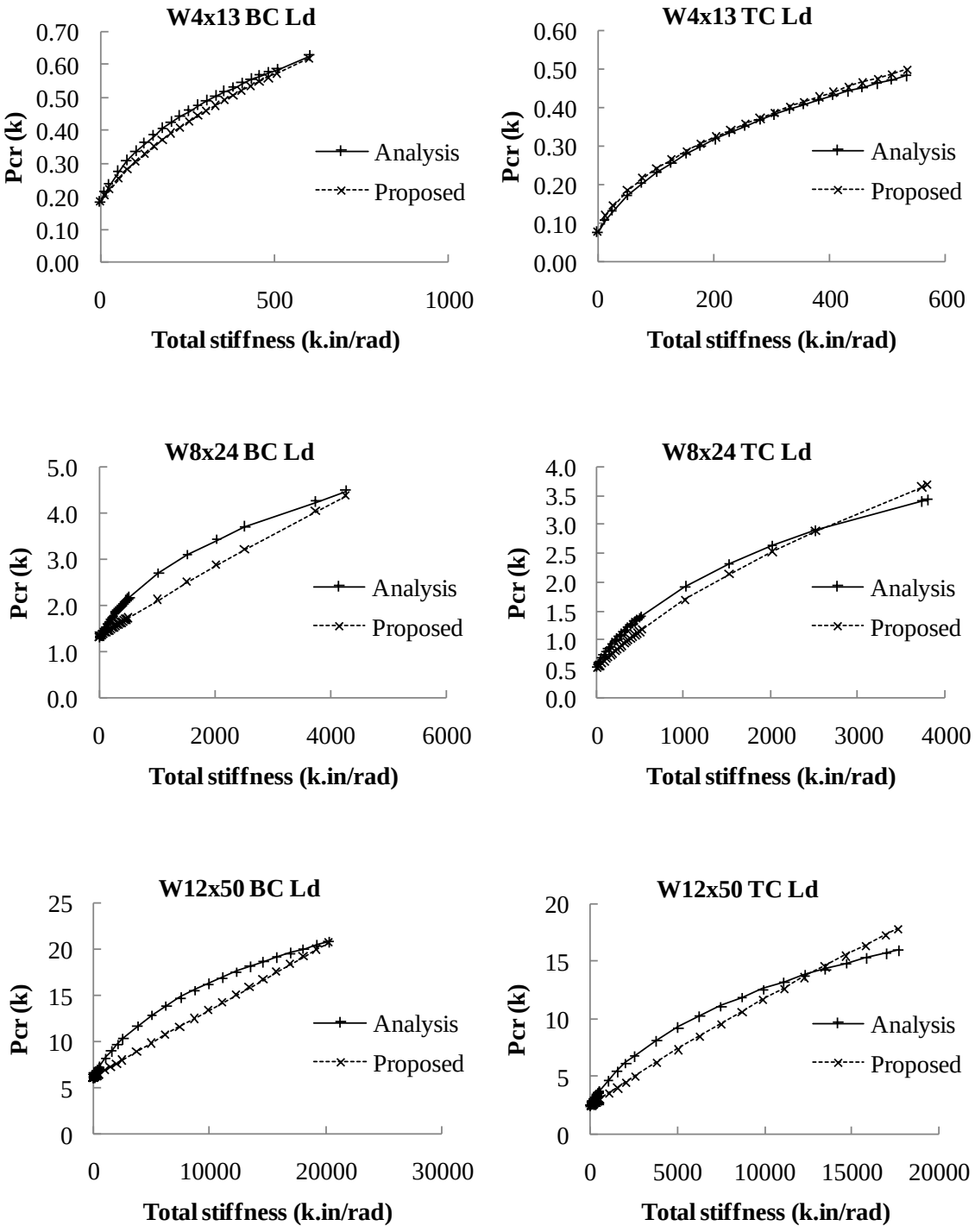

Figure C.2 72-ft span truss with 3-ft depth

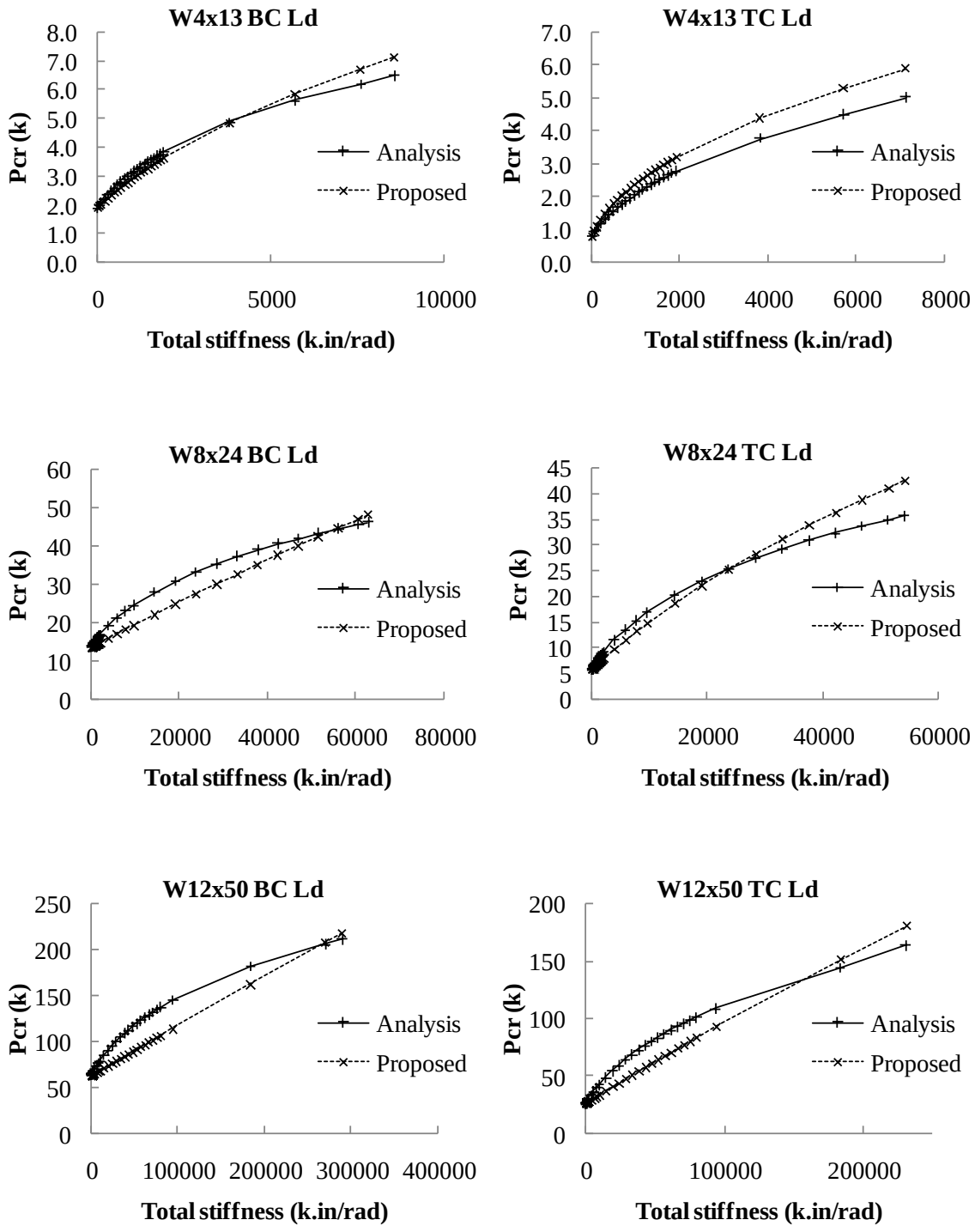

Figure C.3 48-ft span truss with 6-ft depth

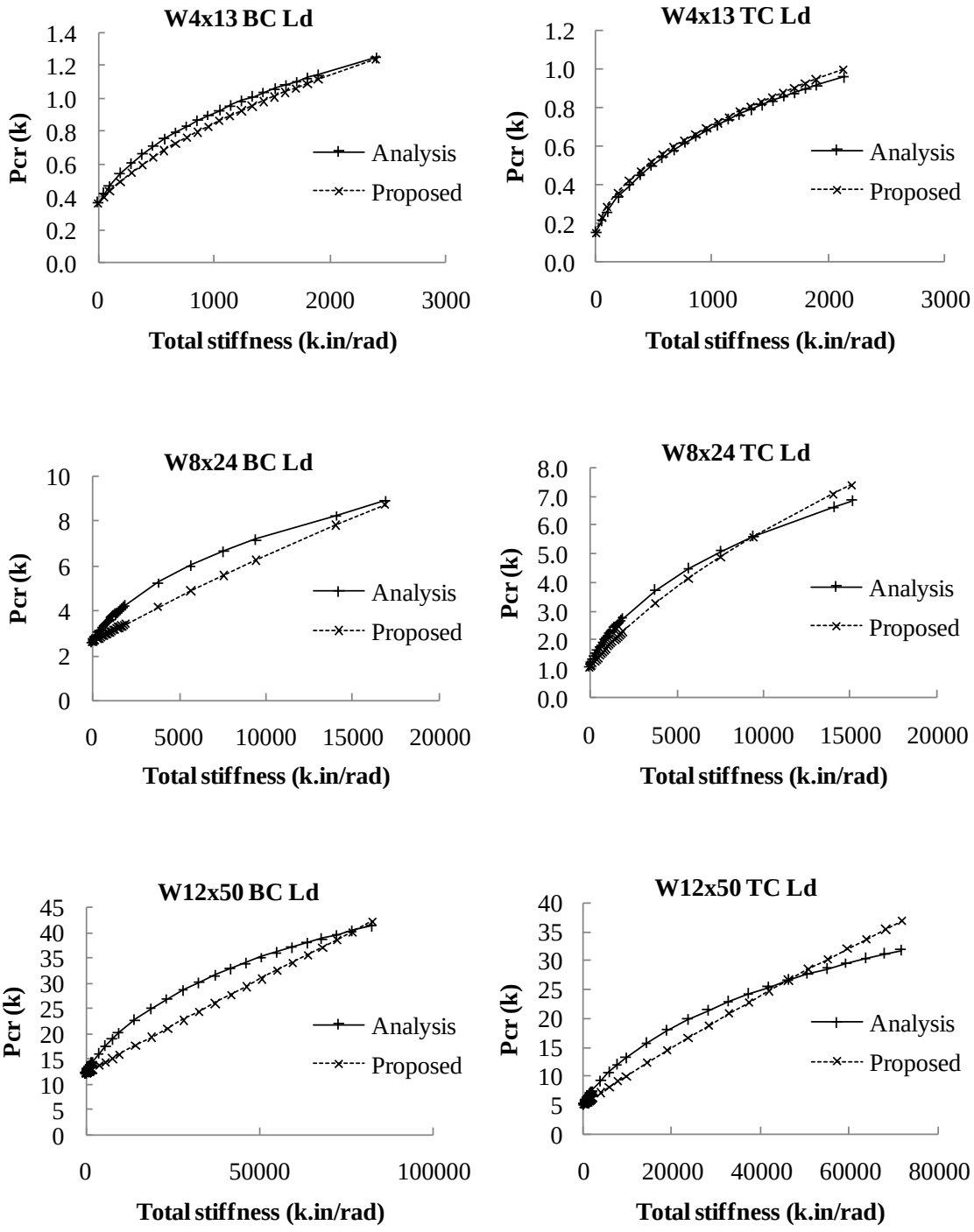

Figure C.4 72-ft span truss with 6-ft depth

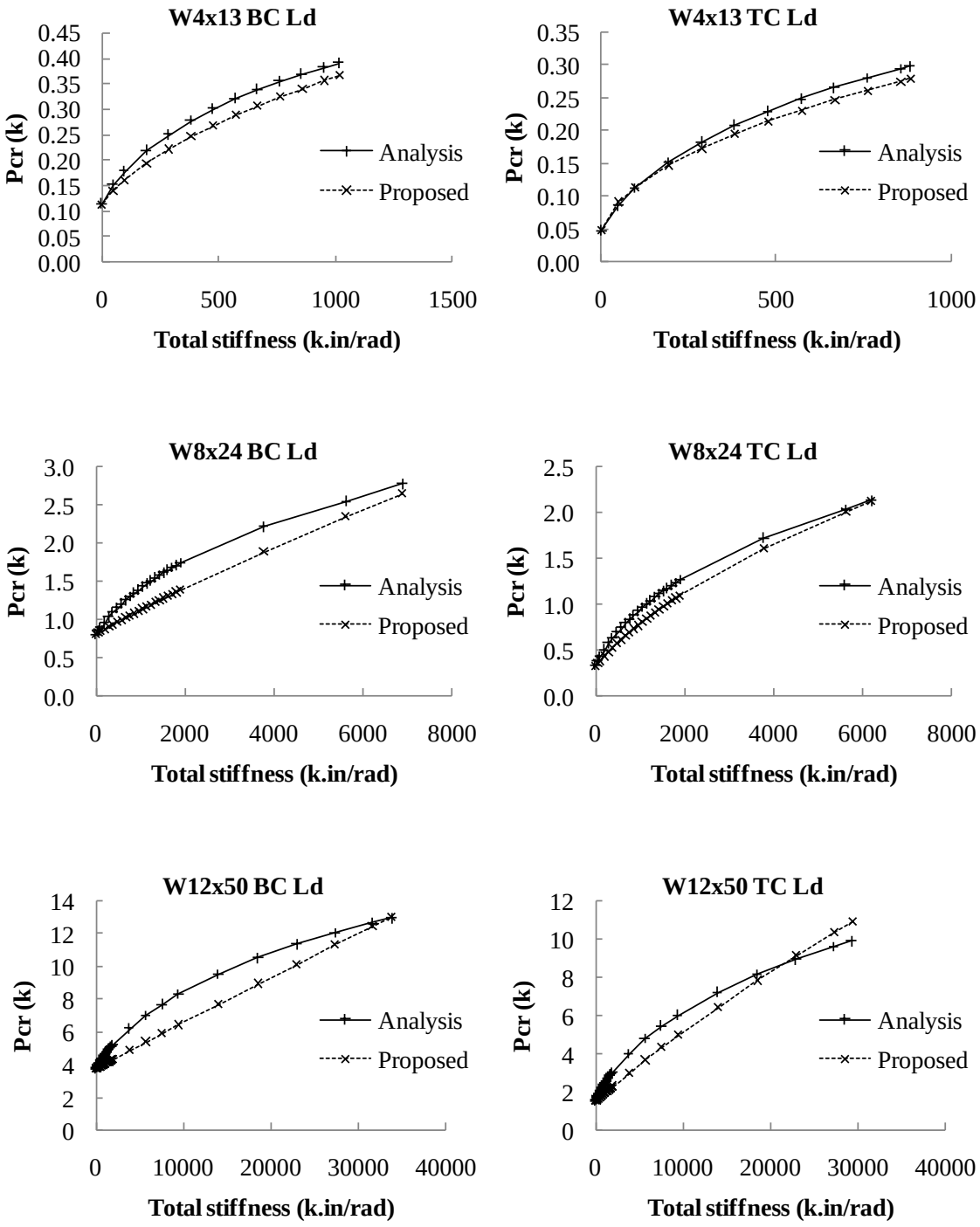

Figure C.5 96-ft span truss with 6-ft depth

C.2.2 Uniform Moment Cases

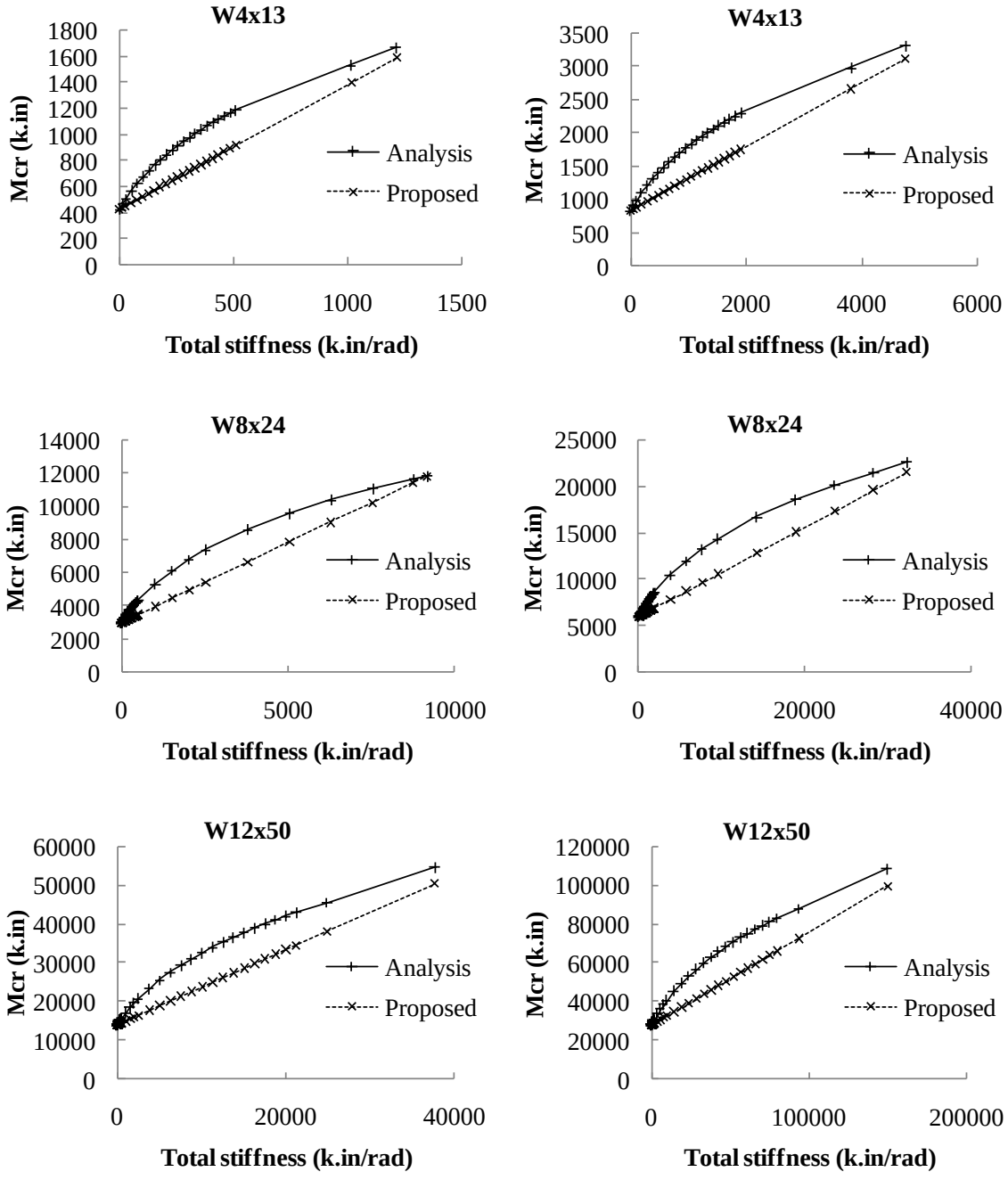

A) 3-ft depth B) 6-ft depth

Figure C.6 48-ft span truss

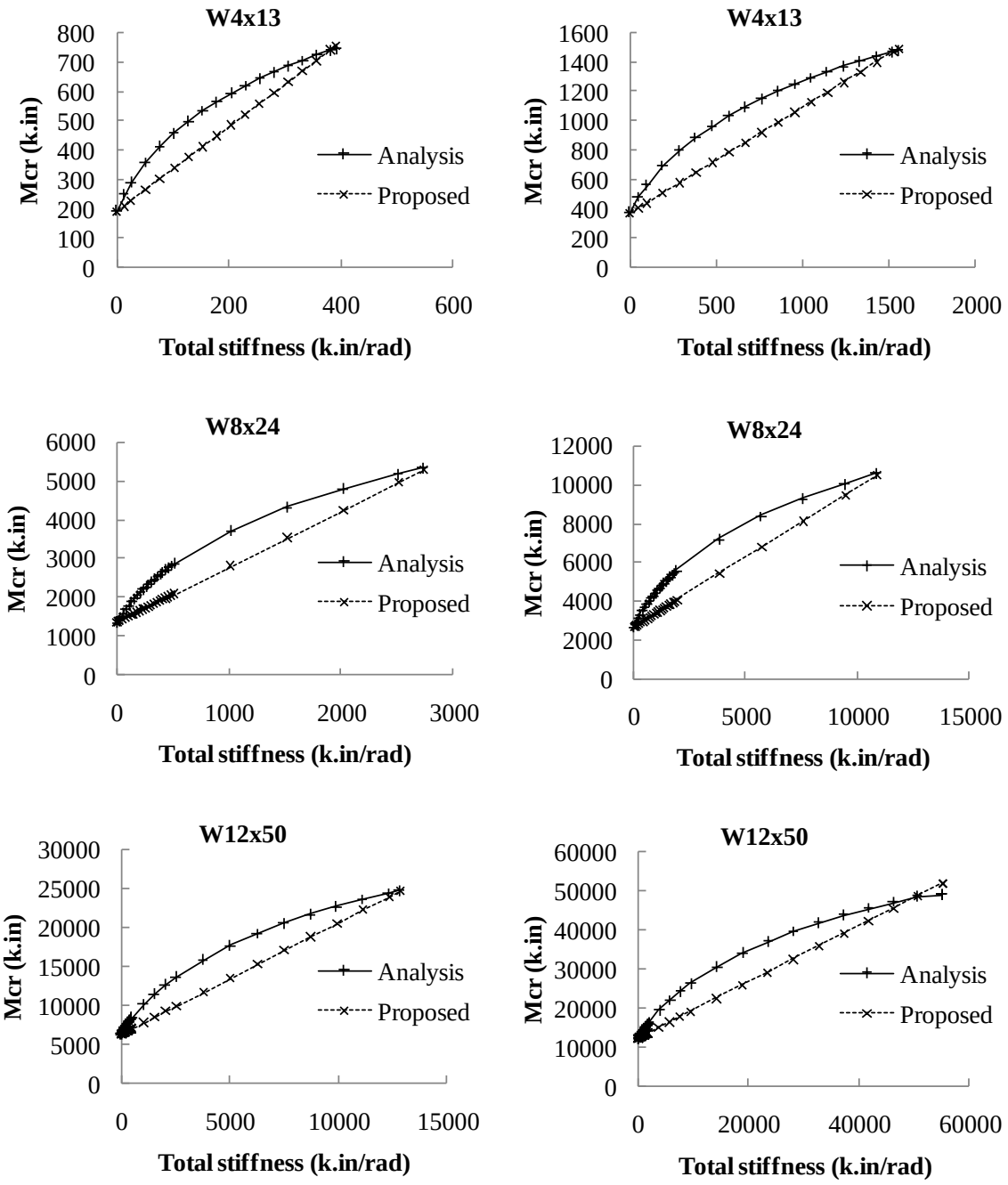

A) 3-ft depth B) 6-ft depth

Figure C.7 72-ft span truss

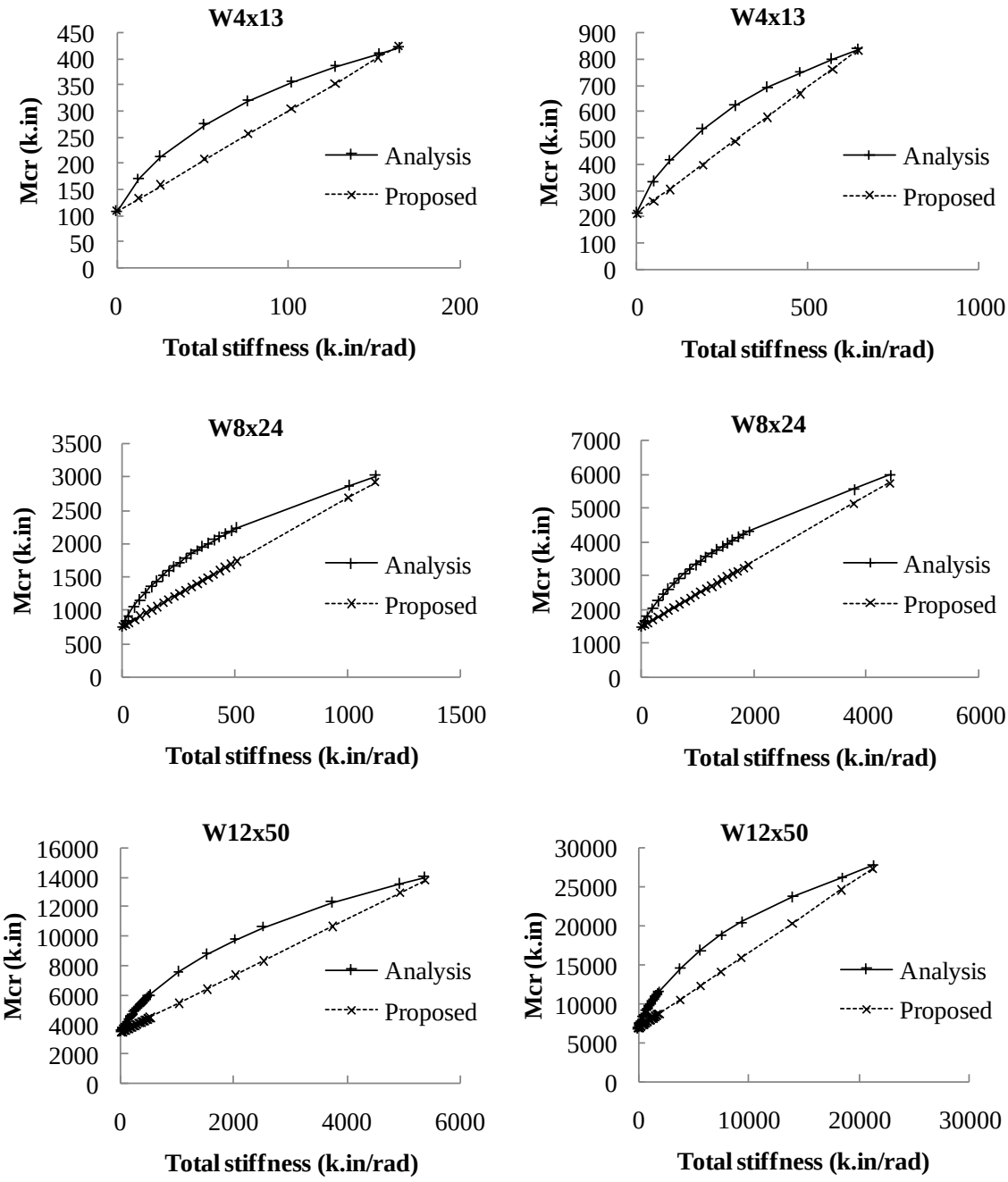

A) 3-ft depth B) 6-ft depth

Figure C.8 96-ft span truss

References

American Association of State Highway and Transportation Officials (AASHTO), AASHTO LRFD Bridge Design Specifications, 4th ed., Washington, DC, 2007.

American Institute of Steel Construction (AISC), Manual of Steel Construction, Chicago, IL, 2005a.

American Institute of Steel Construction (AISC), Code of Standard Practice, Chicago, IL, 2005b.

American Institute of Timber Construction (AITC), Timber Construction Manual, 5th ed., Engle wood, CO, 2005.

ANSYS Inc., "Elements Reference", Release 11.0 Documentation for ANSYS, Canonsburg, PA, 2010.

Collings, D., Steel-Concrete Composite Bridges, Thomas Telford, London, UK, 2005.

Deaver Jr., J.E., Laboratory Tests on Torsional Braces for Steel Bridge Girders with Normal Supports, Master Thesis, University of Houston, Houston, TX, 2003.

Deblauw, R., Master Report, The University of Texas at Austin, Austin, TX, 2007.

Dux P. and Kittipornchai K., "Elastic buckling strength of braces beams", *Steel Construction: Journal of the Australian institute of steel construction*, Vol. 20, No. 1, pp. 2-20, May, 1986.

Engesser, F. "Die Zusatzzkräfte und Nebenspannungen eisemer Fachwerkbrücken", Vol I, Die Zusatzkrafte, 1982, Vol. II, Die Nebenspannungen, 1893, Julius Springer, Berlin, Germany. In *Structural Stability Research Council (SSRC), Guide to Stability Design Criteria for Metal Structures, 5th ed., Ziemien R.D. ed., John Wiley & Son, New York, NY, 2010.*

Engesser, F. "Die Sicherung offener Brücken gegen Ausknicken", *Centralbl. Bauverwaltung*, 1884 p. 415, 1885, p. 93. In *Structural Stability Research Council (SSRC), Guide to Stability Design Criteria for Metal Structures, 5th ed., Ziemien R.D. ed., John Wiley & Son, New York, NY, 2010.*

European Committee for Standardization (CEN), Eurocode 3: Design of Steel Structures – Part 1-1: General rules and rules for building (EN 1993-1-1), Brussels, 2005.

Galambos, T.V., Structural Members and Frames, Prentice Hall, Upper Saddle River, NJ, 1968.

Helwig, T.A.; Frank, K.H.; and Yura, J.A., "Lateral-Torsional Buckling of Singly-Symmetric I-Beams", *ASCE Journal of Structural Engineering*, Vol. 123, No. 9, pp. 1172-1179, September, 1997.

Helwig, T.A.; and Yura, J.A., "Torsional Bracing of Columns", *ASCE Journal of Structural Engineering*, Vol. 125, No. 5, pp. 547-555, May, 1999.

Holt, E.C., "Buckling of a Pony Truss Bridge" in The Stability of Bridge Chords without Lateral Bracing, Report No. 2, The Pennsylvania State College, PA, 1952.

Holt, E.C., "The Analysis and Design of Single Span Pony Truss Bridges" in The Stability of Bridge Chords without Lateral Bracing, Report No. 3, The Pennsylvania State College, PA, 1952.

Iwicki, P., "Stability of Trusses with Linear Elastic Side-Supports", *Thin-Walled Structures*, Vol. 45, pp. 849-854, 2007.

Leigh, J.M., "Bridging Spacing for Longspan Steel Joists" in *Masoumy, G., Lateral Torsional Buckling of Steel Joists and Joist Systems, D.SC. Dissertation, Washington University, Saint Louis, MO, May, 1980.*

Masoumy, G., Lateral Torsional Buckling of Steel Joists and Joist Systems, D.SC. Dissertation, Washington University, Saint Louis, MO, May, 1980.

Meck, H.R., "Experimental Evaluation of Lateral Buckling Loads", *Journal of the Engineering Mechanics Division*, pp. 331-337, April, 1977.

Philips, B.A., Bracing Requirements for Elastic Steel Beams, Master Thesis, The University of Texas at Austin, May, 1991.

PN-90/B-03200 Steel Structures. Design rules, in *Iwicki, P., "Stability of Trusses with Linear Elastic Side-Supports", This-Walled Structures, Vol. 45, pp. 849-854, 2007.*

Quadrato, C.E., Stability of Skewed I-Shaped Girder Bridges Using Bent Plate Connections, Ph.D. Dissertation, The University of Texas at Austin, Austin, TX, 2010.

Southwell, R.V., "On the Analysis of Experimental Observations in Problems of Elastic Stability", *Proceedings of the Royal Society of London*, Vol. 135, No. 828, pp. 601-616, April, 1932.

Structural Stability Research Council (SSRC), Guide to Stability Design Criteria for Metal Structures, 5th ed., Ziemien R.D. ed., John Wiley & Son, New York, NY, 2010.

Schibler, W., "Das Tragvermögen der Druckgurte offener Fachwerkbrücken mit parallelen Gurten", *Instutut fuer Baustatik, Eidgenoessische Technische Hochschule, Zurich Mitteilungen*, No. 19, In *Structural Stability Research Council (SSRC), Guide to Stability Design Criteria for Metal Structures, 5th ed., Ziemien R.D. ed., John Wiley & Son, New York, NY, 2010.*

Tall, L. (ed.), Structural Steel Design, 2nd ed., John Wiley and Son, New York, 1974.

Timoshenko, S.P., and Gere, J.M., Theory of Elastic Stability, McGraw-Hill, New York, 1961.

Wang, L., and Helwig, T.A., "Critical Imperfection for Beam Bracing Systems", *Journal of Structural Engineering*, Vol. 131, No. 6, pp. 933-940, 2005.

Winter, G., "Lateral Bracing of Columns and Beams", *Trans. ASCE*, Vol. 125, Part 1, pp. 809-825, 1960.

Wongjeeraphat, R. and Helwig, T.A., "Stability Bracing Requirements for Truss Systems", *Proc. of 2009 Annual Stability Conference*, SSRC, Phoenix, Arizona, pp. 177-197, 2009.

Yarimci, E., Yura, J.A., and Lu, L., Techniques for Testing Structures Permitted to Sway, Lehigh University, Bethlehem, PA, 1966.

Yura, J.A., Phillips, B., Raju, S., and Webb, S., Bracing of Steel Beams in Bridges, The University of Texas at Austin: Center for Transportation Research, Austin, TX 1992.

Yura, J.A., "Fundamentals of Beam Bracing", *Engineering Journal*, American Institute of Steel Construction, 1st Quarter, pp. 11-26, 2001.

Yura, J.A., Helwig, T.A., Herman, R., and Zhou, C., "Global Lateral Buckling of I-Shaped Girder Systems", *Journal of Structural Engineering*, Vol. 134, No. 9, pp. 1487-1494, 2008.

Zhi-gang, M., "Study on Load–Carrying Capacity of Uniplanar Steel Pipe Truss", *Journal of Civil Engineering and Architecture*, Vol. 2, No. 1, January, 2008.

Ziemian, R.D. and McGuire, W., "Tutorial for MASTAN2 Version 3.0", John Wiley and Son, New York, NY, 2007.